

Thesis Title:

**The contribution of the extra-cellular
matrix to tissue mechanics and
morphology during development**

Candidate Name:

Ricardo Barrientos

*A thesis submitted in partial fulfilment for the degree of Doctor
of Philosophy.*

September 2019

Field:

Biophysics and Developmental Biology

Institution:

MRC Laboratory for Molecular Cell Biology, UCL

and

CoMPLEX, Department of Computer Science, UCL

Supervisors:

Yanlan Mao

Ewa Paluch

I, Ricardo Barrientos confirm that the work presented in this thesis is my own. Where information has been derived from other sources, I confirm that this has been indicated in the thesis.

Abstract

Extra-cellular matrices are ubiquitous in biological systems, implicated in both mechanics and signalling. The effect of extra-cellular matrix on cell shape *in vitro* is well established, however much less is known about how the extra-cellular matrix affects tissue morphology *in vivo*.

During development, the extra-cellular matrix surrounding growing tissues must adapt to the changing size and shape of the cellular mass. Physically, whether the extra-cellular matrix contributes to tissue shape depends on the relative mechanical properties between the cells and their extra-cellular matrix. As cells grow, they apply a tension to their surrounding extra-cellular matrix; how the extra-cellular matrix responds depends on their comparative stiffness. When the extra-cellular matrix is stiff compared to cells, stress may be generated at their interface as the cells grow. In this case the tissue may change shape to minimise this stress. However, any stress build-up may be relaxed over time by remodelling of the extra-cellular matrix. Biologically, stress may induce signals in the cells, allowing dynamic regulation of cell and extra-cellular matrix mechanical properties.

This work is concerned with determining how the extra-cellular matrix contributes to the morphology of a growing tissue, using the wing disc of *Drosophila Melanogaster* as a model system. The wing disc is a larval-stage, highly proliferative, single-cell thick, epithelial tissue folded into a sac, surrounded by a thin extra-cellular matrix. The mechanical properties of this tissue are inferred using a combination of biophysical and genetic techniques. Relative stiffness of cells and their extra-cellular matrix is experimentally measured using atomic force microscopy. Remodelling rates of the extra-cellular matrix are inferred by measuring turnover rates of its components, either *in vitro* using fluorescence-recovery, or *in vivo* using temporal genetic knockdown. By combining these measurements with theoretical models of tissues, the relative importance of stiffness and remodelling to tissue shape can be determined.

Impact Statement

A lot of medical research is currently focused on developing technology to grow organs in the lab. If organs can be grown, then they may be used for transplantation into humans, potentially reducing organ waiting lists and saving lives. The extra-cellular matrix is a vital component of tissues. Understanding how the extra-cellular matrix contributes to tissue development is a necessary step in growing organs *in vitro*. In this work I have looked at how the extra-cellular matrix contributes to the correct morphology, and function, of a developing tissue. This work may therefore contribute to research growing organs *in vitro*. Further, many diseases are caused by, or require, the extra-cellular matrix. For example, miss-regulation of extra-cellular matrix mechanics allows tumours to grow, and metastasise. Understanding the role of the extra-cellular matrix in functional tissue may explain how miss-regulation of the extra-cellular matrix can cause dysfunctional tissue.

Contents

1 Introduction	17
1.1 Mechanics and Morphology	18
1.1.1 Mechanical Properties	18
1.1.2 Proteins as Polymers.....	20
1.1.3 Cell Mechanics and Morphology	21
1.1.4 Tissue Mechanics and Morphology	22
1.2 Model System	23
1.2.1 Growth	28
1.2.2 Morphogens.....	30
1.3 Cells	34
1.3.1 Membrane	34
1.3.2 Cortex.....	35
1.3.3 Polarity.....	39
1.3.4 Adhesion	40
1.4 Cell-Matrix Adhesions	43
1.4.1 Integrin.....	43
1.4.2 Integrin-Associated Complex.....	45
1.4.3 Dystroglycan	50
1.5 Extra-Cellular Matrix	52
1.5.1 Laminin	53
1.5.2 Collagen	54
1.5.3 Heparan-Sulphate Proteoglycans	56
1.5.4 Glypican	57
1.5.5 Syndecan.....	58
1.5.6 Perlecan	58
1.5.7 Nidogen.....	61
1.5.8 Sparc	62
1.5.9 Matrix Metalloproteinase.....	62
1.5.10 Disintegrin.....	66
1.5.11 Lysl Oxidase.....	67

1.5.12 Peroxidasin	67
1.6 Hypothesis	69
1.6.1 Hypothesis	69
1.6.2 Aims	71
1.6.3 Implications.....	71
2 Results	73
2.1 Results Section 1: Structure and composition of the wing disc extra-cellular matrix..	73
2.1.1 Methods.....	74
Fly lines.....	74
Ex vivo Culture method	75
Confocal microscopy	77
Fluorescence Intensity Measurements	80
Electron microscopy.....	81
Statistics	82
2.1.2 Results.....	84
2.1.3 Discussion	98
2.2 Results Section 2: Perturbations to the wing disc extra-cellular matrix.....	101
2.2.1 Methods.....	101
Fly lines.....	101
Confocal Microscopy	103
Treatment Protocols	104
Temperature shift	108
2.2.2 Results.....	112
Genetic perturbations	112
Protease treatments	118
Permeabilisation treatments	126
Temporal genetic perturbations	127
2.2.3 Discussion	131
2.3 Results Section 3: Elastic properties of the wing disc extra-cellular matrix.....	138
2.3.1 Methods.....	138
Fly lines.....	138
Micropipette Aspiration	139
Atomic Force Microscopy.....	145
2.3.2 Results.....	163
Treatments	163
Perlecan.....	167

2.3.3 Discussion	170
2.4 Results Section 4: Dynamic properties of wing disc extra-cellular matrix.....	174
2.4.1 Methods.....	174
Fly lines.....	174
Fluorescence recovery	174
Temperature shift	179
2.4.2 Results.....	184
Intra-cellular turnover	184
Extra-cellular turnover	187
2.4.3 Discussion	194
3 Conclusions.....	199
3.1 Cell contractility and the ECM	199
3.2 Remodelling of the ECM	200
3.3 Outlook.....	203
4 References	205

Figures

Figure 1. <i>A wing disc is a single-cell thick epithelial sac surrounded by an extra-cellular matrix.</i>	24
Figure 2. <i>The wing disc is a highly proliferative tissue, growing in size exponentially over a four-day period.</i>	27
Figure 3. <i>Morphogens pattern the wing disc epithelium, defining growth rates and cell fates.</i>	31
Figure 4. <i>Many cell and tissue shapes may be possible through variation of adhesion, polarity and surface tension.</i>	42
Figure 5. <i>Mechanical properties of the extra-cellular matrix are hypothesised to define its response to cellular growth and proliferation during wing disc development.</i>	70
Figure 6. <i>Fluorescently labelled extra-cellular matrix proteins allow measurement of protein concentration with wing disc size.</i>	81
Figure 7. <i>Fixation changes extra-cellular matrix structure and wing disc morphology.</i>	83
Figure 8. <i>The extra-cellular matrix forms a thin, continuous layer around the wing disc.</i>	85
Figure 9. <i>The extra-cellular matrix remains continuous around the wing disc during growth.</i>	87
Figure 10. <i>Perlecan and laminin appear continuous across the wing disc extra-cellular matrix.</i>	88
Figure 11. <i>The extra-cellular matrix appears to exhibit a fibrous and layered structure.</i>	90
Figure 12. <i>Integrins form clusters, with one cluster centred at the basal surface of each cell.</i>	90
Figure 13. <i>Collagen fibres show some co-localisation with integrin clusters.</i>	91
Figure 14. <i>Actin filaments form a variety of ordered structures on the basal surface of cells.</i>	92
Figure 15. <i>Myosin forms ringlets on the basal surface of cells.</i>	93

Figure 16. <i>The extra-cellular matrix at the pouch becomes thicker as the wing disc ages.</i>	94
Figure 17. <i>Extra-cellular matrix thickness at the peripodial epithelium and hinge of the columnar epithelium are thinner than at the pouch.</i>	95
Figure 18. <i>Cellular protrusions pass through layers of the extra-cellular matrix.</i>	96
Figure 19. <i>Collagen, laminin and perlecan concentrations increase per unit area of extra-cellular matrix as the wing disc grows in size.</i>	97
Figure 20. <i>Using temporal knockdown, interaction between ECM proteins may be elucidated.</i>	109
Figure 21. <i>Metalloproteinase knockdown has no considerable affect on wing disc morphology.</i>	115
Figure 22. <i>Perlecan knockdown leads to constricted wing disc morphology, while perlecan overexpression leads to a spreading out.</i>	116
Figure 23. <i>Integrin knockdown leads to considerable ectopic folding of the wing disc.</i>	117
Figure 24. <i>Degradation of the extra-cellular matrix with collagenase causes a sudden and considerable change of wing disc morphology.</i>	120
Figure 25. <i>Inhibition of myosin contractility reduces the extent of morphological change induced by subsequent extra-cellular matrix degradation.</i>	121
Figure 26. <i>Inhibition of myosin contractility after extra-cellular matrix degradation does not recover the original wing disc morphology.</i>	122
Figure 27. <i>Degradation of cell cortices reduces the extent of morphological change induced by subsequent extra-cellular matrix degradation.</i>	123
Figure 28. <i>Degradation of heparan sulphate does not change wing disc morphology.</i>	124
Figure 29. <i>Degradation of heparan sulphate does not affect perlecan concentration in the wing disc extra-cellular matrix.</i>	125
Figure 30. <i>The extra-cellular matrix is not dependent on cells to maintain integrity.</i>	126
Figure 31. <i>The extra-cellular matrix does not degrade ex vivo over hours timescale.</i>	127

Figure 32. <i>Perlecan degrades from the extra-cellular matrix via fast and slow mechanisms.</i>	128
Figure 33. <i>Temporal knockdown of extra-cellular matrix components reveals complex dynamic effects on other extra-cellular matrix components.</i>	129
Figure 34. <i>Laminin knockdown causes structural changes to collagen in the extra-cellular matrix of the wing disc.</i>	130
Figure 35. <i>The extra-cellular matrix may balance cellular contractility.</i>	133
Figure 36. <i>Micropipette aspiration determines sample stiffness by applying pressure to its surface and measuring the size of resultant deformation.</i>	143
Figure 37. <i>Atomic force microscopy measures sample stiffness by indenting with a cantilever of known stiffness and measuring the indentation-deflection relationship.</i>	146
Figure 38. <i>Wing disc stiffness as measured by atomic force microscopy varies considerably from point to point.</i>	155
Figure 39. <i>Correct stiffness measurement requires careful consideration of sample preparation.</i>	156
Figure 40. <i>After discarding erroneous stiffness measurements, resulting indentation-deflection curves fit the Hertz model well.</i>	160
Figure 41. <i>Wing disc stiffness decreases systematically ex vivo.</i>	160
Figure 42. <i>Degrading the extra-cellular matrix with collagenase leads to a considerable reduction in effective tissue stiffness.</i>	164
Figure 43. <i>Degradation of the cell cortices reduces effective tissue stiffness to a similar level to extra-cellular matrix degradation.</i>	165
Figure 44. <i>Effective stiffness increases with increasing wing disc size.</i>	166
Figure 45. <i>Perlecan knockdown significantly increases effective tissue stiffness.</i>	169
Figure 46. <i>Perlecan knockdown significantly increases the rate of effective stiffness increase with wing disc size.</i>	169
Figure 47. <i>Collagen turnover rates can be measured genetically.</i>	182
Figure 48. <i>Integrins are mostly immobile over an hour-long period.</i>	184
Figure 49. <i>Integrin and myosin have similar turnover rates but dissimilar mobile fractions.</i>	185
Figure 50. <i>Collagen turnover occurs at timescales on the order of days.</i>	186

Figure 51. *Collagen concentration has a net increase over time per unit area of extra-cellular matrix.*187

Figure 52. *Collagen turnover occurs at an increased rate in pouch and hinge regions of the wing disc.*190

Figure 53. *Loss of perlecan reduces collagen turnover rate.*191

Figure 54. *Without perlecan collagen can still turnover but at a greatly reduced rate.*192

Figure 55. *Collagen turnover rate is greater on the outer surface of the extra-cellular matrix.*194

Figure 56. *Regulation of extra-cellular matrix area, and therefore cell shape, during tissue growth may depend on both cell contractility and cell proliferation.*201

Abbreviations

ECM – Extra-Cellular Matrix

IAC – Integrin-Associated Complex

AEL – After Egg Laying

MAS – Muscle Attachment Site

ATP – Adenosine Triphosphate

GTP – Guanosine Triphosphate

RGD – Arginine Glycine Aspartate

HS – Heparan Sulphate

HSPG – Heparan Sulphate Proteoglycan

GFP – Green Fluorescence Protein

SCA – Scarlet Fluorescent Protein

AFM – Atomic Force Microscopy

FRAP – Fluorescence Recovery After Photobleaching

Some gene names are used synonymously with their general protein names, the important ones are:

Trol – *Drosophila* perlecan gene

Vkg – *Drosophila* collagen subunit gene

LanB1 – *Drosophila* laminin beta subunit gene

LanB2 – *Drosophila* laminin gamma subunit gene

LanA – *Drosophila* laminin alpha subunit gene

Wb – *Drosophila* alpha subunit gene

Mmp1 – *Drosophila* matrix metalloproteinase 1

Mmp2 – *Drosophila* matrix metalloproteinase 1

Mys – *Drosophila* beta subunit gene

Mew – *Drosophila* alpha subunit gene

If – *Drosophila* alpha subunit gene

Sqh – *Drosophila* myosin regulatory light chain subunit gene

Utr – Mammalian utrophin transgene.

Some general protein names are used to refer to more specific variants unless otherwise stated:

Collagen – Collagen IV

Myosin – Non-muscle Myosin II

Acknowledgements

I would like to thank my PhD program CoMPLEX, for funding the first three years of my PhD, as well as the MRes year that allowed me to find a subject I wanted to study. I would especially like to thank Lewis Griffin and Guy Moss for accepting me onto the program and providing support. I would also like to thank Gemma Ludbrook who managed the program and also gave plenty of support. I would like to thank Yanlan Mao for accepting me into her lab and funding me for the last year of my PhD and helping me along the way. I would like to thank all past and present members of the lab. Maria Duda trained me to dissect larvae and use microscopes. Rob Tetley helped me greatly with his fly knowledge. Melda Tozluoglu has been especially helpful in teaching me about the mathematical side of tissue mechanics. Nargess Khaligaribi generously invited me to contribute to her paper. Alice roycroft was very supportive, especially at the bench. Fellow PhD students Natalie Kirkland, Filippos Ioannou and Alejandra Guzman Herrera have also been very supportive. I would like to thank Ewa Paluch for helpful discussions. I would like to thank past and present members of the Paluch lab for helping me and sharing reagents. I would especially like to thank Davide Cassani for showing me how to micropipette, and providing helpful experimental advice. I would like to thank my thesis committee, including Buzz Baum, Guillaume Charras, Andrew Oates and Shiladitya Banerjee for providing excellent advice. I would also like to thank Guillaume Charras for letting me to use his atomic force microscopy equipment, Malti Vaghela for helping me with analysis of indentation-deflection curves and Richard Thorogate for training me on the atomic force microscope and fixing it when it every time it broke. At the LM CB I would like to Paul Topham for fixing everything, especially the micropipette-forging filament many times. I would like to thank Andrew Vaughn, Ki Hng and Kathryn Scherer for training me on microscopes and keeping them working.

I would like to thank all the people who were willing to socialise with me through my PhD. On my program, David, Ben, Tess and Andrew. At the LM CB, Henry, Davide, Dani, Nez, Sascha, Agathe, Matt, Gabriel, Sophie, Melanie, Joe, the whole Mao lab

and many more, I can't name everyone. I would like to thank Houseman and Square Tavern for taking care of me on Friday evenings. At home, I would like to thank Lewis who was always there to take my mind off things. I would like to thank my carer Megan for looking after me the last year or so. I would like to thank my parents who have given me emotional support and financial safety, I should probably thank my sister too. I would also like to thank my gran and aunts for being extremely supportive, and providing me a second home in London.

1 Introduction

The evolution of complex morphology has been necessary for the function and survival of multicellular organisms in the environment. The complex morphology of organisms is precisely and reproducibly controlled. To do this, biological systems must arrange cells precisely from microscopic through to macroscopic scales. This is achieved partly through complex patterning of tissue by regulatory signals, but also through mechanics. In order for cells to change shape, they must generate forces, and difference in forces drive changes in shape. The accumulation of cell shape changes at microscopic scales in turn drives tissue shape changes at macroscopic scales. To produce consistent morphology, regulatory systems of organisms must precisely control the patterning of these force differences. Therefore, mechanics are an integral part of development. There are many elements, mechanical and regulatory, that are required for the precise and accurate development of morphology in biological systems. This introduction is concerned with these elements, and in particular those elements that contribute mechanically.

This introduction is ordered as follows. Firstly in §1.1, a definition of the mechanical properties considered, and an outline of how they may contribute to tissue morphology is given. Secondly in §1.2, a description of the wing disc, which is the tissue to be studied, will given, including how growth and patterning contribute to its morphology. Thirdly in §1.3, the elements of cells that contribute to its shape and mechanics is considered, including membrane, cortex, polarity and adhesions. Fourthly in §1.4, adhesions that bind cells to their extra-cellular matrix will be considered in detail. Fifthly in §1.5, the extra-cellular matrix itself will be considered, focusing on the components that compose it and their known function. Finally in §1.6, the overarching hypothesis that will be interrogated in this work will be described. When reviewing published results, particular focus will be given to the wing disc where possible, otherwise to other tissues in the fly, and if necessary to

other organisms. This is necessary because the function of biological mechanisms have often evolved with specificity in different organisms, and therefore details cannot always be translated between them.

1.1 Mechanics and Morphology

Biological tissues can be viewed as composite materials. Cells divide tissues into units, each potentially exhibiting different mechanical properties. The mechanical properties of cells are coupled together through adhesions, either directly through cell-cell adhesions or indirectly *via* an extra-cellular matrix (ECM) and cell-matrix adhesions ^[1], and the mechanical properties of the ECM itself are then coupled to cells too. The composite of these component mechanical properties defines the combined, effective mechanical properties of the tissue ^[2]. However, tissue mechanical properties can be active, in the sense that they can change over time, depending on the programmatic regulation of its constituent cells. Time is important when considering mechanics in biological systems, because the mechanical properties most biological materials exhibit a time-dependent response to force ^[2].

1.1.1 Mechanical Properties

Viscous materials are materials whose resistance to deformation decays with time resist deformation inversely with time under an applied force ^[3]. The viscosity of the material defines the rate at which resistance to deformation is relaxed over time. Elastic materials will deform reversibly under an applied force. When a force is applied to an elastic material it will deform. When the force is removed, an elastic material will return to its original undeformed shape. The amount of deformation resulting from an applied force depends on the materials stiffness. A stiff material will deform less in response to a force than a soft material. At fine scales, constituents of viscous materials can rearrange to relax stress, and viscosity emerges from friction between these constituents. Constituents of elastic materials cannot rearrange, so stress remains ^[3].

Viscoelastic materials will deform irreversibly under an applied force, depending on the period of time the force is applied ^[2]. When a force is applied to a viscoelastic material it will deform, just like an elastic material. However, when the force is removed the material may recover only part of its original un-deformed shape. The longer the force is applied, the more of the material's original shape is lost. This is because the stress in the material due to deformation is being relaxed over time. Relaxation occurs because the microscopic structure of the material is being remodelled. The time over which relaxation occurs depends on the remodelling rate of the material. At timescales much less than the remodelling rate, the material will behave elastically, while at timescales much greater than the remodelling rate the material will behave viscously. Consideration of timescales is therefore very important when considering the mechanics of materials. This is especially true in tissues, which are composite materials where viscoelastic timescales can vary by orders of magnitude between components ^[2].

Plastic materials also deform irreversibly, but as a function of force not time. Plasticity emerges from the force driven rearrangement of a materials constituents. Elastoplastic materials are often characterised by an elastic regime at low force and a plastic regime at high force. Onset of the plastic regime is characterised by a yield stress. Viscoelastoplastic materials combine all three mechanical properties ^[2].

Viscous and elastic properties of materials are passive in the sense that they describe a response to an external force. However, biological systems can also exhibit active mechanical properties. Active mechanical properties emerge from forces generated by constituents of the material itself. Contractility is an example of an active mechanical property ^[2].

1.1.2 Proteins as Polymers

The viscoelastic properties of biological materials are closely related to polymer physics. Polymer physics describes the behaviour of materials composed of long molecules called polymers^[4]. Polymers are treated as flexible strings able to move through many conformations. In solution solvent molecules constantly bombard polymers. These thermal fluctuations drive stochastic changes in polymer conformation, but tend to some average size. The solubility of polymers can change their average end-to-end length. Soluble polymers can swell, while insoluble polymers can collapse^[5]. Cross-linked polymers form networks. Strong crosslinks are relatively unaffected by thermal fluctuations and so remodel on long time scales. Weak crosslinks will remodel under thermal fluctuations and so remodel on short timescales. When a polymer network is deformed, the distribution of polymer sizes changes. However, thermal fluctuations from solution apply forces to drive the polymers back to the preferred size distribution. This entropic response gives the polymer network elasticity, while crosslink remodelling gives it viscosity^[4]. Polymers and proteins are similar, however proteins are encoded with complex interactions that usually lead to predictable structures not considered in the more stochastic treatment of polymer physics. Polymer physics does provide some intuition about the behaviour of biological materials.

Considering polymer behaviour on a spectrum from dense and networked to diffuse and free may be a way to bridge the gap between mechanics and signalling. A polymer that is small or insoluble may diffuse quickly through a dilute solution^[4]. If such a polymer were to change its size or solubility upon interaction with another polymer then its diffusivity may change. If this polymer were actually a protein, then these interactions could be highly specific to certain other proteins. Diffusing and interacting solutes are the basis of reaction-diffusion systems implicated in biological patterning^[6].

1.1.3 Cell Mechanics and Morphology

The simplest physical picture of a cell is as a region of space enclosed by a membrane. The membrane segregates mass from the external environment, allowing the development of an ordered system within the cell. This ordered system includes the conversion of small, simple molecules into large, complex macromolecular machines. To accumulate mass, machinery on the membrane allows the influx, and to a lesser extent efflux, of selected molecules into the cell. As cells accumulate mass, and become more ordered, a differential pressure develops across the membrane. A significant source of cell pressure is osmotic pressure, which develops as a result of differences in solute concentrations between a cell and its external environment ^[7]. This cell pressure applies a tension across the cell membrane, driving its expansion. In order to maintain cell size, a cell cortex that lines the inner surface of the membrane contributes contractility. The cell cortex is formed of a stiff actin filament network. Cortical contractility is generated by non-muscle myosin II, referred to here as just myosin, which actively pulls filaments of the actin meshwork together. This contractile force counterbalances the expansive pressure force across the cell membrane, allowing cells to maintain and regulate their size. Due to volume to area constraints, there is likely to be some optimum size for a functional cell. For example, monopoleudic cells may not be able scale their transcription rates with cell size indefinitely, and so protein production rates may not be able to scale with cell size wither. Therefore, cells proliferate in order to continue to survive. For cells to proliferate they must divide, and for cells to divide they must change shape ^[7].

The most energetically favourable shape for a cell is a sphere, which is the shape that maximises volume while minimising surface area ^[8]. Hence cells in suspension will generally form a spherical shape. Deviations from a sphere will occur due to fluctuations in stress across the cell surface, for example thermal fluctuations of the solution. On average a cell will approximate a sphere, which is rotationally symmetric. In order for a cell to achieve shapes other than a sphere it must break this symmetry. Symmetry can be broken *via* polarity systems in the cell. Polarity

systems generally involve sets of factors that interact antagonistically, driving their segregation into domains. Different polarity factors can recruit different components, which define different mechanics in different domains, driving different cell shapes ^[8]. Cell division is driven by polarity factors defining a ring-shaped domain partitioning the cell into two. Within the ring domain, polarity factors alter cortical mechanics, including increasing contractility, which generates a furrow that divides the cell. Symmetry can also be broken through adhesion to substrates and other cells ^[9]. Adhesion is mediated by adhesion machinery, which are components that integrate into the membrane, and protrude into the extra-cellular space and bind to specific targets. Adhesion components can target substrates such as extra-cellular matrices or adhesion components of other cells ^[1]. When a cell makes contact with a substrate, if adhesion is stronger than pressure forces then the cell will attempt to maximise contact with the surface, and so the cell will spread on a surface ^[8]. Adhesion-mediated spreading is another way for cells to break their symmetry. Adhesion components are often closely connected to polarity factors, to allow cells to define their polarity according to external cues ^[10].

1.1.4 Tissue Mechanics and Morphology

To produce a tissue from cells requires only that cells can grow, divide and adhere to each other. With only these elements the tissue would again have some energetically favourable shape approaching a sphere. By allowing cells polarity, any number of adhesive or non-adhesive domains may be defined per cell, which would generate some order in the arrangement of cells within the tissue, but not necessarily break symmetry. However by defining different mechanics or polarities to different subsets of cells, the symmetry of the tissue could be broken. Morphogens are factors secreted by cells, and diffuse across the tissue to form concentration gradients ^[11]. These morphogen gradients pattern the tissue and provide cells with positional signals. Signals provided by morphogens then define the programmatic activity of the cells. In this way, spatially defined subsets of cells can

have different polarity activities and mechanical properties, effectively breaking tissue symmetry and defining tissue shape.

Most tissues have an ECM. ECM can take many forms, but generally forms a network of collagen fibres that spans the tissue^[12]. The ECM may be implicated in defining tissue mechanics and morphology in many ways. Like cell-cell adhesions, it may couple cells of the tissue together *via* cell-matrix adhesions^[1]. It may act as a cue for defining the polarity of cells^[10]. The ECM may provide a highway for morphogens to cross the tissue^[13]. The ECM may act as an exoskeleton, contributing stiffness to the tissue greater than that provided by cells^[14]. The ECM may remodel slowly, helping maintain tissue morphology against stochastic changes in cell shape^[12]. Relatively little is known about the role of the ECM in defining tissue morphology. It is the aim of this work to determine how the mechanical properties of the ECM contribute to morphogenesis of tissues.

1.2 Model System

The model system used to study tissue development in this work is the *Drosophila Melanogaster* imaginal wing disc. *Drosophila* is a genus of fruit fly and is a particularly useful model system due to its short life cycle, the wealth of knowledge already accumulated about its development and the plethora of genetic tools developed along the way. The wing disc is the larval precursor organ of the adult fly wing. The wing disc is a single epithelial monolayer, folded to form a flat sac, with two distinct, opposing layers, surrounding a lumen^[15]. The geometry of the wing disc is shown in Figure 1. The top-bottom axis has been defined here to describe the axis of the whole wing disc, while the apical-basal axis is reserved for the direction perpendicular to the surface of the epithelial sheet. Apical is the direction pointing inward toward the lumen, and basal points outward. The top epithelial layer – the peripodial epithelium, is a thin membrane of squamous cells. The bottom epithelial layer – the columnar epithelium, forms the bulk of the wing disc. The columnar

epithelium is pseudo-stratified, meaning its nuclei are generally wider than their apical or basal surface areas; cells therefore pack together by distributing nuclei across their apical-basal axis. A transitional, cuboidal phase occurs between peripodial and columnar around the perimeter of the wing disc. An extra-cellular matrix (ECM) is maintained across the external, basal surface of the wing disc^[16]. An analogue of the basal ECM is present along the apical surface of the columnar epithelium with a very different composition^[17]. This apical ECM will not be considered in this work.

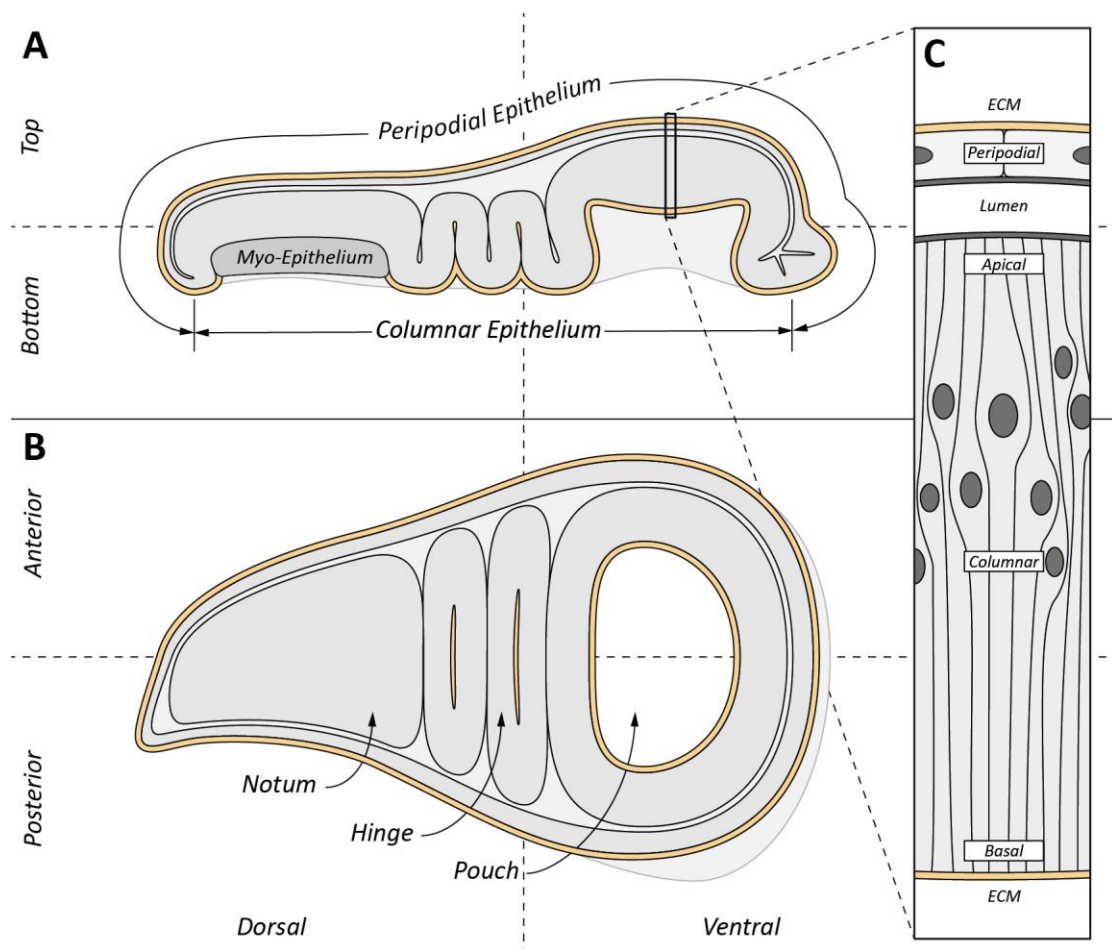


Figure 1. A wing disc is a single-cell thick epithelial sac surrounded by an extra-cellular matrix. **A** and **B** show cross-sections of the wing disc are shown on the left. **A**, shows a cross-section is taken along the midline of the anterior-posterior axis. Peripodial and columnar regions of the epithelium are indicated, as well as the myo-epithelium. **B**, shows a cross-section is taken along the midline of the top-bottom axis. Pouch, hinge and notum regions are indicated. **C**, shows a magnification of a

section of peripodial and columnar epithelia. Apical and basal surfaces the cells are indicated, and the ECM is shown as a thin strip on the basal surface (yellow).

Folds form only in the columnar epithelium, while the peripodial remains unfolded. Three regions can be loosely defined along the dorsal-ventral axis of the wing disc, the pouch, hinge and notum^[15]. The pouch is formed of a flat oval region encircled by a down-fold around its perimeter. The hinge is formed of two full folds emerging ventrally from the pouch fold. The notum is a relatively flat region emerging from the hinge. The basal surface of the notum is lined with myoepithelial cells.

The wing disc begins as about 50 cells at around 24h after egg laying (AEL). Cells first enlarge by approximately six times, and then begin dividing. During initial division average cell size reduces until growth rates and division rates equilibrate^[18]. By 48h AEL, the wing disc gains its flat disc like shape with thick columnar and thin peripodial epithelia. Over the course of subsequent wing disc growth, cells maintain a steady, uniform growth rate and divide approximately every 12 hours^[19], with a slight decrease in size and infrequent apoptosis. Small clusters of cells have synchronised cell cycles, although synchronisation is not inherited and not stable. At around 84h AEL the columnar epithelium folds to form the hinge. Over subsequent growth, these folds deepen so that neighbouring apical surfaces become apposed, and similarly for basal surfaces, Figure 2. At onset of pupation at 120h AEL, the wing disc begins eversion from which point division and growth cease. Before eversion, the wing disc contains approximately 50,000 cells and this size determines the final adult wing size^[18].

Cells of the wing disc are assigned fate according to nested groupings defined by patterns of morphogens. Some of the largest groupings are called compartments. Compartments are groups of cells of the same lineage that do not mix with cells of other compartments. The first compartments to form are the anterior and posterior, and derive from different embryonic founder cells. The boundary between anterior and posterior compartments is smooth and distinct, due to differing adhesive, and

cytoskeletal, properties at apposing anterior to posterior cell surfaces. The second compartments to form are dorsal and ventral. Further subdivisions are made with weaker lineage-boundary enforcement ^[20].

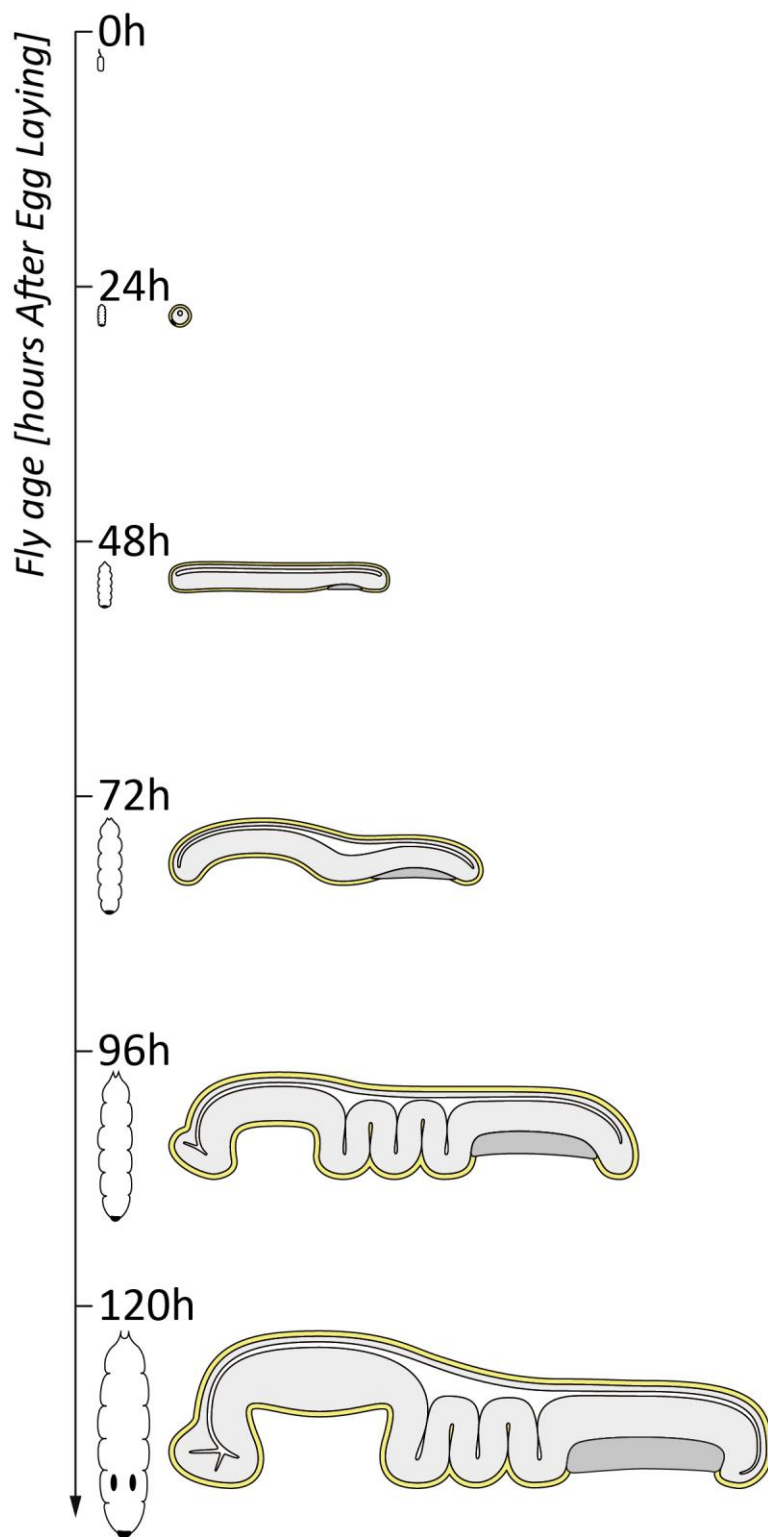


Figure 2. The wing disc is a highly proliferative tissue, growing in size exponentially over a four-day period. Growth of the larva (left), and wing disc (right), are shown for 24h intervals After Egg Laying (AEL). Between 72h and 96h AEL the wing disc produces its distinctive folds. The ECM (yellow) also grows with the wing disc.

1.2.1 Growth

The wing disc is a highly proliferative tissue, growing in size exponentially over a four-day period. During this period the wing disc develops its shape precisely and reproducibly. Wing disc morphology may develop as a result of or in spite of this growth. Growth is therefore the context in which wing disc morphology should be studied. Cells can grow in both size and number, and these two quantities are tightly coupled through the cell cycle ^[19]. Two *Drosophila* proteins important for cell cycle regulation are Cyclin E (CycE) and E2f1. Overexpression of CycE or E2f1 in the wing disc increases cell number and decreases cell size. E2f1 knockout leads to increase in cell size, but reduced proliferation ^[19].

It has been shown that certain compartments of the wing disc can regulate their size regardless of cell growth or proliferation rates. Changing cell division rates by overexpression of CycE or E2f1 in the whole, or part of, the posterior compartment did not change its final size ^[19]. E2f-null mutants in an Rps mutant background grow much faster than they divide, but they do eventually stop growing. It is thought that cells in these clones are unable to sustain a certain amount of mass with a single nucleus ^[19]. Polyploid cells, which have multiple nuclei, can grow much larger and tend to have sizes proportional to their number of nuclei. Polyploid cells induced in the wing disc also did not affect posterior compartment sizes relative to wild type haploids ^[18].

Factors that define cell growth can be intrinsic or extrinsic. Intrinsic growth regulation is autonomous to the cell. An example of an intrinsic growth regulator is ribosomal proteins (Rps) that form protein synthesising ribosomes. The *Drosophila* genome encodes 79 Rps. The mutation of most Rps is lethal when homozygous. Heterozygous mutations of most *Drosophila* Rps cause developmental delay *via* reduced growth rates. Despite a reduced growth rate, heterozygous Rps mutant cells grow to the same size as wild type cells ^[21]. Extrinsic growth regulation is the

regulation of growth by factors external to the tissue. An example is the hormone protein insulin found in the *Drosophila* haemolymph that can signal insulin receptors to define global growth rates. Mutants of some Insulin receptors show similar small-fly phenotypes associated with starvation^[18]. Another type of hormone Ecdysone can control morphogenesis, including wing disc development. This is achieved by triggering morphogenetic events with temporal pulses of Ecdysone^[22], for example by regulation of integrin expression^[23]. The prothoracic gland is a tissue implicated in size-assessment. Reduced prothoracic growth causes developmental delay in larvae. However this developmental delay allows other tissues to grow for longer, leading to overgrowth by pupation time. Release of Ecdysone from the Prothoracic Gland is implicated in initiation of pupation^[24]. Both intrinsic and extrinsic regulation mechanisms can sometimes be coupled. Cell competition tends to drive Rps mutant cells out of the wing disc. However, competition between wild type and Rps-mutant cells does not occur between compartments. If entire compartments are filled with Rps mutant cells then development can be slowed to wait for the compartments to grow sufficiently^[18], possibly due to extrinsic factors.

In some tissues, large variation observed in cell growth and division rates does not account for the small variation observed in cell size. It therefore seems cells are able to measure their size, and alter their growth and division rates accordingly. This mechanism could mean smaller cells grow faster relative to larger cells. In some systems there is evidence of cell cycle checkpoints at which a cell remains until it reaches a certain size. In other systems there is some evidence cells measure their growth rate not their size^[25]. There is some evidence of cell size control in *Drosophila*. During ventral furrow formation in the embryo, conservation of volume is a driving factor in cell shape^[26]. If and how cells measure their size is an open question^[25].

1.2.2 Morphogens

How compartments of the wing disc are able to regulate their size is also an open question. Many hypotheses have been suggested, and most of them involve morphogens^[18]. One hypothesis is based on the assumption that the gradient of morphogen concentration scales with tissue growth. If cells were able to measure the local gradient then they could alter their growth rates accordingly, forming a feedback loop that could stabilise compartment size. The ability of cells to measure small differences in concentration is established with cytokine-following cells^[18].

The wing disc is patterned by many morphogens, Figure 3. Decapentaplegic (Dpp) is a morphogen expressed in a stripe of cells along the anterior-posterior boundary of the wing disc. Dpp is secreted, and diffuses away from its source forming a concentration gradient across the tissue^[27]. Engrailed (En) is expressed uniformly in the posterior compartment of the wing disc from the earliest stages. En induces posterior cells to express and secrete Hedgehog (Hh). Hh diffuses into the anterior compartment, establishing a short concentration gradient. Hh induces anterior cells close to the anterior-posterior boundary, where Hh concentration is high, to express and secrete Decapentaplegic (Dpp). Dpp diffuses into both the anterior and posterior compartments, establishing short concentration gradients. Dpp specifies cell fate in a concentration-dependent, and therefore position-specific way. For example, a transcription factor Spalt is induced at high Dpp concentration in a narrow band around the anterior-posterior boundary, while another transcription factor Omb is induced at lower Dpp concentrations in a broader band. A similar process forms dorsal and ventral compartments, along whose boundary is expressed another morphogen, Wingless (Wg). Where Wg and Dpp meet is the distal region of the wing disc that becomes the adult fly wing, while the proximal region becomes half of the adult fly notum^[18]. The Wg expressing cells along the dorsal-ventral boundary have reduced division rate, and will form the adult wing margin^[28].

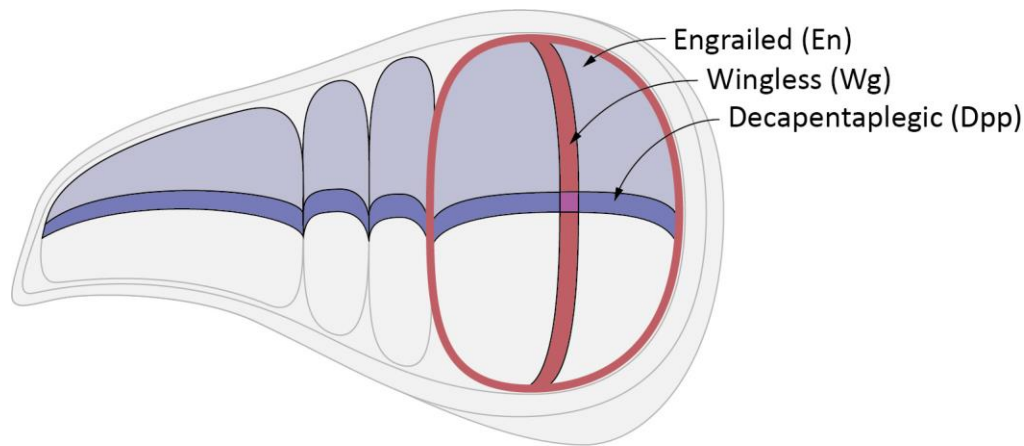


Figure 3. Morphogens pattern the wing disc epithelium, defining growth rates and cell fates. En morphogen (light blue) defines the anterior compartment of the wing disc, while Dpp (blue) and Wg (red) are expressed in bands of cell along the anterior-posterior and dorsal-ventral compartments respectively.

Morphogens therefore tightly regulate the pattern of wing disc fate, and therefore its morphology. For example ectopic clones expressing Dpp and Wg overlap, becoming extra winglets replete with veins in adult flies^[18]. Coupling of cell fate, morphology and mechanics is further revealed by ectopically expressing cell fate specifying transcription factors. Clones in backgrounds with expressing different cell fate transcription factors leads to cysts. Cyst formation is driven by promotion of filamentous actin and myosin cell-cell interfaces between the two populations of cells^[29].

A confounding problem with wing disc growth is its uniformity despite its dependence on complex patterning by morphogens^[27]. For example loss of Dpp leads to wing disc undergrowth, while uniform expression of Dpp causes overgrowth^[30]. It appears growth of cells depends on Dpp gradients, perhaps through comparison of Dpp signalling between neighbouring cells^[31]. Morphogen regulation of growth can also change over time. For example, the onset of the Wg gradient that drives growth at early stages of wing disc development is also required for cessation of growth at late stages^[18]. Morphogen regulation of development is therefore complicated, and may not be intrinsically intuitive. On the possibility of secondary morphogens regulating wing disc size, Day and Lawrence state “This would be a

blatant violation of Occam's razor, but his razor has proved too useful a standby in the increasingly baroque world of developmental genetics" ^[18]. This could in fact be the simplest developmental program that can pattern multiple tissues both temporally in series and parallel. Alternatively this developmental program may be this convoluted simply because it works, and more elegant programs have not been evolved.

Interestingly, the developmental program of the wing disc is intrinsic to its cell. Wing discs and even fragments of wing discs can grow and regenerate when dissected from larvae and transplanted into adult flies, attaining roughly its correct size. The number of precursor cells required for regeneration can be as few as 5 ^[20]. This result suggests wing discs have a mechanism to regulate growth and patterning that emerges from cellular interactions. This mechanism functions irrespective of cellular composition; subsets of cells can be removed, growth and division rates can be accelerated and decelerated in any combination, for any combination of cell subsets, and correct growth and pattern is still achieved. Each and every cell has the latent ability to establish and maintain this mechanism. Only perturbations to the mechanism itself can deregulate growth and patterning. Any factor required for correct function of this mechanism constitutes this mechanism.

Another possible regulator of growth is mechanics. The Hippo pathway can be regulated by multiple cell-cell adhesion proteins, and so could provide a mechanism for cells to compare morphogen levels with their neighbours ^[20]. A model of growth regulation involves transduction of mechanical forces. Morphogens released from the distal region of the wing disc pouch induce local growth. Distal cell growth puts proximal cells under tension. Cells under tension up-regulate growth, this proximal growth eventually compresses the distal cells, and cells under compression down-regulate growth ^[32]. Patterns of tension consistent with this model have been found experimentally ^[33]. The Hippo pathway provides a mechanism for transduction of mechanical forces ^[20]. The Hippo pathway is composed of a core complex, or cassette, that phosphorylates Yki. When not phosphorylated, Yki can enter the nucleus inducing a transcriptional cascade leading to cell proliferation. Activity of the

Hippo cassette is regulated by many upstream factors^[34]. Most of these upstream factors are cell-cell adhesions or polarity factors, and involve sequestering or degrading components of the Hippo complex. Hence the Hippo regulation is highly dependent on cell shape and interaction with neighbouring cells. Upstream factors can also be mechano-sensitive proteins such as alpha-catenin^[34]. In *Drosophila* the majority of reported Hippo regulation originates apically and laterally. Although there is evidence of integrins contributing to Hippo regulation in vertebrates^[34], there are few reports in *Drosophila*.

1.3 Cells

1.3.1 Membrane

The cell membrane is formed of a lipid bilayer. Lipid molecules have a hydrophilic head and a hydrophobic tail driving their self-assembly into bilayers. Proteins can associate with the membrane; either loosely on the surface or strongly by embedding within the hydrophobic innards. Both lipids and membrane-associated proteins can diffuse along the membrane. However, this diffusion is two-dimensional, reducing degrees of freedom, which causes slower diffusion than in three-dimensions. Proteins are dense within the membrane, so dense that no lipid is unaffected by protein. Membrane-associated proteins may associate or dissociate with the membrane over time. Cell membranes are curved partly by forces exerted on it, but an intrinsic curvature can also be built into the membrane by the mechanics and geometry of lipids and membrane-associated proteins ^[35].

Due to its low dimensionality and surface fluidity, the cell membrane may exhibit interesting mechanics. Cell membranes have a low shear modulus due to their fluidity in the plane of their surface, but a higher elastic modulus, but these properties can change as a result of associated-proteins and binding to the cortex ^[36]. There is evidence that cells can change their pressure. Cells in culture tend to round up during division, this process is in part due to an increase in cell pressure. The increased pressure during rounding leads to blebs, which indicate enough pressure to drive detachment of the membrane from the cortex ^[37]. Due to a low elastic modulus in the plane of the membrane, an increase in pressure would not be expected to increase cell size much ^[36]. However the cell membrane could expand if lipids were to turnover with a net increase. Osmotic pressure is regulated by ion transporters in the membrane, which can drive changes in cell pressure that may contribute to cell rounding ^[37]. Membrane tension may also play a mechano-sensing role. Ion channels could be opened by tension, inducing signalling. Membrane-associated proteins could be curvature sensing, by dissociating from the membrane

if curvature moves out of some preferred range; the dissociated protein would then affect signalling ^[36].

1.3.2 Cortex

The cortex is a thin, dense cross-linked network of actin filaments underlying the inside of the cell membrane ^[9]. Actin is a monomeric protein that polymerises to form filaments. New actin filaments are initiated by actin monomers binding to filament-nucleating proteins. Actin filaments polymerise as additional monomers bind to the free end of the filament. Actin filaments are therefore polarised in the sense that they have one potentially polymerising end, called the plus end, and one potentially depolymerising end, called the minus end. The plus end of the actin filament can be in two states, either a free polymerising state, or a locked non-polymerising state when bound by a filament capping protein. Actin filaments can be severed either mechanically or by severing proteins. Actin monomers are ATPases, which are enzymes that bind to ATP and catalyse its decomposition into ADP and a free phosphate ion. When bound to ATP, actin monomers preferentially bind to filament plus ends. When filament-bound ATP decomposes to ADP the monomer is destabilised increasing its likelihood of depolymerising from the minus end. Hence the basal depolymerisation rate of a filament is determined by the actin-ATP lifetime. At the population level, Actin filament abundance is determined by the rate of filament growth versus disassembly. Actin filament growth rate is determined by the abundance of filament-nucleating proteins and the abundance of free filament ends. The abundance of free filament ends is determined by the abundance of capping proteins and the severing rate of existing filaments ^[38].

Many actin-binding proteins regulate actin filament dynamics. arp2 and arp3 form a complex that nucleates actin filaments at angles to existing filaments causing branching. Profilin promotes actin-ATP binding and polymerisation. Cofilin promotes actin filament disassembly. Phospholipids bound to the plasma membrane nucleate

actin filaments, helping localise the cytoskeleton to the membrane^[38]. GTPases, similar to ATPases, are enzymes that bind to GTP and catalyse its decomposition to GDP and a free phosphate ion. Rho GTPases help localise different actin binding proteins to different domains of the cells. When activated Rho GTPases bind to and regulate certain actin-binding proteins. In vertebrates, Rho activation induces actin stress fibres, while Rac activation induces branched Actin filaments^[38].

The *Drosophila* genome encodes six actin genes. These variants differ by only a few amino acids, and are highly conserved with similar homology to vertebrates. Despite their similarity, each actin variant has specific temporal and spatial expression. Four of these actins, are expressed exclusively in muscles. The remaining two are non-muscle actins, one is expressed from embryonic to pupal stages and the second, called Actin5C, is expressed ubiquitously^[39].

The *Drosophila* genome encodes one profilin gene, Chicadee (Chic). Chic knockdown in cultured *Drosophila* cells prevents spreading^[40]. The *Drosophila* genome encodes arp2 and arp3. The arp2/3 complex is required for lamellapodia. Inactivation of arp2/3 complex in *Drosophila* cell culture causes circularly spread cells to become stellate^[40]. The *Drosophila* genome encodes two tropomyosins. Tropomyosin binds along actin filaments, with each tropomyosin dimer covering six to seven monomers. Tropomyosin protects against severing of Actin filaments^[41].

Formins are a class of actin-binding protein that associate with plus ends of filaments during elongation, mediating recruitment of monomers. Formins are auto-inhibitory, and remain inactive until binding Rho GTPases, which induce activation^[42]. This control allows precise spatial localisation of formin activity to specific cell domains and tissue regions. The *Drosophila* genome encodes six formins; Diaphanous (Dia), Cappuccino (Capu), Disheveled-Associated Activator of Morphogenesis (Daam), Formin Related in Leukocytes (Frl), Formin3 (Form3) and Fhos^[42]. Dia is mainly active in the apical domain, and is implicated in regulation of both actin filament structure and myosin contractility, especially during cell division^[43]. Daam is also apically localised^[44], and is implicated in bundling actin filament as well as

crosslinking actin filaments with microtubules ^[45]. Daam and Frl are associated with planar cell polarity in tissues such as the trachea, but not in other tissues that make use of planar cell polarity ^[46]. Capu is also implicated in crosslinking actin filaments with microtubules ^[47]. Form3 is associated with forming actin filament bundles in the trachea ^[48].

Fhos is associated with nucleation and bundling of actin filaments as well as increasing polymerisation rate ^[49]. Fhos is expressed in imaginal discs. Fhos knockout causes mostly pupal lethality, but with some adult fly escapers that exhibit wrinkled wings. In the wing disc Fhos RNA is expressed throughout but with increased expression in the pouch and notum regions and considerable up-regulation either side of Wg-expressing Dorsal-Ventral boundary. Rok is able to phosphorylate Fhos, and Rok expression induces stress fibres in cells expressing Fhos. In the wing disc, expression of Fhos lacking its auto-inhibitory domain promotes actin filaments causing both apical invagination and basal expansion, while expression of full length Fhos affects neither actin filament levels nor morphology ^[42]. These results suggest Fhos has potential to regulate wing disc morphology.

Enabled is another actin-binding protein that increases filament polymerisation rate. However unlike formins, enabled does not nucleate actin filaments. The *Drosophila* genome encodes one enabled, called Enabled (Ena). Enabled and Dia often co-localise and perform similar functions ^[50]. Neither Knockout nor miss-localisation of Ena in imaginal discs affect polarisation or cytoskeletal organisation ^[51]. Actin-binding proteins filamin and fascin are filament bundling proteins. These proteins are often related to the formation of filopodia. The *Drosophila* genome encodes one filamin protein, Cheerio, which is associated with tumour invasion in imaginal discs ^[52]. The *Drosophila* genome encodes one fascin, Singed and its partner Forked. Singed and forked are associated with tracheal filopodia and the thick actin filament bundles forming *Drosophila* hairs and bristles ^[53]. Cher has been proposed to have mechanics-sensitive properties. A mechano-sensitive domain in Cher is masked when the protein is relaxed, but is revealed when under tension allowing signalling.

It has been shown that revealing of the mechano-sensitive domain stabilises the protein ^[54].

Cofilin, cyclase-associated proteins and capping proteins inhibit actin polymerisation directly or indirectly. Cofilin severs actin filaments and promotes monomer dissociation from the minus end. Capping proteins bind actin filament plus ends to prevent polymerisation and cyclase-associated proteins sequester actin monomers to prevent association with plus ends. A combination of arp2/3 and CPs generate a short, branched actin network found in the leading edge of migrating cells. The *Drosophila* genome encodes one CAP, called Capulet (Capt), and one Cofilin, called Twinstar (Tsr). The *Drosophila* genome encodes two CPs, Capping Protein Alpha (Cpa) and Capping Protein Beta (Cpb), which dimerise to become functional ^[55]. Loss of Cpb, Capt and Tsr all lead to accumulation of actin filaments. Capt can also activate Yki ^[56]. Also, loss of Cpa or Cpb can inhibit accumulation of Yki in the nucleus ^[57]. Hence actin filament organisation affects, mechano-sensitive pathways. Gelsolin is a secreted actin filament capping and severing protein. Gelsolin is expressed in the fat body and is found in the haemolymph ^[58], opening the possibility of cell non-autonomous cortex regulation.

Myosin is a primary source of contractility in the cortex. Non-muscle myosin II (referred to here as myosin) is composed of six subunits, two heavy chains, two regulatory light chains and two essential light chains. At one end of each heavy chain is a head domain that binds to actin filaments in an ATP dependent manner, at the opposite ends are domains that allow heavy chains to dimerise. Two pairs of each light chain binds to a region in between the actin-binding and dimerisation domains of each heavy chain. Around twelve of these myosin hexamers then bind together to form a myosin minifilament with actin-binding domains located at both ends. The pair of actin-binding domains on each hexamer can bind to and processively walk along an actin filament. The minifilament can bind two actin filaments, one on each end and processively walk along each independently. This action has the effect of sliding actin filaments relative to one another ^[1]. This sliding drives contraction of the actin network, rather than expansion ^[9]. Myosin activity can be regulated *via* its

regulatory light chains. Rho kinase can activate myosin by phosphorylating its regulatory light chain, allowing actin filament binding ^[1].

Actin filaments turnover on the order of tens of seconds. As a result the cortex is viscoelastic, behaving as an elastic solid at timescales less than seconds and as a viscous fluid at timescales greater than minutes. The contractile action of myosin on the actin network can lead to flows of actin-myosin at fluid timescales. Myosin can also stiffen the actin network by acting as a cross-linker when an external tension is applied ^[1]. This viscoelastic behaviour has been measured during *Drosophila* embryogenesis ^[59]. In terms of morphogenesis, viscoelastic behaviour of the cortex allows cells to remain unaffected by short timescales fluctuations of forces but integrate long-term morphological forces driving tissue shape changes.

1.3.3 Polarity

Cells in the wing disc and epithelial tissues in general exhibit three main polarity domains, apical, lateral and basal. These domains define the prismatic shape of epithelial cells, with apical and basal domains defining the ends of the prism and lateral domain the sides. These domains are established and maintained by complexes of polarity factors. Polarity complexes involved in epithelial polarisation include key proteins Crumbs (Crb), Par and Lethal Giant Larvae (Lgl). Crb is a trans-membrane protein that binds other polarity factors such as Discs Lost (Dlt), Stardust (Sdt) and the Par complex, composed of Bazooka (Baz), Par6 and Atypical Protein Kinase C (aPKC). The Crb complex localises to and defines the Apical domain. The Lgl complex includes Disc Large (Dlg) and Scribble (Scrib) and localises to the Lateral domain, and excludes Crb to the Apical domain. Cellular polarity is inherited from the Oocyte, and is disseminated down through development of the fly ^[60].

1.3.4 Adhesion

Cell polarity is tightly linked with adhesions. The lateral domain is populated by many cell-cell adhesions. It is likely that these cell-cell adhesions both define and are defined by the lateral domain. The most prominent cell-cell adhesion is cadherin, which localises to the adherens junction, a ring just below the apical domain. Cadherins are trans-membrane proteins that form homodimers extra-cellularly with apposing cells. Intra-cellularly, cadherins form complexes with proteins such as the catenins that connect cadherin with the cell cortex. Cadherins are therefore implicated in mechanically adhering cortices of neighbouring cells. In fact the adherens junction exhibits a higher concentration of cortex relative to other domains, suggesting an important contribution to cell mechanics ^[10].

Mechanically, factors such as contractility and pressure generate a tension across the surface of the cell. This surface tension acts to minimise the surface area to volume ratio, driving rounding of the cell. When a cell adheres to a substrate, adhesion acts to bind the cell surface to the substrate surface ^[61]. If the substrate surface is not congruent with the cell surface, then the adhesion will attempt to deform the surfaces to rebalance the forces. The relative deformation of cell and substrate will depend on adhesion strength and the relative stiffness of cell and substrate surfaces. If adhesion is strong compared to the stiffness of the surfaces, then the interfacial surface will be maximised. In this case if the substrate is much stiffer than the cell surface then the cell will spread on the substrate. If the cell surface is much stiffer than the substrate then the substrate may bend around the cell. If adhesion is weak compared to cell surface tension and substrate stiffness then the cell will remain rounded.

For cell-cell adhesion the substrate for a cell is another cell. Generally cells in tissues have similar surface tensions, so cell-cell adhesion generates approximately flat cell-cell interfaces. However, if there is asymmetry in cell surface tensions, then more curved interfaces may occur. For cell-matrix adhesions, the substrate is usually an ECM. In cell cultures the ECM is usually a layer on a glass slide, which is much stiffer

than cells and so will drive cell spreading depending on the adhesion of the given cell type. In tissue the ECM may vary in stiffness and shape, allowing many configurations of spread or rounded cell shapes ^[8]. For example, in tubular tracheal tissues the curved ECM may contribute to the flat curved morphology of tracheal cells. In tissues both cell-cell adhesions and cell-matrix adhesions contribute to cell shape. In epithelial tissues competition between cell-cell and cell-matrix adhesion strength ^[10] may drive cell shape ^[8]. If cell-cell adhesions are stronger than cell-matrix adhesions then cells may become flatter and wider, like squamous epithelia. If cell-matrix adhesions are stronger than cell-cell adhesions then cells may become taller thinner, like columnar epithelia. Similar cell-cell and cell-matrix adhesions could lead to cuboidal epithelia. However, this picture assumes cell surface tension remains constant and uniform. In reality, interaction between adhesion and polarity means different adhesions can have different contractility, either directly by recruiting actin filaments ^[1], or indirectly *via* polarity factors.

In the wing disc, the morphology of the columnar epithelium may be driven by changes in cell shape. Differences in apical, lateral and basal tensions have been implicated in driving the folds of the hinge ^[62]. Interestingly, two of the hinge folds appear to fold *via* different balances of forces between the three domains. One fold is driven by increases in surface tensions in the lateral domain of cells that reduces cell height. The other fold is driven by reduction in basal and lateral surface tension due to loss of cell-matrix adhesion. This latter phenomenon suggests a role in cell-matrix adhesion in maintaining cell surface tension in the basal domain ^[62]. These results point to intrinsic force generation as a method of cell shape and tissue morphology control. In contrast, extrinsic force generation can occur when stress is generated between sets of cells, for example through differential growth. An example of extrinsic growth has been shown to generate folds in the chick gut. Differences in growth rate between two well-adhered tissues, the gut tube and mesenteric sheet, induces an interfacial stress that results in mechanical instability and buckling of the combined tissues ^[63]. It is also conceivable that differences in growth between cells and their ECM could also drive buckling.

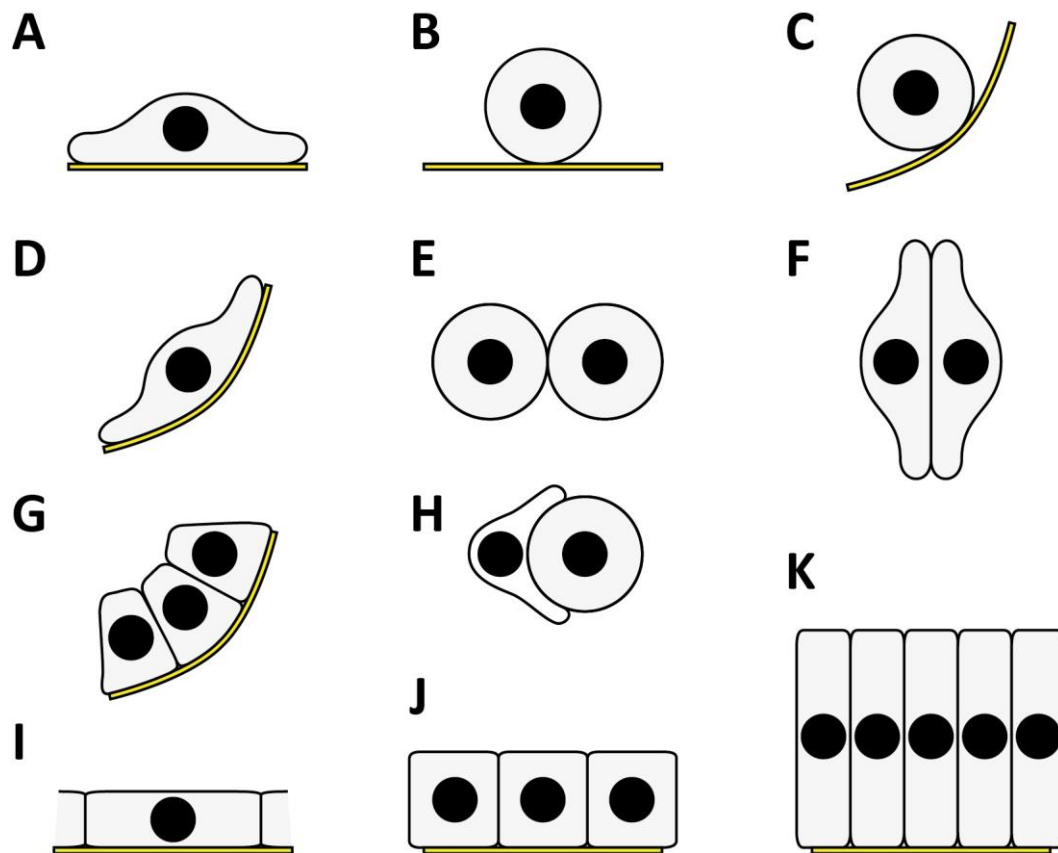


Figure 4. Many cell and tissue shapes may be possible through variation of adhesion, polarity and surface tension. **A**, if cell-matrix adhesion strength is greater than surface tension, cells may spread on an ECM. **B**, if surface tension is greater than cell-matrix adhesion strength cells may round-up. **C**, if surface tension and cell-matrix adhesion are greater than ECM stiffness, cells may curve the ECM. **D**, If cell surface tension and ECM stiffness are similar, both may curve. **E**, if surface tension is greater than cell-cell adhesion strength then cells may bind loosely. **F**, if cell-cell adhesion strength is strong cells may spread on each other. **H**, if one cell has higher surface tension than the other, the softer cell may spread on the more rounded cell. **G – K**, if cells both adhere to each other and to an ECM, they may form epithelial-like tissues. **I**, if the cell-matrix adhesion is stronger than cell-cell adhesion squamous-like epithelia may form, or **K**, columnar epithelia for the opposite. **J**, if cell-cell and cell-matrix adhesion are similar, cuboidal epithelia may arise. **G**, If the substrate is soft compared with cell surface tension, cells may curve the ECM.

1.4 Cell-Matrix Adhesions

1.4.1 Integrin

Integrins are associated with both mechanical adhesion to the ECM and signal transduction^[64]. Generally, a single integrin is composed of two protein subunits of types alpha and beta respectively. The *Drosophila* genome encodes two beta subunits and five alpha subunits. In the wing disc two alpha subunits and one beta subunit are expressed, giving two integrin variants. The two alpha subunits are named Inflated (If) and Multiple Edematous Wings (Mew) and the beta subunit is named Myospheroid (Mys). Integrins containing Mew and If are referred to here as PS1 and PS2 respectively, where PS means Position Specific, derived from the difference in spatial patterning of the two integrins. In the wing disc PS1 integrins localise mainly to the region dorsal-wise of the dorsal-ventral pouch boundary, and to a much lesser extent ventral-wise. PS2 integrins localise almost exclusively ventral-wise to the dorsal-ventral pouch boundary, except for some small patches dorsal-wise^[65]. Other Integrins present in *Drosophila* include one beta subunit Integrin Betanun Subunit (Itgbn), and three alpha subunits including Scab (Scb) that forms PS3^[66]. Phylogenetic analysis suggests alpha Integrin subunits diverged into two families before vertebrates split from invertebrates, of which PS1 and PS2 are representative respectively. PS1 is most homologous to vertebrate alpha3, alpha6 and alpha7. PS2 is most homologous to vertebrate alpha5, alpha8, alphaV and alphaIIb. PS3 appears unique to *Drosophila*, with no clear vertebrate homologs, and PS4 and PS5 are also part of this unique PS3 family^[67].

In *Drosophila*, muscle attachment sites (MASs) are useful environments to study integrins due to elevated expression of, and dependence on, ECM adhesion. At these muscle attachment sites only PS2 is present^[68], likely due to requirement for RGD mediated binding. Mutations of If show a variety of phenotypes at muscle adhesion sites, including detachment from the ECM and detachment from the cytoskeleton^[69].

An amino acid sequence RGD is a well-established integrin ligand. It has been shown that a *Drosophila* cell line expressing PS2 will spread on surfaces coated with RGD^[70]. An ECM protein tiggirin, expressed at MASs, contains an RGD sequence, while another ECM protein Laminin A does not. *Drosophila* cells expressing PS2 spread on tiggirin, but not on laminin A, while *Drosophila* cells expressing PS1 do not spread on tiggirin, but do on Laminin A. Therefore PS1 appears not to recognise RGD but some other sequence^[71]. The other laminin variant, Laminin W, contains an RGD site, so should bind PS2.

If has two isoforms^[72], and Mys has two isoforms^[73], both differing in the splicing of one exon. Different isoform combinations have been shown to affect PS2 binding specificity. *Drosophila* cells lines expressing certain PS2 variants spread more on surfaces coated with RGD fragments than others, although all variants spread better than cells expressing no PS2^[74]. Further, the context of the RGD site also affects its specificity. *Drosophila* cells expressing one PS2 variant spread more on RGD-containing tiggirin fragments than RGD-containing laminin W fragments^[74]. Furthermore, PS1 integrins binding to Laminin A require the whole trimer, rather than just a fragment with Laminin W^[74]. Experiments *in vivo* show Laminin W often co-localises with PS2^[74]. Dependence on integrin variants can also change with development. In developing pupal wings Mys knockout can be rescued with either isoform, however this is not the case in the embryo^[73].

Integrin adhesion properties are can be described by two mechanisms, activation and clustering respectively. Activation involves an integrin conformation change between an inactive, low-affinity, retracted state and an active, high-affinity extended, state. Clustering can increase the strength of adhesion to the ECM^[75]. In the wing disc, integrins form clusters on the basal surface of cells^[76]. Expression of a dominant-negative integrin lacking its extra-cellular domain, leads to loss of laminin from the ECM, as well as considerable changes in wing disc morphology such as ectopic folding and cell shortening^[77]. In the adult fly the dominant-negative integrin induces wing blistering . It is suggested the transformation of cells from columnar to cuboidal induced by the dominant-negative integrin is due to mechanical adhesion,

given the mutant integrin retains its intracellular domain ^[77]. Although I expect binding of integrin to the ECM helps cluster it at the basal domain, and therefore its loss may affect cell polarity. Integrins have also been shown to affect cell shape in the oocyte follicular epithelium, which becomes squamous as it matures. During this transition Integrins are switched from PS1 to PS2. This switch is associated with a change in cytoskeletal organisation *via* up-regulation of actin-nucleating factors enabled, diaphanous and profilin ^[78].

1.4.2 Integrin-Associated Complex

There is some evidence for signalling induced by integrins in the embryo, where loss of integrins leads to separation of cells from their ECM and a reduction in signalling of certain pathways. Integrin mutants lacking an extra-cellular domain can still induce some signalling, showing cell-matrix adhesion is not always required for signalling ^[64]. The Mys cytoplasmic tail contains no enzymatic activity in itself, and so requires the binding of Integrin Associated Complex (IAC) proteins to mediate signalling ^[79]. Intracellular Integrin-associated proteins include: talin, integrin-linked kinase, pinch, parvin, paxillin, vinculin, focal adhesion kinase and tensin ^[80].

Talin is possibly the most important IAC protein, required for correct function of integrins. The *Drosophila* genome encodes one talin protein, called Rhea. In the wing disc talin co-localises with Integrin, forming clusters. Here, talin and integrin are co-dependent, loss of one causes loss of the other ^[76].

Talin exhibits two integrin-binding sites ^[81] that target the cytoplasmic tail of Mys ^[82] and an actin-binding site, on opposite ends of the protein. Talin is able to dimerise. Talin also exhibits multiple vinculin-binding sites ^[82]. Correct localisation of talin to the cytoskeleton requires both actin-binding domains and integrin-binding domains ^[68]. PS2 integrin is also required for correct localisation of talin at MASs ^[68].

It has been shown that the two integrin-binding sites target the two sites on Mys respectively ^[81], raising the possibility of different functions. At MASs, integrin and talin form clusters that attach the cytoskeleton of cells to the ECM. One of the integrin-binding sites of talin is required for activation of integrin at MASs. Loss of this integrin-binding site leads to detachment from the ECM. However, constitutively active PS2 recovers this phenotype ^[83]. The integrin-binding site that induces integrin activation also stabilises the integrin, as measured by its turnover ^[81]. Therefore talin-mediated activation and binding of integrin to the ECM may stabilise the integrin complex. A Mys mutant lacking the targets for talin integrin-binding sites is still able to recruit talin. However, further recruitment of IAC proteins pinch and paxillin is disrupted, suggesting some interdependence ^[83]. It is hypothesised that stochastic activation of integrin could lead to transient binding of the ECM. Activated integrins then recruit talin dimers, nucleating a cluster. The bound talin dimer then able to bind and activate nearby inactive integrin, growing the cluster ^[83]. This would be an example of outside-in signalling.

Talin has been shown to be mechanics-sensitive in vertebrates, by unfolding under tension to reveal vinculin-binding sites ^[82]. The *Drosophila* genome encodes one vinculin gene, called Vinculin. Interestingly, flies lacking vinculin are viable and fertile ^[84]. At MASs, vinculin contributes to paxillin recruitment, while vinculin appears to antagonise tensin recruitment to the IAC ^[82]. Vinculin has an auto-inhibition domain. Constitutively active vinculin forms cytoplasmic aggregates in MASs, which recruit other IAC proteins such as talin, tensin, integrin-linked kinase, parvin and pinch, but not integrin or actin. This aggregation is dependent on talin, suggesting vinculin interacts with the IAC *via* talin ^[82].

The actin-binding and dimerisation domains of talin are closely located. Both dimerisation and the actin-binding domain are required for proper actin binding at MASs ^[85]. Vinculin-binding sites of talin can also mediate actin binding ^[86]. Relative contributions of actin-binding sites or vinculin-binding sites to talin-actin binding are dependent on developmental stage. At MASs the talin binds primarily *via* actin-binding sites, while during germ-band extension vinculin-binding sites appear to

contribute most. Also, both mechanisms can induce a wing blister phenotype ^[86]. In wing discs, actin-binding sites are not required to form clusters ^[85], suggesting vinculin binding sites are sufficient to mediate actin binding.

Structure of proteins in the IAC can be uncovered using Forster resonance energy transfer. In the pupal wing, the IAC appears compact, with talin found close to integrins, and vinculin bound closely to the talin actin-binding domain. In contrast, MASs show the IAC stretched, with talin further away from integrins and vinculin further from the talin actin-binding domain. Super resolution imaging shows talin pulled away from integrins at MASs, hence the loss of proximity, whereas pupal wing IAC proteins co-localise closely. Loss of muscle myosin at MASs brings talin and integrin closer together, showing contractility stretches the IAC ^[86]. It has therefore been suggested that the IAC exhibits two configurations, either parallel or perpendicular to the membrane. When parallel, talin dimers bind two integrins *via* all four integrin-binding sites. When perpendicular, two integrin-binding sites of the talin dimer are unbound due to tension applied by actin at actin-binding sites. In both cases vinculin can substitute actin-binding sites ^[86]. These different configurations could then alter further recruitment IAC proteins and in turn alter signalling.

IAC proteins integrin linked kinase, pinch and parvin form a complex called IPP. The *Drosophila* genome encodes one integrin linked kinase, called Ilk. Ilk requires integrins to localise to IACs of MASs ^[87]. The *Drosophila* genome encodes one pinch, called Steamer Duck. Pinch mutants are also embryo-lethal. At MASs, pinch mutants cause muscle detachment, reduce filamentous actin and binding of actin to membrane ^[88]. The *Drosophila* genome encodes one parvin gene, called Parvin. Parvin knockout is late-embryonic lethal, as with Ilk and pinch ^[89]. Knockout of either Ilk, pinch or parvin is embryo-lethal, and exhibits a muscle-ECM detachment phenotype. All three require integrins and talin to localise to IACs of MASs. Neither pinch nor parvin are required for Ilk localisation to IACs ^[87]. Parvin is completely dependent on Ilk for localisation to IACs, while only partially dependent on pinch. Partial parvin loss due to Pinch loss can be restored by Ilk over-expression ^[89].

Overexpressed Ilk localises to the cytoplasm of MASs, suggesting IACs can become saturated at this overexpression concentration. Ilk exhibits a membrane-localisation domain and an IAC-localising domain, only the latter is required for localisation to IACs in MASs, as well as regulation of Ilk concentration. Over-expressed pinch can still localise to IACs but with reduced stability. Ilk can be phosphorylated, delocalising it from IACs to the cytoplasm of MASs ^[87]. In embryos, parvin is recruited to the leading edge of epithelia during dorsal closure. Parvin is not required for localisation of Ilk, pinch or paxillin to IACs ^[89].

In the wing disc, Ilk, pinch and parvin are all co-dependent for localisation to IACs, while talin is not dependent on any of the three. Pinch is localised to cell membranes in wing discs, and the basal surfaces of pupal wings ^[88]. Loss of Ilk, pinch or parvin in the wing disc does not appear to affect filamentous actin structure ^[89]. Neither does loss of Ilk affect clustering of integrins on the basal surface of wing disc cells ^[90]. Therefore in the wing disc IPP proteins are interdependent, but their loss does not affect either the integrins or actin. However, parvin overexpression induces cell apoptosis in the wing disc, as well as disruption of filamentous actin. Co-overexpression of parvin with Ilk rescues cells from apoptosis ^[91], suggesting parvin unbound from the IAC drives apoptotic signalling. However, filamentous actin remains disrupted with co-overexpression of Ilk and parvin, as well as disruption to laminin structure, even when apoptosis is directly repressed. Rho1 was also up-regulated upon Ilk and parvin overexpression, suggesting these IAC proteins can affect cortical and ECM structure ^[91]. It is suggested parvin up-regulates Rho1, which in turn up-regulates filamentous actin and JNK pathways in parallel. The JNK pathway leads to apoptosis, but it is hypothesised Ilk inhibits this pathway but not the filamentous actin ^[91].

Fluorescence recovery experiments have shown the IPP complex stabilises integrins at the membrane of MASs. Stabilisation properties of the IPP complex are also associated with contractility. Detachment of MASs due to hyper-contractility becomes more severe with loss of IPP proteins. Increased contractility stabilises

integrins, which is prevented by loss of parvin ^[90]. It is thought the IPP complex provides mechanical-sensitivity to IACs by inhibiting turnover when under tension. It has been shown that integrin turnover at MASs is driven by endocytosis, and loss of endocytosis can prevent focal adhesion formation ^[92]. Therefore it is possible the IPP complex regulates endocytosis-driven integrin turnover depending on mechanical tension of the IAC. There is also some evidence that Ilk and pinch localise to IACs with different ratios when contractility at MASs is reduced ^[93]. Further, different types of contractility can localise different ratios of IAC proteins to IACs of MASs. Muscle myosin contractility was found to localise vinculin most, while non-muscle myosin contractility was found to localise pinch ^[93], suggesting IACs configure differently for different mechanical functions.

The *Drosophila* genome encodes one paxillin. Paxillin overexpressed in wing discs causes blisters in adult fly wings. It has been shown that phosphorylation of cofilin rescues paxillin overexpression flies from wing blisters. This suggests paxillin has a role in regulating filamentous actin structure ^[94]. Focal adhesion kinase is an important protein in vertebrates, implicated in remodelling of Integrins. The *Drosophila* genome encodes one focal adhesion kinase, Fak56. Fak56 is ubiquitously expressed with concentrations in muscle and nervous tissues. Interestingly, loss of Fak56 has few phenotypes, despite being active and phosphorylated in wild type. However overexpression Fak56 has multiple phenotypes, for example the wing produces blisters similar to Integrin loss. Overexpression of Fak56 in the wing disc reduces both integrin and talin concentrations, however focal adhesions still form ^[95]. Elsewhere Fak56 is associated with fate determination and tumour suppression ^[96]. The *Drosophila* genome encodes one tensin, called Blistery due to the wing blister phenotype of its knockout. Localisation of tensin to IACs of MASs requires talin and Ilk ^[97]. Mutations of tensin cause disruption to filamentous actin in oocytes ^[98].

1.4.3 Dystroglycan

The *Drosophila* genome encodes one dystroglycan. Dystroglycan has multiple isoforms, including short forms and a long form. A domain lost in the short form is expected to be glycosylated. Glycosylation is a post-translational protein modification, attaching glycosyl groups. In the follicular epithelium, the short form of dystroglycan is expressed but the long form is not. In these cells dystroglycan is localised to the basal domain of cells ^[99]. In vertebrates the cytoplasmic tail of dystroglycan binds dystrophin in muscle tissues and utrophin in epithelial tissues. The *Drosophila* genome encodes one homolog for both dystrophin and utrophin, called Dystrophin ^[99]. As well as dystrophin, dystroglycan forms complexes with syntrophins and sarcoglycans. Syntrophins are cytoplasmic and contain domains associated with signalling. Dystrophin is cleaved into two subunits, alpha and beta, that remain non-covalently bound. The alpha subunit is secreted and binds to ECM proteins, while the trans-membrane beta subunit binds to intra-cellular dystrophin, which in turn binds actin filaments and other proteins ^[100]. In the follicular epithelium, dystrophin is also localised to the basal domain cells, and there is co-dependence between dystroglycan and dystrophin for this localisation ^[99].

When dystroglycan is knocked down in the follicular epithelium, cells lose their polarity, either delaminating or undertaking apoptosis. In cells that remain, loss of Dg causes miss-localisation of apical marker Disc Lost ^[60] and lateral markers neurexin and contactin to the basal surface ^[99]. Presence of another lateral marker Dlg was reduced considerably ^[60]. Similar polarity loss was observed in antennal discs lacking dystroglycan. In egg chambers, fibres of filamentous actin align along the circumferential axis. With loss of dystroglycan, actin fibre alignment is lost. Laminin fibres observed along the circumferential axis of the egg chamber also became misaligned with dystroglycan loss ^[60]. Overexpression of dystroglycan also appears to miss-localise Laminin to the lateral and apical surfaces of cells ^[60]. Dystroglycan has also been associated with cell fate specification in the follicular epithelium ^[101]. In salivary gland epithelia, both intracellular and extracellular dystroglycan domains are to maintain correct cell polarity ^[102].

Perlecan has been shown to directly bind dystroglycan. In the *Drosophila* follicular epithelium, perlecan loss leads to defects in cell polarisation, similar to loss of dystroglycan. In perlecan knockout clones, localisation of dystroglycan and dystrophin to basal cell surfaces is lost. Conversely, dystroglycan knockout clones show normal localisation of perlecan. Similarly, in perlecan knockout clones integrin localised correctly, but localisation of Laminin became diffuse. Laminin A knockout did not affect either dystroglycan or perlecan localisation ^[99]. Overexpression of either forms of dystroglycan in the follicular epithelium leads to ectopic accumulation of laminin and perlecan. This suggests dystroglycan can recruit these ECM components, and glycosylation is not required to do this ^[99].

Dystrophin and dystroglycan are expressed in wing discs ^[103]. Dystroglycan knockdown and some dystrophin mutants cause loss of a cross-vein in the adult fly wing. A screen for genetic mutants that change this cross-vein-loss phenotype identified genes related to muscle function, neuronal migration, morphogen pathways, polarity and the cytoskeleton. For example, Fhos, a homolog of vertebrate Formin is found to interact with dystrophin and dystroglycan ^[103]. A second screen for dystroglycan related proteins found Cam, Capt and Mbl as possible interacting partners, suggesting a connection with actin dynamics ^[104].

1.5 Extra-Cellular Matrix

The composition of ECMs can affect their structure greatly. There are many different components found to form the ECM. A certain type of ECM called basal lamina, or basement membrane, forms thin layers on the basal surface of epithelial tissues. Components that are found ubiquitously in basement membrane are collagen, laminin and perlecan. Basal lamina is distinct from other ECM types due to its two dimensional, as opposed to three-dimensional, structure. This structure emerges from its composition, and specifically the presence of non-fibrillar collagen types ^[105]. Only non-fibrillar collagen types have been found in *Drosophila* and therefore exhibits only basal lamina ECM. Basal lamina is therefore the focus of this work and the term ECM will be used synonymously with basement lamina. Similarly, the *Drosophila* genome encodes relatively few collagen types. Therefore the term collagen will be used synonymously with collagen IV unless specifically stated.

In vertebrates, ECM is constructed by self-assembly, whereby ECM components bind each other and polymerise to form networks. Initiation of ECM self-assembly generally requires laminin, which binds cell-matrix adhesions on cell surfaces, polymerises with itself and facilitates binding of further ECM components. Collagen is thought to bind laminin and covalently cross-link with itself. Further binding of other ECM components such as perlecan and nidogen lead to a mature ECM ^[105].

In *Drosophila*, some ECM components are tissue specific, such as pericardin ^[106] that is located around cardiac tissues, or tigrin ^[107] that is located around muscle tissues. There are also multiple variants certain ECM components, which can again be tissue specific. Some ECM proteins can be post-translationally modified, adding further variation in ECM composition. Differences in ECM composition likely alter the properties of the ECM to suit different functions. In the wing disc, the ECM forms a basal lamina. Many of the key ECM proteins are conserved between mammals and flies, including laminin, collagen, perlecan, nidogen and sparc. However, there are some mammalian proteins missing in flies such as fibronectin and vitronectin ^[71].

Importantly, many proteins of the wing disc ECM are not produced by wing disc cells^[16]. A separate adipose tissue, the fat body, produces ECM proteins and secretes them into the haemolymph, which is a *Drosophila* circulatory system. From the haemolymph, ECM proteins are deposited on to, or recruited by, the wing disc ECM. Therefore ECM production is neither cell, nor tissue autonomous. However, recruitment of ECM proteins from the haemolymph could be cell or tissue autonomous, and once recruited the ECM structure could be modified locally. In this section I detail the known properties of ECM proteins I expect are relevant to the ECM of the wing disc.

1.5.1 Laminin

Laminin is a trimer composed of one alpha, one beta and one gamma subunit. The *Drosophila* genome encodes one beta subunit and one gamma subunit called Laminin B1 and Laminin B2 respectively. The *Drosophila* genome also encodes two alpha subunits called Laminin A (LanA) and Wing Blister (Wb). Therefore there are two possible Laminin variants. Laminin takes the form a cross, where the three subunits intertwine to form one long arm, and then split to into the three short arms. It has been shown that all three subunits must be present for functionality, and a lack of LanB1 prevents secretion of the trimer. In *Drosophila*, loss of LanA and LanB1 are both lethal at late embryonic stage^[108, 109]. Wb mutants are non-lethal but display a blistered wing phenotype from which its name is derived. Wb contains an RGD sequence in the exposed part of its long arm^[110]. LanA does not contain an RGD sequence, implying some other sequence is involved in binding integrin. A possible binding sequence in LanA is IKVGV. This is similar to sequence IKVAV in vertebrate homologs of LanA, which has been shown to affect cell spreading^[109, 111], however this binding mechanism may be specific to neurons. Also sequence LRE is present in LanA, which is implicated in neuronal attachment in vertebrate LanA homologs^[109, 112].

In the *Drosophila* embryo, Laminin is required for Collagen IV and Perlecan to integrate into the ECM. With a LanB1 mutant Perlecan and Collagen IV remain diffuse and irregular, respectively, in the extra-cellular space of the embryo. Also, LanB1 mutant embryos show a similar phenotype to embryos lacking Collagen IV [108].

1.5.2 Collagen

Collagen fibres are composed of three protein subunits wrapped in a helical formation to form a fibril. Each fibril of collagen IV has a globular head domain, a tail domain and a long thin helical middle [113]. Head domains of collagen fibrils can dimerise, allowed by high extra-cellular chloride concentrations and facilitated by peroxidase. This head-head bond is first oligomerised in presence of chloride, and then covalently bonded with sulfilimine cross-links by peroxidase. This final step is expected to give the collagen bond, and the ECM its tensile strength. Four tail domains of collagen fibrils can bind together, facilitated by lysyl oxidase. The four tail domains bind laterally, two parallel and two antiparallel. The four tail domains first bind non-covalently, but are then stabilised by disulphide and nondisulfide cross-links. This ordered binding of collagen fibrils is thought to generate sheet-like diamond-shaped lattice, although lateral helical interactions may also produce super-coiled structures [113].

There are two collagen types present in flies, a homolog of mammalian collagen IV and a homolog of mammalian collagens XV/XVIII. Collagen IV forms basal lamina, and contributes the majority of collagen in the wing disc ECM. The *Drosophila* genome encodes two collagen IV subunits, Viking (Vkg) and Collagen at 25C (Cg25C). It has been shown that collagen IV fibrils are heterotrimers of Vkg and Cg25C [16]. Collagens XV and XVIII are part of the multiplexin type of collagens. Multiplexin collagens are structurally distinct from other collagen types and exhibit glycosaminoglycan side chains. The *Drosophila* genome encodes one multiplexin collagen called Multiplexin (Mp). Mp has known roles in neuron development and

has been implicated in correct wingless patterning. Mutants for Mp have a wing margin phenotype, possibly related to defective wingless patterning ^[114].

Throughout larval stages collagen is produced mainly in the fat body. The fat body secretes collagen in its trimeric form into the haemolymph. In the haemolymph collagen fibres diffuse, and eventually accumulate on surfaces of other tissues such as the wing disc ^[16]. Integration of other ECM components such as laminin, nidogen and integrins in the wing disc ECM are not dependent on the presence of collagen, except perlecan, which does require collagen to integrate. Knockouts for Vkg or Cg25C are embryo lethal. Temporal knock down of Collagen IV beginning at early larval stages are not lethal until pupal stages. Temporal knockdown of Vkg and Cg25C knockdown for a 96h period during larval stages have been found to induce a columnar to cuboidal epithelium transition in the wing disc. Wing disc morphology induced by these knockdowns is consistent with collagenase degradation of the wing disc ECM, which leads to an unravelling of the tissue on the order of minutes after treatment ^[16].

During oogenesis, *Drosophila* eggs elongate from spheres to ovoids, while increasing in volume. During this process the follicular epithelium rotates three times inside its ECM shell, which requires integrin and collagen. This rotation generates collagen fibres that become aligned along the direction of rotation ^[115]. By measuring the effective stiffness of the egg it has been suggested these aligned collagen fibres give the ECM anisotropic stiffness that in turn causes anisotropic growth of cells that gives the egg its ovoid shape ^[14].

Collagen has been implicated in mediating diffusion of the morphogen Dpp through ECM ^[116]. Domains in both Vkg and Cg25C allow binding of Dpp with its shuttling complex. In the *Drosophila* ovary, collagen restricts diffusion of Dpp through the ECM to maintain correct cell fate signalling. In contrast, in the *Drosophila* embryo, collagen increases Dpp signalling, which is explained by collagen-facilitated binding of Dpp with other Dpp-binding partners ^[116]. In the wing disc, Dpp is secreted and has been shown to diffuse through the ECM. Collagen knockdown prevents this Dpp

signalling, but not Hh or Wg signalling^[117]. Ectopic binding of secreted Dpp to collagen can reduce Dpp diffusion and prevent correct Dpp signalling^[118]. Interestingly, Dpp ectopically expressed in the fat body can find its way to the basal surface of the wing disc. Most of the Dpp accumulates at the ECM surface, but a fraction also diffuses in between the cells forming a basal to apical gradient that induces the same phenotype in the wing disc as uniform Dpp overexpression^[117].

1.5.3 Heparan-Sulphate Proteoglycans

A group of ECM proteins exhibit a type of post-translational modification that adds to them multiple Heparan-Sulphate Glycosaminoglycan (HS GAG) side chains. These proteins are called Heparan-Sulphate Proteoglycans (HSPGs)^[119]. These HSPGs can be divided into further subtypes, called Glypicans, Syndecans and Perlecan, depending on the properties of their core protein. Glypicans are bound to the membrane *via* a GPI anchor. Syndecans are also membrane-bound, but *via* a trans-membrane domain, and have Chondroitin-Sulphate side chains along with HS GAG side chains. Perlecan is not membrane-bound and so is released into the ECM. HS GAG side chains are implicated in sequestering secreted signalling factors within the ECM. This sequestration has the effect of restricting and controlling the diffusion of these signalling factors.

The *Drosophila* genome encodes one Perlecan, one Syndecan and two Glypicans. The two Glypicans are named Division Abnormally Delayed (Dally) and Dally-Like (Dlp). The Syndecan is named Syndecan (Sdc). The Perlecan is named Terribly Reduced Optic Lobes (Trol). In the wing disc HS-mediated restricted diffusion is thought to define gradient patterns of morphogens such as Hedgehog (Hh)^[120], Decapentaplegic (Dpp) and Wingless (Wg)^[121].

1.5.4 Glypican

Glypicans Dally and Dlp have been shown to affect diffusion of morphogens in the wing disc ECM. A morphogen Wg is secreted in a stripe of cells along the dorsal-ventral boundary of the wing disc pouch establishing an extracellular gradient that tails off with increasing distance from this boundary^[121]. Loss of Dally causes a reduction in Wg diffusion, and loss of both Dally and Dlp causes a compound reduction in Wg diffusion^[122]. However it has also been shown that Dlp behaviour is more complex^[123]. When Dlp concentration is low, it can act cooperatively by delivering Wg to its cell surface receptor, reducing its diffusion distance. When Dlp concentration is high, it act competitively by sequestering Wg away from its receptor, extending its diffusion distance.

The role of HS GAG side chains in binding morphogens is not entirely clear. In some cases only the core protein of Dally and Dlp is necessary for morphogen binding, with HS GAG side chains only improving affinity^[123, 124]. Further, this affinity can be altered extra-cellularly by modifying HS GAGs *via* a secreted endosulphatase named Sulf1. Sulf1 removes specific sulphate groups from HS GAGs, changing the affinity of the Glypican. It has been shown that desulfation of Dally by Sulf1 can reduce Wg binding. Furthermore, Wg has been shown to up-regulate Sulf1 suggesting a possible feedback mechanism^[125].

Glypicans are not purely localised to the basal ECM, they are found in all domains of the cell. The GPI anchor that keeps glypicans attached to the cell membrane also directs the protein to the apical domain surface. The GPI anchor has been associated with Endocytosis and cycling of Dlp from the apical to basal-lateral cell domains^[126]. This cycling has been implicated in Hh diffusion. The role of Dally and Dlp in Hh diffusion is a complex process. For example, the presence of basal-lateral cytonemes have also be implicated in Hh gradient formation^[127].

1.5.5 Syndecan

Syndecan has no known role in the wing disc, but has been implicated in axon guidance in neuronal tissues ^[128].

1.5.6 Perlecan

Perlecan is a single protein to which heparan sulphate chains can be added post-translationally. Vertebrate perlecan has five domains. Domain II has a domain related to low-density lipoprotein receptors. Domain III has a domain similar to N-Terminal regions of vertebrate laminin subunits α and β , which are short arms. Domain IV has domains similar to neural cell adhesion molecules. Domain V has domains similar to the C-Terminal region of vertebrate laminin α subunit. Trol has domains III, IV and V, but not Domain I. Also, Trol extends vertebrate Domain II, increasing the number of low-density lipoprotein receptors from four to twenty-two ^[129]. Trol has around 30% homology in domains III, IV and V compared with mammalian perlecan and insignificant homology in domain II ^[130]. The structure of Trol domain V suggests fly and vertebrate perlecan homologs have different ligands. Trol contains at least two RGD binding sites, one in domain V and one in domain III ^[131].

By looking at RNA transcription, it has been shown that Trol is expressed in imaginal discs as well as the fat body ^[131]. However other experiments have shown perlecan in wing disc ECM originates from the fat body ^[132]. Collagen IV is required for Perlecan to integrate into the wing disc ECM. Knockdown and overexpression of perlecan is nonlethal prior to the pupal stages. Changes to perlecan expression lead to morphological phenotypes in wing disc. Perlecan knockdown causes a narrowing of the wing disc along the anterior-posterior axis and an elongation of the columnar epithelium along the apical-basal axis, giving the tissue a compacted appearance. Perlecan overexpression causes a widening of the wing disc along the anterior-posterior axis and a shortening of the columnar epithelium along the apical-basal

axis, giving the tissue a flattened appearance ^[16]. Perlecan knockdown causes a reduction in apical cell area in the wing disc pouch, but without changing either distribution of polygon edge number or the pattern of cell orientation ^[117]. Polygon edge number is an indicator of tension across individual cells. Greater cell tension drives cells to minimise their surface areas, which in epithelial tissues leads to more efficient hexagonal packing. Despite driving Trol knockdown throughout development, leading to distorted wing discs, adult fly wing have no visible phenotype ^[117]. However, larvae hemizygous for a hypomorphic Trol mutant G0271 take one day longer to reach third instar, at which point the mutation becomes lethal ^[129].

An osmotic shock can drive a transient increase in cell volume, increasing wing disc size and hence apply a tension to its ECM. When inflated this way, the wing disc ECM stretches with the cells. However, after perlecan knockdown, the wing disc ECM can rupture when stretched this way. When collagenase treatment is applied to Wing discs with perlecan knockdown, the columnar epithelium transforms to a cuboidal, similar to collagenase of wild type wing discs. Electron microscopy images of the wing disc show the ECM becomes thinner when perlecan is knocked down ^[16].

Many of the results described previously were determined in *Pastor-Pareja and Xu 2011* ^[16]. The authors hypothesise that perlecan knockdown leads to an “increase in [ECM] tension” or a “decrease in elasticity”. However there is ambiguity in these statements. If a viscoelastic material has less elastic properties implies the material has more viscous properties. I assume what they mean is not that the ECM becomes less elastic, but that perlecan is less stiff than collagen. Hence if the two components were arranged in series then the ECM as a whole would be softened by relatively more perlecan, and stiffened by relatively less perlecan than collagen. However collagen and perlecan could be arranged in parallel, which would mean the tissue remains stiff regardless of perlecan concentration. Also, by changing ECM stiffness, perlecan only changes the magnitude of deformation induced by a tensile force applied to the ECM. To change the magnitude of tension itself, perlecan would need to regulate active sources of force in the tissue. Unlike cell cortices, there is no

known source of active contractility in the ECM. The authors suggest perlecan could be affecting cell contractility, and cite a paper establishing such a link; however the paper they cite has since been retracted. I believe an overlooked source of active force is cellular growth. As cells grow and proliferate, they may apply a tension to the ECM. By softening the ECM, perlecan may be allowing it to deform with the growing cellular mass. However, this ignores remodelling of the ECM, which will relax any tension applied to the ECM and is likely to occur on cell growth and proliferation timescales.

It is also possible that through perlecan's role in morphogen transport its absence could affect cell growth rates. Dally and Dlp have well-established roles in controlling morphogen gradients in the wing disc. However, despite Trol having many of the same characteristics as these other glypicans, there is little evidence of Trol affecting signalling in the wing disc. Reporters of Hippo Pathway activity Death Associated Inhibitor of Apoptosis 1 (Diap1) and Expanded (Ex) show no difference when Trol is knocked down^[117]. Concentrations and gradients of Dpp reporters, pMAD and SALM, are unaffected by Trol knockdown. In other tissues Trol has been implicated in some signalling roles. Quiescent Neuroblasts in the larval nervous system require Trol to switch to maintain cell proliferation. It has been shown in this case that binding of Trol is necessary for Hh signalling^[133]. Trol also promotes Wg and Dpp signalling in the second instar larval brain. However Trol no longer affects Wg and Dpp signalling in the larval brain at third instar despite continued Dpp and Wg signalling^[13]. These results show the role of Trol in signalling can vary considerably between tissues and stages of development. Assuming perlecan is binding morphogens directly, its ligand specificity maybe being changed, or perlecan itself is being changed, perhaps *via* differing HS GAG modification or *via* differing isoforms. This variety of specificity may be unsurprising given HSPGs have variation in HS GAG modification.

At the neuromuscular junction, perlecan knockout leads to a reduced size, and different morphology of this structure. Sulfateless is a protein involved in attaching heparan sulphate side chains to perlecan. Loss of sulfateless prevents addition of

heparan sulphate side chains. Knockdown of sulfatase alone in muscles causes reduced muscle size. Combining sulfatase knockdown and perlecan knockout does not exacerbate or recover the reduced muscle size observed with perlecan knockout alone. Introducing a secondary source of heparan sulphate side chains by expressing a secreted variant of Dally does recover some of the muscle size defects of perlecan knockout^[134]. Therefore, heparan sulphate side chains appear to contribute to tissue-size control of perlecan. Perlecan helps mediate extracellular Wg in this tissue, and its heparan sulphate side chains contribute to this function^[134]. It is possible that reduced muscle growth in perlecan knockout is a result of reduced Wg signalling, however the mechanical role suggested in the wing disc may also contribute here.

1.5.7 Nidogen

Nidogen is found ubiquitously in ECMs, and is conserved between vertebrates and invertebrates, however surprisingly loss of nidogen does not affect viability of mice or flies^[135]. Nidogen is present in the wing disc ECM, but nidogen knockout does not affect the wing disc ECM. However, nidogen knockout does lead to holes in the fat body ECM. Nidogen binds both laminin and collagen *via* different domains, suggesting the ability to crosslink them. Furthermore, loss of nidogen reduces co-localisation of laminin and collagen in fat body ECM, supporting a cross-linking role. Nidogen knockout does not affect perlecan localisation, but interestingly combined knockdown of nidogen and perlecan causes pupal lethality where single knockdown of either are viable to at least larval stages^[135]. Osmotic shock causes wing discs to inflate, likely exerting tension on its ECM, and leads to the wing disc 'bursting'. Nidogen knockout reduces the time taken for wing discs to burst during osmotic shock^[136], implying the ECM has become weaker.

1.5.8 Sparc

In vertebrates, *sparc* has been implicated in both promotion and suppression of tumour growth, but is not well understood. In the wing disc, *sparc* is up-regulated in competing cells, but not simply as a result of apoptosis. Dpp overexpression can inhibit *sparc* up-regulation, but is unaffected by Wg and JNK pathways. *Sparc* knockdown in loser cells speeds up competition and apoptosis, while *sparc* overexpression in loser cells prevents their apoptosis, before activation of Caspase. However, *sparc* overexpression does not block apoptosis in general, for example apoptosis in the wing disc pouch is not blocked.^[137] Loss of *sparc* is lethal at larval stages and leads to accumulation of ECM components such as laminin, collagen and perlecan at the fat body surface^[138]. *Sparc* has therefore been implicated in transporting ECM proteins such as collagen and perlecan from the fat body to target tissues. To do this, *sparc* is thought mediate dissolution of otherwise insoluble ECM components into the haemolymph^[16].

1.5.9 Matrix Metalloproteinase

The *Drosophila* genome encodes two matrix metalloproteinases, Mmp1 and Mmp2. Both Mmps contain a Catalytic domain, a C-Terminal hemopexin domain for binding substrates and inhibitors, an N-Terminal pro-domain that is cleaved for activation, and a signalling domain. Glycosylphosphatidylinositol (GPI) anchors are glycolipids that can be attached to the C-Terminal of proteins by post-translational modification. Both Mmps contain cleavable GPI anchors, allowing them to be either membrane-bound or secreted. Mmp1 has close homology to vertebrate MMP-28 and MMP-19. Mmp2 has close homology to MMP-11, MMP-25 and MMP-17. Therefore Mmp1 and Mmp2 represent different groups of mammalian matrix metalloproteinases. The distinction between the two Mmps is their substrate specificities Some specificity is shown *in vitro*, where Mmp1 but not Mmp2, can cleave casein substrates, while Mmp2, but not Mmp1, can cleave gelatin substrates^[139]. The *Drosophila* genome also encodes one Tissue Inhibitor of Metalloproteinases

(Timp). Timp can inhibit both Mmp1 and Mmp2 activity *in vitro* ^[140]. Loss of Timp causes wing blisters. Reck is another possible Mmp inhibitor, that inhibits Mmp1 in tumours ^[141]. Reck RNA is expressed in a strip around the periphery of the wing disc pouch ^[142]. Mmp2 RNA is expressed throughout the wing disc, with patches of minimal expression at the pouch center and Hinge-Notum fold. Mmp1 RNA is expressed at an insignificant level across the wing disc, with only a small patch of strong expression in the notum region ^[143].

There are six unique isoforms predicted for Mmp1 all with identical catalytic and hemopexin domains. There is only one isoform of Mmp2 predicted to be secreted. Only some Mmp1 isoforms exhibit a GPI anchor ^[139]. There is some evidence that when inactive both Mmps can contribute to cell adhesion ^[139]. Mmp2 and one isoform of Mmp1 has been found to exhibit an adhesive function. This adhesion is observed only when the proteolytic activity of the Mmps have been inhibited, either *via* mutation of the catalytic domain or by overexpression of Timp ^[139]. Cell adhesion has also been implicated in Mmp1 activity. A screen for interacting partners of Mmp1 hemopexin domains identified a transmembrane protein Ninjurin A (Njia). Njia interacts with specificity among the Mmp1 isoforms and does not interact at all with Mmp2. Overexpression of NjiA leads to increased cell adhesion *in vitro*, and this adhesion is dependent on the presence of Mmp1. However, this adhesion is not cell autonomous, suggesting Mmp1 cleaves Njia to produce a secreted signalling fragment ^[144].

Mmp1 null-mutants have tracheas that appear taut during growth, and eventually snap ^[145]. Mmp1 null-mutants grow slower and form smaller wing discs. This phenotype is hypothesised to be caused by hypoxia induced by tracheal defects. Timp overexpression in only the trachea causes the same phenotype. Further, Timp overexpression in imaginal discs does not affect their size, supporting the hypothesis that tracheal defects affect wing disc size *via* hypoxia ^[146].

The hemopexin domain is thought to provide specificity of Mmps to certain substrates. Some evidence for this specificity has been shown for Mmp1, where the

Mmp1 catalytic domain is required in larval stages for both trachea elongation and trachea invasion of discs, while the hemopexin domain is required only for trachea invasion of wing discs^[145]. Therefore in some contexts the hemopexin domain is required but not in others. It has been suggested hemopexin specificity could be related to the proteins to be remodelled – trachea elongation requires remodelling of apical ECM proteins such as chitin, whereas trachea-disc invasion requires collagen remodelling. Tissue invasion also requires the hemopexin domain of Mmp1^[141]. During pupal stages cells of the fat body fat body are dissociated, and both Mmps have been associated with this process. Loss of Mmp1 or Mmp2 delays fat body dissociation and loss of both Mmps or overexpression of Timp extends this delay further. Interestingly, overexpression of Mmp2 accelerates dissociation but overexpression of Mmp1 does not, suggesting some functional differences between Mmps. In this tissue it has been shown both Mmp1 and Mmp2 degrade cadherins, but Mmp1 does so with much greater efficiency. Therefore it appears Mmp1 and Mmp2 have overlapping but distinct roles, at least in this context. Interestingly, this specificity appears to be independent of hemopexin domains^[147].

There is some evidence of Mmps used to remodel the ECM. The Trachea makes contact with, and attaches to, the basal surface of the columnar epithelium around the notum region during wing disc development. In a mature state, cells of the two tissues come into direct contact. However before contact, both tissues are covered in ECM, and therefore ECM between the two tissues must be remodelled to achieve contact. It has been shown that a secreted signalling factor FGF attracts the trachea to the correct region of the wing disc. Interestingly, ectopic expression of this signalling factor leads to misplaced contact of the trachea with the wing disc^[148]. Normally, the circular section of the trachea becomes flattened against the wing disc surface as it integrates. Loss of Mmp2, but not Mmp1, prevents the trachea from flattening or integrating onto the wing disc surface, and remains circular in section. Interestingly, function of Mmp2 in this situation is tissue specific, loss of mmp2 in only the trachea, or both the trachea and wing disc, produce the phenotype described. However, loss of Mmp2 in the wing disc alone produces the opposite, a more flattened trachea than wild type^[148]. This result suggests Mmp2 activity can be

controlled with precise locality. I would expect given their proximity, Mmp2 release by either tissue would diffuse into the ECM of the apposing tissue. However, this result implies Mmp2 released by the two tissues are not redundant. Perhaps suggesting Mmp2 or, its regulation, is sequestered in the ECM of the tissue from which it is secreted.

Mmps have been shown to be important for tumour growth and invasion of tissues in flies, possibly through remodelling. Two types of tumour, generated by knockout of either polarity factor Lgl or cell proliferation regulator Brain Tumour (Brat), either induce Mmp1 expression or not, respectively. For the former, Mmp1 contributes to metastasis of the mutant cells. For the latter, signals are sent to surrounding wild type cells to increase Mmp1 expression ^[146]. Combining knockout of polarity factor Scribble and overexpression of mutant Ras (RasV12) in clones, highly invasive tumours can be produced in the wing disc. The JNK pathway mediates invasiveness of these tumours. Expression of Mmp1 again contributes to tumour invasion, which is regulated downstream of the JNK pathway. Interestingly Mmp2 also contributes to tumour invasion, despite only Mmp1 being regulated by JNK ^[149]. Loss of either Mmp cause defects in wing disc eversion, a process also dependent on the JNK pathway. It has been shown that deactivation of the JNK pathway reduces Mmp1 and Mmp2 expression in the wing disc ^[141]. Ectopic expression of Mmp2 in the wing disc can induce a damage-response from the organism. This response involves damaged cells releasing cytokines that localise haemocytes, again dependent on the JNK pathway ^[150].

Degradation of the ECM *in vivo* with Mmp2 affects wing disc morphology. Expression of Mmp2 in the wing disc leads to a columnar to cuboidal transition, similar to that observed with collagenase treatment. Applying Mmp2 as a pulse *in vivo*, then allowing it to repair, leads to cells recovering their columnar shape ^[16]. Degradation of the ECM with Mmp2 can affect cell proliferation in the wing disc. EdU staining is a way of measuring cell proliferation rates. Overexpression of Mmp2 in the wing disc pouch shows a reduction in EdU at the anterior and posterior most regions. A pulse of Mmp2 overexpression only during larval stages allows adult wings to form, and

these wings are smaller but with the same cell density suggesting a reduction in cell proliferation^[117]. Mmps have been implicated in some folding of the wing disc. Expression of Mmps in pouch folds is required for fold formation^[151].

1.5.10 Disintegrin

As neighbouring class of proteins contain both matrix metalloproteinase and disintegrin domains, called A Disintegrin And Metalloproteinase (ADAM). ADAMs share the same catalytic domain exhibited by Mmps but also contain a disintegrin domain, which can bind to integrins. By binding integrins of the same cell, disintegrins have the potential to inhibit cell-matrix adhesion. By binding to integrins of other cells, disintegrins could form cell-cell adhesions. The *Drosophila* genome encodes five known ADAM proteins, called Kuzbanian, Kuzbanian-like, Tace, Mind-meld and Meltrin^[152]. ADAM proteins are known to affect many morphological processes during fly development, especially in the cardiac and neural tissues. However, most functions reported for fly ADAMs implicates them in cleavage of cell surface receptors, not the ECM, for example Kuzbanian and Kuzbanian-like are known to cleave cell-surface receptor Notch^[153]. Timp has been shown to inhibit vertebrate homologs of both Tace and Kuzbanian *in vitro*^[140].

Another class of ADAM, called ADAM-TS include thrombospondin-like repeats. The *Drosophila* genome also encodes three ADAM-TS proteins. One ADAM-TS, called AdamTS-A, is associated with cell migration^[154], but is also associated with tissue morphology. Loss of AdamTS-A has been shown to give a similar tissue elongation phenotype to perlecan knockout in the central nervous system of larvae^[155]. AdamTS-A does not require perlecan to drive tissue elongation, and AdamTS-A overexpression does not rescue the perlecan knockout phenotype. Perlecan overexpression alone does not affect central nervous system morphology but does rescue the AdamTS-A loss phenotype. AdamTS-A overexpression leads to an increase in perlecan, a decrease in collagen and no change in laminin levels in the central nervous system ECM. AdamTS-A loss leads to an increase in collagen. It is unclear from this work if AdamTS-A is degrading collagen, if so it could be relaxing any stress

applied to the ECM by the rapidly growing cellular mass of the central nervous system during larval stages. Homologs of AdamTS-A in mammals are known to degrade chondroitin sulphate. As covered previously, perlecan knockout stop cell proliferation early during its development, and AdamTS-A knockout behaves the same. However, both perlecan and AdamTS-A knockdown do not stop cell proliferation, and lead to the elongated central nervous system phenotype. It is therefore suggested that cellular growth may contribute to this morphological phenotype ^[155].

1.5.11 Lysyl Oxidase

Lysyl oxidase is a secreted protein, known to covalently crosslink four tail domains of collagen fibrils in vertebrates ^[113]. Increased crosslinking of collagen by lysyl oxidase is expected to increase ECM stiffness. Increased ECM stiffness is known to promote tumour invasion ^[156]. The *Drosophila* genome encodes two lysyl oxidase-like proteins, Loxl1 and Loxl2. Loxl1 is expressed throughout fly development with peaks at pupal stages, while Loxl2 expression occurs mainly in adult flies. Fly Loxls can be inhibited using a drug called BPAN introduced into their food. A low concentration of BAPN moderately extends development time, while high concentrations severely extend development time and reduce viability ^[157]. Knockout of Loxl1 or Loxl2 show no clear phenotype during larval development, while their combined knockout causes shortening in the optic stalk of the eye disc, suggesting some redundancy between the two. Combined Loxl1 and Loxl2 knockout does not affect ECM thickness in the eye disc but does reduce the effective stiffness of the tissue, suggesting a reduction in ECM stiffness ^[158].

1.5.12 Peroxidasin

Peroxidasin is a secreted protein known to crosslink two head domains of collagen fibrils in vertebrates. The *Drosophila* genome encodes one peroxidasin, Pxn. Hypomorphic mutants of Pxn lead to larval lethality ^[159]. In *Drosophila* Pxn requires

bromine to cross-link collagen in the ECM, and larvae fed on bromine-deficient diets exhibit similar phenotypes to Pxn loss^[160].

1.6 Hypothesis

During larval development, the wing disc grows in size exponentially. However, the ECM that encapsulates the wing disc must respond to this growth. Considering the mechanics of this interaction has led to the following hypothesis, also summarised in Figure 5.

1.6.1 Hypothesis

The wing disc is a highly proliferative tissue. Cells grow and divide approximately every twelve hours. During this exponential growth the ECM forms a thin layer across the basal surface of the wing disc tissue. Cells of the wing disc epithelium are single cell thick; therefore cell density can be expressed as the number of cells per unit area of ECM. I assume cells will have a preferred basal surface area that is dependent on their cell-matrix adhesion strength. As a result I expect cells to exert a tension on the ECM that is some increasing function of their number per unit area of ECM. The preferred basal surface area of cells defines a preferred cell number per unit ECM area at which no tension is applied to the ECM. As cells proliferate their number will increase, but their number per unit area of ECM will depend on ECM area, which in turn depends on the mechanical response of the ECM to any applied tension.

I assume that the ECM is a viscoelastic material. Whether the ECM behaves predominantly elastically, viscously or both will depend on its remodelling rate. The limiting cases are; at timescales much shorter than the remodelling rate the ECM will behave elastically and at timescales much longer than the remodelling rate the ECM will behave viscously. If the ECM behaves elastically, then its response to tension will depend on its stiffness. A stiff ECM will deform less under an applied tension than a soft ECM. If the ECM behaves viscously, then its response to tension will depend on its remodelling rate. A faster remodelling ECM will resist deformation for less time than a slow remodelling ECM.

If the remodelling rate of the ECM is much faster than the proliferation rate of the cells, then the ECM area will grow as cells proliferate. In the limit of fast ECM remodelling the ECM would instantaneously relax any tension, and cells would be able to maintain their preferred basal surface area at all times. If the remodelling rate of the ECM is much slower than the proliferation rate of the cells, then tension will increase across the ECM as cell number per unit ECM area increases. In the limit of soft ECM, the ECM would deform to accommodate the preferred cell number per unit area. In the limit of stiff ECM, the ECM would not deform at all under applied tension, and both cell number per unit area and applied tension would increase with cell proliferation rate. These are limiting cases on a spectrum of remodelling rate and stiffness.

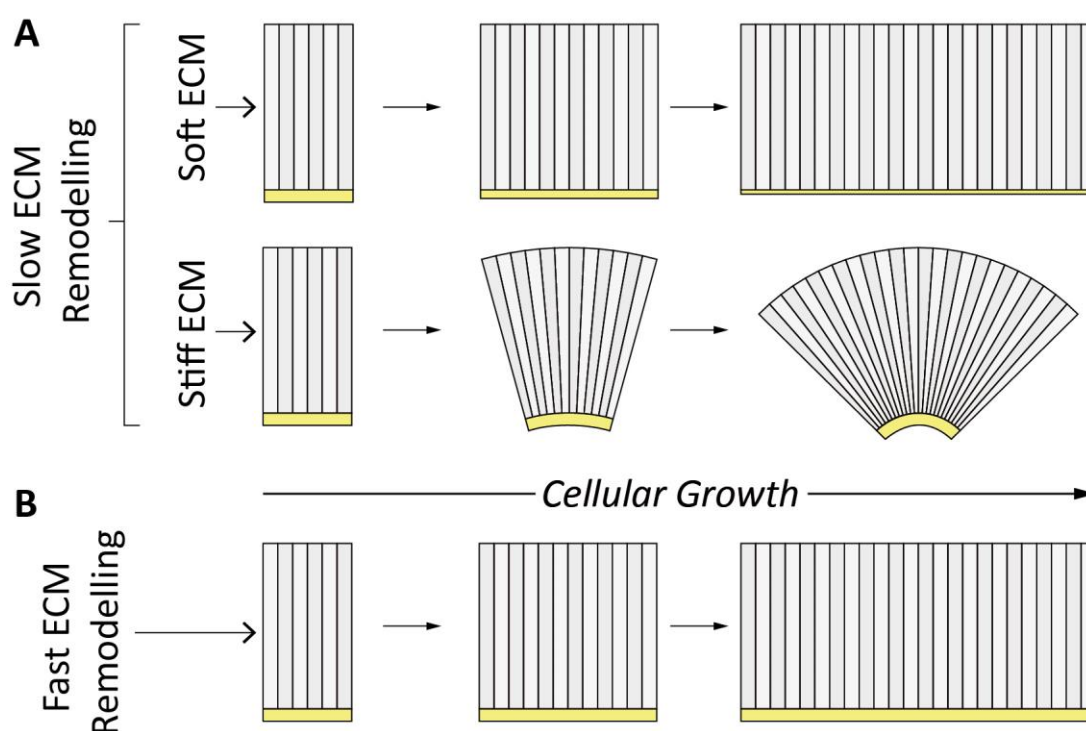


Figure 5. Mechanical properties of the extra-cellular matrix are hypothesised to define its response to cellular growth and proliferation during wing disc development. **A**, if the ECM remodels slowly relative to cell proliferation then it may respond elastically. If the ECM is much softer than cells then it may become stretched by the cell layer as it grows. If the ECM is much stiffer than cells, then stress may develop between the two, potentially leading to buckling. **B**, if the ECM remodels much faster than cells grow, then it may grow with the cells, relaxing any stress that may build up.

1.6.2 Aims

This hypothesis raises two questions:

- 1.** Do cells in the wing disc apply a tension to the ECM, and if so, how do cells apply this tension.
- 2.** What are the mechanical properties of the ECM and how do they affect the response of the ECM to cellular growth in the wing disc.

Answering these two questions should help understand how the cells and their ECM interact during wing disc growth, and whether this interaction contributes to wing disc morphology.

1.6.3 Implications

Understanding the mechanical behaviour of the ECM may contribute to understanding morphological development of the wing disc. When the ECM is stiff and remodels slowly, stress is expected to build up in the ECM as cells proliferate. This stress could lead to mechanical instability and buckling, in which cells can achieve a greater surface area by curving out of the otherwise flat basal plane. If the ECM is stiff and remodels slowly, then it is possible that buckling could contribute to the curvature observed in the hinge and pouch of the wing disc. From apical cell-cell junctions it is observed that cells exhibit fluidity in their arrangement by exchanging neighbours. ECM remodelling rate may act as a rate-limiting step on cell rearrangements, however cell-matrix adhesion remodelling would be more important in this case. Cells have been shown to exhibit mechano-sensitivity. An increase in cell compression due to confinement by a slow remodelling ECM may trigger mechano-sensitive pathways affecting cell growth or fate.

2 Results

To interrogate the hypothesis I needed to understand both the geometry of the ECM and its mechanical properties. I have divided the results into four sections. To begin, I have studied the structure of the ECM and how it changes with wing disc age, §2.1. I have then perturbed cells and their ECM to try to understand how the cells and ECM interact, and how that interaction affects wing disc morphology, §2.2. I have then considered the elastic properties the tissue, to try to understand how the ECM contributes to tissue stiffness, §2.3. Finally, I have considered the dynamics of the ECM, and how remodelling may affect its role during wing disc development, §2.4. For each section I begin by describing the methods used, I then present and describe the results, and finally I discuss the meaning of the results.

2.1 Results Section 1: Structure and composition of the wing disc extra-cellular matrix

This section is concerned with understanding the structure of the ECM in its natural state. Specifically, how the ECM structure changes spatially across the wing disc, and also how the ECM structure changes with time as the wing disc grows. To elucidate ECM structure I have made use of electron microscopy. This section is also concerned with the components that contribute to the structure of the ECM, again both spatially and temporally, and how components co-localise. To do this, I have made use of fly lines containing fluorescently labelled proteins.

2.1.1 Methods

Fly lines

There exist many genetic resources in the *Drosophila Melanogaster* model system. Libraries of fly lines have been produced by randomly inserting P-elements into fly DNA. The effect of the insertion depends on both the location of insertion and the contents of the P-element. If a P-element is inserted into a gene then it may prevent correct transcription of the gene, for example if the P-element is not in the same reading frame as the gene. If the P-element is inserted just right, then the genetic code contained in the P-element may be transcribed with the gene. If the P-element contains a gene coding for a fluorescent protein then, if inserted correctly into an endogenous gene, the expressed protein will be tagged with the fluorescent protein. This is an example of a protein trap. Successful protein trap lines must be characterised to confirm the fluorescent protein does not generate new phenotypes. If no phenotype is observed, the protein trap line can be used to observe the sub-cellular localisation and dynamics of the protein in live tissues.

The likelihood of generating a correctly inserted P-element for a given gene depends partly on the structure of the gene. Some P-elements are designed to work in specific regions of the gene. For example, a P-element can be designed to act like an artificial exon, flanked by splice acceptors, and therefore must be inserted in non-coding introns^[161]. Hence the probability of a P-element inserting into an intron of a given gene depends on the size and number of introns in that gene. Libraries of fluorescently tagged proteins are therefore not comprehensive. Different transposable elements show different affinities for certain genetic regions. P-elements are known to have hot- and cold-spots, genes where insertion is more or less likely to happen. Other transposable elements, such as Minos-elements, have less preferential insertion, and so have been used to target genes that P-elements miss^[162].

Other collections of fly lines take a more direct route to fluorescently tag proteins. A copy of a gene, including its upstream regulatory region, is isolated, and combined with a fluorescent protein gene at one of the terminals. This transgene is then inserted back into fly DNA at a specific, non-deleterious, location. The insertion is therefore an extra, fluorescently tagged copy of the gene that is hopefully expressed with the same pattern as the endogenous gene^[163]. Unfortunately I have found these extra-copy fluorescently-tagged proteins provide much lower fluorescence intensity than the endogenous protein trap variety. I have tried to use protein trap lines where possible, but often these lines are not available for my protein of interest.

I have used protein trap lines for ECM proteins to observe their localisation in the wing disc. The protein trap collection^[161] contains fly lines with GFP inserted into endogenous Viking (VkgGFP; VkgG00343 FBID: *FBti0153267*) and Trol (TrolGFP; TrolG00022 FBID: *FbaI0243608*). The collection of transgenes tagged with GFP, FlyFos^[163], contains Laminin B1 (LanB1GFP; LanB1fTRG00681 FBID: *FBti0198899*), Laminin A (LanAGFP; LanAfTRG00574 FBID: *FbaI0339089*), Sparc (SparcGFP; SparcfTRG00032 FBID: *FbaI0339548*) and Nidogen (NdgGFP; NdgfTRG00638 FBID: *FBti0198644*). Another collection of transgenes tagged with YFP, FlyProt^[164], contains Inflated (IfYFP; IfCPTI004152 FBID: *FBti0143597*) and Mew (MewYFP; MewCPTI001678 FBID: *FBti0143875*). I have also obtained a fly line containing endogenous Myspheroid tagged with GFP (MysGFP), a gift from Nick Brown. I have used two UAS-VkgScarlet (UAS-VkgSCA) fly lines, gifts from Besaiz Sanchez and Brian Stramer, one on the second chromosome and the other on the third. I have driven these using the Vkg and Cg25C regulatory fragment driving Gal4, CgGal4^[16].

Ex vivo Culture method

Dissection and live imaging is performed in insect culture medium. A problem with culturing wing discs *ex vivo* is no method has yet been established that is able to keep wing discs proliferating for longer than 24 hours^[165]. It has generally been

found that once dissected, proliferation rates of cells reduce regardless of culture conditions, and go through one round of division at most before cessation. Cell proliferation cannot be reactivated *ex vivo* by overdriving cell growth genes, or by inhibiting stress-activated genes. However, implanting dissected wing discs back into an adult fly abdomen can reactivate proliferation. Neither hyper-oxidative nor hypo-oxidative conditions prevent cessation. Co-culture with dissected fat body and brain tissues do not affect cessation. Using haemolymph extracted from flies or larvae has a worse outcome than established insect mediums. Only by supplementing media with hormones has some success been found. By adding a bovine insulin cell proliferation cessation can be delayed, but not prevented ^[165]. A steroid hormone Ecdysone has been shown to extend proliferation further than bovine insulin, but again does not prevent eventual cessation of proliferation ^[166]. Hence, *ex vivo* wing disc culture is not perfect, and is clearly missing some complex set of factors, even before ECM components are considered.

I have used a culture protocol established by Dye et al ^[166], shown to prolong wing disc proliferation the longest of the protocols published so far. Grace's insect medium is used as a base. I receive Grace's media (Sigma-Aldrich, G9771-1L) as a powder, which I add to around 900mL of distilled water, at room temperature, while stirring until the powder is dissolved. While still stirring, I add 1.05g of BisTris (Sigma-Aldrich, VB9754-25G) until dissolved. I then adjust the pH of the mixture to 6.6 by adding NaOH. I then add more distilled water to achieve a final volume of 1L. I then filter the mixture using a pump and membrane with 0.2µm pore size, in a tissue culture hood. I then divide the filtered medium into 10mL aliquots while still under the hood, and store them at 4°C. Before use, I open an aliquot of medium and add 500µL of Fetal Bovine Serum (Sigma-Aldrich F4135-500ML) and 100µL of Penicillin-Streptomycin (ThermoFisher, 15140-122) to obtain 5% and 1% concentrations respectively. The Fetal Bovine Serum and the Penicillin-Streptomycin are stored in 500µL and 5mL aliquots, respectively, at -20°C. I then add 0.5µL of a 0.05mg/mL stock of Ecdysone (Sigma-Aldrich, H5142) kept at -20°C. I then lightly shake the media and allow it to warm to room temperature. Once hormones have been added, I never use the media for more than three days due to inevitable fungal infections.

I take larvae from their fly tubes and immerse and wash them in distilled water in a concave glass well. For dissection, I add 0.8mL of media to a glass concave dissecting plate. I dissect the larvae by pinching and pulling the head from the body using forceps. The wing discs can be found attached to the head matter by both trachea and other, thinner tubes. I remove as much of these tubes as possible to isolate the wing disc. However, some trachea is often left attached to the notum and hinge because it is hard to remove without damaging the wing disc. Isolated wing discs are moved using a P200 pipette and 200 μ L pipette tip to a glass well containing more media. Wing discs must be kept immersed in media at all times, if allowed to dry they disintegrate.

Confocal microscopy

When imaging, it is important that the wing discs are immobilised so that they do not leave the field of view, that they are kept immersed in media at all times and are brought as close to the coverslip as possible. For live imaging I use one of three methods to mount wing discs, each with their own benefits. The first method, established by Restrepo et al ^[167], uses a filter chamber (Merck Millicell Cell Culture Insert, PI8P01250), which is a tube of hard plastic with an 8 μ m pore size filter paper stuck to the bottom. Wing discs are placed in a 10 μ L blob of media in the middle of a 35mm glass-bottomed dish (World Precision Instruments, FD35-100), the filter chamber is placed on top of the blob, filter paper down. The filter chamber is then filled with 200 μ L of media. Finally, a sheet of lens cleaning tissue (Sigma-Aldrich, WHA2105841) is repeatedly folded in half parallel to the short side to form a strip. This strip is wetted with distilled water and placed in a ring around the inside edge of the glass-bottomed dish, humidifying the chamber. The lid of the dish is put in place and sealed shut using parafilm. In this method, the wing discs are immobilised by the surface tension of the media between the glass bottom and the filter. Plenty of media is supplied *via* the media in the chamber and the dish is kept humid by the damp lens tissue, keeping the wing disc immersed.

The second method, established by Dye et al ^[166], uses filter paper rather than a chamber, to confine the wing disc. A hole is punched into double-sided sticky tape (Tesa, 5338), using a hole-punch. The hole-punched sticky tape is adhered to the surface of a 35mm glass-bottomed dish, to form a makeshift well. Wing discs are placed in the well in about 10 μ L of media. The wing discs are then oriented as required, and as much excess media is removed without letting the wing discs dry. Quickly, a piece of 5 μ m pore size filter paper (Sigma-Aldrich, WHA70602513) is adhered on top of the sticky tape, sealing the well, turning it into a pocket. Around 2mL of media is then added on top of the pocket, filling the dish. Finally, the lid is put in place and sealed using parafilm. In this method, wing discs are immobilised partly by surface tension of the media but also due to confinement within the pocket. By adding plenty of media on top, the wing discs are kept immersed. A benefit of this method is that wing discs can be forced up close to the glass bottom of the dish. The amount of confinement the wing discs experience can be controlled by changing the amount of excess media is left in the well before sealing.

The third method, which is one I developed, uses a piece of coverslip to flatten the wing discs. A coverslip of 0.08mm thickness is carefully broken into pieces by hand. I select pieces of coverslip that are approximately 4mm in size. I place a coverslip piece into a 35mm glass-bottomed dish. I coat the piece of coverslip with around 1 μ L of a tissue adhesive called cell-tak. The cell-tak is smeared to coat as much of the coverslip piece as possible. The dish with the coverslip piece is warmed to 25°C on a hot plate, until the cell-tak is dry. Following the cell-tak instructions, the dried cell-tak is washed once with ethanol. I then fill the dish with 2mL of media. I bring the wing discs into the dish but not onto the piece of coverslip. With forceps, I 'waft' each wing disc to orient and place it on the cell-tak. Wing discs usually stick immediately upon contact with the cell-tak. Once all wing discs are stuck to the piece of coverslip, I flip the piece of coverslip using two pairs of forceps and allow it to settle. The stuck wing discs remain stuck during flipping, and once flipped, the wing discs are flattened between the piece of coverslip and glass bottom of the dish. Finally, the dish lid is put in place and sealed with parafilm. Usually, the piece of

coverslip does not move when transferring the dish to the microscope, so the wing discs remain in place. The benefit of this method is the wing discs are very well immobilised and flattened right up-against the glass. The drawback of this method is the discs may be a little deformed by the flattening, and therefore is not suitable for analysing wing disc morphology. Also the surface area the wing discs have in contact with the media is reduced, so this method should not be used for long-term imaging.

I use the filter chamber method for situations where I want the wing discs to have plenty of space to move, for example when I expect the morphology to change during treatment. A drawback is wing discs have enough space to move laterally under the chamber, so can sometimes leave the field of view over time. The filter paper method addresses this issue by giving wing discs less space to move. Also, by creating a pocket, wing discs are shielded by any flow of media that could move them. Therefore I usually prefer the filter paper method above the filter chamber method. The coverslip method I use when I am only interested in measuring fluorescence levels on the basal surface of the wing disc. By flattening the wing disc, its basal surface is brought right up against the coverslip, whereas in the other methods the curvature of the columnar epithelium creates a gap, which attenuates any emitted fluorescent light. This is good for measuring ECM fluorescence levels, where the long-term health of the wing disc is less of a concern.

Wing discs are imaged live using an inverted Zeiss LSM 880 microscope. This microscope is capable of confocal and super resolution 'Airyscan' imaging. Images were taken either with a 25x water lens or a 40x oil lens.

I prefer to image wing disc ECM components in live rather than fixed conditions due to creases forming during fixation, Figure 7 A, B. These fixation artefacts are likely caused by osmolarity-induced volume changes in the cellular mass. There are protocols using sucrose to alter the fixative osmolarity, however I did not pursue this past initial tests due to the greater efficiency of live imaging. Images of how adding switching from PBS to the media of live wing discs is shown in Figure 7 C. The reduced osmotic pressure caused by switching from PBS to media appears to deflate

the wing disc. In particular the lumen collapses, causing the peripodial epithelium to hug the apical surface of the columnar epithelium. A similar lumen collapse is seen when wing discs are fixed with 4% PFA in PBS Figure 7 D. These issues raise questions of what the osmotic conditions are like *in vivo*, and whether the wing disc lumens are normally collapsed or inflated. From here on I assume the insect media we use for live culture is closer to *in vivo*, and I treat the morphology of fixed wing discs and the structure of their ECM with caution.

Fluorescence Intensity Measurements

To determine change in ECM components with wing disc size, I have measured both fluorescence intensity and wing disc size for different fluorescently labelled ECM proteins. I have mounted them using the coverslip flattening method describe previously. This method minimises the attenuation of fluorescence measured from the ECM by keeping it consistently close to the objective. This method also flattens the wing discs so that the columnar epithelium is relatively flat. I can then measure wing disc size consistently without changes in pouch doming affecting the result. To characterise wing disc size I obtain an image stack of the whole, or most, of a wing disc ECM using a Zeiss LSM 880 confocal microscope with 40x oil objective at 0.6X digital zoom. The wing discs imaged, exhibit the ECM protein of interest labelled with GFP. From images of the fluorescently labelled ECM protein I can determine both its concentration in the ECM and the wing disc shape. I then sum the image stack to obtain a single image. On this image I manually draw a circular region that best follows the perimeter of the pouch region of the wing disc. The shape of the wing disc may vary slightly, and manual region fitting is inherently variable, generating error in the measurement. However, any errors in fitting this region are hoped to be negligible compared with the range in wing disc sizes measured. To measure fluorescence intensity I draw a smaller region as close to the pouch center as possible. I do not place the region on non-epithelial structures such as the trachea. I then take the mean fluorescence intensity of that region. I repeat this process for wing discs across a range of ages between 72h and 96h AEL to obtain

pairs of wing disc size and protein fluorescence intensity. This process was repeated for each fluorescently labelled protein. The proteins considered were laminin (LanB1GFP), collagen (VkgGFP) and perlecan (TrolGFP).

For each protein dataset I performed a linear regression using the SciPy library in python allowing the gradient and intercept to vary freely. From the linear regressions, I took the gradients as a measure of change in fluorescence intensity with wing disc age. I also obtained the standard deviations from the linear regressions to characterise the significance in difference between gradients for different proteins.

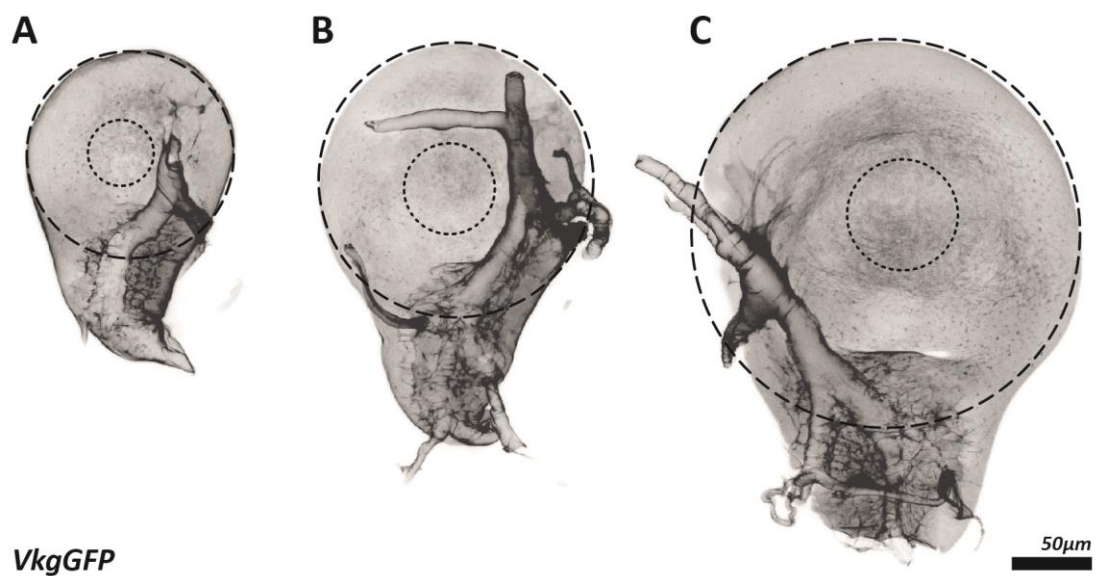


Figure 6. Fluorescently labelled extra-cellular matrix proteins allow measurement of protein concentration with wing disc size. A – C shows summation projections of collagen in the ECM of wing discs of different sizes. The dashed circles indicate the characteristic diameter for the wing discs, the dotted circles indicate the region from which fluorescence intensity is measured.

Electron microscopy

To generate electron micrographs of the wing disc ECM, wing discs were dissected and fixed in a mixture of 2% formaldehyde and 1.5% glutaraldehyde in PBS for 30 minutes. Fixed wing discs were then embedded in 2.8% low melting point agarose

dissolved in PBS. Once set, blocks of wing disc-containing agarose were cut out and secondarily fixed for 1 hour in a mixture of 1% osmium tetroxide and 1.5% potassium ferricyanide at 4°C. Further fixation and contrast enhancement was achieved with, 1% thiocarbohydrazide for 20 minutes, 2% osmium tetroxide for 30 minutes, 1% uranyl acetate overnight at 4°C and lead aspartate for 30 minutes at 60°C, with extensive washes in double distilled water between incubations. Samples were then dehydrated in increasing concentration of ethanol solutions and embedded in Epon resin. The 70nm ultrathin resin sections were cut with a diamond knife (Diatome) using an ultramicrotome (UC7; Leica) and sections were collected on formvar-coated slot grids. Wing discs were imaged using a 120kV transmission electron microscope (Tecnai T12; FEI) equipped with a CCD camera (Morada; Olympus SIS). *All steps after dissection were performed by Jemima Burden of the MRC LMCB Electron Microscopy Facility.*

To measure ECM thickness from electron micrographs, the perpendicular distance was measured for multiple positions across multiple images for each morphological region and each wing disc age grouping. The mean and standard deviation was then plotted for each group of measurements.

Statistics

In Figure 16 and Figure 17, length measurements for each age were found not to be normally distributed, therefore nonparametric tests were used. For Figure 16 a Kruskal-Wallis test was used to determine if any of the three groups were significantly different, which they were, then a Mann-Whitney U test was applied to each pair giving significance labels shown. For Figure 17 a Mann-Whitney U test was applied to find the significance label shown. For Figure 19 A – C linear regressions were applied to each data set and plotted as a solid line. To determine if gradients differed significantly between linear fits, the R functions `lm` and `emtrends` was used to determine significant difference for each pair. Significance labels are based on p values of a given test and are assigned not significant (ns) if the p-value was greater than 0.05, (*) if less than 0.05, (**) if less than 0.01, (***) if less than 0.001 and (****) if less than 0.0001.

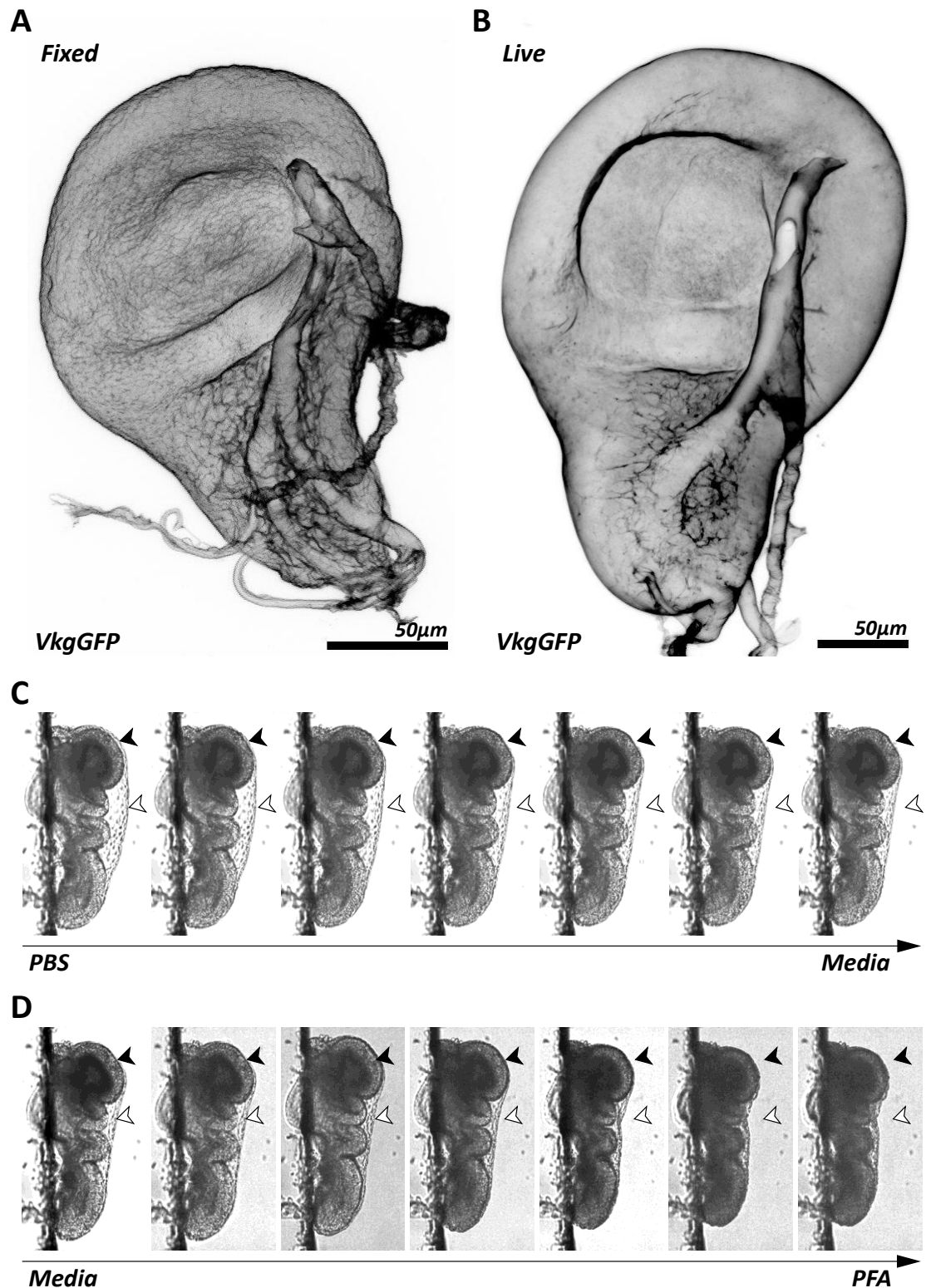


Figure 7. Fixation changes extra-cellular matrix structure and wing disc morphology. Maximum projections of VkgGFP for wing discs under fixed, **A**, and live, **B**, conditions. **C** shows sections of a wing disc over time after switching from PBS to medium. **D** shows sections of a wing disc over time after switching from medium to PFA. In **C** and **D**, filled and hollow arrows at each time point indicate the position of the peripodial epithelium at the initial time point.

2.1.2 Results

I have used fly lines with fluorescently tagged ECM proteins to observe their localisation across the wing disc. Some images of fluorescently tagged ECM proteins in the wing disc have been published previously, including VkgGFP^[16]. In these cases I still obtained my own images in the hope of uncovering more detail. Both VkgGFP, TrolGFP and LanB1GFP show a thin, continuous layer of fluorescence along the basal surface of the wing disc epithelium, Figure 8, Figure 9 and Figure 10. In live wing discs it appears the peripodial collagen is at a lower concentration Figure 9, however this is just due to attenuation of fluorescence signal, in fixed wing discs where attenuation is negligible, the concentration of the peripodial ECM appears similar to columnar Figure 8.

The pouch region of the columnar epithelium is fairly flat and uniform unlike hinge and notum regions. In the pouch region of the ECM Figure 9, collagen is apparent across the whole surface but shows some variation in concentration. In older wing discs, Figure 9 B, C, there appears a band of relatively low collagen concentration across the pouch along the anterior-posterior axis, indicated by pairs of inverted black arrows in magnifications Figure 9 B'', C''. This band of diffuse collagen likely co-localises with the band of cells that defines the dorsal-ventral compartment boundary and expresses the morphogen Wg. A thinner, less prominent band of reduced collagen fluorescence appears along the dorsal-ventral axis, indicated by pairs of inverted white arrows in magnifications Figure 9 B'', C''. This band likely co-localises with cells that define the anterior-posterior compartment boundary and express the morphogen Dpp. Collagen concentration in the central pouch region appears generally increased compared with the periphery. Perlecan and laminin also exhibit increased concentration in the central pouch region, enclosed by arrows in Figure 10, and to a lesser extent exhibit low fluorescence bands in older wing discs indicated by pairs of inverted black arrows in Figure 10 C, F. Imaging collagen at greater magnification shows the increased concentration is partly due to high

concentration fibres that cross the ECM Figure 11, which are less dense in the wing disc periphery.

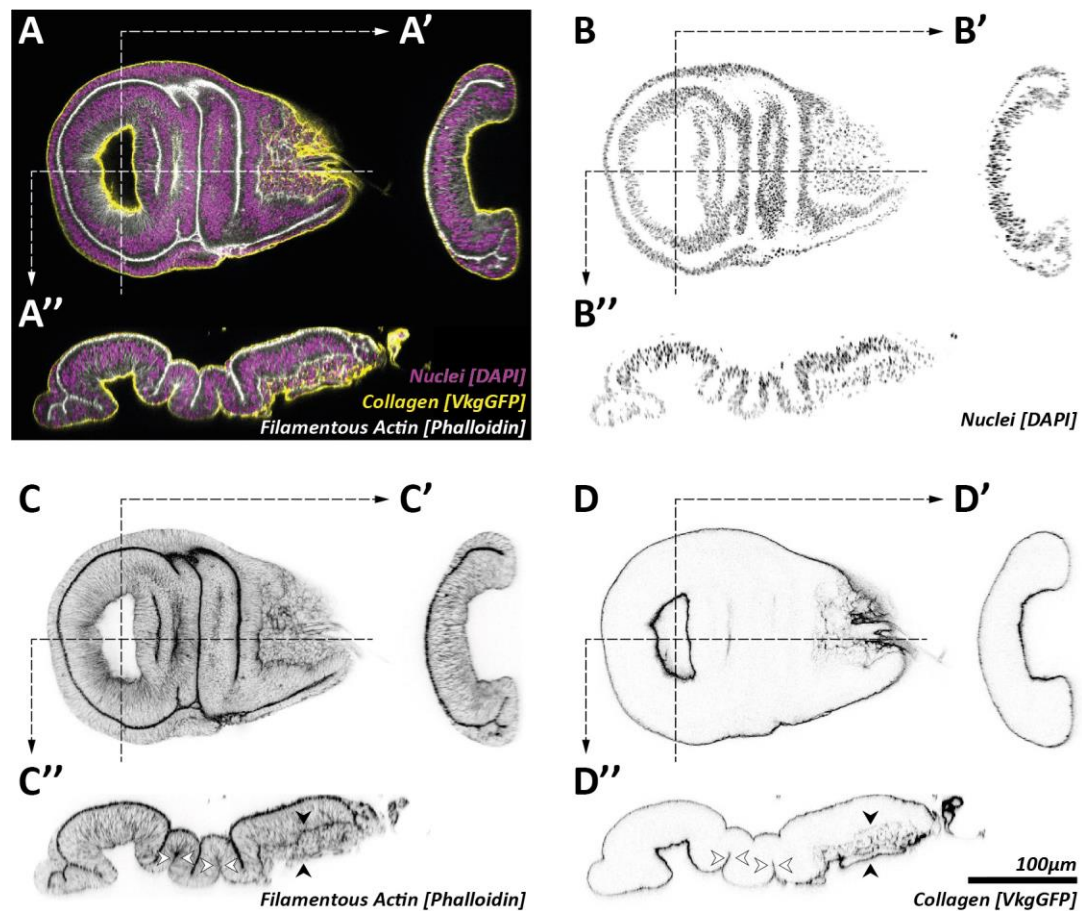


Figure 8. *The extra-cellular matrix forms a thin, continuous layer around the wing disc. A – D show fluorescent images of one slice of one wing disc. A' – D' show cross-sections of the wing disc along the anterior-posterior axis of the pouch region. A'' – D'' show cross-sections of the wing disc along the dorsal-ventral axis. In C'' and D'' apposing basal surfaces of hinge-hinge and hinge-notum epithelial folds are indicated by pairs of white inverted arrows. In C'' the layer of myoepithelial cells below the notum epithelium are indicated by pairs of inverted black arrows, and collagen surrounding these myoepithelial cells are similarly indicated in D''. The wing disc shown is approximately 120h AEL and has been fixed.*

At hinges of older wing discs, basal surfaces of the columnar epithelium appose each other, indicated by white arrows in Figure 8 C'' and D'', sandwiching the ECM between them. It is unclear if each of the two apposing epithelia have their own ECM, forming a bilayer, or if ECMs combine to form a single layer. For younger wing

discs the hinge columnar epithelia do not appose, and the ECM is separated, Figure 9. For older wing discs the basal surface of the folding columnar epithelium forms a point of high curvature, Figure 9 A'', D''. If the ECM is a bilayer, its curvature at this point is considerably greater than the ECM curvature at any other point along this epithelium. This is of interest because if the ECM is stiff enough, it may prefer lower curvature, and so this point of high curvature may either be discontinuous or have different mechanical properties.

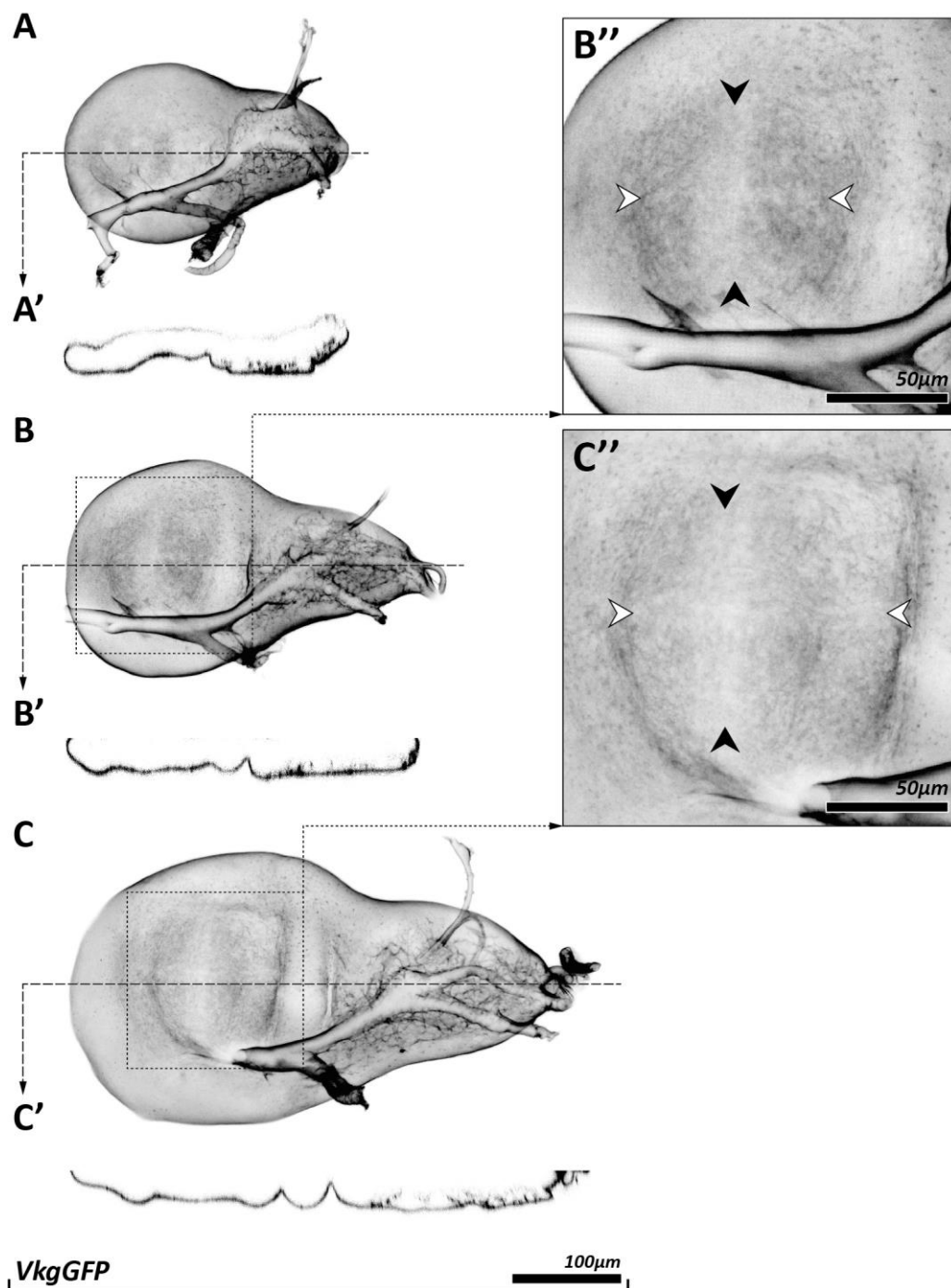


Figure 9. The extra-cellular matrix remains continuous around the wing disc during growth. **A – C** show summation projections of wing discs expressing endogenously labelled Vkg, a subunit of collagen. Wing discs from **A – C** are increasing in age, with **A** around 72h AEL, **B** around 84h AEL and **C** around 96h AEL. **A' – C'** show cross-sections of the wing discs shown in **A – C** indicated by the dashed line. **B''** and **C''** are magnifications of their respective wing disc pouches, black arrows subtend the band of low concentration Vkg along the dorsal-ventral boundary, white arrows subtend the similar but less prominent band along the anterior-posterior boundary. All wing discs were imaged live.

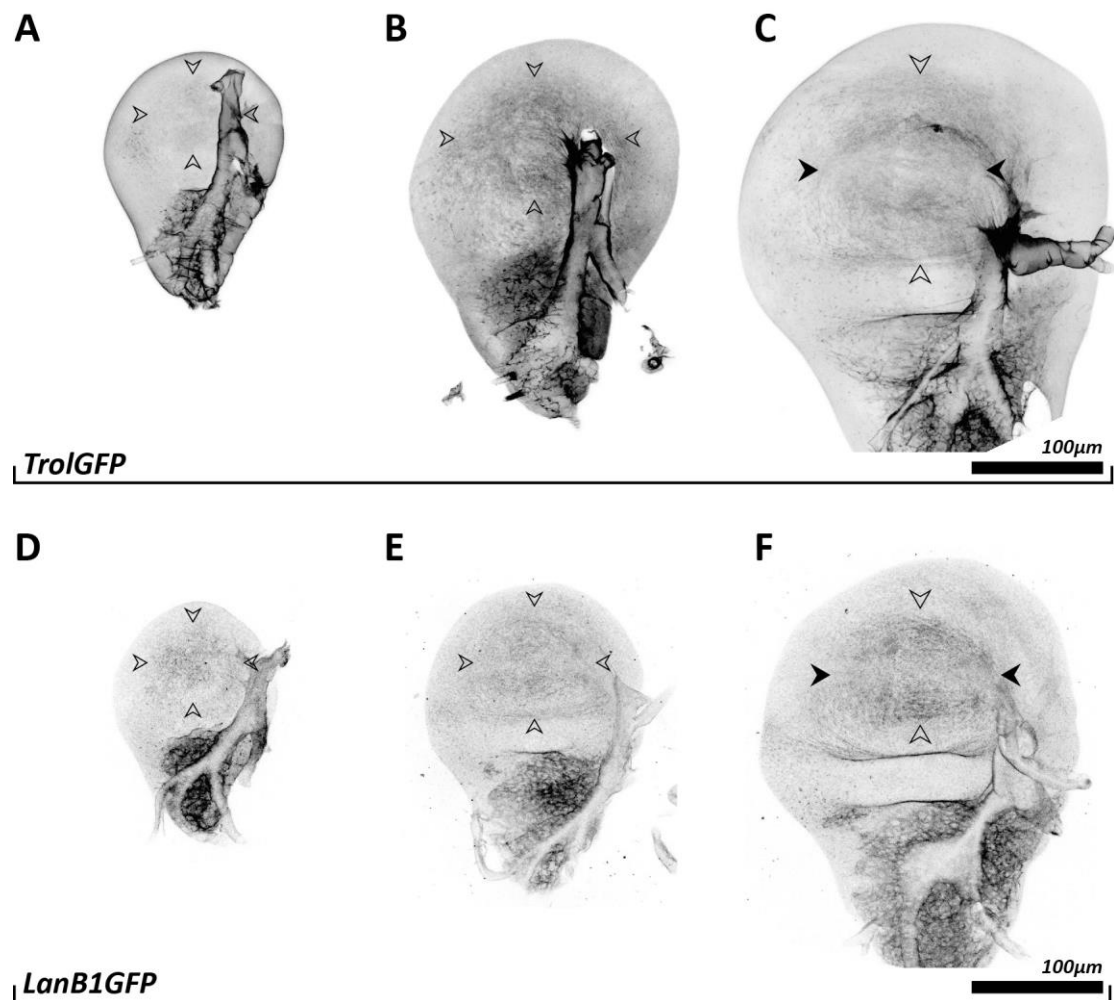


Figure 10. *Perlecan and laminin appear continuous across the wing disc extra-cellular matrix. A – C* shows perlecan distribution in the ECM of wing discs of increasing age. **D – F** shows laminin distribution in the ECM of wing discs of increasing age. **A** and **D** are approximately 72h AEL, **B** and **E** are approximately 84h AEL and **C** and **F** are approximately 96h AEL. Region enclosed by arrows indicate more concentrated perlecan and laminin in the pouch. Pairs of inverted black arrows in **C** and **F** subtend bands of reduced perlecan and laminin respectively. All wing discs have been imaged live.

At the notum, myoepithelial cells line the basal surface of the columnar epithelium, and appear as an aggregation of spherical cells, indicated by black arrows in Figure 8 C'. These myoepithelial cells appear completely covered in ECM, Figure 8 D'' indicated by black arrows, possibly due to the lack of polarity suggested by their spherical shape. Again, the ECM covering these cells are of higher curvature, so

might be of different mechanical properties. It may be more likely the myoepithelial ECM is different given the considerable difference in cell type to the epithelium. Laminin, and to a lesser extent perlecan, are much more concentrated around the myoepithelial cells compared with other regions of the wing disc Figure 10. Remaining trachea also attaches around this area. It has been previously shown the ECM requires different regulation at points where trachea and columnar epithelium meet to adhere the ECMs of these two cell layers ^[148]. If so, a similar process may be at play between apposing columnar epithelia at the hinge.

With increased resolution, finer structure is observed in the ECM. Around the pouch area collagen appears to form fibres of high fluorescence, Figure 11 A. It is unclear how these fibres connect with the otherwise uniform, sheet-like fluorescence signal. They may be agglomerations of collagen fibrils, perhaps aligned to form fibres. Alternatively they could be 'ruffles' in the sheet that appear brighter by overlaying each other in the plane.

From images of fluorescently labelled integrin subunits it can be seen that integrins appear to form clusters, Figure 12. Generally, a single cluster appears to form for each cell. These clusters appear fairly uniformly across the columnar epithelium, but with some variation in size and shape. Integrin clusters show some co-localisation with collagen fibres, indicated by white arrows in Figure 13 A'''. Some collagen fibres appear to subtend integrin clusters, and collagen fibres appear denser in regions with more integrin clusters. From images of fluorescently labelled actin filaments, it appears cortical actin on the basal surface form a range of structures. Often actin filaments form asters Figure 14 B, C, possibly co-localising with integrin clusters. Actin filaments also form waves of aligned bundles Figure 14 A. These bundles appear partially aligned with collagen fibres, however, actin structures also appear more dense where collagen structures are less dense. Myosin forms high-concentration ring-like structures on the basal surface of cells Figure 15, and there appears to be a single ringlet per cell. Like integrin clusters, these ringlets can vary in size and shape

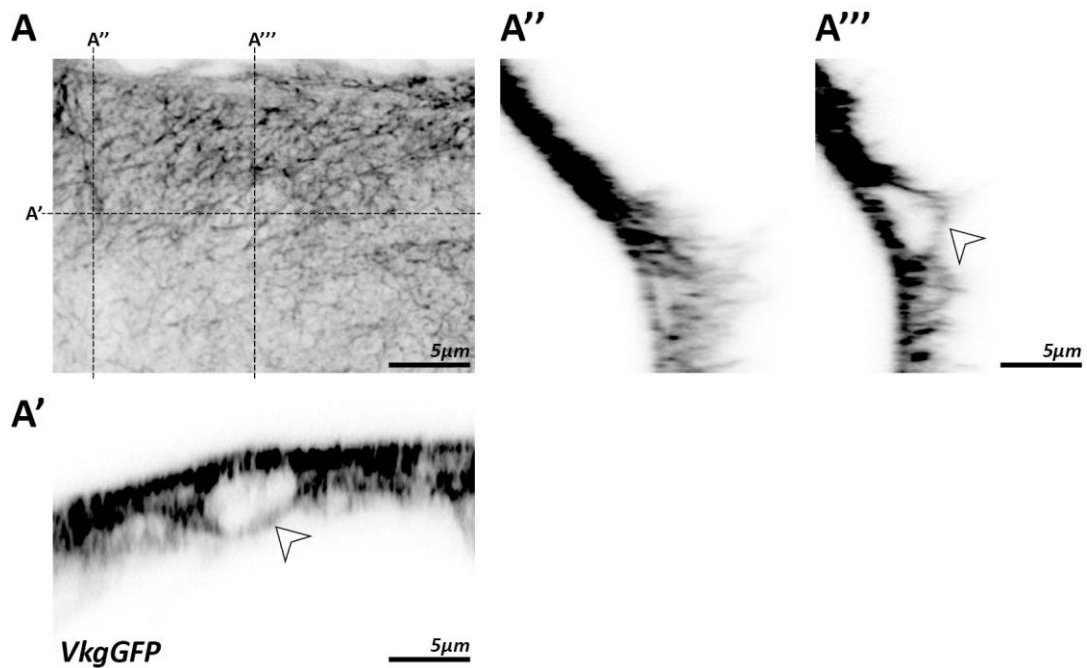


Figure 11. The extra-cellular matrix appears to exhibit a fibrous and layered structure. **A** shows the high magnification maximum projection of VkgGFP in the pouch region of a mature wing disc. Dotted lines on **A** indicate sections shown in **A'**, **A''** and **A'''** of the image stack. Arrows in **A'** and **A'''** indicate transverse holes in the ECM layer.

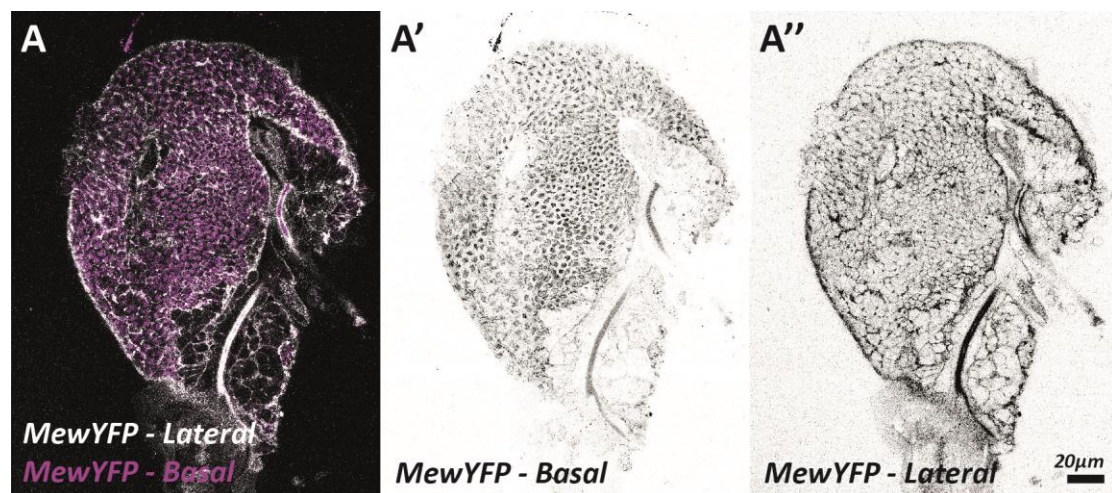


Figure 12. Integrins form clusters, with one cluster centred at the basal surface of each cell. **A** shows an approximately 72h AEL wing disc with basal integrin clusters and cell outlines marked with lateral integrin. **A'** shows basal integrin alone, basal integrin was obtained by maximum projection. **A''** shows lateral integrin obtained by taking a slice above the basal surface of the wing disc. Lateral integrin is much lower concentration than basal, so has been artificially increased in brightness.

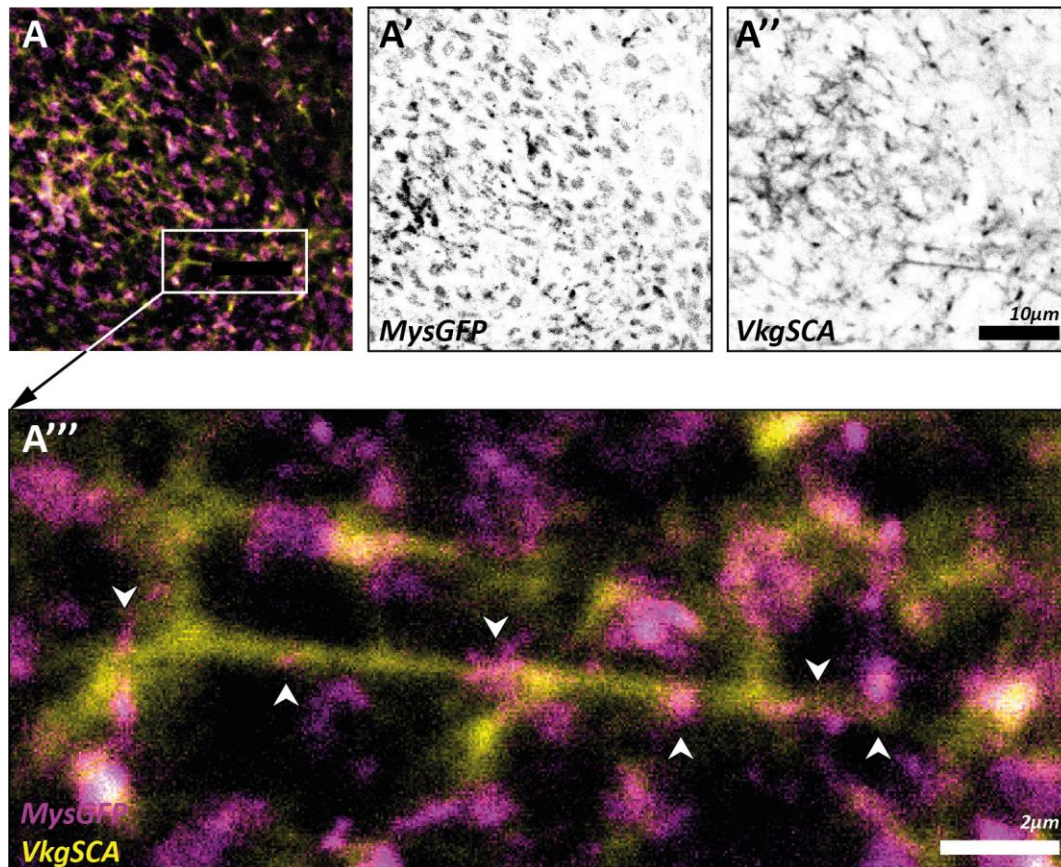


Figure 13. Collagen fibres show some co-localisation with integrin clusters. **A** shows an example of high resolution images of integrin (Mys) and collagen (Vkg) in the wing disc pouch. **A'** and **A''** show separated integrin and collagen channels respectively of composite image **A**. **A'''** shows a magnified view of a collagen fibre in **A**, integrin clusters that appear to colocalise with this collagen fibre are indicated by white arrows. All wing discs are imaged live.

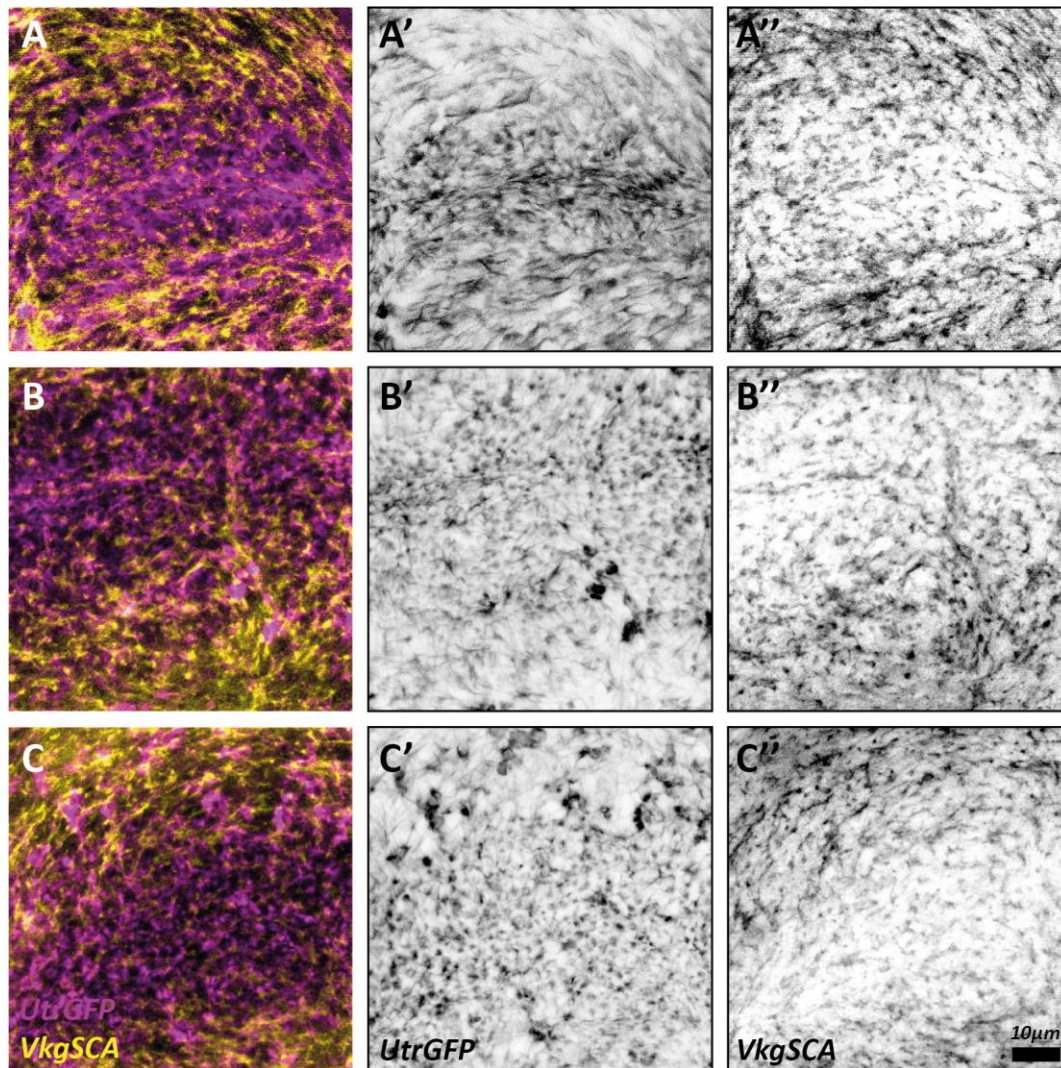


Figure 14. Actin filaments form a variety of ordered structures on the basal surface of cells. **A – C** show three examples of high resolution images of filamentous actin (Utr) and collagen (Vkg) in the pouch ECM. **A' – C'** and **A'' – C''** show separated filamentous actin and collagen channels respectively of composite images **A – C**. All wing discs are imaged live.

Even at high resolution, detailed structure of the ECM is hard to discern. Using electron microscopy, much more detail can be seen, and shows the ECM is much more heterogeneous than light microscopy suggests. Electron micrographs of the ECM of the wing disc pouch at three ages, 72h, 96h, 120h AEL, are shown in Figure 16 B, C, D. At all three ages the ECM appears as a nanometres-thick layer of electron-dense material separated by electron-diffuse gaps. Generally, the outer electron-dense layer is thicker than any inner layers. For 72h AEL wing discs, few inner

electron-dense layers are observed, and the outer layer makes multiple contacts with the cells, Figure 16 B. Electron-diffuse gaps can be seen, especially at boundaries between cells. For 96h AEL wing discs, more inner electron-dense layers appear, forming a buffer between the outer layer and cell surfaces, Figure 16 C. For 120h AEL wing discs this buffer has grown considerably, and the basal surface of cells appear to inter-digitate with inner electron-dense layers of ECM, Figure 16 D. The distance between basal cell surface and the nearest outer electron-dense layer of ECM is quantified in Figure 16 A. Quantified this way, the pouch ECM thickness at 72h, 96h and 120h AEL were found to be $(0.11\pm 0.04)\mu\text{m}$, $(0.3\pm 0.2)\mu\text{m}$ and $(1.1\pm 0.8)\mu\text{m}$ respectively. The mean thickness of the ECM as quantified this way, increases with the age of the disc. However, the variance also increases considerably, reducing the significance of the difference between these distributions. Different maturation behaviour is observed in the protruding part of the hinge, as shown in Figure 17 B, C. The hinge ECM thickness at 96h and 120h was measured to be $(0.14\pm 0.02)\mu\text{m}$ and $(0.31\pm 0.09)\mu\text{m}$ respectively. The thickness of the ECM at the Hinge at both 96h and 120h AEL is comparable to the thickness of the pouch ECM at 72h AEL Figure 17 A. Between 96h AEL and 120h AEL the ECM thickness increases very little. The peripodial ECM thickness at 72h has been measured to be $(0.10\pm 0.04)\mu\text{m}$.

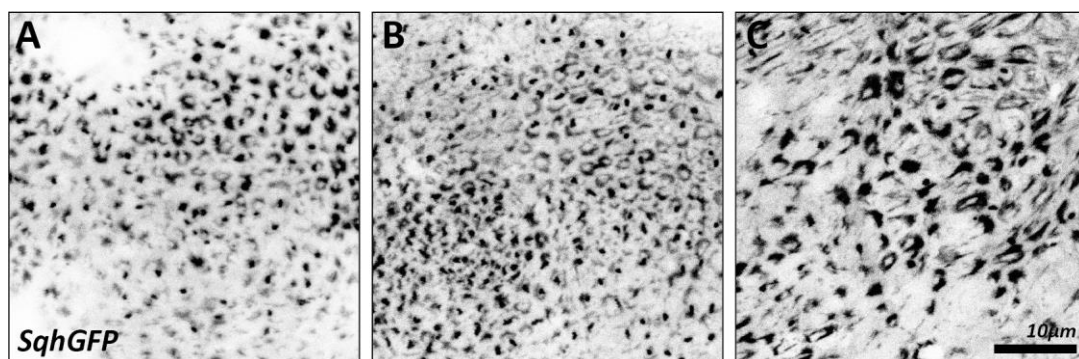


Figure 15. *Myosin forms ringlets on the basal surface of cells.* A – C show summation projections of myosin (Sqh) on the basal surface of the pouch of three different wing discs. All wing discs are imaged live.

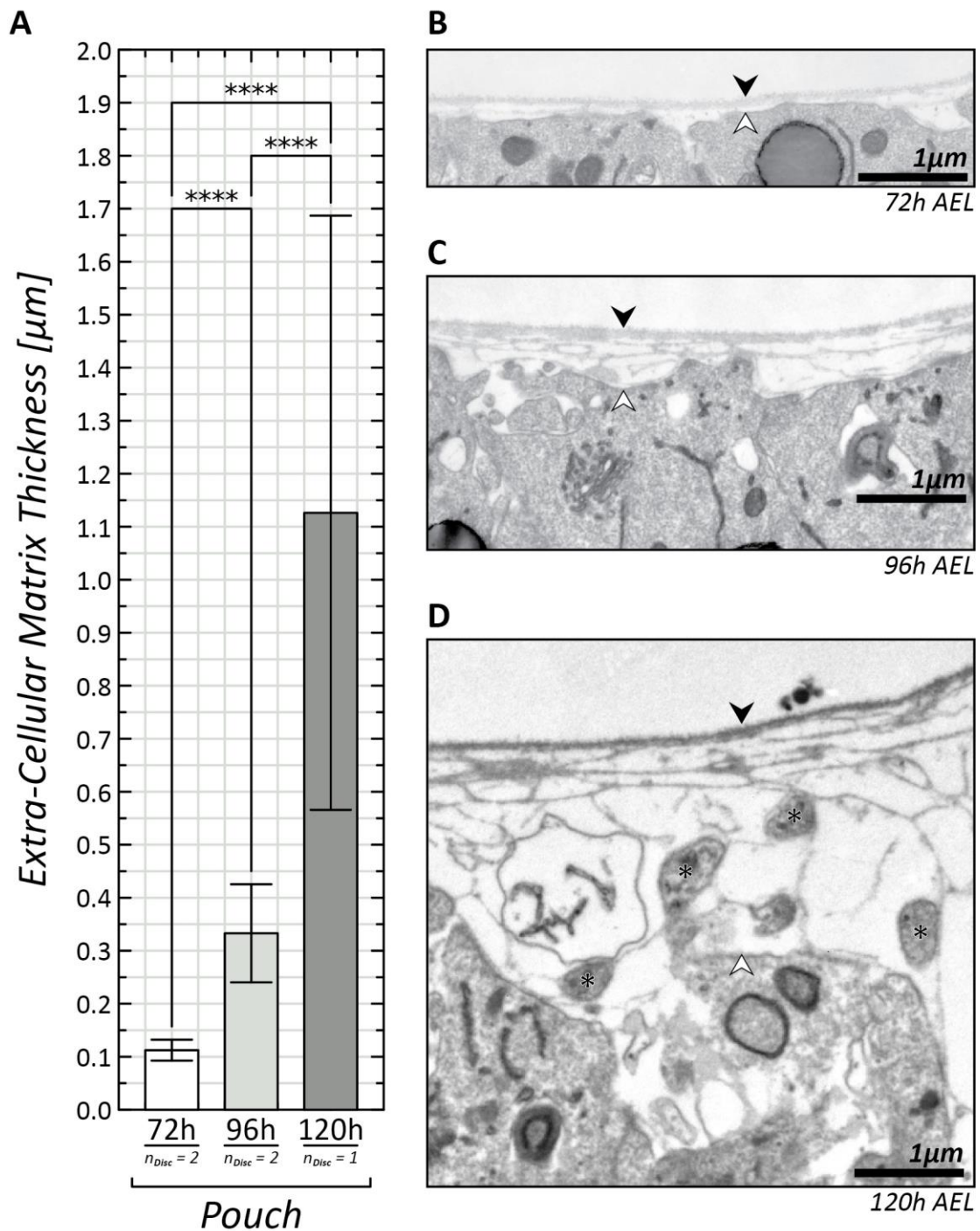


Figure 16. The extra-cellular matrix at the pouch becomes thicker as the wing disc ages. **A** shows measurements of ECM thickness obtained from electron micrographs around the pouch region of wing discs taken from larvae approximately 72h, 96h and 120h AEL. **B**, **C** and **D** show example electron micrographs of pouch ECM at 72h, 96h and 120h AEL respectively. Hollow and filled arrows show in **B**, **C** and **D** indicate the inner and outer surfaces of the ECM respectively. Asterisks indicate putative cellular protrusions into the ECM.

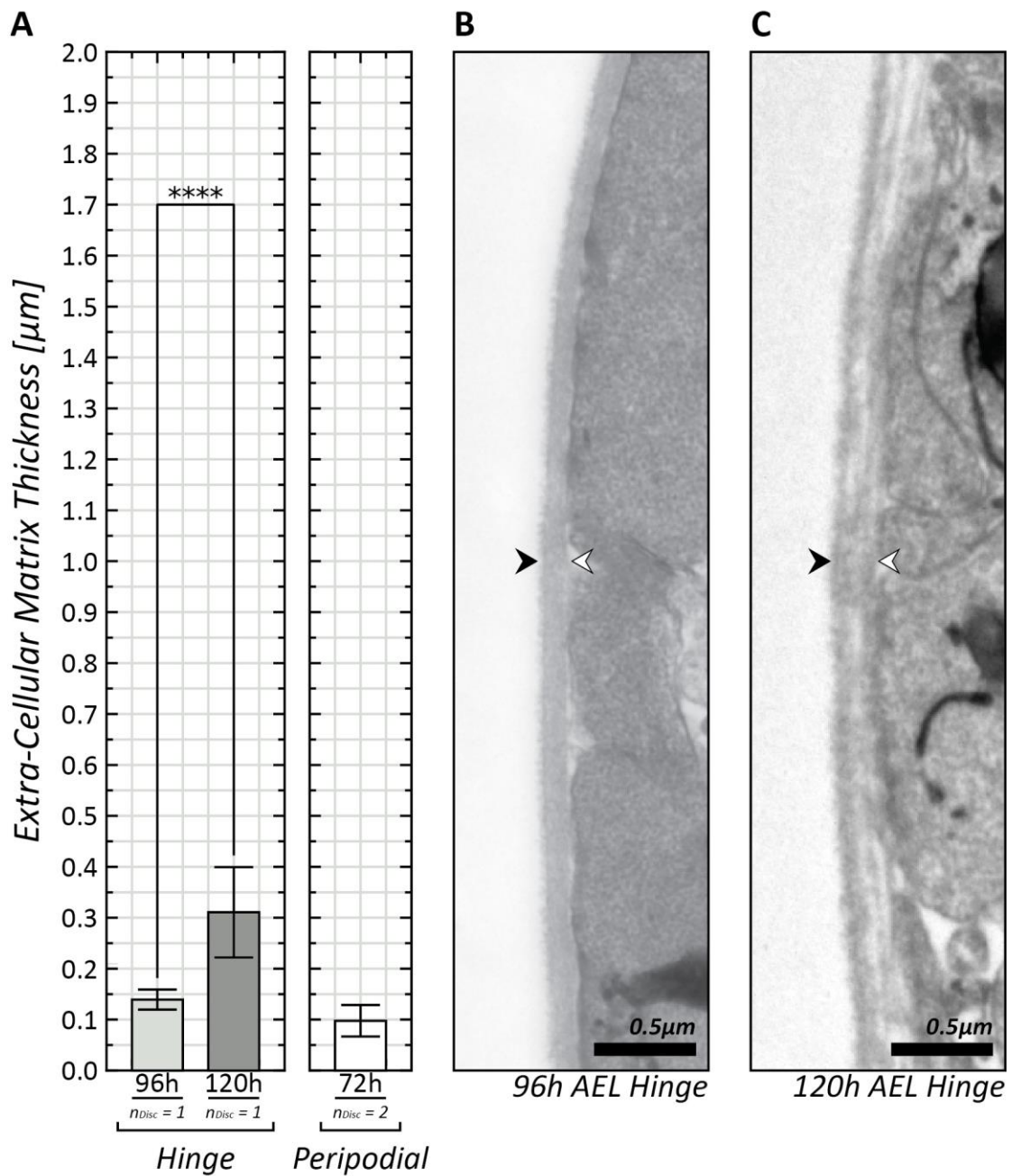


Figure 17. Extra-cellular matrix thickness at the peripodial epithelium and hinge of the columnar epithelium are thinner than at the pouch. **A** shows measurements of ECM thickness obtained from electron micrographs of the hinge of the columnar epithelium and peripodial epithelium at various larval ages. **B** and **C** are example electron micrographs of the hinge ECM at approximately 96h and 120h AEL respectively. Hollow and filled arrows show in **B** and **C** indicate the inner and outer surfaces of the ECM respectively.

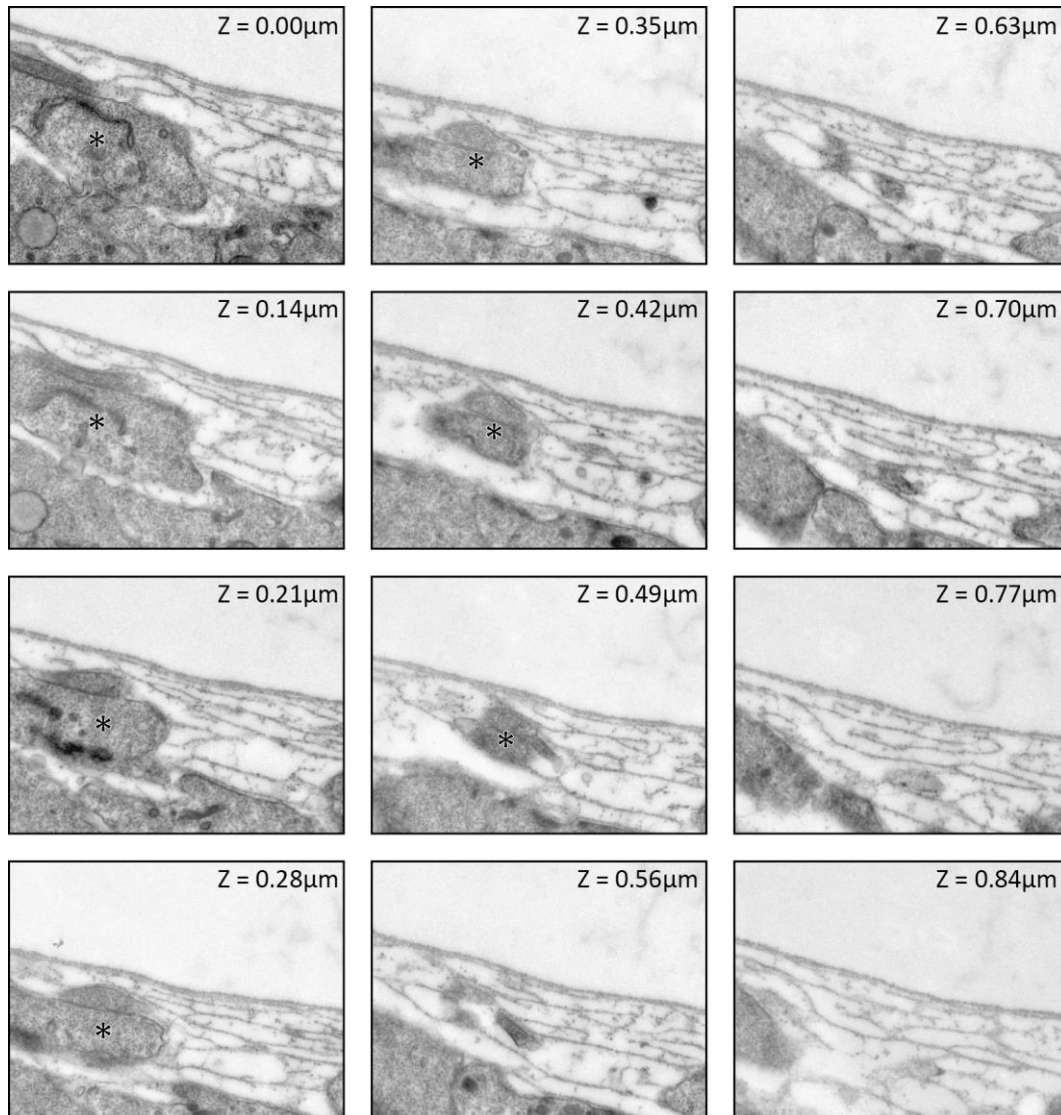


Figure 18. Cellular protrusions pass through layers of the extra-cellular matrix. A series of electron micrograph sections through the ECM are shown with the depth indicated. Asterisks indicate a single cellular protrusion as it passes through the ECM.

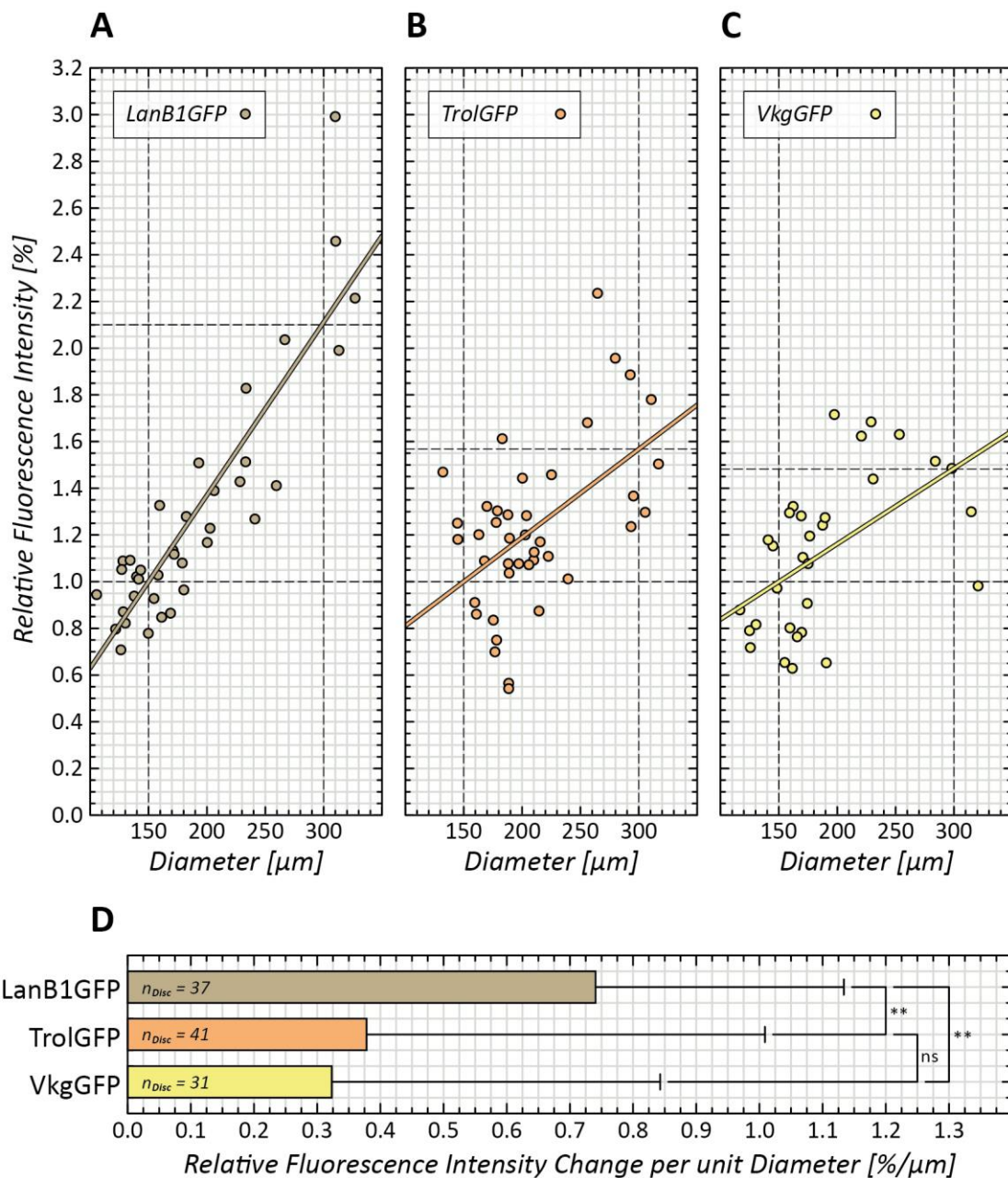


Figure 19. Collagen, laminin and perlecan concentrations increase per unit area of extra-cellular matrix as the wing disc grows in size. **A – C** are scatter plots of relative fluorescence intensity against characteristic diameter for each wing disc for laminin (LanB1), perlecan (Trol) and collagen (Vkg) respectively. Solid lines in **A – C** are linear fits to the data. Relative fluorescence intensity is the measured fluorescence intensity normalised by the fluorescence intensity at 150 μm characteristic diameter estimated by the linear fit. **D** shows the rate of change in fluorescence intensity with respect to the characteristic diameter.

Given the clear increase in ECM thickness with increasing wing disc age observed in Figure 16 A, I was interested to know how concentrations of ECM components would change too. Change in fluorescence intensity of laminin, perlecan and collagen with wing disc size are shown in Figure 19 A – C. All three components appear to increase with wing disc size. The rates of fluorescence intensity change with respect to wing disc size are shown in Figure 19 D. Estimated change in fluorescence intensity with characteristic diameter for laminin, perlecan and collagen are $(0.74 \pm 0.06)\%/ \mu\text{m}$, $(0.38 \pm 0.10)\%/ \mu\text{m}$ and $(0.32 \pm 0.09)\%/ \mu\text{m}$. Laminin fluorescence intensity increases at a significantly greater rate than collagen and perlecan, which increase with similar rates.

2.1.3 Discussion

In this section I have found that the structure of the ECM changes considerably with wing disc age. At early ages the wing disc ECM forms a single electron-dense layer covering the basal surface of the epithelium. As the wing disc ages the single electron-dense layer delaminates, forming multiple electron-dense layers separated by electron-diffuse spaces. At later ages the electron-diffuse spaces become much larger, allowing the electron-dense layers to become much more three-dimensional. At all ages a single thick electron-dense layer is observed on the outer-most surface of the ECM and another electron-dense layer is observed on the inner-most surface making contact with cell surfaces. Also at later ages, cellular protrusions appear to pass between electron-dense layers of the ECM. Concentrations of laminin, perlecan and collagen increase with wing disc age, although it is unclear if these concentration increases are proportional to the overall increase in ECM thickness. Laminin concentration increases at approximately twice the rate of perlecan and collagen suggesting some complexity to the localisation of these ECM components within the layered ECM structure.

The thickness of the ECM also varies spatially. Wing discs have on average a thinner ECM at the hinge than at the pouch. It may be that the process of fixation, especially the complex fixation for electron microscopy, may introduce artefacts, as has been mentioned in the methods of this section. However, assuming these images are representative of live, one interpretation is that the hinge ECM is under tension, which pulls the electron-dense layers taut, while the pouch ECM is relaxed, allowing layers to separate. Similarly, increase in curvature from pouch to hinge may contribute to changes in morphology. Alternatively, delamination of electron-dense layers may be induced by dynamics at the basal surface of the cells. Basal surfaces of pouch cells at 120h AEL appear to form protrusions that move laterally through inner electron-dense layers of ECM Figure 16 D. Sections of these protrusions can be seen as blobs of cell floating between inner layers of ECM. It is possible these protrusions are actively delaminating electron-dense layers of ECM. By comparison, basal surfaces of hinge cells at 120h AEL are smooth. It is unclear whether changes in basal cell surface morphology induce ECM delamination or vice-versa, or whether they are both reacting to some external factor such as a local compression of the tissue. There is some evidence that basal cellular protrusions are present in live wing discs, as indicated by arrows in Figure 11 A' and A''. In these high resolution sections, a protrusion-shaped gap can be seen passing through the collagen. These sections also show spikes of collagen pointing toward the cellular mass, which could be ECM squeezing between gaps between cells.

When ECM component fluorescence intensity is measured as the sum over the depth of the ECM, as done in Figure 19, we cannot infer whether concentration of the component changes with age, because the depth of the ECM may also change, and electron microscopy results suggest ECM depth does change with age, Figure 16. Given these measurements suggest both quantity of ECM component and ECM depth increase with age, it may be that concentrations remain constant. However, this cannot be determined with these results, especially given the heterogenous structure of the ECM, and the different rates of increase of different ECM components.

Spatially, ECM component concentrations appear to change across the columnar ECM, and these changes may coincide with compartment boundaries, indicated by black arrows in Figure 9 B'', C'', Figure 10 C, F. This suggests the overlying cells are differentially regulating the structure of the ECM in these areas. These particular cells definitely have different fates than their neighbours given they express Dpp and Wg morphogens. It may be they express Mmps, which would degrade the ECM and make it more diffuse in their vicinity. However, the ECM below these compartment boundaries may be the normal ECM state given other ECM in the periphery of the pouch and at the hinge have similar concentrations. Therefore it may be the pouch that is unique in sequestering more ECM. In fact, increases in ECM component concentration in the pouch appear to be a result of fibrous collagen structure, suggesting some differential ECM regulation in this area.

Integrins form a cluster at the basal surface of each cell, Figure 12. Myosin forms a ring at the basal surface of each cell Figure 15, possibly around the integrin cluster, although this has not been determined. Cortical actin appears to form fibres that run along the basal surface of cells such that it is hard to discern cell boundaries, Figure 14 A. These actin fibres also appear to be ordered relative to collagen fibres but, again, further analysis would be required to determine correlation between the two. Cortical actin also appears to sometimes form asters, Figure 14 B, C, which may co-localise with myosin rings, integrin clusters or both. Collagen fibres appear to sometimes co-localise with integrin clusters, although the frequency of these events has not been quantified. These fibres may be generated by integrins, particularly during cellular reorganisation such as cell division. Alternatively, these fibres could result from cell apoptosis, however apoptosis is not thought to be a regular occurrence in the wing disc^[168]. If collagen fibres were generated by cell division, then it would explain why the compartment boundaries exhibit far less fibres, because cells in these compartment boundaries have been shown to proliferate far less than normal^[28].

2.2 Results Section 2: Perturbations to the wing disc extra-cellular matrix

This section is concerned with applying ECM-related perturbations to the wing disc and using the resulting response to help understand the role of the ECM. A coarse method I have used is to remove the ECM entirely by degrading it using proteases *ex vivo*. More specific proteases can degrade specific ECM components. I am also interested in the interplay between cellular mechanics and the ECM, so I have also used drugs targeting cortical machinery. Using genetic perturbations I have been able to inhibit or promote production of specific ECM components *in vivo* and observe their effect on wing disc morphology. It is also possible to apply genetic perturbations with temporal control, allowing more subtle dynamic effects to be determined.

2.2.1 Methods

Fly lines

Binary expression systems are genetic tools used extensively in flies. They are composed of two inserted sequences, a transcriptional activator and its target promoter. The most ubiquitous binary expression system in flies is the Gal4-UAS system^[169]. The transcriptional activator, Gal4, is usually placed under the control of an effector of a gene with a desired expression pattern. The target promoter, UAS, is placed in control of some transgene of interest. In cells where Gal4 is expressed, it activates UAS, which in turn drives expression of the transgene. The transgene is therefore expressed in the desired pattern. The utility of binary expression systems is their modularity. Collections of fly lines have been established with Gal4 under the control of different effectors. Any Gal4 line can be crossed with a line containing a UAS promoted transgene to quickly express that transgene in a tissue of choice. Other binary expression systems include LexA-LexO and QF-QUAS, which along with

Gal4-UAS, act independently of one another, allowing different transgenes to be expressed in patterns simultaneously. A transcriptional repressor, Gal80, provides further utility. Gal80 is usually placed directly under the control of a desired effector. Where Gal80 is expressed, Gal4 activation of UAS is repressed, allowing further refinement of the transgene expression pattern. Furthermore, a temperature sensitive variant, Gal80ts, can be switched from active to inactive *via* a temperature change from 18°C to 29°C, allowing direct temporal control of transgene expression [170].

A common way to prevent cells from producing a certain protein is *via* RNA interference (RNAi). Short interfering RNA are short double-stranded fragments of a target gene RNA. When present in a cell, short interfering RNA are incorporated into endogenous gene-silencing machines called RNAi-induced silencing complexes. These complexes then bind and degrade messenger RNA of the target gene, preventing translation [171]. A synthetic sequence coding for precursors of short interfering RNA can be inserted into fly DNA. An inserted RNAi gene is usually placed under a UAS promoter to allow expression to be controlled both spatially and temporally. RNAi is usually referred to as a knockdown, rather than a knockout for null-mutants, because silencing of the gene is not complete. Different RNAis can have different knockdown efficiencies. Efficiency depends on the region of the target gene used. When RNAi are designed, the target sequence is chosen to cover as many isoforms of the gene as possible. Efficiency also depends on where in the DNA the RNAi sequence is inserted. In many collections of RNAi fly lines the sequence is targeted to a specific location, so that expression levels remain consistent between lines [172].

To start inferring functions of ECM proteins in the wing disc, I have knocked down their expression using RNAi. For this screen I have used Gal4 under the control of Actin5C (Act-Gal4; FBID: *FBti0012293*) effector to drive RNAi against ECM proteins fairly ubiquitously in the organism, throughout development. The RNAi lines I have used are UAS-VkgRNAi (VDRC 106812, FBID: *FBti0123104*), UAS-TroIRNAi (VDRC 24549, FBID: *FBti0096489*), UAS-LanB1RNAi (VDRC 23119, FBID: *FBti0082958*), UAS-

LanB2RNAi (VDRC 42559, FBID: *FBti0089007*), UAS-LanARNAi (VDRC 18873, FBID: *FBti0093928*), UAS-WbRNAi (VDRC 3141, FBID: *FBti0085776*), UAS-NdgrRNAi (VDRC 109625, FBID: *FBti0141528*), UAS-Mmp1RNAi (BDSC 31489, FBID: *FBti0130783*) and UAS-Mmp2RNAi (BDSC 31371, FBID: *FBti0130784*). Other transgenic lines I have used are UAS-Trol (DGRC 201233, FBID: *FBti0109477*), UAS-Mmp1 (BDSC 58702, FBID: *FBti0164924*) and UAS-Mmp2 (BDSC 58704, FBID: *FBti0164926*). A dominant negative chimera of Myspheroid is the cytoplasmic domain fused the trans-membrane domain of another protein. This chimeric MysDN can dimerise and has been shown to recover some signalling of wild type Mys, however it cannot bind ECM proteins because it contains no extra-cellular domain^[77]. UAS-MysDN, was a gift from Maria Martin-Bermudo.

Confocal Microscopy

For screening morphological phenotypes, dissected wing discs were fixed, stained and mounted for confocal imaging. To fix, dissected wing discs were treated with 4% PFA in PBS for 30 minutes, then washed three to four times with either PBS or PBT. PBT is 0.3% Triton (Triton X-100, Sigma Aldrich) dissolved in PBS. Fixed discs were then stained with a mixture of Phalloidin 647 at 1:200 and DAPI at 1:1000 for 30 minutes, and then washed three to four times with PBS. Wing discs were fixed and stained in concave glass wells. To mount, strips of double-sided sticky tape were stuck to a glass slide, with a gap of approximately 2mm forming channels parallel to the short edge of the slide. Channels were then filled with fluoromount. Fixed and stained wing discs were moved from their glass wells to a blob of fluoromount on a spare slide, transferring as little PBS as possible. From the blob of fluoromount on the slide, wing discs were transferred to the fluoromount in the channel using forceps. Once all wing discs were transferred to the channel, the fluoromount was allowed to set for approximately 40 minutes, before covering with a glass coverslip. Approximately 10-20 wing discs were dissected for each genotype. Often, multiple genotypes were mounted onto a single slide with multiple channels, one genotype for each channel.

Fixed wing discs were imaged on a Leica SP8 inverted, confocal microscope. A stack of images was taken for each wing disc with a 40x oil objective at 0.75x digital zoom. To automate imaging, a stack was first set up for each wing disc, then each stack was automatically imaged in turn over night. Leica software saves all these stacks in a single proprietary image file, which was automatically broken down into one tiff image file per stack using an FIJI script. From these individual stack files, sections and projections were taken manually using FIJI.

Treatment Protocols

To remove the ECM I have used Collagenase. Collagenase is perhaps incorrectly named because it gives the impression of a collagen-specific protease, however it does not degrade collagen alone. Most commercially bought collagenases are blends of proteases designed for dissociating cells in culture and tissues. There are many different blends of collagenase, with each variant supposedly better suited to a certain cell or tissue type. The variant I have used is CLS-1 (Worthington). CLS-1 is listed as containing collagenase, caseinase, clostripain and trypsin. The collagenase ingredient in CLS-1 is composed of two isoforms of a collagenase from an unspecified source, which is expected to cleave collagen preferentially at a bond between glycine and a neutral residue. So although this collagenase contains a supposedly collagen-specific protease, the other proteases packaged with it will contribute to non-specific proteolysis.

A published collagenase treatment protocol ^[16] involves dissecting wing discs in PBS, then applying collagenase at 0.5% in PBS at 37°C for 1 minute. The collagenase they used is different to the one used here, so to determine a concentration of CLS-1 to use, I calculated the activity of the collagenase used in the published protocol and used the concentration of CLS-1 that should give the same activity. The activity I calculated was approximately 125 U/mg, giving me a CLS-1 concentration of 1.62 mg/mL. As discussed previously, I expect media to better approximate *in vivo*

osmolarity than PBS, so I further deviated from the published protocol by dissolving the CLS-1 in media, therefore keeping wing discs in media at all times. To determine if the CLS-1 concentration was sufficient to degrade the ECM, I applied single, double and half concentrations to wing discs and found the single concentration almost completely eliminated the VkgGFP fluorescence signal from wing discs. I assume the high temperature used in the published protocol is to increase the rate of proteolysis, however I found this step unnecessary and achieved complete ECM degradation within minutes. So finally, the protocol I have used for all wing disc collagenase treatments is 1.62 mg/mL CLS-1 in media for 5 minutes at room temperature. The CLS-1 is shipped as dry flakes in a glass pot, which is stored at 4°C. Before treatment the CLS-1 flakes are dissolved in media to the right concentration, this mixture is kept for no longer than a day in case of collagenase activity decay. The treatment was applied to wing discs in glass wells, and was washed away by replacing with media four to five times.

As expected, I found CLS-1 to degrade many ECM components with the protocol described, showing it is not specific to collagen. Another variant of collagenase, CLSPA (Worthington) has much lower levels of non-collagenase proteases, which I hoped would be more specific. Treating wing discs with CLSPA at the same activity as CLS-1, I found the degradation was much slower, taking up to an hour for the VkgGFP signal to completely degrade. Treating wing discs with CLSPA at 1000 U/mL, VkgGFP signal was lost much quicker, over about 10 minutes. However, at this higher concentration LanB1GFP signal was also lost over a similar time frame. Hence I found CLSPA to be both unspecific to collagen and weaker than CLS1. It may be that the secondary proteases are still effective at this concentration. If so, at lower concentrations, CLSPA may still cleave collagen, but the cleaved collagen remains bound to the ECM by other intact components, and so retaining the VkgGFP signal. Alternatively, the collagenase component of CLSPA itself can target other ECM components as substrates for degradation. Another collagenase variant, Dispase 1 (Sigma-Aldrich), is an unknown proprietary blend. Wing discs treated with Dispase 1 at 0.2 mg/mL in media for 5 minutes were able to eliminate VkgGFP and LanB1GFP

signals. In the end I decided to proceed with CLS-1 as my collagenase treatment, and accept that it degrades the ECM as a whole.

I have used a heparanase to degrade the heparan-sulphate side-chains associated with Perlecan and other proteoglycans. I have used a Heparanase I and III blend (H3917, Sigma-Aldrich). HS3917 is shipped as a powder, which I dissolved to a 0.5mg/mL in PBS stock solution stored at -20°C. I treated wing discs with HS3917 diluted to 0.025mg/mL in media for 20 minutes. Heparanase action was confirmed by staining for cleaved heparan-sulphate chains using anti-heparan-sulphate (3G10, Amsbio).

I have used Rok inhibitor Y27632 (Y0503, Sigma-Aldrich) to reduce cell contractility. The effect of Y27632 has been previously established in the wing disc ^[173], and I use these concentrations as a guide. Y27632 is shipped as a powder, which is dissolved to 9.62 g/mL (20mM) in distilled water, and stored at -20°C. To treat wing discs, stock Y27632 is diluted to 1.60 g/mL (5mM) in media. Wing discs are maintained in Y27632 throughout the given experiment, and any measurements or fixation are applied after an initial incubation period of at least 20 minutes.

I have used Latrunculin-A (L5163, Sigma-Aldrich) to inhibit polymerisation of Actin into filaments. The effect of Latrunculin-A has been established in the wing disc ^[173], and I use these concentrations as a guide. Latrunculin-A is shipped as a powder, which is dissolved to 422 mg/mL (10mM) in ethanol and stored at -20°C. To treat wing discs, stock Latrunculin-A is further dissolved to 4.22 mg/mL (100µM) in media. Wing discs are maintained in Latrunculin-A throughout the given experiment, and any measurements or fixation are applied after an initial incubation period of at least 20 minutes.

I was interested in finding a treatment similar to CLS-1 or Y27632 that disrupts the ability of integrins to bind to the ECM. Initial research led me to the disintegrin Echistatin (E1518, Sigma-Aldrich), derived from snake venom. When injected into mammals, Echistatin targets platelets, preventing their aggregation by preferentially

binding and blocking their integrins. Echistatin is used in cell culture to help dissociate cells, like collagenase. Echistatin is shipped as a powder, which I dissolved to 0.01 mg/mL in distilled water, and stored at -20°C. As a first approach, I simply treated wing discs with Echistatin at a high concentration of 0.5 µg/mL in media to attempt to observe any effect on morphology down the dissection microscope. Unfortunately I observed no effect on wing disc morphology.

A possible reason for a lack of phenotype associated with Echistatin is its integrin specificity. Echistatin contains an RGD sequence, which, as described previously, §1.4.1, is present in Wb, one of two laminin alpha subunits. This RGD sequence is expected to bind integrins containing If, one of the two integrin alpha subunits known to be present in the wing disc. Therefore, Echistatin should only bind a subset of integrins. To block all integrin activity in the wing disc would require a mixture of disintegrins that together would target all integrin types simultaneously. Integrins are of great interest due to their use as therapeutics ^[174]. Many different disintegrins have been isolated from snake venoms ^[175], and most of these disintegrins target RGD-binding integrins. However, some target non-RGD binding integrins, and some even bind RGD-binding integrins in a non-RGD-dependent manner, such as Lebein-2 and Lebein-1 respectively. It has been established that Lebein-1 and Lebein-2 are specific to mammalian $\alpha 3\beta 1$, $\alpha 6\beta 1$ and $\alpha 7\beta 1$ integrins, which are the closest homologs to *Drosophila* Mew-Mys integrins ^[176]. Echistatin has been found to bind mammalian $\alpha 5\beta 1$ amongst other integrins ^[177], which is a reasonably close homolog to If-Mys. Another disintegrin, Ocellatusin has also been found to bind mammalian $\alpha 5\beta 1$ integrin ^[178] but with a greater potency than Echistatin. My concern with these RGD-binding disintegrins is if they are highly specific to a given mammalian integrin, they are unlikely to work on the *Drosophila* homolog due to what I presume are considerable genetic differences. A best bet would be a disintegrin that has been shown to work on all the closest mammalian homologs to If-Mys, like the Lebeins have with Mew-Mys mammalian homologs. I have yet to find a disintegrin that suits If-Mys in this way. Also Lebeins are not commercially available. For these reasons, I have not progressed any further with disintegrin treatments.

I have killed cells by permeabilising them using a high concentration of the surfactant Triton (Triton X-100, Sigma Aldrich). To degrade cells I immersed wing discs in approximately 3% Triton in PBS for 10 minutes, before washing resultant ECM shells four or five times with PBS.

Temperature shift

To avoid the pre-larval lethality of some genetic perturbations I have made use of Gal80ts, which is a temperature sensitive variant of Gal80. At around 18°C, Gal80ts is active and inhibits the Gal4 activation domain from initiating transcription of a transgene. At around 29°C, Gal80ts is deactivated, allowing Gal4 to drive transcription of a transgene. By keeping flies at 18°C, otherwise lethal UAS-driven transgenes can be kept silent allowing flies to develop through to larval stages, then shifting larvae to 29°C can activate the transgene to observe its effect on wing discs.

I first applied temperature shift experiments in an attempt to observe morphological phenotypes of the wing disc. However, after applying some knockdowns for 24h or more I found no observable phenotype, for example when using UAS-LanB1RNAi. I considered the lack of phenotype could be due to the given protein not being important for wing disc morphology. I also considered that the knockdowns could be much weaker in larval compared with embryonic stages. Another possibility is that ECM proteins are considerably stable, and that knockdown periods of days is not enough to eliminate them. With all these possibilities, I decided I wanted to directly observe the effect of certain knockdowns directly by combining a protein knockdown with its corresponding fluorescently labelled variant. For example, driving VkgRNAi expression temporally in a VkgGFP background. By directly observing its effect, I would be able to determine if the knockdown was functioning and the timescale over which the knocked down protein would leave the ECM. I then took this further, by driving a knockdown for one protein, and observing the effect of the knockdown on a different fluorescently labelled protein. By looking at how one

ECM component is affected by another, I could infer how these components affect one another.

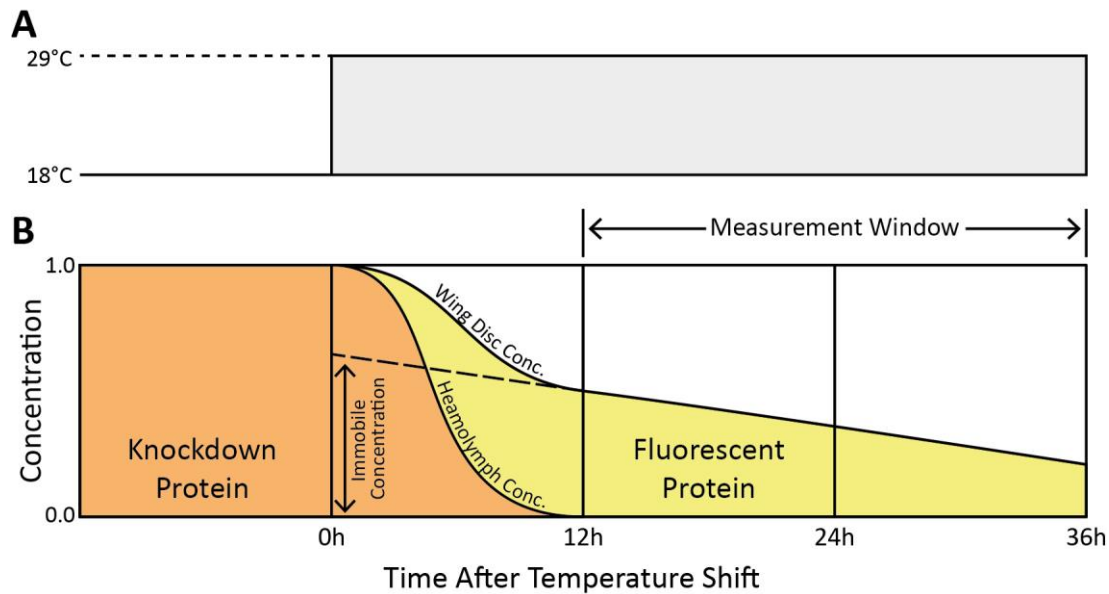


Figure 20. Using temporal knockdown, interaction between ECM proteins may be elucidated. **A**, at 0h the temperature shift is applied, moving larvae from 18°C to 29°C. **B**, Initiation of a protein knockdown at 0h induces a reduction in production of that protein. It is assumed that by 12h the concentration of the knocked down protein in the haemolymph (orange) has become negligible. Therefore the response of the fluorescently labelled protein in the wing disc ECM (yellow) after 12h is a result of only the degradation of the knocked down protein from the wing disc ECM. The immobile concentration is the amount of fluorescently labelled protein lost that is accounted for by its linear reduction in the measurement window (dashed line).

Using this method I have been able to obtain measurements of the change, and rate of change, of protein concentrations within the ECM. An assumption I have made is that the protein knockdown reaches steady state within 12 hours after the temperature shift. By steady state knockdown, I mean that protein production rates have been reduced to negligible levels, secretion of the protein by the fat body has ceased, and the concentration of the protein in the haemolymph has reach a constant negligible level. Therefore, after 12 hours the knocked down protein is no longer being added to the ECM of the wing disc, and subsequently, any measured change in concentration of the fluorescent protein is due to a change in concentration of the knocked down protein. This 12 hour assumption is based on the reported 12 hour inactivation time of Gal80ts^[179]. However, this assumption

remains untested. The expected response of a temporal protein knockdown on a fluorescently labelled protein is described in Figure 20. It may be that there is some feedback between production and deposition of ECM components, however this is hard to determine and is likely to occur at the fat body tissue not the wing disc.

To make the crosses I bred a driver fly line for each protein of interest, composed of a Gal4, TubGal80ts and the fluorescently labelled protein. I crossed virgins of fly lines containing the knockdown to males of a given driver line. I split each cross across four tubes so that I had four copies of each cross, labelled A, B, C and D. Each copy would be used for one time point in the experiment. All these tubes were kept at 18°C. I then flipped these four tubes once per day to generate a series of tubes for each copy, and I discarded tubes more than nine days old. 36 hours before dissection I transferred some tubes from 18°C to 29°C. The tubes transferred were of the correct age to be the equivalent of 72h to 120h AEL at 25°C at the time of dissection. Tubes from copies B and C were transferred from 18°C to 29°C at 24h and 12h before dissection respectively. At the time of dissection, I dissected wing discs from 29°C tubes of copies A, B and C, as well as from 18°C tubes of copy D. The wing discs were taken from larvae that were roughly equivalent in size to 96h AEL larvae at 25°C. I dissected around 8 wing discs from each copy, or time point.

Wing discs were then mounted using the piece of coverslip method described in §2.1.1. Wing discs from all time points were stuck to one piece of coverslip, but segregated into rows to identify the different time points when under the microscope. By flattening the wing discs with a piece of coverslip, the ECM around the pouch region was pushed flat up-against the bottom of the dish, which minimises the attenuation of the fluorescence signal when imaging further from the objective. Wing discs were imaged using the Zeiss LSM 880 microscope in confocal mode with a 40X oil objective at 0.6X digital zoom. Stacks of images were taken for each wing disc covering the thickness of the ECM. By imaging all time points in one dish within a few hours of each other I am minimising the effect of any variation in laser power over time.

Each image stack was then summed to obtain a single image for each wing disc. The fluorescence intensity in each summed image is a measure of the amount fluorescently tagged protein per unit area in the ECM. I obtained the average fluorescence intensity for each wing disc by measuring the mean fluorescence intensity of a circular region in the pouch using FIJI. I had therefore obtained a dataset consisting of sets of wing disc fluorescence intensities across four time points, 0h, 12h, 24h and 36h. I then normalised the fluorescence intensity of wing discs at all time points to the average wing disc fluorescence intensity of the 0h time point. Because the 0h time point represents the fluorescence intensity before knockdown, by normalising to this value I obtain the fractional change in fluorescence intensity at subsequent time points.

I then applied a linear regression to the latter three time points, 12h, 24h and 36h. From the fitted line I obtained a gradient and associated standard deviation. This gradient represents the change in fluorescence intensity, and therefore the change in protein concentration over time due to the applied genetic perturbation. Importantly, this is a measure of the fluorescence intensity change over a specific timescale, which is days. From the function of the fitted line, I obtained the predicted fluorescence intensity at the 0h time point, which I call the immobile fraction. The difference between the predicted and measured fluorescence intensity at 0h measures how much of the fluorescence intensity change at days timescales, which I am calling the immobile fraction, accounts for the fluorescence intensity change at hours timescales, which I am calling the mobile fraction. If the absolute difference is significantly less than unity, then the mobile fraction is likely to exist, in which case the rate of fluorescence intensity change is most likely described by two mechanisms, one at days timescales measured by this experiment, and one at hours timescales that is inferred by this experiment but whose exact rate is undetermined. Calling the days-timescale fluorescence intensity change immobile is obviously a misnomer given that it is mobile, but is supposed to be a reference to the part of a FRAP experiment that is usually hidden.

This process was repeated three times for each condition, obtaining three values for rate of fluorescence intensity change and three values for immobile fraction. For each condition, the mean of the three fluorescence intensity change rates and the mean of three immobile were plotted. Importantly, the fluorescence intensity used is actually the integration of concentration across the thickness of the ECM. As described in §2.1.2, both the thickness of the ECM, Figure 16, and the measured integrated-concentration of certain ECM components increase with wing disc age, Figure 19. In this experiment I am sampling wing discs of ages in some window around 96h AEL, and I have so far ignored the fluorescence intensity to wing disc size scaling, hence I expect a range of fluorescence intensities at each time point regardless of knockdown. Any significant trends will therefore have to contend with this in-built age-based variation. However, it is possible to measure wing disc size from the images taken in this experiment, so the age-dependence of fluorescence intensity could be accounted for in the future.

Statistics

In Figure 33 scatter plots for five genetic conditions are shown. Each condition has been fitted with a linear function. The p value on each scatter plot indicates arises from the hypothesis that the gradient of the fitted line is equal to zero. The two coefficients of the linear fit, gradient and y-intercept, for each group have been more clearly compared in Figure 32. Box and whisker plots have been used to represent the fitted coefficients, where the box represents the coefficient IQR and whiskers represent standard deviation of the coefficient. In Figure 29, a Student's t-test was used to compare fluorescence intensity of control-treatment pairs.

2.2.2 Results

Genetic perturbations

A prime suspect for regulation of ECM turnover are Mmps. Mmps have a well-established role at the beginning of pupation, where up-regulation of Mmp

expression suddenly and quickly degrades the ECM, initiating massive morphological change^[180]. However, this drastic removal of ECM is not of interest here; instead I am interested in a degradation rate mild enough to maintain ECM integrity while promoting turnover. If Mmps do contribute to ECM turnover, I would expect their knockdown to induce a phenotype where the tissue appears compacted, however this is not what I observe. Representative projections and sections are shown for Mmp1 and Mmp2 knockdown in Figure 21 D – I. Surprisingly, these knockdowns do not show any clear morphological phenotype in the wing disc. Larvae of Mmp1 knockdown were found to develop slower than controls, and stopped developing around 72h to 96h AEL, this phenotype has been published and is expected to be due to tracheal defects^[146].

Line	Lethal	Stock
UAS-VkgRNAi	†	VDRC 106812
UAS-LanB2RNAi	†	VDRC 42559
UAS-LanB1RNAi	†	VDRC 23119
UAS-LanARNAi		VDRC 18873
UAS-WbRNAi		VDRC 3141
UAS-Trol		DGRC 201233
UAS-TrolRNAi		VDRC 24549
UAS-NdgRNAi		VDRC 109625
UAS-Mmp1	†	BDSC 58702
UAS-Mmp1RNAi		BDSC 31489
UAS-Mmp2	†	BDSC 58704
UAS-Mmp2RNAi		BDSC 31371
UAS-MysDN		

Table 1. A screen of extra-cellular matrix component genetic perturbations confirms previously identified wing disc morphological phenotypes. The first column gives the name of the fly line used, as described in the methods. The second column shows lethality of genetic perturbations; those with a cross, †, were lethal before larval stages. The third column gives the stock number of the fly line. All genetic perturbations were driven throughout development with ActGal4.

Knockdowns of laminin subunits LanB1 and LanB2 were found to be embryo-lethal, Table 1, which is consistent with published results ^[108, 181]. However, knockdown of LanA was not found to be lethal, which is not consistent with published results showing embryo-lethality of null-mutants ^[109], suggesting this RNAi line is not working. Knockdown of Vkg was also found to be embryo-lethal, which is consistent with published results ^[16, 182]. Overexpression of Mmp1 or Mmp2 was found to be embryo-lethal, which is expected given this is similar to a knockdown of all ECM components, some of which are embryo-lethal in their own right. Knockdown of nidogen shows no clear phenotype in wing disc morphology, Figure 23 G – I, which is consistent with published results ^[136].

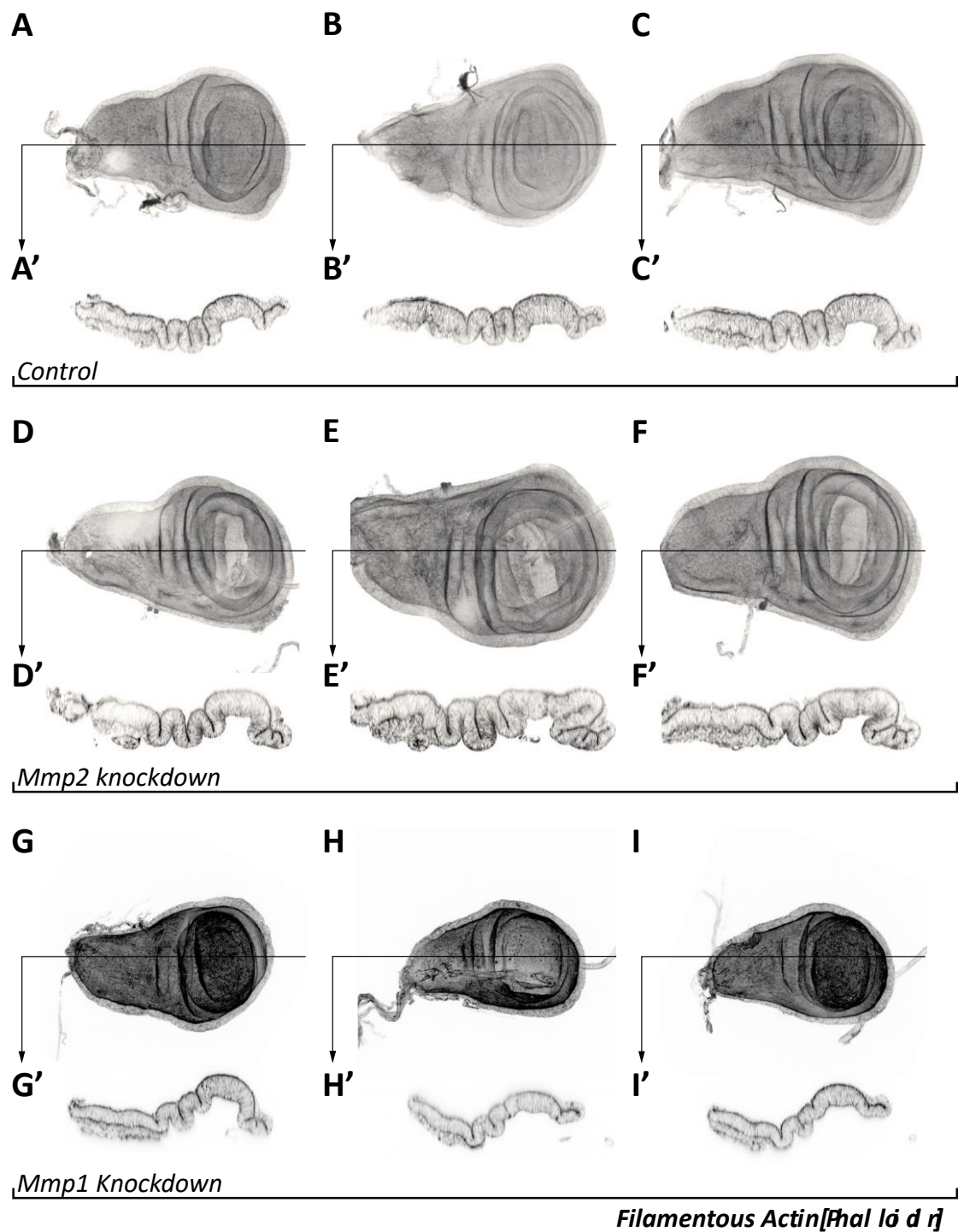


Figure 21. Metalloproteinase knockdown has no considerable affect on wing disc morphology. **A – I** are maximum projections off phalloidin-stained, fixed wing discs. **A' – I'** are the respective sections of **A – I** indicated by the lines with arrowhead. **A – C** show three examples of control wing discs where ActGal4 has driven no transgene throughout larval development. **D – F** and **G – I** show examples of Mmp2 and Mmp1 knockdown, respectively, driven throughout larval development by ActGal4. Wing discs were dissected between 96h and 120h AEL.

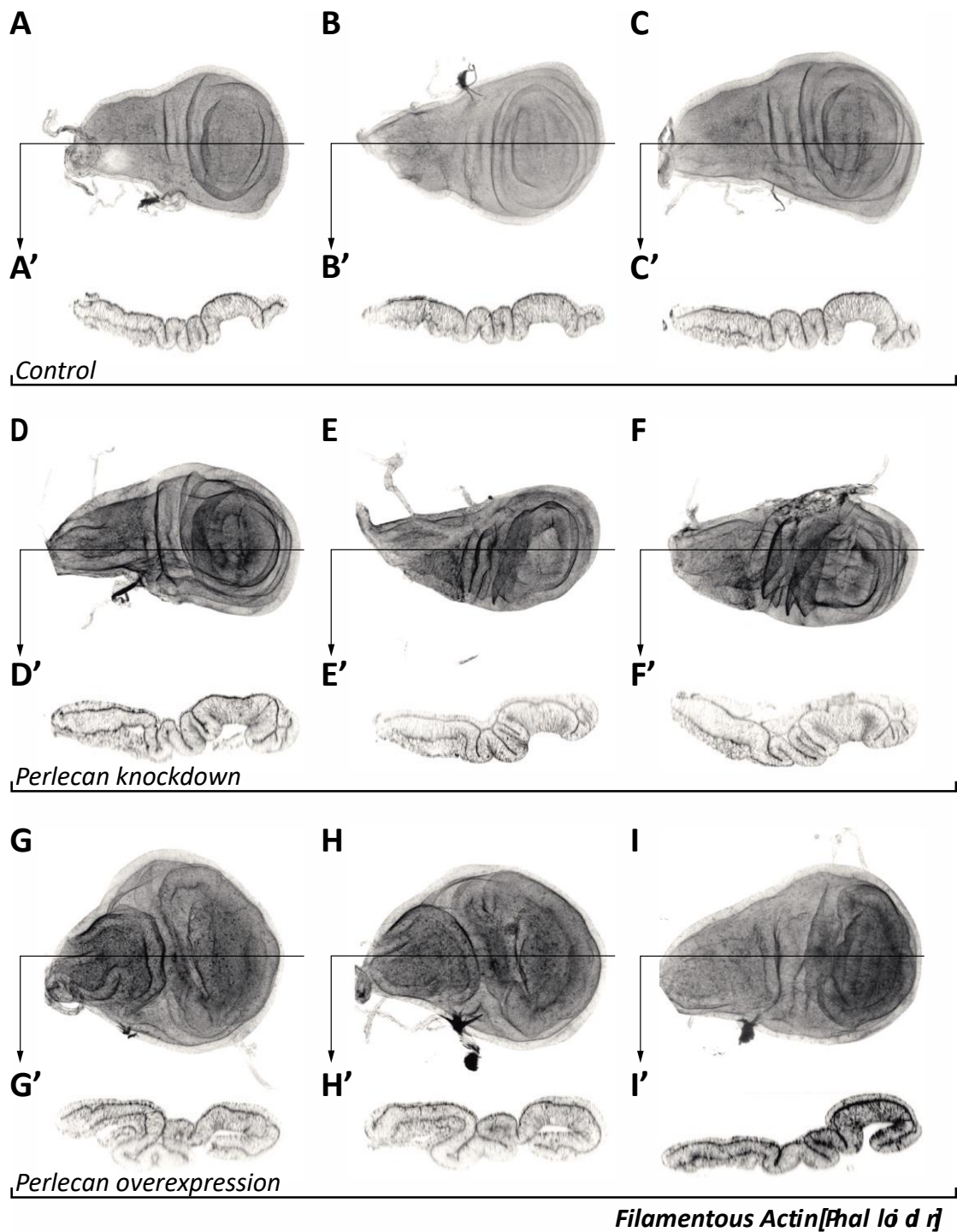


Figure 22. *Perlecan knockdown leads to constricted wing disc morphology, while perlecan overexpression leads to a spreading out. A – I are maximum projections off phalloidin-stained, fixed wing discs. A' – I' are the respective sections of A – I indicated by the lines with arrowhead. A – C show three examples of control wing discs where ActGal4 has driven no transgene throughout larval development. D – F and H – I show examples of Trol knockdown and overexpression, respectively, driven throughout larval development by ActGal4. Wing discs were dissected between 96h and 120h AEL.*

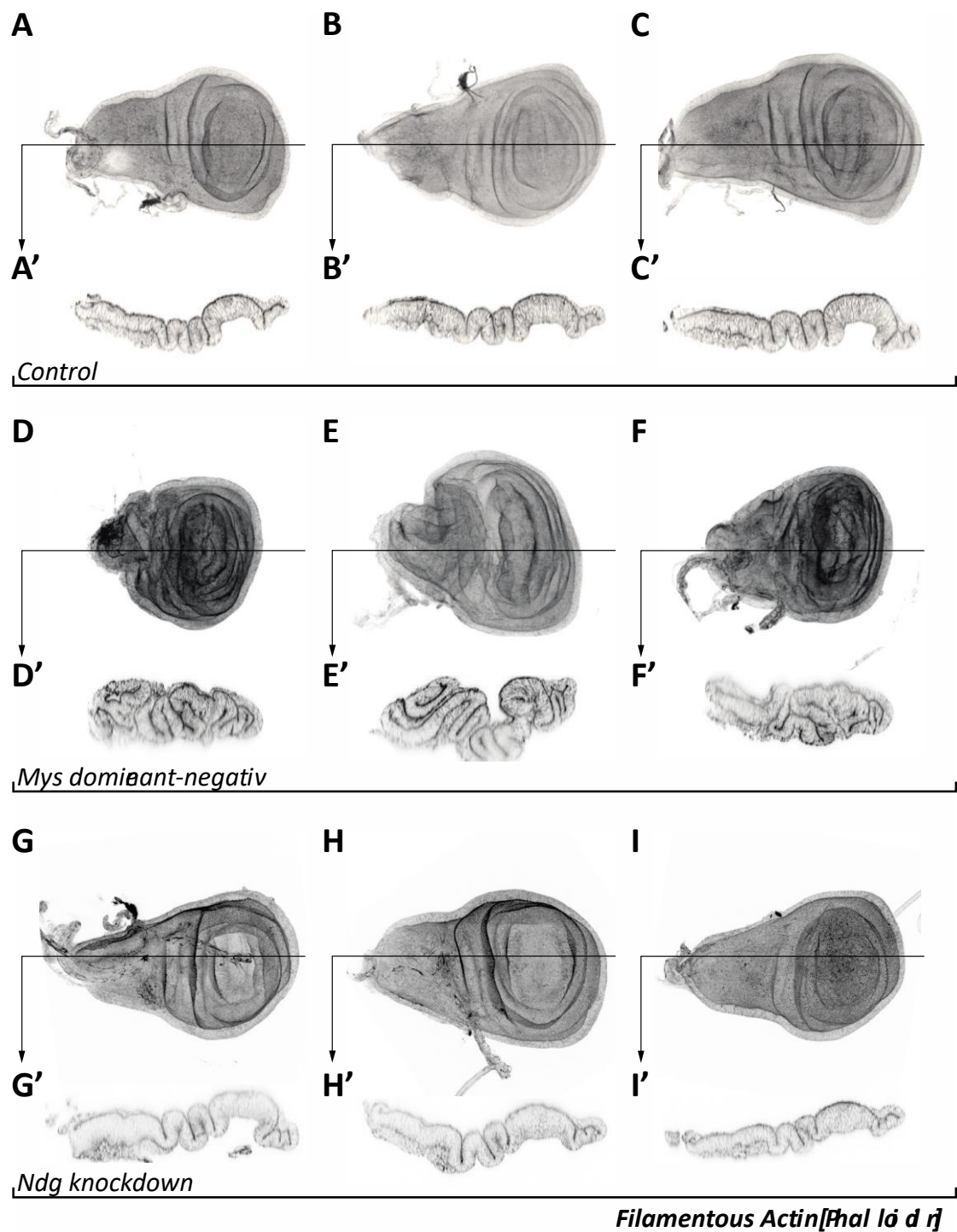


Figure 23. *Integrin knockdown leads to considerable ectopic folding of the wing disc.* **A – I** are maximum projections off phalloidin-stained, fixed wing discs. **A' – I'** are the respective sections of **A – I** indicated by the lines with arrowhead. **A – C** show three examples of control wing discs where ActGal4 has driven no transgene throughout larval development. **D – F** show examples of dominant-negative Mys driven throughout larval development by ActGal4. **H – I** show examples of Ndg knockdown driven throughout development by ActGal4. Wing discs were dissected between 96h and 120h AEL.

A phenotype showing compaction in the wing disc has already been identified for Trol knockdown, as well as the opposing phenotype with overexpression of Trol ^[16]. To attempt to recover these phenotypes I have performed a similar experiment, both knocking down and over expressing Trol, shown in Figure 22 D – I. As can be seen in the sections, Figure 22 D' – F', Trol knockdown causes thickening of the columnar epithelium, while the projections, Figure 22 D – F, show narrowing of the wing disc in the Anterior-Posterior axis. Sections of Trol overexpression show flattening of the columnar epithelium, Figure 22 G' – I', while projections show widening of the wing disc in the Anterior-Posterior axis, Figure 22 G – I. The published phenotype has therefore been recovered. Although the described perlecan phenotype is not quantified here, it has been quantified by others ^[16].

Expressing a dominant-negative chimera of Mys throughout development produce very few larvae. Wing discs of surviving larvae show extreme ectopic folding Figure 23 D – F. These wing discs appear compacted, for example the pouch is folded in on itself as if the columnar epithelium is minimising its basal surface area. This result is difficult to interpret given integrins could be affecting both signalling and ECM localisation. For Figure 21, Figure 22 and Figure 23 wing disc age was not precisely staged, and therefore any differences in wing disc size between phenotypes cannot be interpreted.

Protease treatments

The problem with driving knockdowns throughout development is the difficulty in differentiating the instantaneous effect of losing the protein and the accumulation of these effects over time. Even with temporal knockdown using Gal80ts, knockdowns can take up to 12 hours to take effect. Furthermore, knockdown of ECM components that are secreted affect the whole organism, which may have knock-on effects on the wing disc unrelated to its own ECM. One way to circumvent these problems is to apply treatments to wing discs *ex vivo* to determine the effect in that instant.

Degrading the ECM of wing discs *ex vivo* using collagenase, CLS-1, causes sudden and considerable morphological changes, Figure 24. In general, basal surfaces of columnar epithelia appear to expand. ECM between apposing basal surfaces of fold epithelium is degraded, leading to these surfaces pulling apart and opening the fold basally. Wing discs shown in Figure 24 were not precisely staged, so a selection of wing discs of different sizes are shown, larger wing discs are older while smaller wing discs are younger. For wing discs that appear older, Figure 24 G – I, hinge folds opening basally leads to the wing disc folding in half across the hinge so that apical pouch region moves into apposition with the apical notum region. Expansion of basal surface causes opening and flattening of the pouch region in older wing discs, while some folds keep their shape. For wing discs that appear younger, Figure 24 J – L, basal expansion drives shape change in all regions of the columnar epithelium. In some cases basal expansion is so considerable that pouch and notum columnar epithelia can invert, Figure 24 J, K, and hug apposing epithelia. The final shape of these younger ECM-degraded wing discs is spherical with all the columnar basal surface facing outward, Figure 24 J – L. During this process the peripodial epithelium follows the apical surface of the wing disc, and becomes tucked inside the sphere. CLS-1 treated wing discs that are imaged live show slightly different morphological changes compared with fixed.

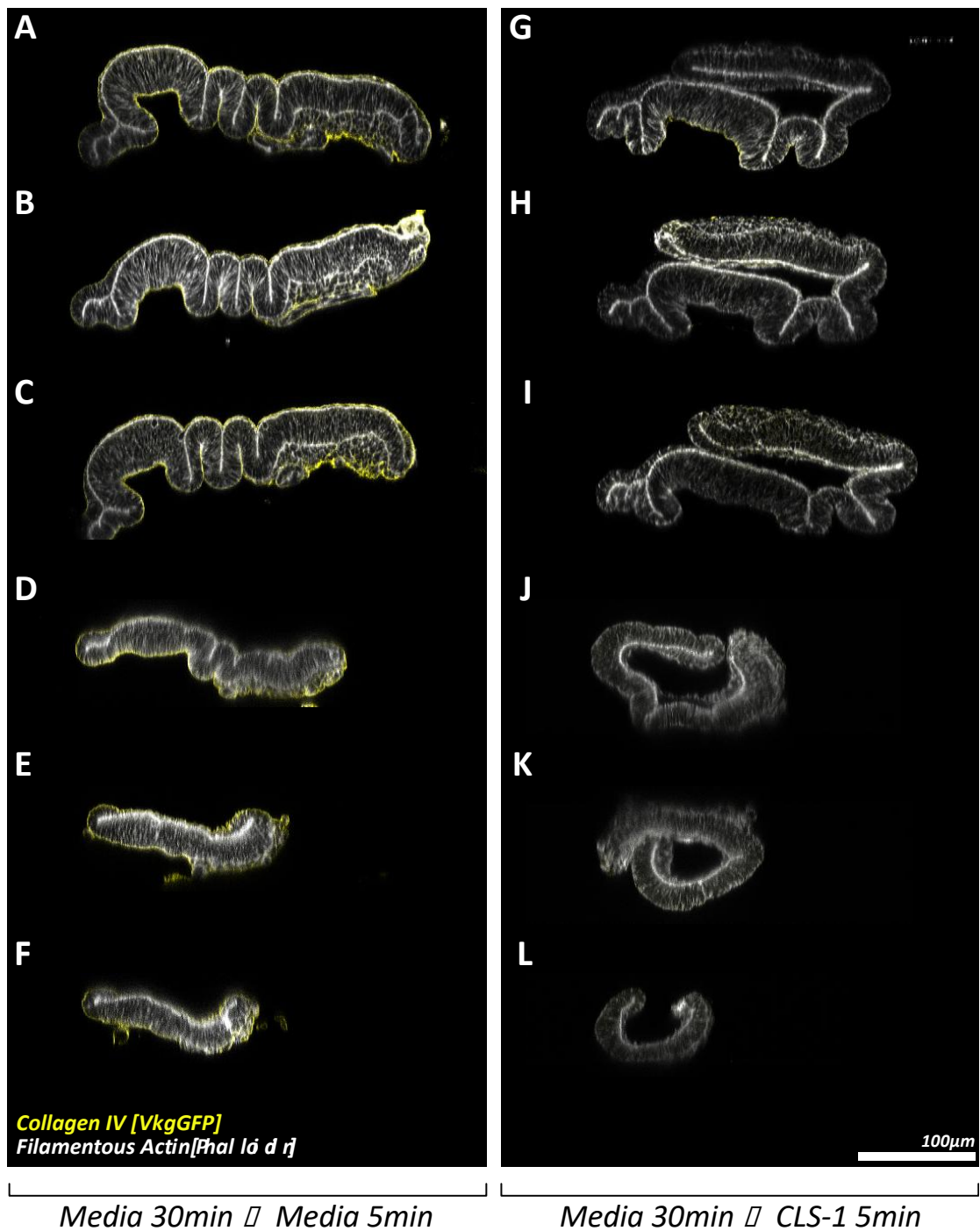


Figure 24. Degradation of the extra-cellular matrix with collagenase causes a sudden and considerable change of wing disc morphology. **A – F** show sections of wing discs fixed after being immersed in media for 35 minutes. **G – L** show sections of wing discs fixed after treatment with media for 30 minutes and CLS-1 for 5 minutes. Wing discs are between 72h and 120h AEL.

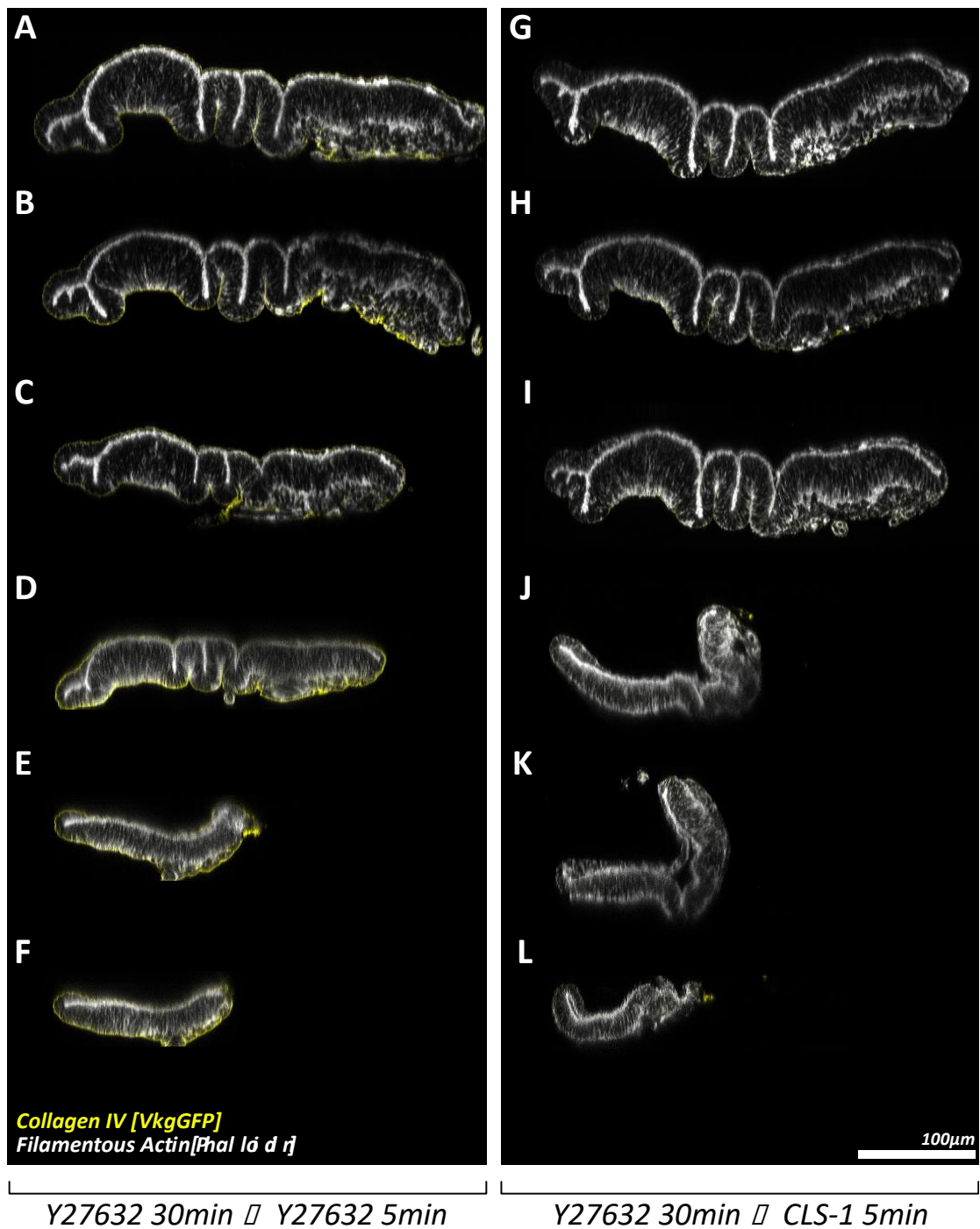


Figure 25. Inhibition of myosin contractility reduces the extent of morphological change induced by subsequent extra-cellular matrix degradation. **A – F** shows sections of wing discs fixed after treatment with Y27632 for 35 minutes. **G – L** shows sections of wing discs fixed after treatment with Y27632 for 30 minutes then CLS-1 for 5 minutes.

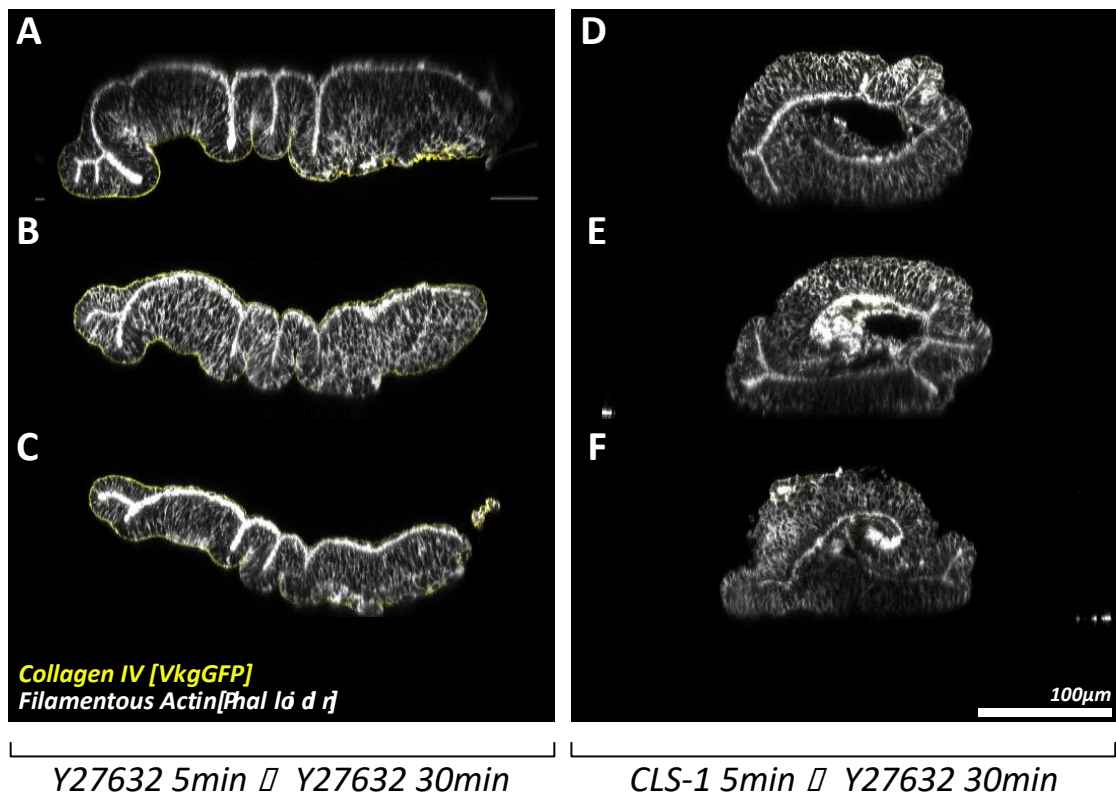


Figure 26. *Inhibition of myosin contractility after extra-cellular matrix degradation does not recover the original wing disc morphology. A – C* shows sections of wing discs fixed after treatment with Y27632 for 35 minutes. *D – F* shows sections of wing discs fixed after treatment with CLS-1 for 5 minutes then Y27632 for 30 minutes.

The deformation resulting from CLS-1 treatment of wing discs suggested the ECM somehow contributes to the balance of forces. I therefore decided to try perturbing contractility, which I expected to be a source of force generation. Y27632 and Latrunculin-A are drugs that have been shown to inhibit Rok activity and inhibit actin polymerisation, respectively, in wing discs^[173]. Pre-treating wing discs with Y27632 for 30 minutes before treating with CLS-1 for 5 minutes appears to prevent or reduce deformation, Figure 25. For this particular experiment. The reverse experiment, in which wing discs are first deformed by pre-treating with CLS-1 for 5 minutes before treating with Y27632 for 30 minutes, does not reverse the deformation, Figure 26. Pre-treating wing discs with Latrunculin-A for 30 minutes before treating with CLS-1 for 5 minutes also appears to prevent or reduce wing disc deformation, Figure 27.

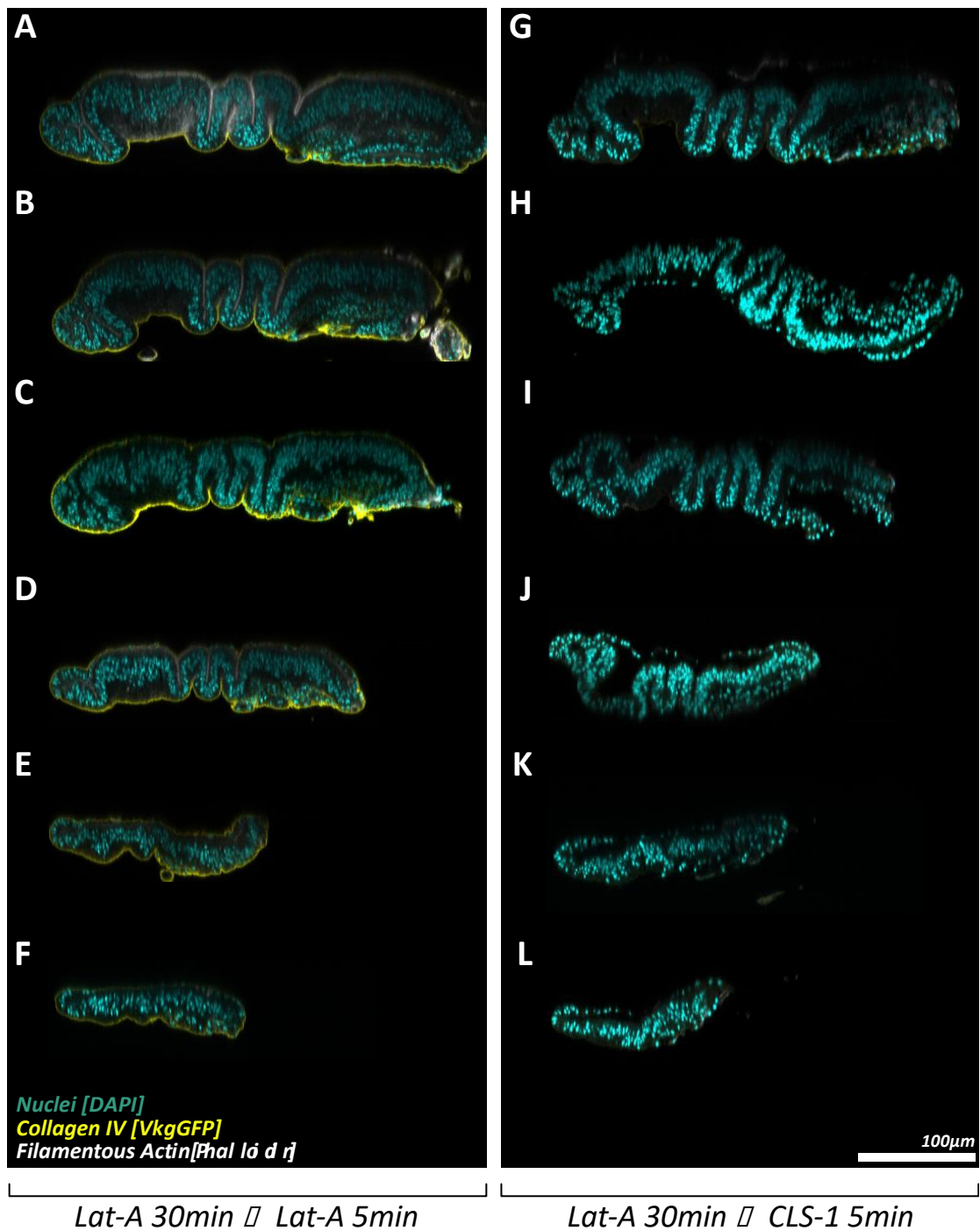


Figure 27. Degradation of cell cortices reduces the extent of morphological change induced by subsequent extra-cellular matrix degradation. **A – F** shows sections of wing discs fixed after treatment with Latrunculin-A for 35 minutes. **G – L** shows sections of wing discs fixed after treatment with Latrunculin-A for 30 minutes then CLS-1 for 5 minutes.

Degrading the heparan-sulphate side-chains of perlecan and other proteoglycans of wing discs *ex vivo* using heparanase HS3 917, does not affect wing disc morphology, Figure 28. This suggests the heparan-sulphate side-chains do not contribute to ECM maintenance of tissue shape. Degradation of heparan-sulphate side-chains does not affect localisation of perlecan in the ECM, Figure 29, suggesting perlecan does not bind the ECM *via* its heparan-sulphate side chains.

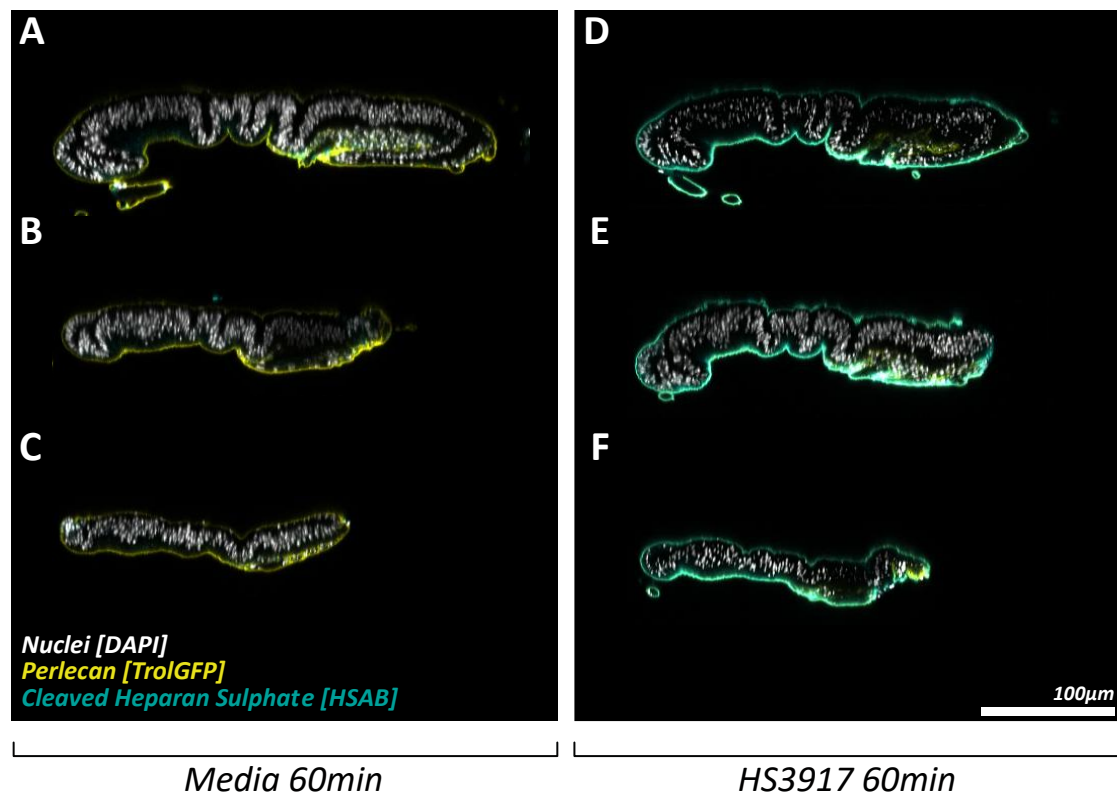


Figure 28. Degradation of heparan sulphate does not change wing disc morphology. **A – C** shows sections of wing discs fixed after incubation in media for 60 minutes. **D – F** shows sections of wing discs fixed after treatment in HS3917 for 60 minutes. All wing discs are stained with 3G10, an antibody for cleaved heparan sulphate.

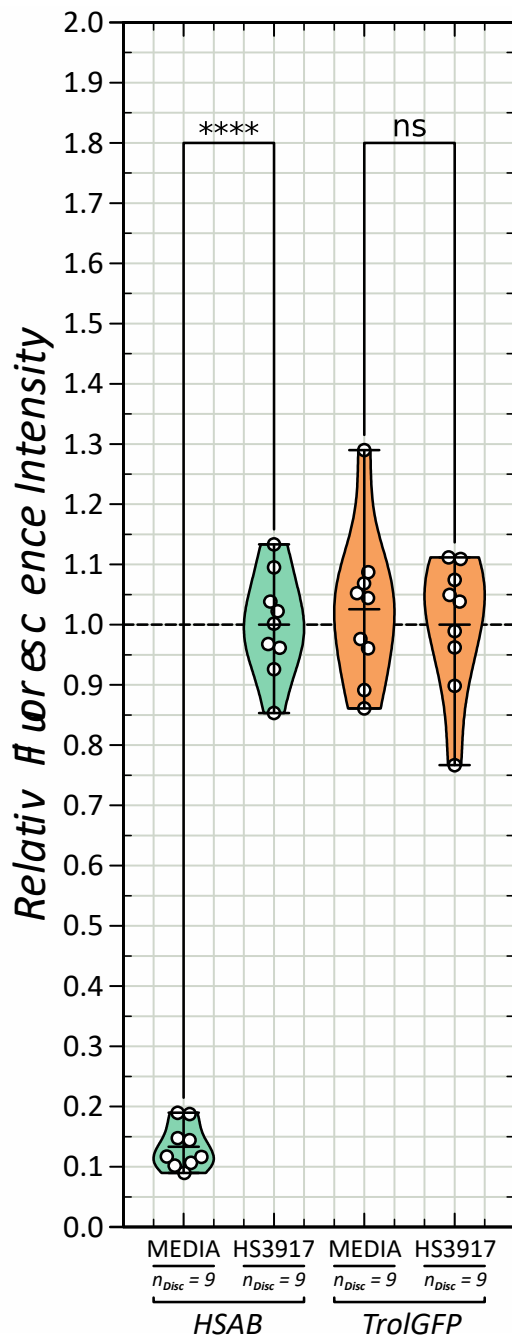


Figure 29. Degradation of heparan sulphate does not affect perlecan concentration in the wing disc extra-cellular matrix. Measurements for TrolGFP and 3G10 (HSAB) fluorescence intensity are shown for wing discs either treated with heparanase HS3917 for 60 minutes or incubated in media for 60 minutes. Mean fluorescence intensity for each wing disc was measured from a circular region of the pouch ECM. HSAB fluorescence intensity measurements are normalised relative to the mean fluorescence intensity of heparanase treated wing disc HSAB fluorescence intensity measurements. Similarly, TrolGFP fluorescence intensity measurements are normalised relative to the mean fluorescence intensity of heparanase treated wing disc TrolGFP fluorescence intensity measurements.

Permeabilisation treatments

It has been shown that cells themselves can be degraded through permeabilisation [183]. Degrading cells of the wing disc does not lead to degradation of the ECM, Figure 30. Signals from VkgGFP, TrolGFP and LanB1GFP remain after permeabilisation, Figure 30, despite some ballooning of the ECM shape, likely due to transient transfer of osmotic pressure from the cells to the ECM. Because wing disc ECM components are produced non-autonomously, the ECM of an *ex vivo* wing disc cannot gain mass. Culturing *ex vivo* wing discs is therefore similar to knocking down all ECM components *in vivo*. Wing discs imaged for 12 hours do not show any change in VkgGFP or TrolGFP signal, Figure 31. However wing discs do curl up over time, this is an effect observed to a small extent in the time after dissection but becomes significant over long timescales.

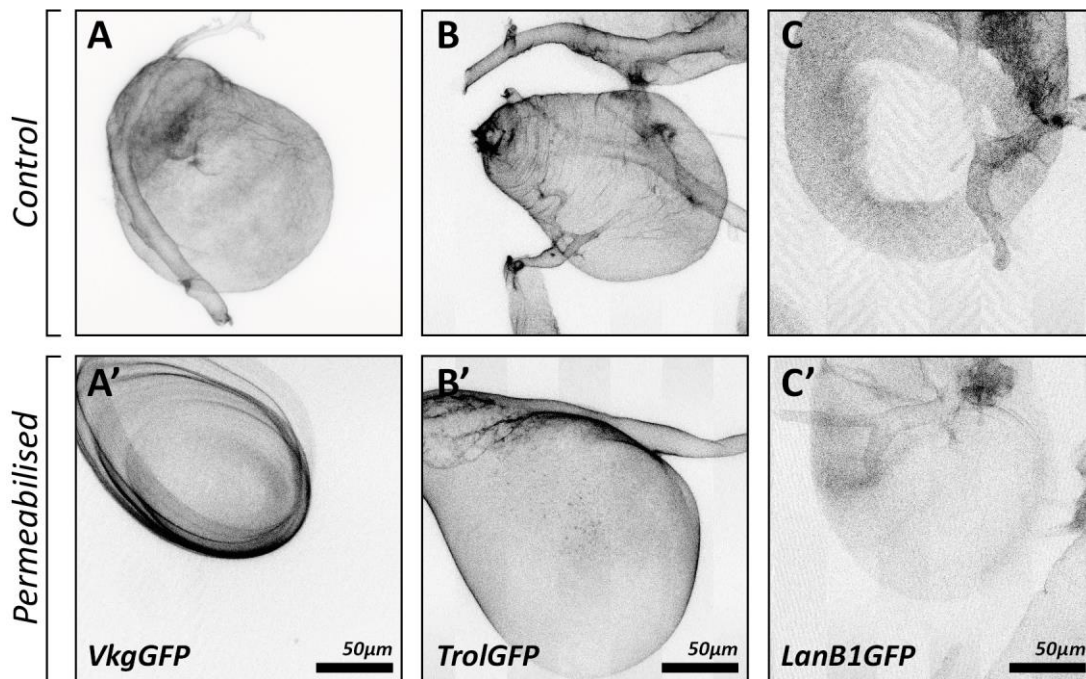


Figure 30. The extra-cellular matrix is not dependent on cells to maintain integrity. **A** – **C** show three different wing discs exhibiting collagen (Vkg), perlecan (Trol) and laminin (LanB1) respectively. **A'** – **C'** show the same wing discs as **A** – **C**, respectively, after treatment with Triton to permeabilise the cells. For **A**, movement of the ECM shell during imaging lead to a distorted image.

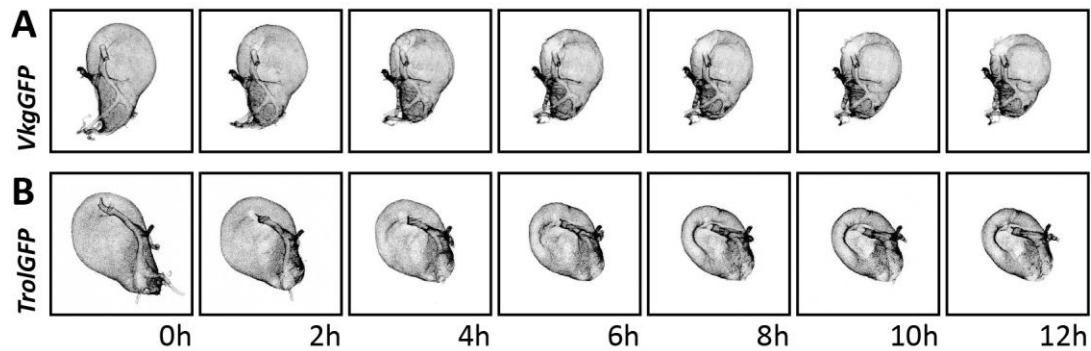


Figure 31. *The extra-cellular matrix does not degrade ex vivo over hours timescale. A and B show collagen and perlecan, respectively, of wing discs immersed in media imaged over 12h.*

Temporal genetic perturbations

Rates of fluorescence intensity change for different genetic perturbations are shown in Figure 32 A and A'. Temporal perlecan knockdown slightly significantly increases collagen concentration in the wing disc ECM over time by $(0.4 \pm 0.2)\%$ per hour, while laminin knockdown does not have a significant effect on collagen, Figure 32 A and Figure 33 A, A'. Temporal perlecan and collagen knockdowns significantly decrease perlecan concentration in the wing disc ECM over time by $(-1.0 \pm 0.2)\%$ per hour and $(-2.2 \pm 0.3)\%$ per hour respectively, while laminin knockdown significantly increases perlecan concentration over time by $(1.1 \pm 0.3)\%$ per hour, Figure 32 A' and Figure 33 B – B''. Temporal knockdown of neither perlecan nor laminin show significant collagen immobile fractions, Figure 32 B. Similarly, temporal knockdown of laminin does not show a significant perlecan immobile fraction, however temporal knockdown of either collagen or perlecan do, Figure 32 B'. Temporal knockdown of perlecan shows a perlecan mobile fraction of $(70 \pm 5)\%$, and interestingly temporal knockdown of collagen shows a perlecan mobile fraction of $(132 \pm 7)\%$, Figure 32 B'.

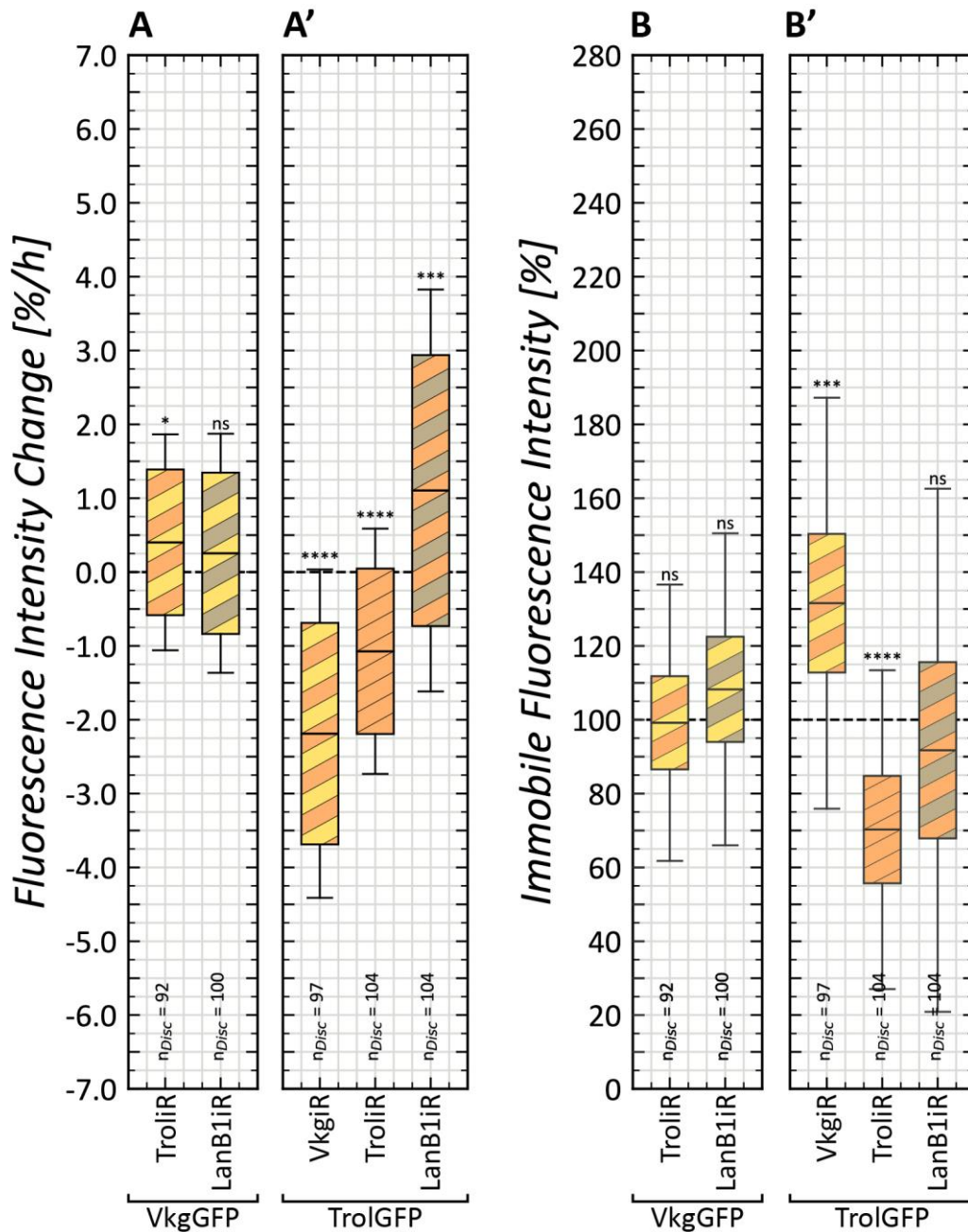


Figure 32. *Perlecan degrades from the extra-cellular matrix via fast and slow mechanisms. A and A'*, fluorescence intensity change is the rate of change of fluorescently-tagged protein between 12h and 36h after knockdown initiation. **B and B'**, immobile fluorescence intensity is the remaining fraction of fluorescence estimated at knockdown initiation given the linear degradation observed between 12h and 26h after knockdown. **A and B** show effect of indicated knockdowns on collagen (VkgGFP), while **A'** and **B'** show effect of indicated proteins on perlecan (TrolGFP).

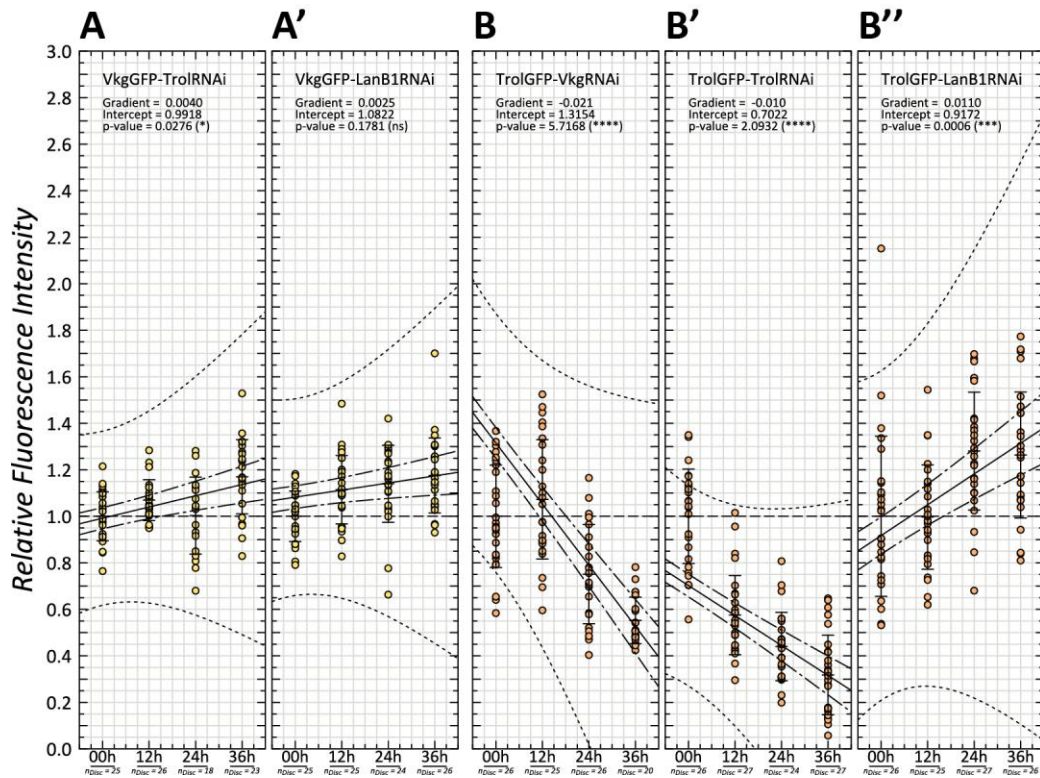


Figure 33. Temporal knockdown of extra-cellular matrix components reveals complex dynamic effects on other extra-cellular matrix components. A – A' and B – B'' are scatter plots showing change in measure fluorescence intensity with time. Solid lines indicate linear fits of fluorescence intensity measurements across 12h, 24h and 36h. Relative fluorescence intensity is measured fluorescence intensity at all time points normalised by the mean fluorescence intensity of the initial 00h time point. Dotted line is standard deviation of linear fit, dotted-dashed line is standard error of linear fit.

At the measured loss rate of approximately 1% per hour, perlecan would take over 4 days to completely degrade from the ECM. However, this total degradation time will be considerably shorter because of its significant immobile fraction. This immobile fraction shows approximately 30% of perlecan is lost within in the first 12h of temporal knockdown, which is a much faster loss rate than the subsequent 24h, Figure 33 B'. Interestingly, with temporal knockdown of collagen, perlecan loss appears to only begin after 12h, Figure 33 B. An interesting phenotype is observed when laminin is knocked down. The wing disc retains its morphology, but VkgGFP fluorescence becomes inhomogeneous across the ECM, Figure 34 A. Collagen appears to form a network of ringlet-shaped high-concentration fibres, which differs from the straighter, more aligned fibres seen in wild type, Figure 34.

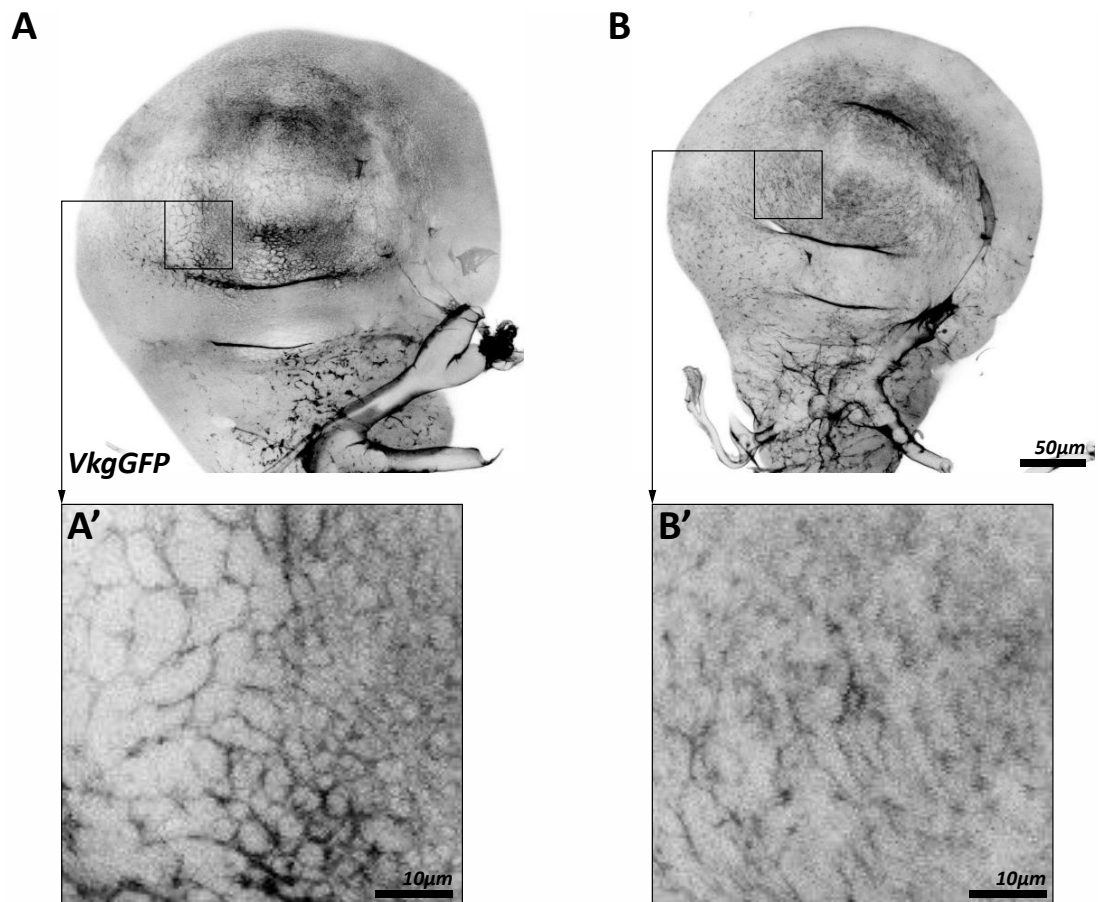


Figure 34. *Laminin knockdown causes structural changes to collagen in the extracellular matrix of the wing disc. A shows VkgGFP as a result of temporal knockdown of LanB1 for 36h with LanB1RNAi. B shows VkgGFP with no knockdown applied. A and B are summation projections of image stacks, and A' and B' are magnifications of regions of interest.*

2.2.3 Discussion

In this section I have characterised the role of the ECM in maintaining wing disc morphology. Degradation of the ECM with collagenase leads to a sudden and considerable deformation of the wing disc consistent with a basal expansion of the columnar epithelium, Figure 24. This result suggests the ECM contributes to maintenance of wing disc shape. The basal expansion triggered by ECM degradation could have both mechanical and signalling origins. The rapid rate of expansion precludes transcription and translation based signalling, but not fast reorganisation of protein-protein signalling networks.

From a mechanical point of view, it may be intuitive to think about cells and their ECM as two adhered elastic materials. Before ECM degradation the cellular layer is held under compression by adhesion to the stiffer ECM layer. When the ECM is degraded the cellular layer is no longer held in compression, and so expands. This picture suggests cells have somehow become compressed within the ECM, perhaps due to cellular growth. However, either sudden degradation of either the actin cytoskeleton, Figure 25, or inhibition of myosin contractility, Figure 27, appears to block this basal expansion. These results suggest basal expansion is being driven by contraction of the actin-myosin cortex. This may be initially confounding; that cortical contraction leads to cellular expansion, but may be explained by taking cell shape into account.

The effect of cortical contractility is to generate a surface tension, and this surface tension will drive a minimisation of the cell surface to volume ratio. A sphere is the shape that has the smallest surface to volume ratio, the prismatic shape of epithelial cells will have a greater surface to volume ratio, and this ratio will increase as these cells become taller and thinner. Hence, the basal expansion of columnar cells after ECM degradation may be the result of contractility minimising surface to volume ratio, and before, the ECM restricts basal surface are expansion. When contractility

is inhibited, this tendency to minimise surface to volume ratio is removed, and cells maintain their shape after ECM degradation, Figure 35. This interpretation assumes surface tension is uniform across the cell, which is unlikely to be true, but will suffice as a first approximation. This interpretation also assumes cells approximately conserve their volumes, which is an assumption that has some precedent ^[26].

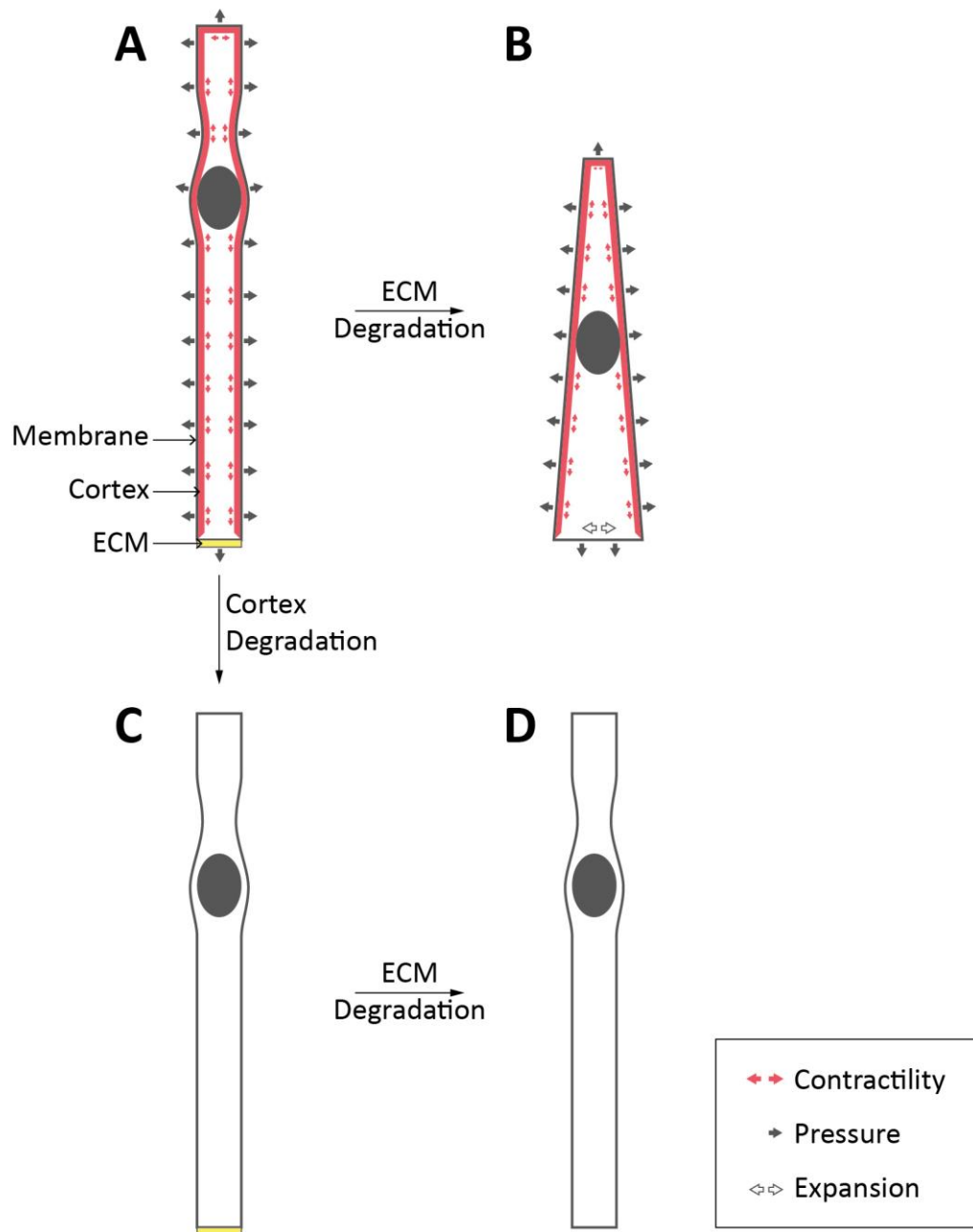


Figure 35. *The extra-cellular matrix may balance cellular contractility.* This figure describes a hypothetical explanation of the ECM degradation results. **A**, with the ECM intact, apical and lateral contractility generates cell pressure, in turn increasing basal expansive stress. This basal expansive stress is balanced by ECM elasticity. **B**, when the ECM is degraded basal expansive stress becomes imbalanced, so it expands, and apical-lateral surface areas decrease to maintain cell volume. **C**, if the contractility is inhibited, then pressure is no longer generated to the magnitude required to induce basal expansive stress, therefore when the ECM is degraded cells maintain their shape, **D**.

An implication of this surface tension hypothesis is that the ECM is maintained under tension by the cells. Inhibition of contractility does not appear to affect wing disc morphology, Figure 25. This suggests the ECM deforms insignificantly under any applied tension. Ablations of the ECM could also expose any tension as recoil. Some preliminary ablations were performed on the wing disc ECM during this project, but showed little to no recoil. However, a rigorous set of ECM ablations, with confirmation that ablation, not bleaching, is occurring would help confirm if the ECM is, or is not, under tension.

An alternative hypothesis is the ECM may contribute to wing disc shape by providing signals that define intrinsic basal contractility. However, any signalling based mechanism must work fast given the deformation occurs within minutes after ECM degradation. It has already been shown that integrins form clusters on the basal surface of cells, Figure 12, and that actin and myosin structures form here, Figure 14 and Figure 15. A first step to determine any fast signalling would be to see if contractility, such as the basal myosin ring, change after ECM degradation. A direct way to measure any change in regulation would be to infer contractility *via* myosin activation by staining for phosphorylated Sqh. This has been attempted, but unfortunately, the protocol used to stain for phosphorylated Sqh produced unusable results, so further work would be required to get this working.

Treatments that degrade specific ECM proteins may reveal their roles in maintaining wing disc morphology. I have been unsuccessful trying to obtain proteases with specificity to certain ECM proteins. One protease that does work is heparinase. However, degradation of heparan sulphate does not affect wing disc morphology, Figure 28, suggesting no contribution to maintaining wing disc morphology. Also heparinase does not affect perlecan localisation within the ECM, Figure 29, so cannot be used to specifically degrade perlecan from the ECM.

Another way to determine the contribution of certain ECM components is to genetically perturb them, by knocking them down or overexpressing them. As an

initial screen of wing disc phenotypes I have knocked down or overexpressed certain ECM components throughout development. ECM components required for survival to larval stages include collagen and laminin, Table 1. Perlecan knockdown leads to wing discs that appear thicker and narrower, while perlecan overexpression leads to wing discs that appear flatter and wider, Figure 22, a phenotype previously reported [16]. Despite some shabbiness, wing discs of Mmp1 or Mmp2 knockdown do not display any clear phenotype, Figure 21. A lack of clear phenotype could be due to redundancy between Mmps; however in the literature it has been shown the two Mmps have distinct roles [147]. Also, published results show Mmp knockouts are not lethal at larval stages [143], so it could be that Mmps simply do not contribute to wing disc development. Alternatively, these Mmp RNAi lines may not be strong enough to further reduce what is probably an already low level of Mmp expression. It may be that Mmps aren't present in the wing disc. Immuno-staining for Mmps would help show their localisation. Unfortunately, published reagents I have tried so far have not provided strong signals for Mmp1 or Mmp2 concentration [139, 143], however other published reagents are yet to be tested [151]. A way to check if Mmp antibodies work would be to stain everted wing discs, where Mmps are known to be expressed [180].

Expression of the dominant-negative integrin MysDN leads to both ectopic folding and compaction of the wing disc, Figure 23. Given the extreme morphological deformation of this phenotype, it is difficult to interpret. Basal cell surfaces appear both expanded and contracted in different regions. In the pouch the basal surface appears confined almost to a point, while the basal surface of the hinge remains expanded like wild type. The whole tissue appears confined within a shell. Further work is required to determine if the ECM is intact for this phenotype. Although it has been shown MysDN recovers some signalling, it may affect some as yet untested signalling pathway that may contribute to this phenotype.

One concern with these temporal knockdown results is that ECM component concentrations may change simply as a result of the increased temperature after temperature shift. If there is some non-negligible increase, then it may account for

the observed increase in collagen as a result of perlecan or laminin knockdowns. Another concern is the assumption knockdowns eliminate levels of ECM components in the haemolymph, which has not been experimentally confirmed. An experiment to confirm this assumption may require taking samples of the haemolymph before temperature shift and 12h after. From these samples concentrations of the knocked down protein in the haemolymph could be measured.

Keeping in mind these concerns, when production of new perlecan is inhibited, perlecan degrades from the ECM Figure 32 A'. However, the amount of perlecan degradation measured over the 24-hour period starting 12 hours after temperature shift does not account for the reduction in perlecan during the initial 12 hours after temperature shift, as described by the immobile fraction, Figure 32 B'. This suggests perlecan may degrade at two rates, one at an hours-timescale and another at a days-timescale. This suggests two populations of perlecan, which for example may differ in isoform or by mechanism of incorporation into the ECM. Perlecan has been shown to require collagen to bind the wing disc ECM^[16], while dystroglycan has been shown to recruit perlecan in other tissues^[99], these two proteins may therefore be a good starting point. Neither laminin nor perlecan knockdown affects levels of collagen within the ECM. Extending this temporal knockdown experiment to other ECM-associated proteins such as integrin and dystroglycan may affect collagen concentration.

A highly stable ECM is not unexpected given its integrity under perturbations and treatments obtained here. The ECM remains intact when cells are degraded Figure 30, suggesting the ECM has its own integrity independent of cells. This shows the ECM has its own structural integrity, in the sense that cells do not keep the ECM held together, at least once the ECM is established. The ECM could therefore be considered as its own entity, an extra-cellular object. This also shows collagen, perlecan and laminin are all bound together to form a single composite material. Further, there is insignificant degradation of perlecan or collagen when wing discs are cultured *ex vivo* for extended periods of time Figure 31, showing that under these conditions the ECM is highly stable, at least over this timescale. The

implication is that either these ECM components are stable over this timescale *in vivo* too, or some destabilising factor is present *in vivo*, but lost once *ex vivo*.

Although loss of laminin does not affect collagen concentration, it does cause a change in collagen structure within the ECM, Figure 34. These collagen fibre ringlets are similar to outlines of cells, which suggests vertices of these cables could co-localise with either cell vertices or even cell integrin clusters, a bit like a Voronoi diagram or its dual. This structural change in collagen suggests laminin is in some way contributing to the homogeneity of collagen, perhaps by directly binding collagen or by mediating bonds between cell-matrix adhesions and collagen. Collagen fibres appear mainly in the pouch region suggesting some difference in the ECM in this region compared to other regions. These cables are similar to the structure of collagen after fixation, Figure 7, suggesting this structural change is due to some physical process, like dehydration.

2.3 Results Section 3: Elastic properties of the wing disc extra-cellular matrix

This section is concerned with applying biophysical experimental techniques to determine the contribution of wing disc components to its stiffness. Specifically, how the ECM contributes to the effective stiffness of the wing disc. Other contributions to wing disc stiffness are also considered, such as contractility and cortical stiffness. The contribution of the ECM component perlecan to effective tissue stiffness is also determined.

2.3.1 Methods

Fly lines

To visualise the wing disc live, I have used three lines that have strong GFP fluorescence throughout the wing disc and mark cell outlines clearly. The first line is *yw;VkgGFP;SqhCherry* (*SqhCherry*, BDSC 59024 *FBID: FBti0164920*), which is *VkgGFP* described previously §2.1.1, with a copy of *Sqh* labelled with cherry fluorescent protein under control of the *Sqh* regulatory sequence inserted onto the third chromosome. The *SqhCherry* signal is relatively weak due to competition with endogenous *Sqh* expression, however it is bright enough to see the wing disc outlines. This line allows both the ECM and the wing disc cells to be observed simultaneously. The second line is *yw,SqhAx3;SqhGFP*; (*SqhGFP*, BDSC 57144 *FBID: FBal0035707 and FBti0073027*)^[184], which is a copy of the *Sqh* gene labelled with GFP under control of its own regulatory sequence, inserted into the second chromosome, with *SqhAx3* on the first chromosome, which is a null mutation of the endogenous *Sqh* gene. The inserted *SqhGFP* rescues the *Sqh*-null mutant, providing strong cytoplasmic signal and an even stronger cortical signal. The third line is *Ubi-GFP-CAAX* (*CAAX-GFP*, DGRC 109824 *FBID: FBtp0011013*)^[185], which is GFP fused to *CAAX*, a membrane-targeting motif, under the control of Ubiquitin regulatory sequence. This line gives a strong, ubiquitous signal, which clearly marks the cell

membranes. I have also recombined CAAX-GFP with ActGal4 onto the same chromosome to both drive genetic perturbations and visualise the wing disc.

Micropipette Aspiration

Micropipette aspiration is a technique used to measure the stiffness of single cells. More recently, micropipette aspiration has been used to measure tissue stiffness. Micropipette aspiration involves applying a suction pressure, or aspiration, to the surface of a material. As the applied pressure increases, the surface of the material is deformed, or aspirated, up into the micropipette. The stiffness of the material can then be determined from the relationship between pressure magnitude and the resulting aspiration size. The stiffer the material, the smaller the aspiration for a given pressure.

A micropipette is made from a glass tube. Using a pipette forge, the glass tube is heated in the center while being pulled from both ends. When the center of the glass tube melts it is pulled apart such that the center thins out until it eventually snaps. The result is two hollow glass needles. The next stage involves a metal heating filament. Before creating a micropipette, a glass rod is melted onto the filament to create a glass bead fused onto the filament. One of the glass needles is put in a movable clamp to hold it in place. Both the filament with glass bead and the clamped glass needle are placed under a microscope. The filament is heated, and the glass needle is brought close to the hot filament, but without touching. The filament heats one side of the glass needle more than the other causing the needle to bend. This bend allows the micropipette to enter the sample dish at one orientation, but meet the sample at a different orientation. Therefore the bend angle is chosen based on the orientation of the pipette holder and the orientation of the sample. Once the filament has caused the glass needle to bend to the required angle, the glass needle is moved away from the filament to cool. The bent glass needle is brought close to the now-cold filament for a second time, but allowed to make contact with the glass bead at a point on the tip side of the bend. The filament is

then heated up, which in turn heats and melts the glass bead. As the glass bead melts it fuses with the glass needle at the point where they make contact. The filament is then cooled, which in turn cools and solidifies the glass bead. As the glass bead cools it shrinks, which in turn pulls on, and eventually snaps, the glass needle. If lucky, the glass needle snaps cleanly, leaving a flat open end, which is the finished micropipette. The diameter of the micropipette depends on the distance along the glass needle at which the snap is made.

The micropipette is held and manoeuvred using an electronic micromanipulator. The micromanipulator allows fine control of the micropipette position, so that contact can be made with the tissue without damage. The micromanipulator is built into a spinning disc microscope used for imaging. The non-tip end of the micropipette is connected to a rubber tube that connects to both a syringe and a reservoir *via* a switch. The syringe is filled with PBS and is used to manually push the PBS through the rubber tubing and either through and out of the micropipette tip or into the reservoir depending on the switch position. The reservoir is filled with enough PBS to submerge the end of the rubber tube. A clamp holds the reservoir in place. The clamp has a micrometre built into it, which allows changes in height of the reservoir to be measured. The microscope is inverted; therefore the direction of imaging is in the upward z-direction. The micropipette is angled such that the tip end is parallel to the x-y-plane.

To be able to capture an image from which the aspiration size can be measured, the aspiration needs to be applied perpendicular to the direction of imaging, so in the x-y-plane. This means the surface of the wing disc to be aspirated must be oriented perpendicular to the x-y-plane. The surface of the wing disc I wish to aspirate is either the columnar or peripodial epithelia. Therefore, the wing disc must be mounted on its side. To do this I first create a shelf using a piece of coverslip placed at the bottom of a 35mm glass-bottomed dish. I then coat the edge of the coverslip with cell-tak, and allow it to dry on a hot plate at 30°C. I then fill the dish with 2mL of media. I then quickly place wing discs into the dish, waft them one by one over to the coverslip so that they make contact with, and stick to, the edge of the coverslip. I

orient the wing discs so that either the columnar epithelium or the peripodial epithelium is stuck the edge of the coverslip, depending on the experiment. The wing discs are therefore immobilised in the right orientation to image aspirations. Example images of wing discs mounted for peripodial and columnar aspiration are shown in Figure 42 A and B respectively.

Once the dish is mounted on the microscope and the micropipette and reservoirs are filled with PBS, the micropipette is manoeuvred into the dish so that its tip is submersed in the media. The micropipette tip is then manoeuvred to the same z-plane in which aspiration will be applied to the wing disc. The switch is set so that fluid can only pass between the reservoir and the micropipette. The pressure difference across the tip of the micropipette is defined by the height difference between the surface of the media in the dish and surface of the PBS in the reservoir. To achieve zero pressure difference, the reservoir is first brought as close to the height of the dish as possible. Then the reservoir height is further fine-tuned until no flow is observed coming from the tip of the micropipette. Microbeads can be added to the media to help observe flow. Once zero pressure difference is achieved, the micropipette tip is brought into contact with the surface of the wing disc. Sometimes the dish needs to be rotated so that the surface of the wing disc and the tip end are parallel so that a seal can be made. Once a seal is made, the reservoir height can be lowered to induce an aspiration pressure to the wing disc surface.

The pressure difference is increased in increments. After each pressure increase, there is a wait period of around 3 minutes before measurement. This is because the tissue has a finite deformation rate, which is defined by its viscosity. This short time scale viscosity will partly be due to friction, but may also be a result of cortical remodelling. Within 3 minutes the aspiration will finish deforming and the final, static deformation is treated as the elastic response of the tissue. Both transmitted and fluorescent light images are taken of this elastic deformation and the height of the reservoir is recorded. Spinning disc microscopes are moderately confocal, so the image is taken in the z-plane of the maximum width of the micropipette tip to capture the maximum length of the aspiration. This process is repeated for each

pressure increment to produce a dataset of pressure-image pairs. Examples of a series of aspiration images is shown in Figure 42 A', B'. Generally the change in reservoir height per increment is kept constant, although it is not necessary. The length of aspiration is measured from each image by drawing a line starting at the point on the aspiration that is furthest into the micropipette and ending at the micropipette tip, while keeping the line parallel to the micropipette length. The diameter of the micropipette is also measured from the images by drawing a line across the width of the micropipette tip.

A model of the relationship between aspiration length and aspiration pressure for a bulk material has been previously established ^[186]. This model treats the material as a homogeneously elastic half-space. A half-space is one of the two volumes produced by cutting infinite space with an infinite plane, therefore the material is approximated as having an infinitely large surface and being infinitely deep. The pipette is modelled as an annular region on the surface of the half-space centred at the origin, Figure 36. Within the inner radius, a , and outer radius, b , of this annular region $a \leq r \leq b$, the surface of the half-space cannot move perpendicular to the surface. A uniform pressure differential, Δp , is applied to the surface of the half-space within the inner radius, $r < a$. The pressure induces a normal deformation of the surface at the origin, L , which is related to Young's modulus E as,

$$\frac{L}{a} = \frac{3\Delta p}{2\pi E} \phi(\eta)$$

where $\phi(\eta)$ is a function dependent on the dimensions of the pipette wall. This model makes a few assumptions. Firstly, by treating the sample as a half-space it is assumed that both the width and thickness of the sample are much greater than the size of the aspiration region. Secondly, the sample is assumed to have homogenous mechanical properties, like Young's modulus. Thirdly, the deformations are assumed to be sufficiently small to treat the elastic response of the sample as linear. This model was developed for the application of micropipette aspiration to endothelial cells. The authors suggest that for this application, the first assumption is of greatest

concern, while the approximate linearity of the experimental measurements allays concerns for the last two assumptions ^[186].

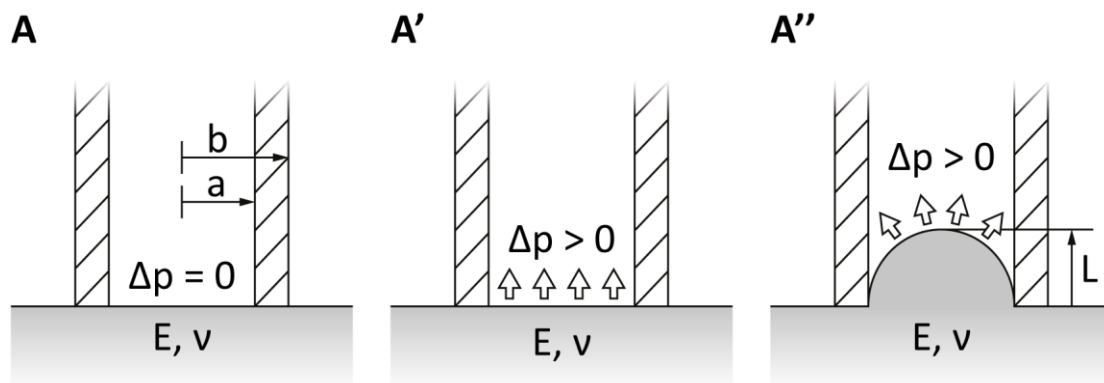


Figure 36. *Micropipette aspiration determines sample stiffness by applying pressure to its surface and measuring the size of resultant deformation. A*, the sample surface (grey) has mechanical properties of Young's modulus E and Poisson ratio ν , the micropipette has inner radius a and outer radius b . **A'**, when a pressure difference $\Delta p > 0$ is applied to the inner region, some time later **A''** an aspiration forms of height L from the tip of the micropipette.

Estimations of the value of $\phi(\eta)$ using finite element simulations have since been published ^[187]. The authors first rewrite the model equation with a consolidated parameter C so that,

$$\frac{L}{a} = \frac{\Delta p}{E} C.$$

They then constructed a cylindrical patch of tissue of radius R , and thickness h with finite element mesh. The micropipette was modelled as the pressure Δp applied within the inner region $r < a$ of an annulus centred at the center of the circular surface of the tissue, and the tissue surface was fixed within the region $a \leq r \leq b$. They then ran multiple simulations varying parameters b , h and R to determine how the value of parameter C changed. They found that for $b/a > 2$, $h/a > 2$ and $R/a > 2$ the value of C was unity. This suggests that if these geometric relations can be satisfied, the parameter C can be ignored. When applied to wing discs I found the third condition satisfied well, as the wing disc is much larger than the aspiration. The

second condition is satisfied for the columnar epithelium, whose apical-basal height is much greater than the pipette tip radius. However, the peripodial epithelium is much thinner than the pipette tip radius, so C is likely to be greater than unity. In fact modelling the peripodial epithelium as a half-space is a poor assumption, so I do not expect the model to give good predictions of Young's modulus.

To infer the contribution of the ECM to tissue stiffness I applied micropipette aspiration to wing discs either treated with CLS-1 or left untreated. CLS-1 treatment was applied, using the protocol outlined in §2.2.1, after mounting the wing discs. For each dataset I fit the model described previously, with $C = 1$, using Mathematica. The Young's modulus was then calculated from the gradient of the fitted line. The final results were grouped according to control or collagenase treatment, peripodial or columnar epithelium. To circumvent problems with the parameter C I decided to ignore absolute values of Young's modulus and instead take a ratio of control against collagenase for each tissue. The assumption here is the parameter C is approximately the same for all measurements of a given epithelium regardless of treatment, therefore this parameter should drop out when taking the ratio.

Having obtained results for collagenase treatment I wanted to continue by trying Rok inhibitor treatments using Y27632 as described in §2.2.1. However, during data collection I experienced a fault with the micromanipulator. While aspirating I would often notice the micropipette drifting out of position, leading to the micropipette tugging on the tissue, and making the results inconsistent. Despite sending the micromanipulator back to the manufacturer to be repaired, the drift was not fixed. Other problems with micropipette aspiration such as the slow rate of data acquisition and the difficulty of imaging the aspiration for older wing discs drove me to seek out other methods for measuring tissue stiffness. In the end I decided to proceed with atomic force microscopy, which has the benefits of being well established and a greater rate of data collection. The only drawback of atomic force microscopy is when indenting, rather than aspirating, more attention needs to be given to how the bulk responds to the applied deformation.

Atomic Force Microscopy

Atomic force microscopy (AFM) is a technique that can be used to measure the stiffness of a sample. AFM makes use of a cantilever with a tip on the end, Figure 37, which is used to indent the sample. The tip is pushed into the sample, which causes both an indentation of the tip into the sample, and a deflection of the cantilever away from the sample surface, Figure 37 C. How much the cantilever indents and deflects depends on the relative stiffness between the cantilever and the sample. If the stiffness of the cantilever is known, then the stiffness of the sample can be inferred from measurements of indentation and deflection. AFM can also measure the height of the sample surface, as the point at which a deflection occurs. Furthermore, by measuring multiple points across the surface of a sample, maps of height and stiffness can be obtained. It is also possible to measure the viscosity of a sample by applying an indentation and measuring how the deflection changes over time.

In the last decade or so, commercial companies have developed integrated AFM systems that combine both machinery and software, allowing more widespread use of this technique, for example in biology. The AFM system I have used is the JPK Cellhesion, which is an AFM built into an Olympus FV1000 inverted confocal microscope. This allows AFM measurements to be combined with confocal imaging concurrently on a single sample. The majority of the AFM is built into a 'head' with three height-adjustable legs that stands on a customised version of the moveable microscope stage. The bottom of the head is therefore offset from the surface of the stage and sample by a distance defined by the height of the legs. The bottom of the head has a slot in which a glass prism can be inserted. This prism is used to hold the cantilever. When inserted, the glass prism protrudes a certain distance out the bottom of the head, and the cantilever sits at the end of this protrusion. The distance the prism protrudes is a little greater than the height of a 35 mm glass-bottomed dish. The cantilever can therefore be brought into contact with a wing disc stuck to the bottom of a 35mm glass-bottomed dish by lowering the head *via* the height-adjustable legs. The back of the cantilever is coated with a reflective material.

The deflection of the cantilever is measured by reflecting a laser off the back of the cantilever, onto a detector in the head. The detector is able to convert the position of the incident laser into an electric signal. As the cantilever deflects, the angle of reflection of the laser changes, which is measured as a change in position on the detector. The height of the fixed end of the cantilever is held in place relative to the head, but is changed relative to the sample using the height-adjustable legs, controlled either coarsely by motor, or finely by piezo. The piezo allows precise measurement of changes in height.

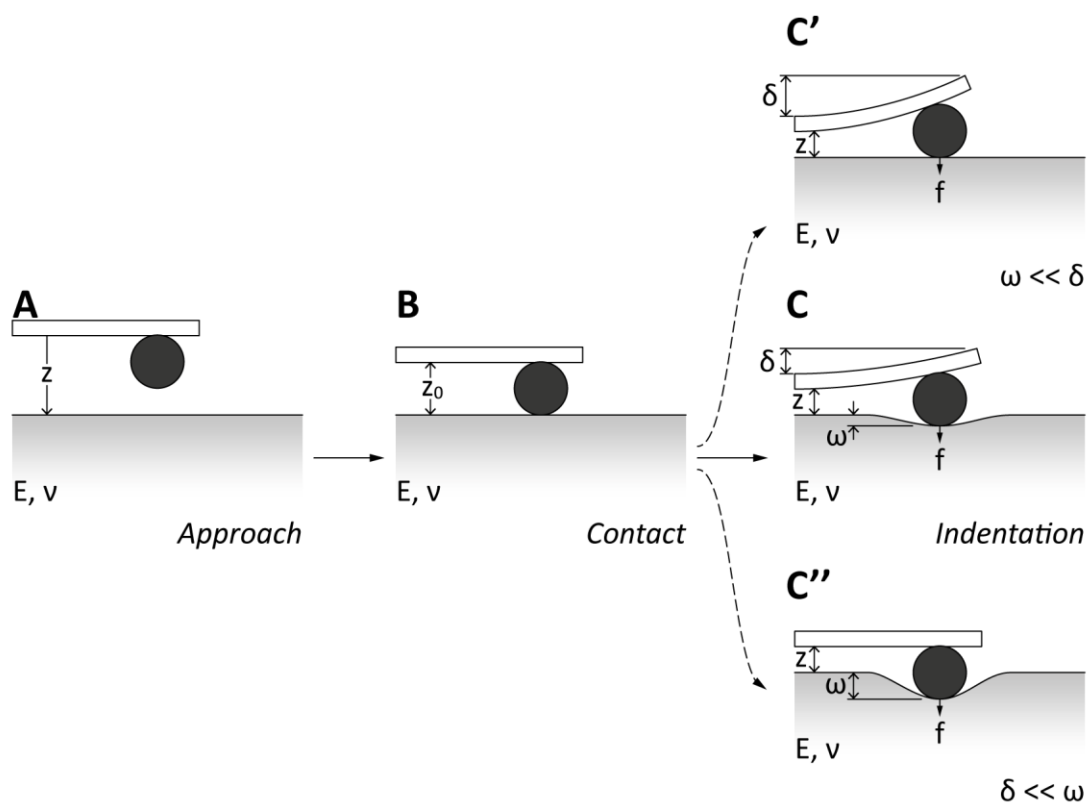


Figure 37. Atomic force microscopy measures sample stiffness by indenting with a cantilever of known stiffness and measuring the indentation-deflection relationship. **A – C**, the sample with Young’s modulus E and Poisson ratio ν is in grey, the cantilever of spring constant k is in white and the bead of radius R in black. **A**, the cantilever first approaches the sample, cantilever height is z . **B**, the bead makes contact with the sample surface at z_0 . **C**, for $z < z_0$ the sample is indented, ω , generating a deflection δ . Extreme cases are shown in **C'** and **C''** for extremely hard and extremely soft samples respectively. The cantilever spring constant is chosen relative to the expected sample stiffness to generate measurable indentations and deflections.

To obtain a measurement, the cantilever tip is first brought close to the sample surface, but without making contact. The cantilever height is then reduced at some constant speed. As the cantilever approaches the sample, a constant deflection is measured. At the point of contact, the cantilever deflection begins to increase. Once the deflection passes some threshold the cantilever velocity reverses, increasing in height at some constant speed. The measurement finishes once the cantilever has returned to its starting position. Throughout this process measurements of cantilever deflection and cantilever height are made at some frequency. These measurements trace a height-deflection curve.

To convert measurements to standardised units the cantilever must be calibrated. The calibration converts cantilever deflection from a voltage, δ_V , measured by the detector to a cantilever deflection measured in meters, δ , and then to deflection force, f , in newtons, which is the force required to displace the cantilever. A measurement is made on a hard surface such as a glass slide. Because the surface is hard the cantilever does not indent, therefore the deflection force, f , depends only on cantilever displacement, z , *via* Hooke's law,

$$f = k\delta = kz$$

where k is the spring constant of the cantilever. The measurement on a hard surface will therefore produce a linear relationship between cantilever displacement and deflection, $z = k_V\delta_V$. With this relationship, cantilever deflection can be converted from units of volts to metres using the cantilever displacement, which has a known unit in metres. A conversion parameter, k_V , in volts per metre can be found from the hard surface measurement by finding the gradient of the deflection-displacement curve. Applying this conversion parameter to any future deflection, $\delta = k_V\delta_V$, converts it from volts to metres. To find the deflection force from the deflection displacement, the cantilever spring constant must be found. There are multiple ways to measure cantilever spring constant, I have used the thermal noise method. Thermal fluctuations in the air can drive oscillations in cantilever deflection. Cantilever oscillations can be treated as a simple harmonic oscillator, which *via* the

equipartition theorem, allows the spring constant k , to be related to the mean square spring deflection $\langle \delta^2 \rangle$,

$$k = \frac{k_B T}{\langle \delta^2 \rangle} = \frac{k_B T}{P}$$

where $\langle \delta^2 \rangle$ is equal to the integral of the power spectrum P . The power spectrum is obtained experimentally by measuring the average deflection power as a function of deflection frequency. A Lorentzian function is fitted to the power spectrum and integrated. From the power spectrum integral the spring constant is calculated ^[188]. This calibration procedure is performed within the JPK AFM software.

The cantilever tip I have used is a fluorescent bead. The cantilevers I have used are manufactured without tips, allowing a bead to be attached by the user. The cantilevers I have used come as a single chip with multiple cantilevers, each with a different stiffness. The manufacturer quotes an estimate of the stiffness of each cantilever, but a more accurate stiffness can be measured for each cantilever using the calibration method described previously. When stuck, the cantilever-bead combination will have a different spring constant to the bare cantilever, so the spring constant of each cantilever has to be obtained first. To stick a bead to a cantilever, fluorescent beads are first dried onto a glass slide. I have used beads of 15 μ m diameter, which fluoresce at far-red wavelengths. A pool of ultraviolet light-activated glue is placed on the same slide as the dried beads. On the AFM, the spring constant of a bare cantilever is measured using the glass slide as a hard surface. While still on the AFM, the tip is moved over to the pool of glue using the moveable stage. The tip of the cantilever is then momentarily dipped into the glue. The cantilever with the blob of glue is then moved over an isolated bead. The tip is then brought into contact with the bead, allowing the glue to capture the bead. If successful, the bead will stay with the cantilever tip as it is lifted from the surface. To solidify the glue, the cantilever tip is irradiated with ultraviolet light for 10 minutes. Usually this permanently bonds the bead to the cantilever tip.

After calibrating the cantilever and attaching a bead, measurements can then be taken for live samples. Before each session, the conversion parameter k_V for the cantilever is re-measured because its value changes between air and fluid media, as well as varying with cantilever position relative to the detector. Sample measurements are taken as described previously. In fluid, if the cantilever moves too fast then hydrodynamic drag can generate a significant and nonlinear deflection of the cantilever during approach. I found that a speed of $1\mu\text{m/s}$ was slow enough to make this approaching deflection insignificant, and thus render hydrodynamic drag negligible. At this speed the indentation timescale is on the order of seconds, which is well below the minutes remodelling timescale of the cytoskeleton, suggesting remodelling contributions can be ignored. I have found that for the wing disc a 10nN maximum deflection threshold is sufficient to produce analysable curves. It is possible to obtain Young's modulus from the indentation-deflection curve produced when either indenting or retracting from the sample. I have chosen to use the indentation method to calculate Young's modulus, and therefore I can discard the retraction data. This allows me to set a faster retraction speed of $10\mu\text{m/s}$, which increases the rate of curve acquisition. The JPK software is connected directly to the microscope stage allowing measurements to be taken automatically over multiple positions with multiple repeats. I set the retraction distance taking into account changes in the height of the tissue between positions. I use a measurement frequency of 10kHz . Measurements are saved in a proprietary format by the software, which I then convert to raw data text files. I then perform processing and analysis on this raw data using a python script I have written.

Raw data for measurements obtained from the software are in terms of cantilever height, z , and cantilever deflection force, f . To make interpretation of results more intuitive, cantilever height measurements are converted to indentation. The indentation, ω , is the difference in cantilever height, z , from the contact point, z_o , minus the deflection, δ ,

$$\omega = z_o - z - \delta.$$

Calculating indentation requires first determining the contact point between sample and tip. The contact point is defined by a discontinuity in deflection change with height. For hard samples the discontinuity is large, and therefore straightforward to detect from derivatives of deflection with respect to height. However, for soft samples the discontinuity can be subtle. To automatically detect the contact point I have adapted a published method ^[189]. The deflection measurements are chronologically ordered. A window is selected consisting of the first 2000 deflection measurements. The standard deviation of the deflections within the window is calculated. This initial window contains only deflections before contact is made with the sample, therefore the standard deviation of these deflections represents the thermal noise of the cantilever when free in the media. The window is then repeatedly shifted along by one measurement and the absolute difference between the first and last deflections of the window is calculated. When the difference in deflections is greater than six times the initial thermal noise, then the process is stopped. The contact region is then assumed to be within this final window, the contact window.

The Hertz model is commonly used to obtain the Young's modulus from an indentation-deflection curve. The Hertz model is another example of a solution to a contact problem. The general case of the Hertz model considers contact between two infinitely large elastic spheres ^[190]. This treatment requires the contact region between the spheres to be much smaller than the size of either sphere. Firstly, this treatment allows boundary contributions to become negligible due to their distance. Secondly, this treatment allows the region outside the contact region to be approximated as the plane of a half-space. Thirdly, this treatment means deformations are small, so that only the linear elastic response need be considered. Furthermore, the sphere surfaces must be frictionless to assume linear elasticity. For contact between a sphere and a plane, the radius of one of the spheres is assumed to be infinite. The surfaces of the bodies cannot conform, which is a further violation of the models assumptions. This model assumes both bodies have uniform mechanical properties ^[191].

When assuming the sphere is much stiffer than the sample, the Hertz model takes the form,

$$f = \frac{4ER^{\frac{1}{2}}}{3(1-\nu^2)}\omega^\gamma$$

where E is Young's Modulus, ν is Poisson ratio, R is tip radius and γ is a factor dependent on tip shape. Cantilever tips can take many shapes, such as cones, cylinders or spheres. I have used a spherical tip, whose contact region has been shown to be predicted well by the Hertz model when indenting tissues ^[192]. Spherical tips have $\gamma = 3/2$. Therefore, the Hertz model predicts a polynomial relationship between indentation and deflection,

$$f = \beta\omega^{3/2},$$

where,

$$\beta = \frac{4ER^{\frac{1}{2}}}{3(1-\nu^2)}.$$

The contact window contains 2000 candidate contact points. To find the best contact point, a least squares fit of the Hertz model is applied to the data for each candidate assuming it to be the contact point. From the candidate contact point, a fit is applied to the data up to a maximum indentation of

$$\omega_{max} = R - (R^2 - R_{max}^2)^{1/2},$$

where R_{max} is the maximum radius of the contact region, which I have fixed at $R_{max} = 3\mu m$. By limiting the indentation depth, analysis is kept consistent, and the assumption of small deformations in the Hertz model is maintained. Both the pre-contact and the post-contact regions are fit to using a linear model and a polynomial Hertz model respectively,

$$f(\omega) = \begin{cases} f_o + \alpha\omega, & \omega < 0 \\ f_o + \alpha\omega + \beta\omega^{3/2}, & 0 \leq \omega < \omega_{max} \end{cases}$$

where $f_o = f(0)$, the deflection force at the contact point. Because these functions are polynomial it is possible to generate exact solutions to the least squares, which I have used to speed up the fitting process. The pre-contact region is fit to first, obtaining a value for α , which accounts for drift in the deflection measurement. The drift is usually negligible, but is accounted for anyway. The post-contact region is fit to second, using the value of α obtained from the linear fit, to obtain a value for β . For both linear and polynomial fits, f_o is allowed to vary as a free parameter, which gives two values f_{lo} and f_{po} respectively. Generally these two values are approximately zero, however when they are large it implies a poor fit and are therefore used as a measure of fit quality^[189]. A measure of fit quality is then used to determine the contact point to use. For the measure of fit quality, Δ , I have used,

$$\Delta = \Delta_e + \Delta_o.$$

Where Δ_e is the mean squared errors of the linear and polynomial least square fits,

$$\Delta_e = \frac{1}{n} \sum_{i=1}^n (f(\omega_i) - f_i)^2,$$

and Δ_o is the square of the difference between contact point deflections of linear and polynomial least square fits,

$$\Delta_o = (f_{lo} - f_{po})^2.$$

The candidate contact point used is the one with the smallest value of Δ . The Young's modulus E is calculated from the fit parameter β as,

$$E = \frac{3\beta(1 - \nu)^2}{4R^{1/2}}.$$

Where the Poisson ratio is assumed to be $\nu = 0.5$, which means the material is treated as incompressible, which is observed in cell culture ^[192]. The radius of the bead $R = 7.5\mu m$. After fitting, a plot is automatically generated showing the fit overlaid on the data. I then manually inspect each fit to determine if it is useable. For example, if the contact point has been incorrectly determined I discard the fit. If the fit at the contact point deviates too far from zero I discard the fit. The majority of poor fits result from indentation-deflection curves that deviate too far from the Hertz model. Usually this deviation is experimental error, for example spikes due to noise in the AFM room, or detritus floating in the dish interfering with the cantilever. However, it is the consistent deviations from the Hertz model that were of concern, as they could suggest violations of the models assumptions.

For the first trials using AFM on wing discs I took measurements at positions in a line along the anterior-posterior axis. The form of the generated curves varied greatly. If the wing disc tissue matched the assumptions of the Hertz Model well, then the experimental measurements should follow the same exponential relationship. However the curves obtained in this initial data collection varied greatly, with only some fitting the Hertz Model well. It could be that deviations from the Hertz Model occur due to heterogeneity in tissue stiffness, for example differences in stiffness between the ECM and the cells, which would violate the homogeneity assumption. However, before considering this possibility, there are other simpler explanations. By looking at sections of the wing disc during indentation, Figure 39 B, it is clear that where the columnar epithelium is not well supported by the coverslip this region of tissue translates rather than deforming. Any translation of the tissue will cause an underestimation of tissue stiffness, and are therefore not useable. As the hinge region is not well supported, and is generally not flat, I have not proceeded with measurements of the hinge. Similarly, the notum region has a layer of myoepithelial cells that I expect to have considerably different properties to the epithelium they cover, I have therefore not proceeded with measurements of the notum. All

measurements I have taken are therefore in the pouch region. The pouch columnar epithelium is flat and well supported, making it the best candidate for good quality, interpretable stiffness measurements.

One problem with indentation in the pouch region is its tendency to come unstuck at the periphery. Where the pouch epithelium comes unstuck, it begins to form a cup shape, whose rim can make contact with the cantilever while indenting, Figure 39 A. If the cupping is considerable enough then this erroneous contact will occur before bead contact, which leads to an underestimation of stiffness and misshapen indentation-deflection curves. This is a problem I have been unable to completely solve. When I mount the wing discs, I make sure there is plenty of cell-tak and discs are flattened to stick them as well as possible. However, it is usually only a matter of time before they become unstuck, so I have had to minimise the time between sample preparation and measurement as much as possible. Further, I have found that younger wing discs have less curvature in the pouch to begin with than older wing discs, and so tend to stick down better. Some treatments, such as CLS-1 increase the likelihood of wing discs becoming unstuck, likely due to degradation of the ECM that binds the cell-tak. Again, I have found no way around this problem, and so I get a lower yield of useable measurements per dish for some treatments compared with others. To confirm each wing disc has remained stuck, I take images of the wing disc cross-section after measurement. If a wing disc has become unstuck, then I cannot trust the measurements, so I do not take the measurement data through to the analysis stage. By limiting indentation measurements to the pouch region and taking into account erroneous contact, I found the indentation-deflection curves to be a consistent shape that fit the Hertz Model well, Figure 40.

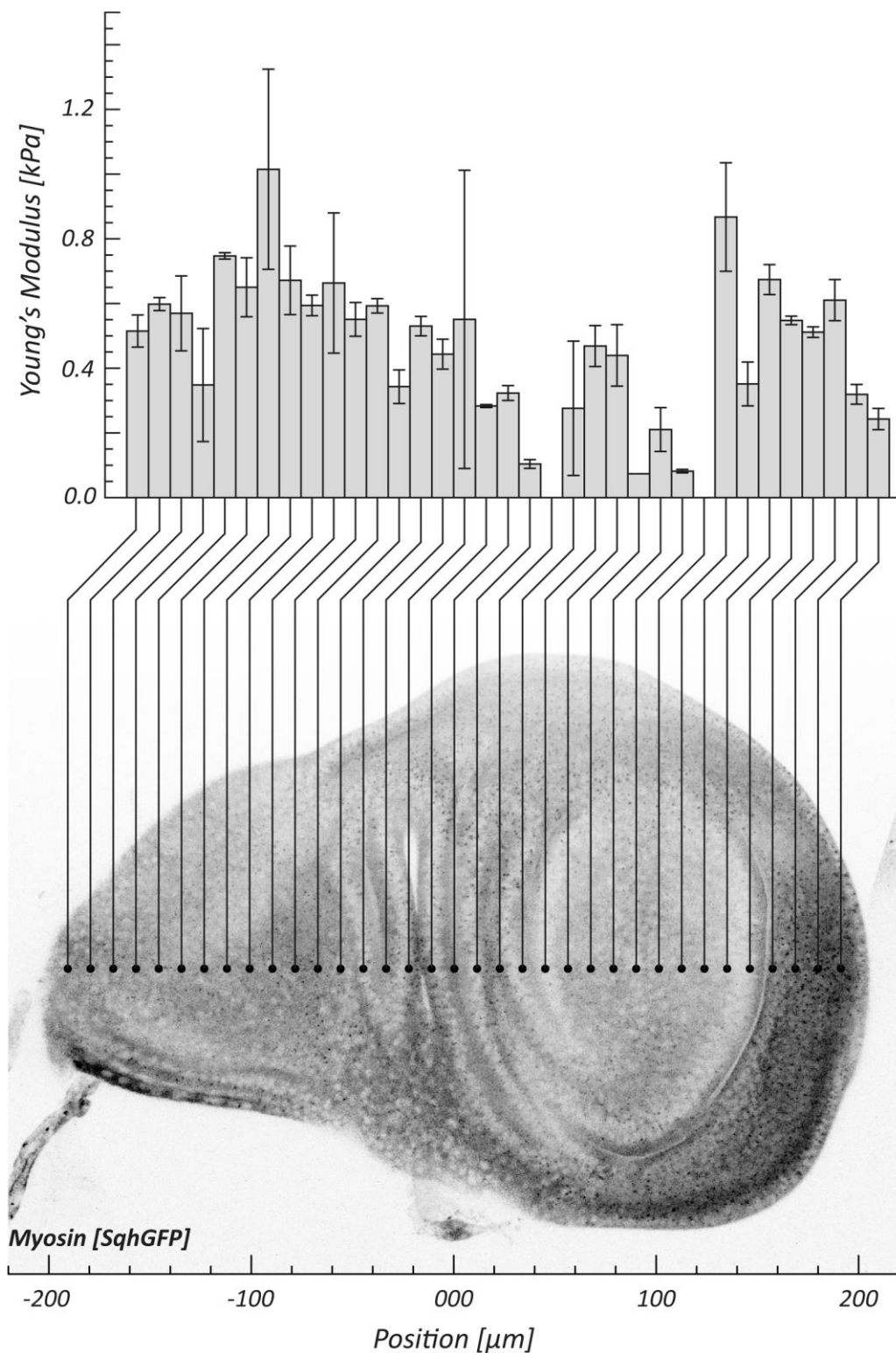


Figure 38. Wing disc stiffness as measured by atomic force microscopy varies considerably from point to point. Measurements of Young's modulus, shown above, for a series of points along the midline of a wing disc, shown in the image below. Error bars are the standard deviation of repeated measurement of a given point. Bars with no error indicate only a single successful measurement at that point. Points with no bar indicate no successful measurements.

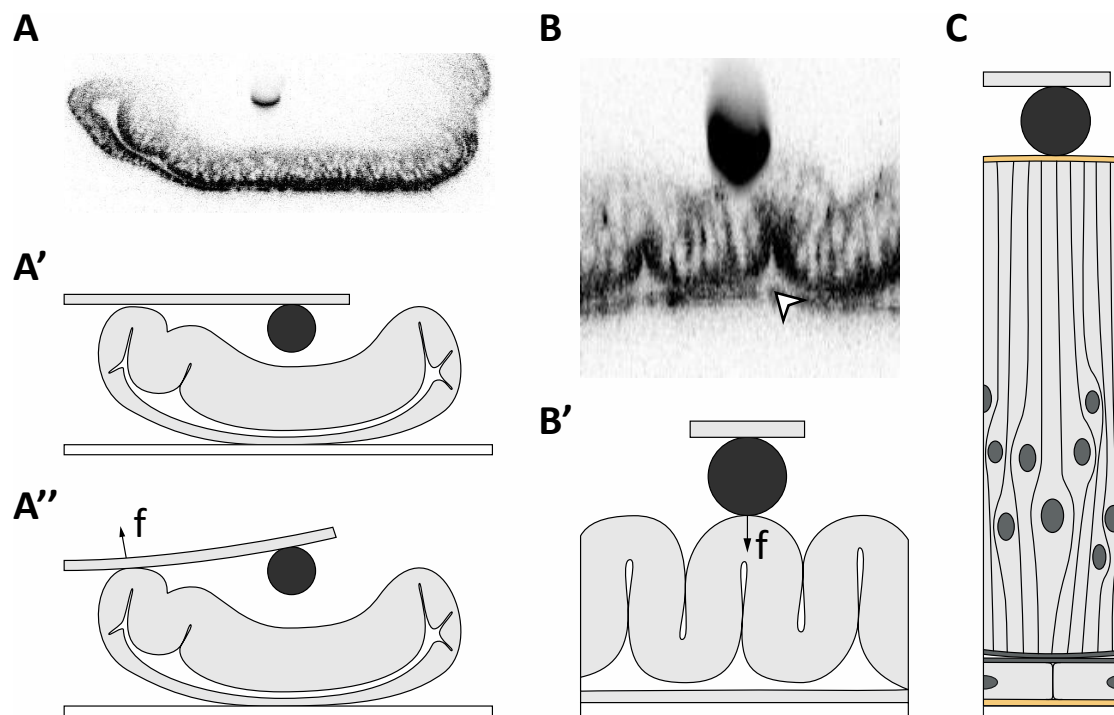


Figure 39. *Correct stiffness measurement requires careful consideration of sample preparation. A*, is a wing disc section showing the bead has not made contact with the sample despite recording a cantilever deflection. **A'** and **A''** describe how the curvature of wing discs can cause erroneous cantilever-sample contact. **B**, is a wing disc section focusing on the hinge region, the hollow arrow indicates regions of the columnar epithelium that are not well supported, shown diagrammatically in **B'**. **C** is a diagram depicting the different layers in the wing disc potentially contributing to the measured 'effective' tissue stiffness.

For the first set of experiments, I wanted to obtain the change in Young's modulus of wing discs due to some treatment. To do this I measured a given wing disc once before treatment, and once after treatment. These treatments would be applied to a whole dish, therefore I had to measure wing discs before treatment in one batch, then apply the treatment to all wing discs in the dish and then measure the same wing discs again as one batch after treatment. This would result in a time delay between measuring before and after treatment for a given wing disc. When analysing these results for the control condition of no treatment, I found wing discs would soften over this time interval by around 15%, Figure 41. I was concerned that this significant softening-over-time may be caused by some part of my protocol. I tried reserving imaging until after all measurements in order to limit photo-damage,

although it didn't seem to help much. I tried replacing the media after measuring each wing disc in order to supply them with plenty of nutrients, which also didn't seem to help much. I tried placing dissected fat bodies into the dish in case it would provide some unknown factor, however this didn't help either. I tried minimising the number of wing discs I imaged to three in order to reduce experiment time, which did help. I was concerned that any excess cell-tak could have dissolved into the media and may be toxic, so I tried replacing the media after mounting the wing discs, which appeared to help. Finally, I was concerned thermal drift may affect measurement of deflection, so I tried recalibrating the cantilever between each wing disc, which didn't appear to help. Over the course of trying out these possibilities, I found the softening-over-time became considerably reduced, Figure 41, but it is not clear that this improvement was from any specific experimental parameter I changed. I think another factor is simply that by practicing the experiment I became faster at it and therefore minimised the measured softening.

The final protocol for AFM with treatments uses the genotype *SqhAx3;SqhGFP* to visualise the wing disc. Indentation-deflection measurements are obtained from 4 wing discs per dish, 4 positions are measured per wing disc and the set of positions is measured 3 times. Treatments are then applied, to the dish. For CLS-1, the media in the dish was replaced with 16.2 mg/mL of CLS-1 in media for 5 minutes then washing four to five times with media before proceeding. The control treatment for CLS-1 is the same protocol but replacing CLS-1 in media with just media. For Y27632, the media in the dish is replaced with 320 mg/mL (1mM) of Y27632 in media and is allowed to remain for 20 minutes before proceeding. The control treatment for Y27632 is the same protocol but with 3.33% distilled water in media. For Latrunculin-A, the media in the dish is replaced with 4.22 mg/mL (100 μ M) Latrunculin-A in media and is allowed to remain for 20 minutes before proceeding. The control treatment for Latrunculin-A is the same protocol but with 1% ethanol in media. After applying the treatment, the 4 wing discs are measured again as before, and in the same order. However the positions on the wing discs are not exactly the same before and after treatment due to slight movement of the dish. Sometimes wing discs become unstuck during or after the treatment process, in which case they are skipped and

the data discarded. Indentation-deflection curves are fit with the Hertz Model to obtain Young's moduli. The three Young's moduli for each point are averaged, then the four Young's modulus for treated or untreated wing disc are averaged. The Young's modulus of a wing disc after treatment is divided by the Young's modulus for that wing disc before treatment to obtain a ratio, Figure 43 A. This ratio is the amount the wing disc has softened as a result of the treatment. To then take into account softening-over-time, I divided the average of Young's moduli for each treatment, CLS-1, Y27632 and Latrunculin-A by its control treatment, media, water and ethanol, respectively, Figure 43 A'. I believe this gives the best approximation of the softening of wing discs as a result of the applied treatment alone.

I have also measured the Young's modulus of wing discs after applying different genetic perturbations. For genetic perturbations I have obtained measurements from at most 6 wing discs per dish, 4 positions are measured 3 times each. Unlike treatments, I can't get a before and after perturbation per wing disc, so instead I measure a set of wing discs for the perturbation and a different set of wing discs for the control condition. The genetic perturbations are Trol knockdown (UAS-TrolRNAi) and Trol overexpression (UAS-Trol) driven throughout development with Act-Gal4, recombined with CAAX-GFP to visualise the wing disc. The control genotype used for this perturbation is just Act-Gal with no UAS driven transgene, again recombined with CAAX-GFP. Indentation-deflection curves are fit with the Hertz Model to obtain Young's moduli. The three Young's moduli for each point are averaged, and then the four Young's moduli are averaged for each wing disc. Young's moduli for wing discs of a given perturbation are then averaged and standard deviation plotted, Figure 45.

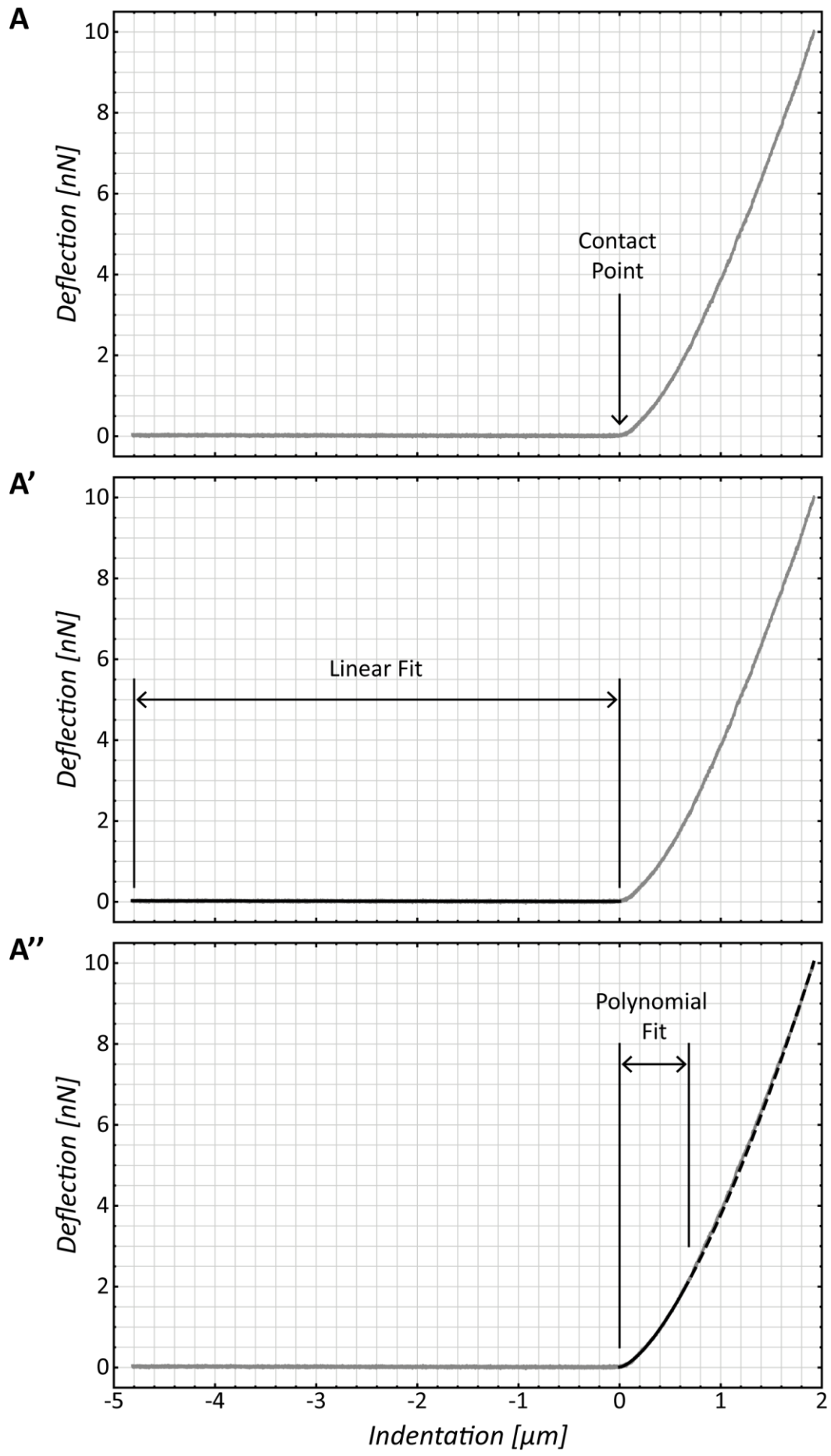


Figure 40. After discarding erroneous stiffness measurements, resulting indentation-deflection curves fit the Hertz model well. **A**, an example of an indentation-deflection curve, data points are shown in grey. **A'**, a linear fit, black solid line, is made to the region of the curve up to the contact point. **A''**, the hertz model is fit the region of the curve after the contact point but below a certain indentation depth, black solid line, the dashed black line is an extension of the fitted hertz model to unfit region of the curve.

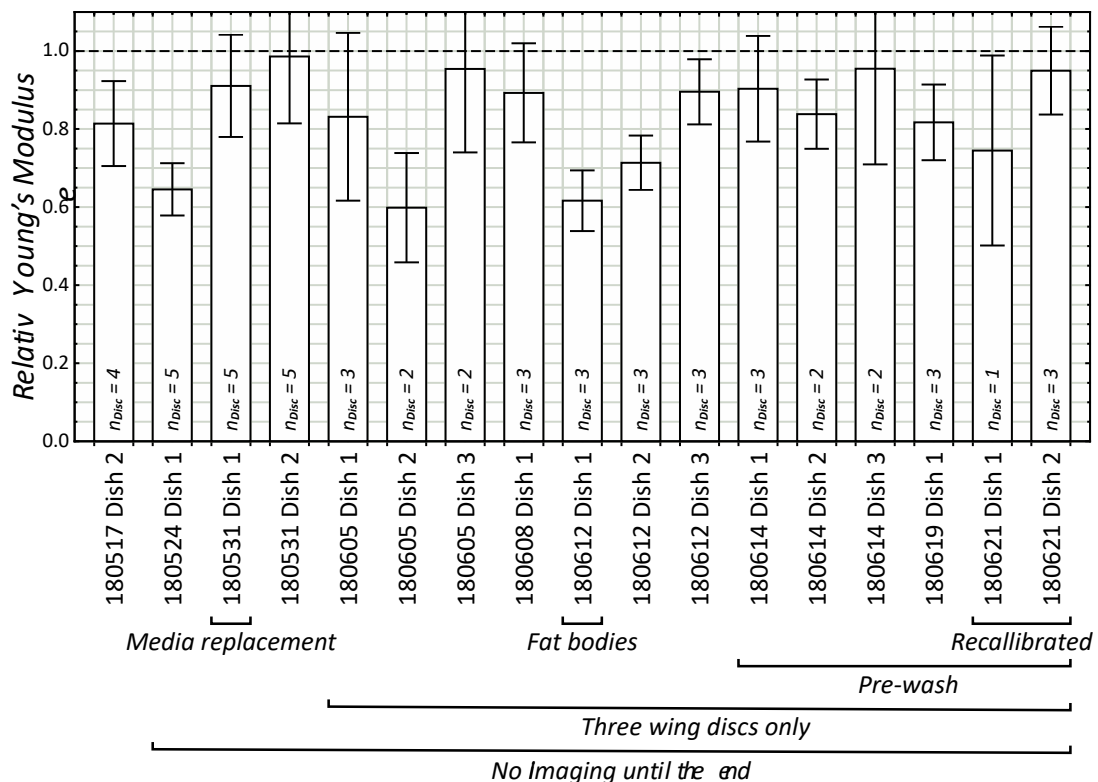


Figure 41. Wing disc stiffness decreases systematically *ex vivo*. Relative Young's modulus is given for a series of wing discs cultured in media. Different experimental setups are indicated. *Media replacement* involves replacing media in the dish between measuring each wing disc. *Fat bodies* have fat bodies dissected and placed in the dish with the wing discs during measurement. *Recalibrated* has the cantilever sensitivity recalibrated between measuring each wing disc. *Pre-wash* involves replacing the media immediately after mounting samples to remove any dissolved cell-tak. *Three wing discs only* are where only three wing discs are measured to cut down on experiment time. *No imaging until the end*, involves dispensing with imaging before treatment.

I have also plotted Young's modulus against size for each wing disc, both for treatments, Figure 44, and perturbations, Figure 46. To measure the wing disc size I have manually drawn a circle around the pouch region of the wing disc, as shown in Figure 44 B – D and Figure 46 B – D. I have then taken the diameter of this circle as an approximate, characteristic diameter of the wing disc. By calling the size 'characteristic' I am trying to acknowledge that this measurement is fairly abstract. I have then performed a linear fit on each set of points. The gradient of the fitted line gives the stress per unit size of each wing disc, while the standard deviation of the gradient can be used to determine if the gradients are significantly different between conditions, Figure 46 E.

Statistics

For Figure 43 A, violin plots with overlaid data points are shown for six conditions. These conditions form three control-treatment pairs. Data points of some of these conditions were found not to be normally distributed, so to test significant difference between pairs a nonparametric Kolmogorov-Smirnov two sample test was applied to each. Results from these tests are shown by lines connecting the violins with a significance label. For Figure 43 A', significant difference between pairs of treatment-control ratios are tested by permutation test. Permutation test involves randomly permuting labels of data points and calculating a new test statistic, T_i . In this case the test statistic used was,

$$T_i = \frac{\hat{E}_{T1}}{\hat{E}_{C1}} - \frac{\hat{E}_{T2}}{\hat{E}_{C2}}$$

and a p value is calculated as the number of permuted test statistics that are less than or equal to the original, unpermuted test statistic, $T_i \leq T$. Calculated bars are shown as lines connecting ratio bars.

For Figure 45A, it was found that data points of one of the groups is not normally distributed, therefore a nonparametric Kruskal-Wallis test was used to determine if there is any significant difference between the means of these populations. It was found that there is, and so a Mann-Whitney U test was applied to each pair, and results indicated as a significance label and line connecting the two. The same nonparametric procedure was used for Figure 45B. In Figure 44 A and Figure 46 A – A'' linear fits were performed using the SciPy *linregress* function. This function provides p values for the hypothesis that the fitted gradient is different than zero, which are shown on the plot.

2.3.2 Results

Treatments

Preliminary results using micropipette aspiration with CLS-1 treatments are shown in Figure 42 C. These results show the columnar epithelium stiffness reduces to approximately 15% after treatment with CLS-1. A reduction to approximately 45% after CLS-1 treatment was found for the peripodial epithelium. A similar result was found using AFM Figure 43 A', where columnar epithelium stiffness reduced (23 ± 3)% after treatment with CLS-1. These results are consistent with the ECM contributing a considerable amount of stiffness to the tissue.

Using AFM I have found wing discs treated with Y27632 fall to (67 ± 6)% of their original stiffness, Figure 43 A'. Wing discs treated with Latrunculin-A fall to (23 ± 2)% of their original stiffness, Figure 43 A'. Latrunculin-A degrades filamentous actin, which effectively removes the cell cortices. By removing filamentous actin, myosin contractility will also be lost, therefore the Y27632 effect is like a subset of the Latrunculin-A effect. Measurements of effective tissue stiffness against wing disc size are shown in Figure 44. Measurements of effective tissue stiffness against wing disc size are shown in Figure 44. A linear regression on this data suggests there a statistically significant change in stiffness with wing disc size.

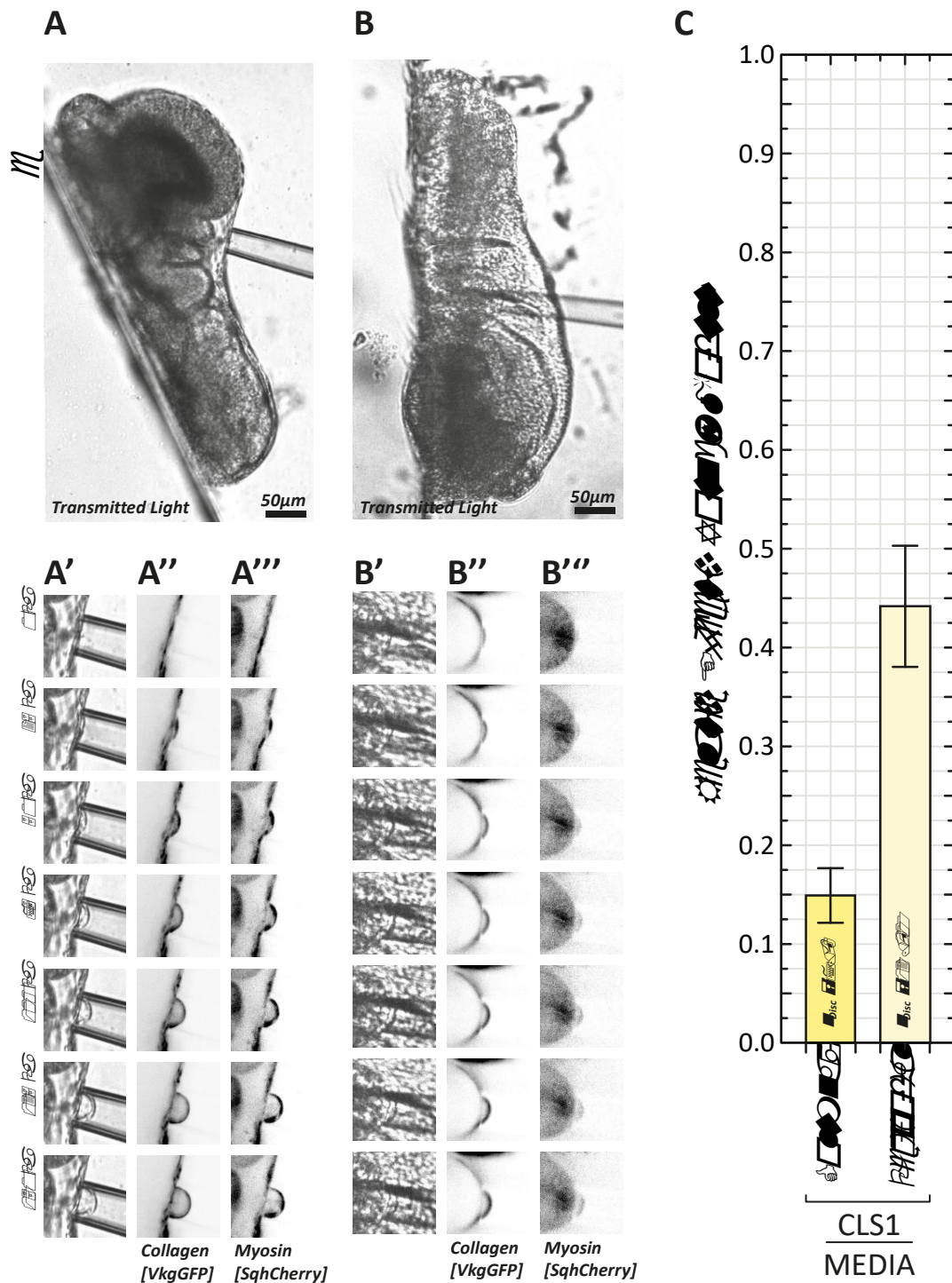


Figure 42. Degrading the extra-cellular matrix with collagenase leads to a considerable reduction in effective tissue stiffness. **A** shows an example of micropipette aspiration of wing disc peripodial epithelium. **B** shows an example of micropipette aspiration of wing disc columnar epithelium. **A' – A'''** and **B' – B'''** show magnifications of aspirations for peripodial and columnar epithelia respectively. **C**, relative Young's modulus is the mean Young's modulus of wing discs treated with CLS-1 normalised by the mean Young's modulus of untreated wing discs.

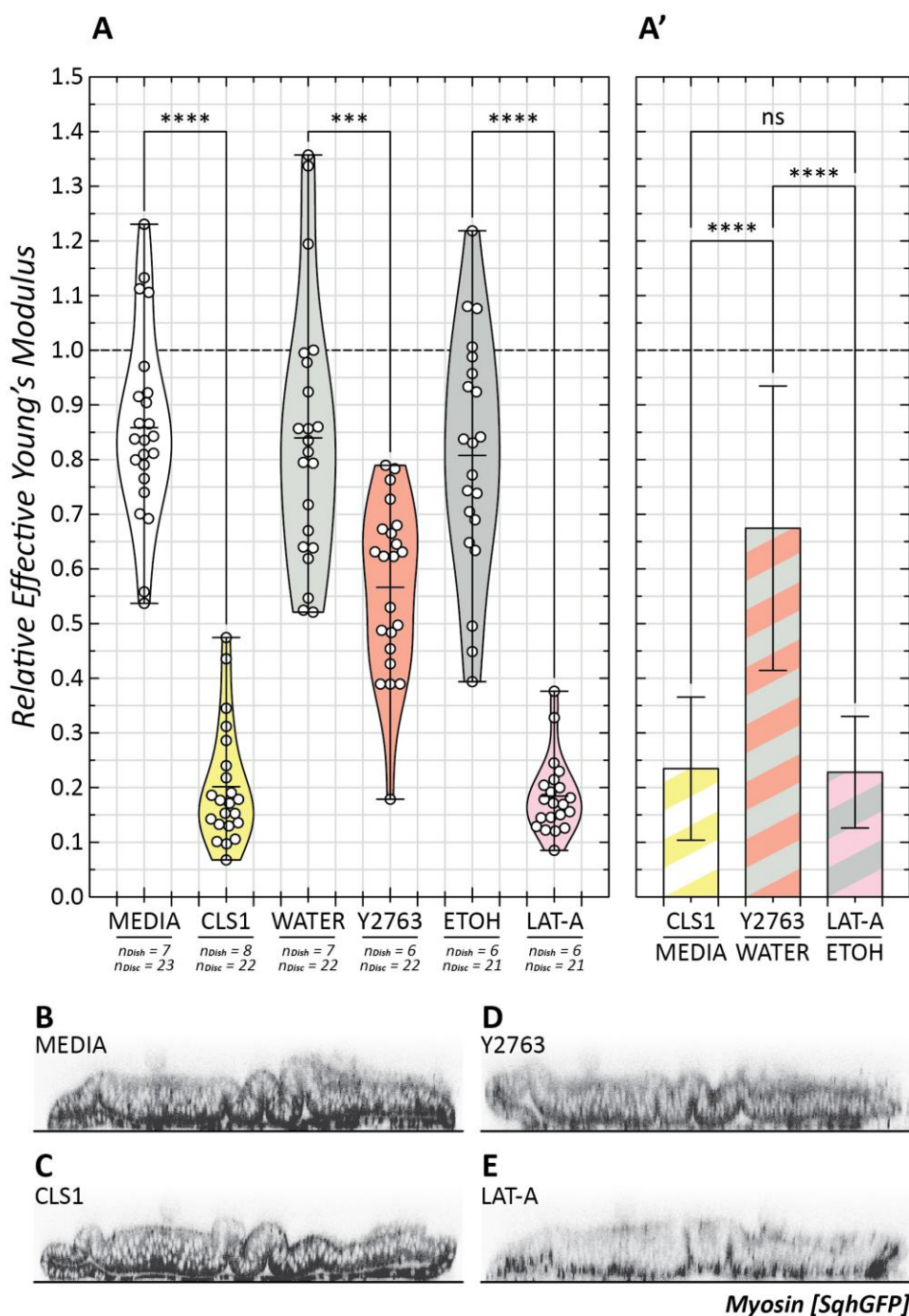


Figure 43. Degradation of the cell cortices reduces effective tissue stiffness to a similar level to extra-cellular matrix degradation. Stiffness measurements of the basal wing disc pouch using atomic force microscopy. **A**, relative effective Young's modulus is measured Young's modulus of a wing disc after treatment divided by its measured Young's modulus before treatment, where dots represent individual wing discs. **A'**, relative effective Young's modulus is the mean Young's modulus of treated wing discs divided by the mean Young's modulus of wing discs treated with its control treatment. Where MEDIA, WATER and ETOH are control treatments of CLS-1, Y2763 and LAT-A respectively. **B – E** show wing disc sections after treatment with media, CLS-1, Y27632 and Latrunculin-A respectively.

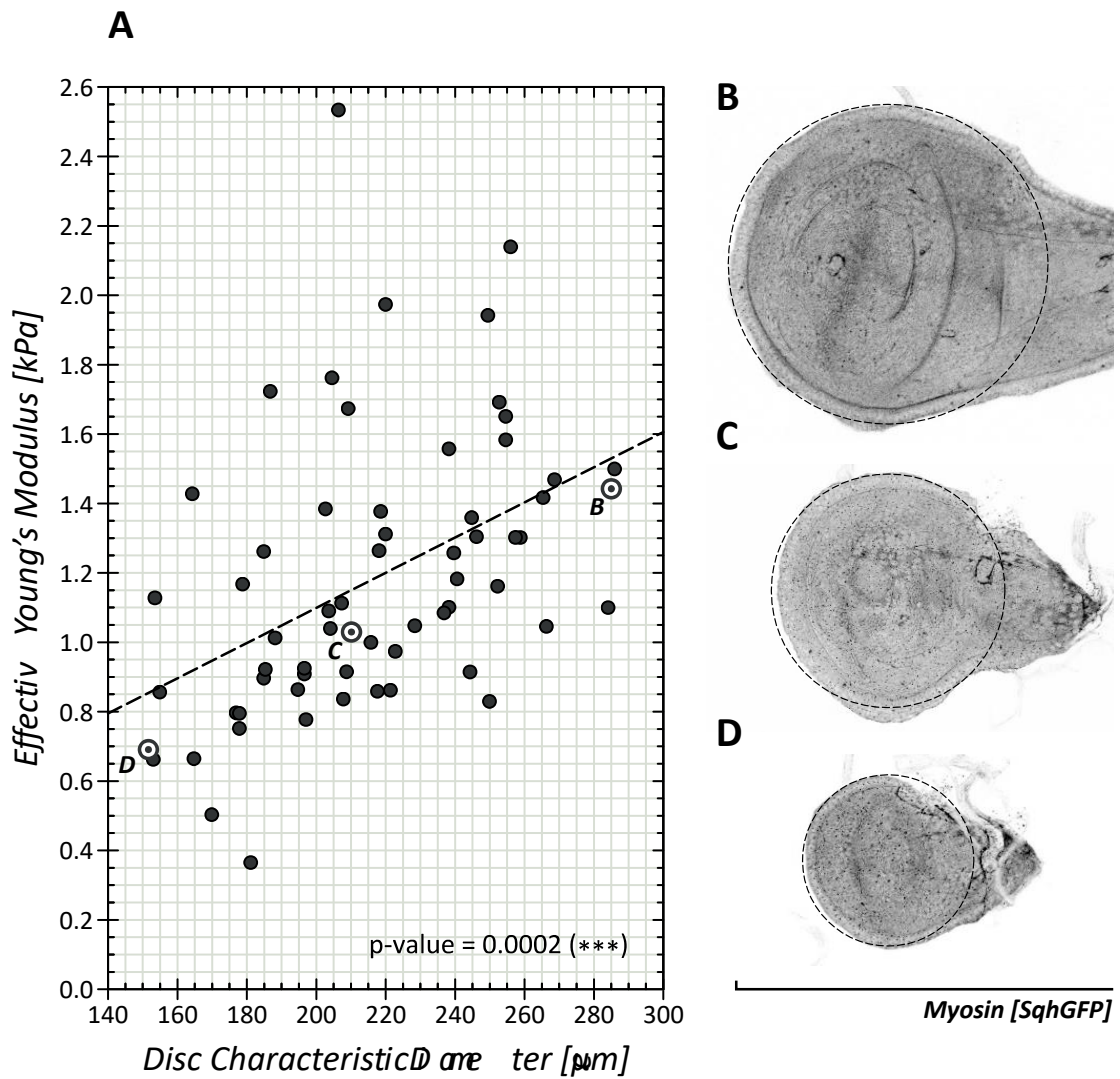


Figure 44. *Effective stiffness increases with increasing wing disc size.* **A** shows a scatter plot of effective Young's modulus against characteristic diameter for individual wing discs measured by atomic force microscopy. **B – D** show summed projections of wing discs whose stiffness have been measured. Characteristic diameter is measured as the diameter of a circle manually fitted to the pouch region of a flattened wing disc as shown with dashed circles in **B – D**. The dashed line in **A** is a linear fit to the data, whose gradient is significantly different from zero.

Perlecan

It was previously reported that perlecan knockdown and overexpression could stiffen or soften the ECM respectively ^[16]. As shown in Figure 22, perlecan knockdown and overexpression have morphological phenotypes in the wing disc, the former appearing to compact the tissue. I wanted to see if these phenotypes correlated with a change in wing disc stiffness. Measurements of effective Young's modulus with perlecan knockdown and overexpression are shown in Figure 45 A. These results show a significant increase in stiffness when perlecan is knocked down compared with control or perlecan overexpression. However, no significant difference is observed between perlecan overexpression and control. The change in effective Young's modulus with wing disc characteristic diameter for perlecan perturbations are shown in Figure 46 A. Qualitatively, the stiffness of perlecan knockdowns tend to increase at a greater rate with respect to wing disc size compared with perlecan overexpression and controls. The change in perlecan concentration in the ECM with perlecan knockdown or overexpression was characterised by measuring the fluorescence intensity of wing discs stained with a perlecan antibody, shown in Figure 45 B. These results show perlecan knockdown reduces perlecan concentration to $(16 \pm 2)\%$ of control concentration, while perlecan overexpression increases perlecan concentration to $(230 \pm 20)\%$ of control concentration.

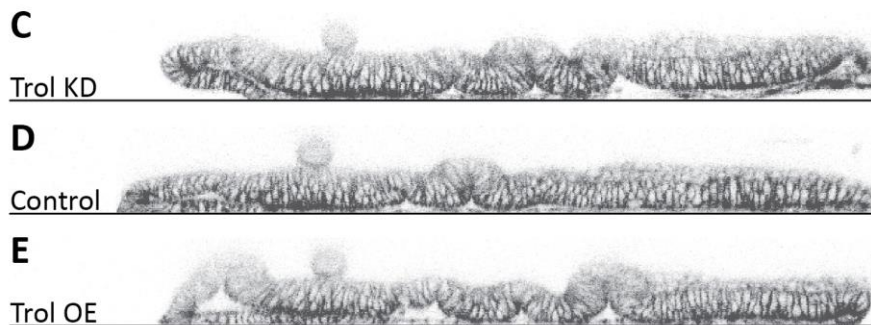
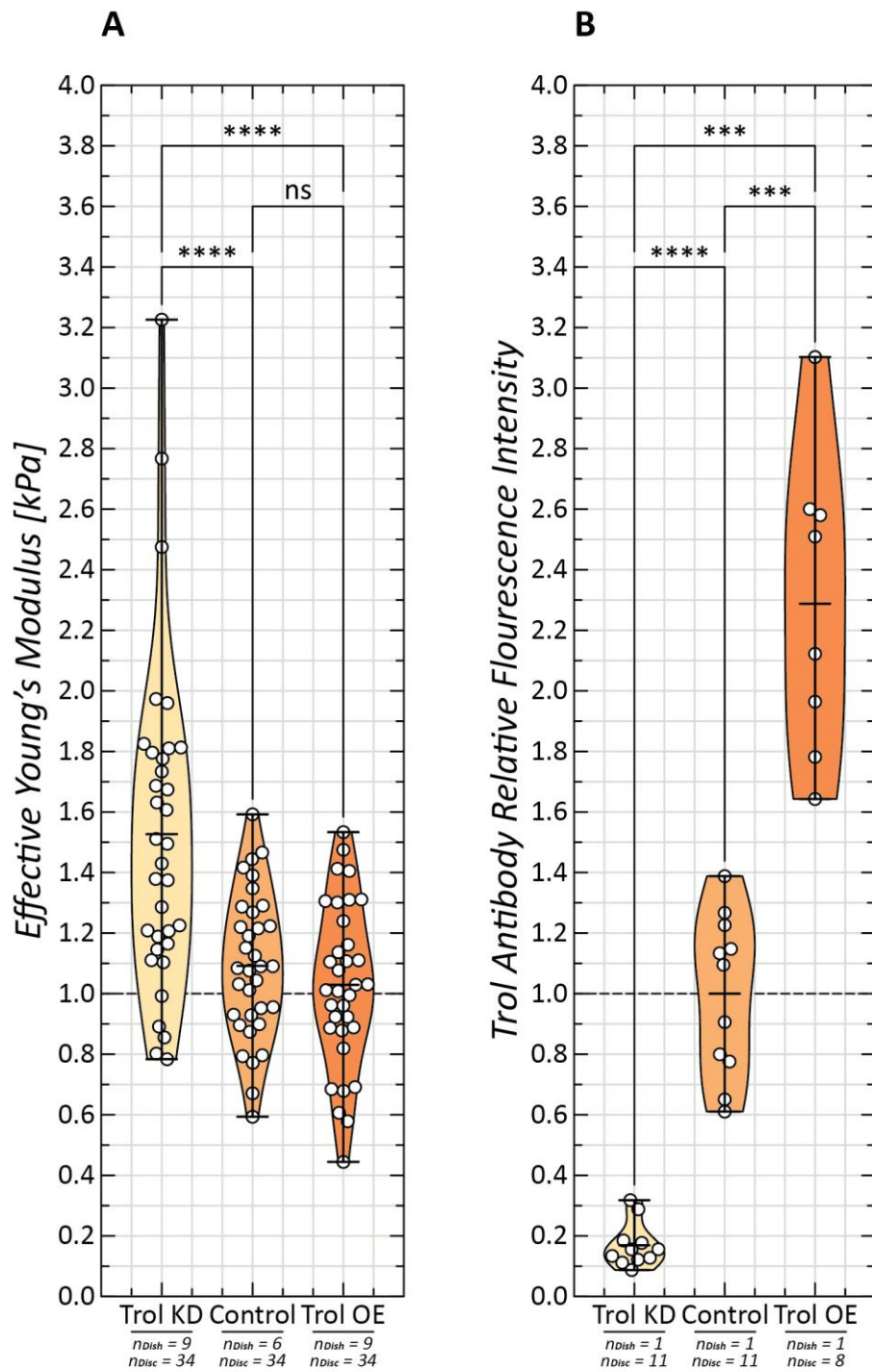


Figure 45. *Perlecan knockdown significantly increases effective tissue stiffness.* **A** shows measurements of effective Young's modulus for perlecan knockdown (Trol KD), perlecan overexpression (Trol OE) and control, where dots indicate individual wing discs. **B** shows the relative fluorescence intensity of a perlecan antibody as a result of perlecan perturbations. **C – E** shows example wing disc sections for perlecan knockdown, control and perlecan overexpression respectively.

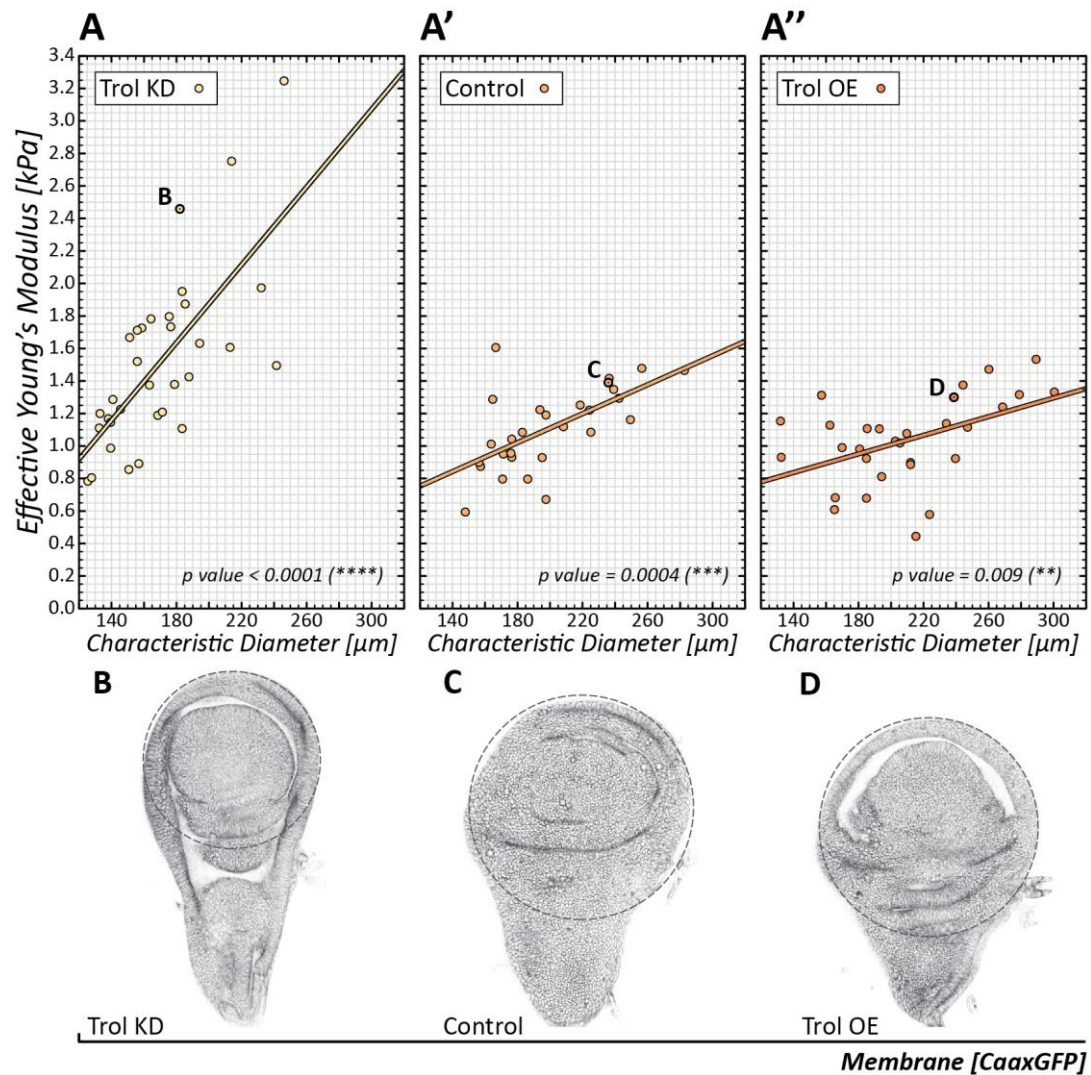


Figure 46. *Perlecan knockdown significantly increases the rate of effective stiffness increase with wing disc size.* **A – A''** are a scatter plots of effective Young's modulus against wing disc characteristic diameter for perlecan knockdown (Trol KD), control and perlecan overexpression (Trol OE) respectively. Solid lines in **A – A''** are linear regressions to data of the respective conditions. **B – D** show summed projections of wing discs for perlecan knockdown, control and perlecan overexpression respectively. Characteristic diameter is measured as the diameter of a circle manually fitted to the pouch region of a flattened wing disc as shown with dashed circles in **B – D**.

2.3.3 Discussion

When indenting the tissue, a deformation is applied to the ECM and basal cell surfaces in a region local to the point of indentation. The act of deforming the ECM and basal cortex of cells should produce an elastic response on the timescale of the indentation, which is on the order of seconds. For the cortex it is established that turnover is on the order of seconds to minutes ^[1]. Assuming turnover is similar to remodelling rate, basal cell cortices are expected to respond elastically to indentation. I also expect the ECM to respond elastically at these short timescales. While basal cell cortices should be directly deformed by an indentation, the lateral cortices may also be slightly reduced in length by this deformation. In a continuous material, the magnitude of deformation per unit volume given a point load should decay with distance from the point according to some inverse power law ^[190], similar to how light intensity decays with distance from a point source. According to this principle, it would be expected that the region of tissue local to the indentation contributes most to the measured effective stiffness. However, a tissue is not continuous. The parts of tissue that respond elastically to the indentation such as cell cortices and ECM actually form surfaces that divide up regions such as the cytoplasm that are expected to respond only viscously. Stress induced by the deformation should therefore decay only through this network of surfaces. I expect confinement of stress to elastic surfaces should reduce its degrees of freedom, effectively reducing the decay gradient compared to an imaginary tissue in which the bulk is continuously elastic

Indentation should also slightly reduce cell volumes. Therefore, although cytoplasm is considered a fluid at indentation timescales, it could still act elastically due its incompressibility. Whether cell volume is conserved on indentation timescales depends on how porous cell membranes are at this timescale. Water and ions are able to move through channels in the cell membrane, and this movement is thought to regulate cell pressure ^[37]. There is evidence that this regulation can be

mechanical, whereby ion channels are opened by increased membrane tension ^[36]. The rate at which molecules can pass through the cell membrane limits adaptation of cell pressure. If the cell membrane is not porous on indentation timescales then volume should be conserved, and act elastically. Assuming small molecules such as water diffuse much faster than indentation rate, a reduction in cell volume results in an increase in cell pressure across all surfaces of the cell. The elastic response from a reduced cell volume should be the elastic response of the cell cortex to a uniformly applied tension. Cell volume changes can therefore couple the apical cell cortex to a deformation of the basal cell cortex. Other cytoskeletal components could also drive more global response of cells, such as microtubules that appear to be able to span the inside of cells ^[151]. Hence there are multiple contributions to the effective stiffness measured.

The effect of Y27632 is to inhibit the phosphorylation of myosin regulatory light chain by Rok. Dephosphorylation of myosin in this way is thought to prevent it from binding filamentous actin ^[4]. Therefore I expect Y27632 to reduce both the contractility and cross-linking activities of myosin. The measured reduction in effective stiffness induced by Y27632 may therefore be a result of reduced contractility and reduced cortical stiffness. The effect of Latrunculin-A is to inhibit actin filament polymerisation, effectively degrading the cortex. Using myosin as a marker of the cortex here, Figure 43 E, but also in the previous section, Figure 27, it is clear the Latrunculin-A treatment eliminates the majority of cortex. The measured reduction in effective stiffness induced by Latrunculin-A is therefore a result of loss of contractility and loss of residual non-contractile cortex stiffness. I expect the only remaining contributions to the effective stiffness measurement are ECM, cell pressure and residual cytoskeletal components. The effect of CLS-1 has been established to a certain extent in the previous section, §2.2.2.

A possible way to determine the contribution of ECM tension would be to ablate basal cell cortices underneath the indented region. A similar, but more difficult, experiment could involve degrading a patch of ECM using the micropipette, and then measuring the change in stiffness inside that patch. If stiffness reduces as much as

applying CLS-1 to the whole wing disc then ECM degradation must affect the tissue locally. Alternatively, apical or lateral cortex could be ablated before indenting to attempt to eliminate tension applied to the ECM. If the reduction in effective stiffness is significant compared with Latrunculin-A, then it may indicate they are the main source of tissue stiffness. Alternatively, there exist genetic tools that target specific domains of cells. The GrabFP tool uses a polarised protein fused with anti-GFP to move a different protein labelled with GFP to either the apical or basal-lateral domains ^[118]. This tool could be applied to a GFP-labelled phosphatase of myosin to inhibit contractility in a certain domain. Greater control may be achieved using opto-genetic tool that allows hyper-activation of myosin with light ^[193]. Either tool could be used in conjunction with indentation to determine the relative contributions of contractility in the different domains of the cell.

A significant increase in effective stiffness has been measured with wing disc size Figure 44. This increase in tissue stiffness may be related to the increase in ECM thickness, Figure 16, and increase in ECM components observed per unit area of the pouch ECM, Figure 19. Generally the shear modulus of a sheet of material will increase with increasing thickness, and this may be what is measured with indentation. A more precise characterisation effective stiffness, such as in Figure 43, at different wing disc ages could help elucidate whether contractility or ECM stiffness contribute to this size-stiffening relationship.

Effective tissue stiffness increases significantly with perlecan knockdown, compared with control wing discs, Figure 45 A. However effective stiffness is not significantly different with perlecan overexpression compared with control. Perlecan knockdown and perlecan overexpression do lead to decrease and increase in perlecan concentration compared with control wing discs. Therefore, perlecan concentration does not scale linearly with ECM stiffness. Perlecan knockdown may increase tissue stiffness by increasing ECM stiffness. However, it is then surprising perlecan overexpression does not decrease measured effective stiffness, because it would be expected to soften the ECM.

From Figure 46 it may appear perlecan knockdown increases the rate of wing disc stiffening with age. However, because perlecan knockdown also affects wing disc size, characteristic diameter becomes dependent on both age and perlecan knockdown. To determine if perlecan knockdown affects stiffness with age an independent measure of age is required, such as staging egg deposition.

2.4 Results Section 4: Dynamic properties of wing disc extra-cellular matrix

This section is concerned with how ECM components and ECM-related components turnover. To determine turnover rates for cellular components integrin and myosin I have used fluorescence recovery after photo bleaching *ex vivo*. For ECM components, *ex vivo* methods are insufficient; therefore I have made use of genetic methods to temporally switch between differently labelled forms of collagen *in vivo* and measure changes over time.

2.4.1 Methods

Fly lines

I have made considerable use of two UAS-VkgScarlet (UAS-VkgSCA) fly lines, gifts from Besaiz Sanchez and Brian Stramer, one on the second chromosome and the other on the third. Often, driving expression of a protein using Gal4-UAS cumulatively with the endogenous protein leads to overexpression and an associated phenotype. However, I observe no phenotype when overexpressing Vkg by driving it throughout development with CgGal4. I have used an interference RNA line targeting green fluorescent protein, UAS-GFPRNAi (GFPRNAi, BDSC 41551, *FBID: FBti0148872*). I have also used a Trol-null mutant, TrolG0271 (BDSC 11848, *FBID: FBti0015659*), which has been previously characterised ^[16].

Fluorescence recovery

I have used fluorescence recovery after photo-bleaching (FRAP) to measure the turnover rates of integrin and myosin in *ex vivo* wing discs. FRAP involves photo bleaching a fluorescently tagged component in some region and measuring how the fluorescence intensity in that region changes over time. These measurements are then used to infer the dynamics of that component *via* a mathematical model.

Generally the molecule of interest is expected to have at least two states of differing mobility, and these states are usually spatially segregated. For example, the molecules may diffuse slower when bound to the cell membrane, but diffuse faster in the cytoplasm. In this case, the recovery of fluorescence in a region bleached on the membrane can show how fast molecules diffuse on the membrane and also how fast molecules move from cytoplasm to membrane ^[194]. Sometimes the low mobility state can be completely immobile on the timescale of the experiment. In this case the mobile fraction is measured as the fraction of fluorescence that recovers over the timescale of the experiment, and only the dynamics of this mobile fraction can be inferred.

The fly lines I used for FRAP were MysGFP and SqhGFP previously described in §2.1.1. In both cases I was interested in the dynamics of the structures they form on basal cell surfaces. To get good images for FRAP, I have had to bring the basal surface of the wing disc right up against the glass bottom of the dish. To do this I have used the method described in §2.1.1, where the peripodial surface of the wing discs are stuck to a piece of coverslip using cell-tak. The piece of coverslip is then flipped, sandwiching the wing disc between the coverslip and the bottom of the dish. This mounting method has the main advantage of pushing the basal surface of the wing disc as close to the objective as possible, and a secondary benefit of immobilising the wing discs. However this method is not ideal because the wing discs are under moderate compression and their media-exposed surfaces are limited. Despite these problems I have had to use this method because wing discs have a tendency to dome-up after dissection, which brings the basal surface of the pouch too far from the coverslip to observe fluorescence. Fortunately, most wing discs mounted using this method appear functioning as indicated by their fluorescence, and those that do not I have avoided imaging. After mounting using this method, I imaged the wing discs for no longer than 90 minutes, which is enough time for two FRAP experiments.

The FRAP experiments were achieved using a Zeiss LSM 880 microscope. To image the fluorescent proteins a 40x oil objective with 3x digital zoom in Airyscan mode

was used. I focused on the basal surface at the center of the pouch columnar epithelium. It was possible to obtain a large enough stack of images covering the depth of the basal surface within 1 minute. I then took a time series of these stacks with an interval of 1 minute for a total of 46 minutes. To bleach GFP I used the same 488nm laser used to image but at a higher intensity. The bleaching intensity was chosen by trialling different intensities and choosing the minimum required to bleach in order to minimise damage. For both MysGFP and SqhGFP, fluorescence tended to form a single cluster around the center of each cell. For SqhGFP the cluster usually formed a ring, while MysGFP formed a dot. For each cluster, I bleached a small circular region on only a part of the cluster. I applied this part-bleaching method to 20 clusters, corresponding to 20 cells, for each FRAP experiment. I applied the bleach after the first frame in the time series. For each FRAP experiment I used a different wing disc. Before processing and analysis, I summed the images of the stack for each frame.

I experienced a small amount of drift of the sample during the time series. This drift was not due to translation of the tissue as a whole, but instead a kind of spreading of the tissue surface on the glass. I expect this spreading was driven by the compression applied to the wing discs by the coverslip piece. The drift was, in some cases, enough to move the bleached region of tissue away from the original bleach region of interest. To realign the two I used a default plugin for FIJI listed under 'Registration' called 'Correct 3D Drift'. For most time series this plugin worked, however some did not work because the drift varied across the image. I discarded the experiments where I could not correct the drift. Often, imaging causes a certain amount of bleaching, which needs to be accounted for in the FRAP measurement. This unwanted bleaching is usually eliminated from the FRAP measurement by normalising the fluorescence intensity in a bleached region with the fluorescence intensity of some unbleached region. By bleaching only part of a cluster I was able to normalise the fluorescence intensity per-cluster. For each bleached region I found a second unbleached region on the same cluster. The normalised FRAP measurement is the mean fluorescence intensity of the bleached region divided by the mean fluorescence intensity of the unbleached region per frame.

Mean fluorescence intensity values for each region and time point were obtained using script I wrote in FIJI, and exported to text files. Measurement text files were then imported into a custom Python script for normalisation and model fitting. Fluorescence intensities of unbleached, f^u , and bleached, f^b , regions were combined to find a normalised fluorescence intensity \tilde{f} per time point i , per cell c , as follows

$$\tilde{f}_{c,i} = \left(\frac{f_{c,i}^b}{f_{c,i}^u} - \frac{f_{c,1}^b}{f_{c,1}^u} \right) \left(\frac{f_{c,0}^b}{f_{c,0}^u} \right)^{-1}$$

where $i = 0$ is the time point before bleaching and $i = 1$ is the time point immediately after bleaching. Normalised fluorescence intensity per time point is then averaged over all cells to find the average normalised fluorescence intensity per time point, \tilde{f}_i . A function modelling fluorescence recovery is then fit to the final averaged normalised fluorescence intensities. The function I have used is

$$\tilde{f}(t_i) = \alpha(1 - \exp(-\tau t_i))$$

where α is the mobile fraction and τ is the time constant^[195]. I have fit this function in Python using the `curve_fit` function from the SciPy library. I assigned a maximum possible value of $\alpha = 1.0$ during fitting. I also passed the standard deviation of the averaged normalised fluorescence intensity for each time point into the fitting function in order to obtain errors on the fitted parameters. I repeated this process for the two components, SqhGFP and MysGFP.

The function used to model fluorescence recovery is derived from the solution to an ordinary differential equation that relates fluorescence of bound, f_b , and free, f_u , components to bound component recovery rate \dot{f}_b

$$\dot{f}_b(t) = k_b f_u - k_u f_b(t)$$

where k_b and k_u are rates of component binding and unbinding respectively ^[195]. Unbound fluorescence is assumed to remain constant while bound fluorescence varies over time. The solution to this ordinary differential equation is

$$f_b(t) = \frac{k_b f_u}{k_u} - k_0 \exp(-k_u t)$$

with an unknown parameter k_0 . At the time zero bleaching eliminates fluorescence of the bound fraction, which is equivalent to $f_b(0) = 0$. Using this boundary value, the unknown parameter can be determined leading to

$$f_b(t) = \frac{k_b f_u}{k_u} (1 - \exp(-k_u t))$$

which gives the function used to fit the data by setting $\tilde{f} \equiv f_b$, $\alpha \equiv k_b f_u / k_u$ and $\tau \equiv k_u$. Therefore the time constant, τ , is just the unbinding rate of the bound component. Steady state $\dot{f}_b(\infty) = 0$ shows the parameter α is the final fluorescence when extended to infinite time. However the parameter α is inferred from the recovery over a short timescale, and hence only gives the steady state fluorescence of the mobile fraction at that timescale.

This model makes a number of assumptions. One assumption is that the component of interest binds by one mechanism and unbinds by another, each with a characteristic rate k_b and k_u respectively. However, there may be multiple mechanisms by which a component may bind or unbind, leading to families of binding or unbinding rates, forming linear combination of solutions to the ordinary differential equation. It is possible for multiple mechanisms of integrin unbinding to exist given both inside-out and outside-in signalling. Multiple mechanisms of myosin unbinding are also likely to exist given the complexity of the cortex. However, in this experiment I am trying to compare the general turnover of these two components, therefore a coarse characterisation of their dynamics is sufficient. Adding more

unbinding rates would require some understanding of the source mechanisms, and if not done properly could lead to over-fitting of the data.

An issue I had with SqhGFP was that it is so dynamic that the shape and intensity of the ring changes over time. An example of shape change can be seen in Figure 49 D, where the ring shrinks in size. This shape change will affect the fluorescence intensity measurements, which contributes to the large standard deviation that develops with time in the time series in Figure 49 B.

Temperature shift

As discussed previously, the problem with studying ECM dynamics of the wing disc is the non-local production of ECM components. It has previously been shown that ECM components such as collagen are produced in the fat body, secreted into the haemolymph and deposited, or sequestered, on the wing disc surface^[16]. When the wing disc is dissected from its larva it no longer has access to a supply of ECM components, which, as discussed previously §2.2.1, shuts down turnover of the ECM. Therefore, to study dynamics of the ECM I have turned to *in vivo*.

Previously §2.2.1, I have used temperature shift to switch on genetic perturbations temporally within developing larvae. Here I have employed this technique again to drive expression of UASVkgSCA temporally in the fat body of developing larvae using CgGal4 in conjunction with TubGal80ts. I have also included a UAS-GFPRNAi to temporally knockdown only the endogenous VkgGFP. Therefore, before temperature shift only the endogenous VkgGFP is expressed. After temperature shift VkgSCA expression is up-regulated and VkgGFP expression is down-regulated *via* GFPRNAi. It is assumed that after some time, VkgSCA is the only form expressed while VkgGFP is near completely knocked down. This experiment is like a genetic analogue of a photo-switching experiment. Importantly, switching between two pools of differently labelled collagen should not affect the total amount of collagen in the system. This experiment is therefore measuring an approximation of collagen

turnover in wild type larvae. Of course, in reality there may be some transient change in total collagen secretion during the switch over if activation and knockdown initiate at different rates. There may also be a long-term change in total collagen if the CgGal driver does not match expression levels of the endogenous Cg effector. In both cases I hope that the haemolymph acts as a buffer to lessen these effects on the wing disc.

Flies of genotype *ywhsflp;VkgGFP,CgGal4,UASVkgSCA;TubGal80ts/(S-T)* were crossed with flies of genotype *ywhsflp;VkgGFP;UASGFPRNAi* in three separate tubes and kept at 18°C. These tubes were flipped every day forming three rows of progressively older tubes. Tubes older than 9 days were thrown away. At 36h before dissection I moved four of the tubes of the first row to 29°C. At 24h before dissection I moved four tubes from the second row to 29°C. At 12h before dissection I moved four tubes from the third row to 29°C. Some of these time points were at early hours of the morning, so I used a heat bath on a timer plug. When switched off the heat bath is at 18°C, which is the temperature of the room, then when switched on the heat bath warms to 29°C. Tubes were placed in the heat bath during the day, then the timer plug was set to switch on the heat bath at the required time, effectively temperature shifting the larvae. At dissection time, about 8 wing discs for each time point were collected. To mount I used the cover slip flattening technique described previously, §2.1.1. By flattening the wing discs right up against the bottom of the dish attenuation due to distance from the objective is minimised. Wing discs for each time point are stuck down in rows on the piece of coverslip. The ECM of the wing discs were imaged using a Zeiss LSM 880 with a 40x oil objective at 0.6x digital zoom in confocal mode. VkgGFP and VkgSCA were imaged using 488nm and 561nm lasers respectively. For each wing disc, a stack of images was taken covering the whole ECM thickness in the pouch region. This entire process was repeated three times on separate days.

The image stacks for each channel for each wing disc were then summed to generate a single image per channel, per wing disc. The mean fluorescence intensity of VkgGFP and VkgSCA was measured from a circular region in the pouch of each wing

disc. To account for variation in laser power between days, I normalised the fluorescence intensities of each dish and channel by the mean fluorescence intensity of the 12h time point of that dish and channel. I then applied a linear regression to the fluorescence intensity means of each dish and channel. The linear regression function used was `linregress` from the SciPy library. The final turnover rates for each channel were taken as the average of the slopes obtained from the linear regressions of each dish. These fluorescence intensity changes for VkgGFP and VkgSCA were then plotted as the percentage change in fluorescence from the 12h time point. The VkgGFP fluorescence intensity change was found to be negative, as expected, the absolute value represents the unbinding rate of collagen. The VkgSCA fluorescence intensity change is positive and represents the binding rate. I assume the time from the moment of temperature shift to the moment of maximum expression of the transgenes is less than 12 hours. Therefore, by 12 hours the rates of VkgSCA and VkgGFP secretion, and hence their concentrations in the haemolymph should have reached steady state. Any change in VkgGFP and VkgSCA concentrations in the wing disc ECM after 12 hours should therefore be a result of the local gain and loss rates of collagen to the ECM. Ideally I would expect the fluorescence intensity changes of VkgGFP and VkgSCA to follow some nonlinear exponential function like with FRAP. However, given the low time resolution of this experiment I expect fitting a nonlinear function would give low confidence in the fitted parameters.

This experiment can also provide spatial information about gain and loss rates of collagen across the ECM of the wing disc. However, more assumptions are required. Once VkgSCA is secreted from the fat body it diffuses through the haemolymph, possibly with the aid of Sparc^[16]. I assume that by diffusing into the haemolymph, VkgSCA becomes well mixed with VkgGFP. If so, I would expect all surfaces of the wing disc to be exposed to a homogenous concentration of VkgSCA, and by extension a homogenous ratio between VkgGFP and VkgSCA concentrations. If this assumption is correct, then any spatial differences in VkgSCA fluorescence intensity across the wing disc ECM would indicate spatial differences in gain rates of collagen. Moreover these gain rates would be defined locally, autonomous to that region of tissue.

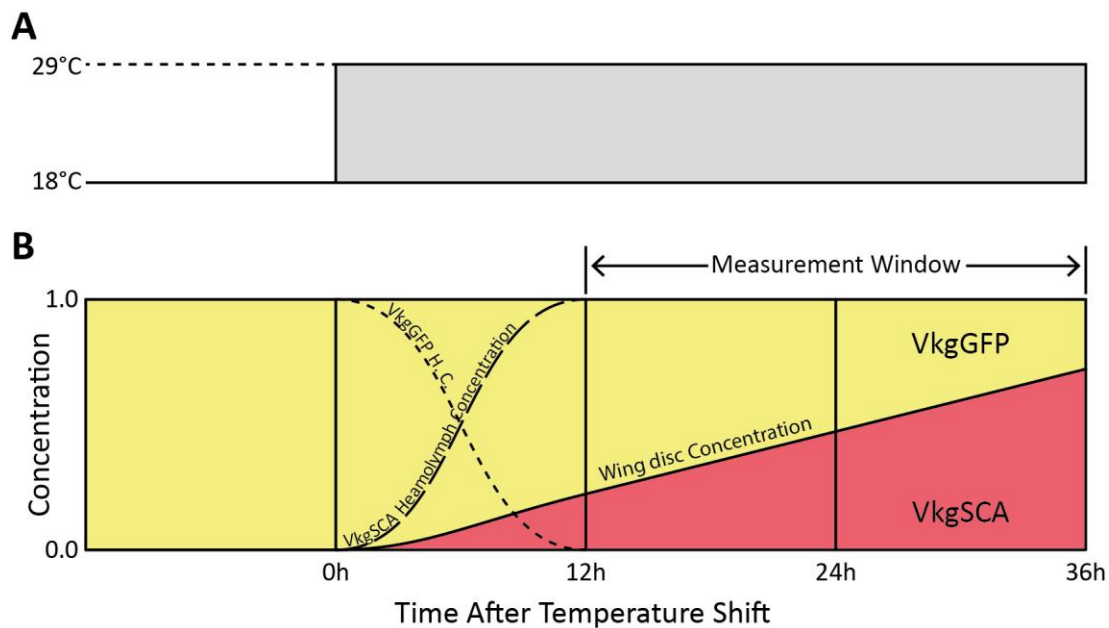


Figure 47. Collagen turnover rates can be measured genetically. **A**, larvae are shifted from 18C to 29C at 0h. **B**, between 0h and 12h after temperature shift the concentration of VkgGFP and VkgSCA in the haemolymph are assumed to decrease and increase respectively. From 12h to 36h a linear change of VkgGFP and VkgSCA is expected to be measured.

Unlike FRAP, the measured change in fluorescence intensity is not a direct measure of turnover. As the tissue grows its ECM surface area increases to accommodate the growing cellular mass, and as shown in Figure 16, the thickness of the ECM grows too. An increase in ECM surface area will have the effect of diluting the measured collagen fluorescence. Conversely, an increase in ECM thickness will increase the ECM volume per unit surface area, effectively increasing the measured collagen fluorescence.

Temperature shift experiments have also been performed in larvae with a perlecan-null mutant *TrolG0271*. These particular experiments did not include the UAS-GFPRNAi. I instead applied a pulse of VkgSCA by temperature shifting at approximately 12h before dissection. Because I have only obtained one time point from these experiments I can't calculate turnover rate. I also cannot compare fluorescence between repeats due to changes in laser power. Therefore for these experiments I focus on spatial differences in fluorescence levels. The perlecan gene

is on the X chromosome, so males with the *perlecan* mutant were selected. Larvae hemizygous for the *perlecan* mutation were identified by their slow development, small size and transparency. Correct identification of *perlecan* mutant larvae was confirmed upon dissection, by the clear morphological phenotype of the imaginal discs and other tissues.

Statistics

For Figure 49 A, B, the exponential function described previously was fit to the data using the SciPy *optimize* function. The resulting fitted curve is overlaid on the data as a solid line. In Figure 48 the coefficients and their standard deviations are shown as bar plots. A Student's t-test was used to compare a given coefficient between SqhGFP and MysGFP.

For Figure 51, data from three repeats are pooled into scatter plots for measurements of VkgGFP or VkgSCA in three genetic conditions. Linear regressions were fitted to each, shown as a solid line. Standard deviation and standard error are shown as dotted and dotted-dashed lines respectively. The. For Figure 50, a box and whisker plot is used to directly compare gradients of the linear regressions shown in Figure 51. The boxes on this plot represent the IQRs of the linear regression gradient, while the whiskers represent the standard deviation. Significance labels directly above each box and whisker are the significant difference between the fitted linear regression gradient and a gradient of zero with the same variance. The measurements in Figure 50 of either VkgGFP or VkgSCA, because these measurements are of different things they are not compared with each other, however comparisons are made between different genetic conditions of either VkgGFP or VkgSCA. An ANCOVA was used to determine if the gradients of any of the genetic conditions was significantly different than the gradient of the pooled data. When the ANCOVA suggested a significant difference, pairwise comparisons were made between genetic conditions. Results between pairwise comparisons are indicated by connected lines and significance labels. These statistics were calculated using R functions *lm* and *emmeans*.

2.4.2 Results

Intra-cellular turnover

Mobile fractions of integrin (Mys) and myosin (Sqh) obtained from FRAP experiments are shown in Figure 48 A. According to these measurements (100 ± 4)% myosin is mobile within the 45-minute timescale of the experiment. In contrast only (21.4 ± 0.7)% of integrin is mobile on this timescale. Fluorescence recovery rates obtained by FRAP applied to integrins and myosin are shown in Figure 48 B. There is no significant difference between the recovery rates of the mobile fractions of integrin and myosin, and their means are (10.6 ± 0.8)% per minute and (10.9 ± 0.9)% per minute respectively.

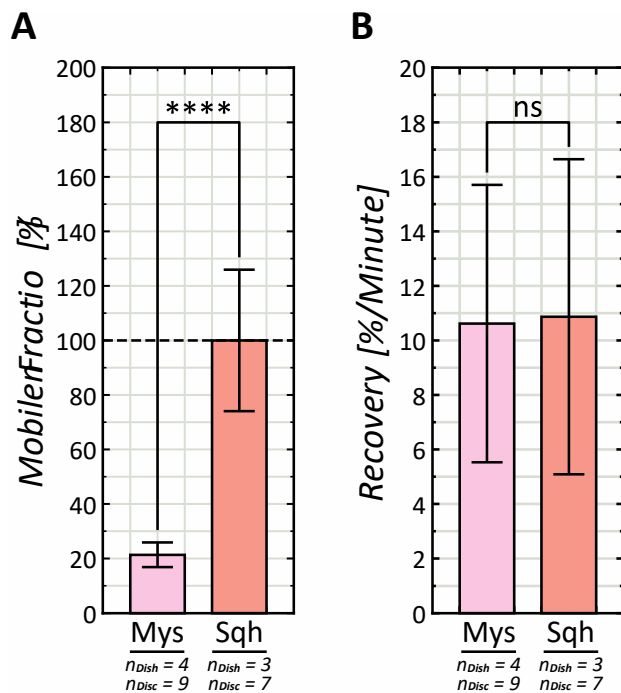


Figure 48. *Integrins are mostly immobile over an hour-long period. A*, shows the mean immobile fractions of integrin (Mys) and myosin (Sqh). **B**, shows the mean recovery time constants of integrin and myosin after photo-bleaching.

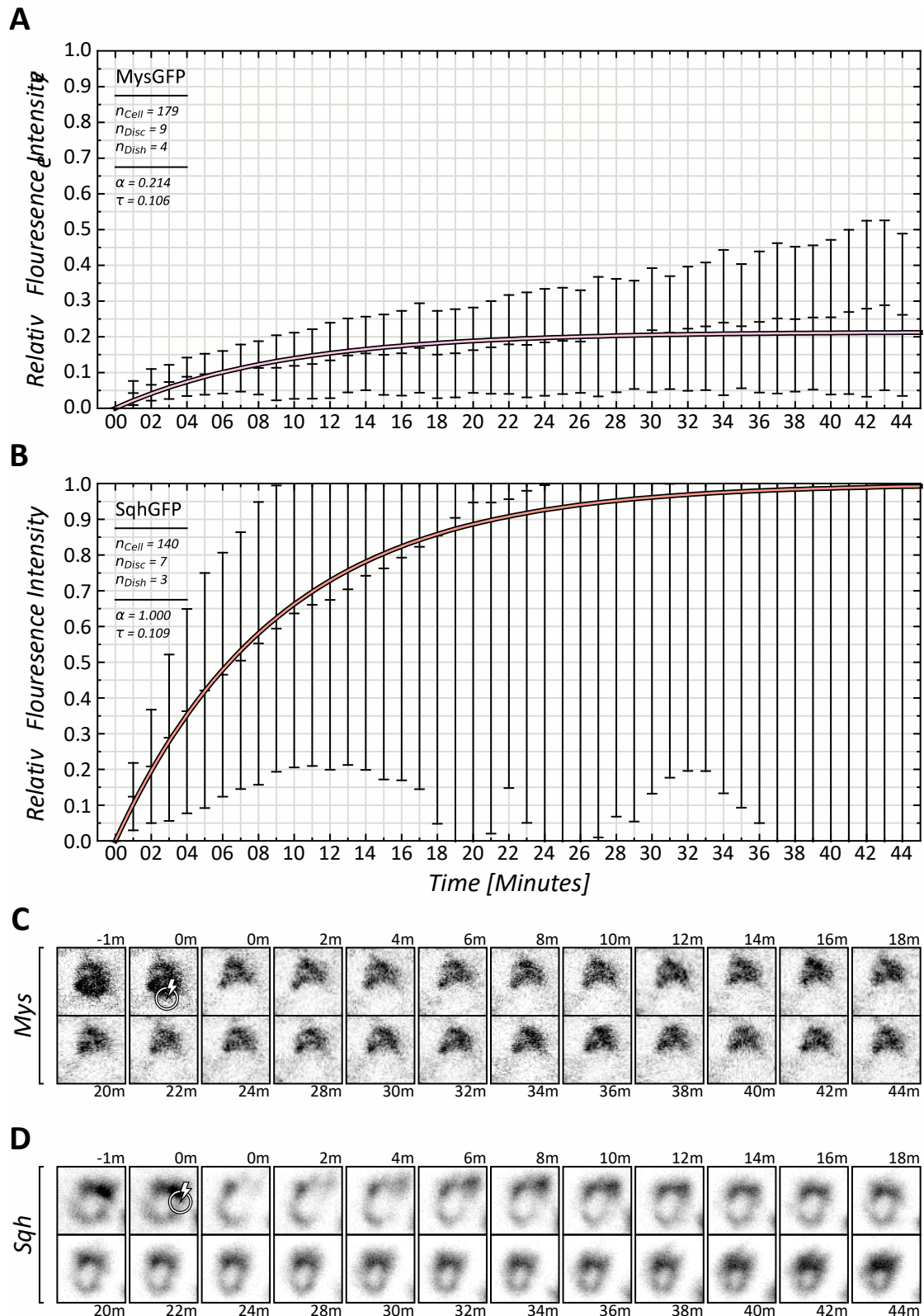


Figure 49. *Integrin and myosin have similar turnover rates but dissimilar mobile fractions. A and B show FRAP time series for integrin (Mys) and myosin (Sqh) respectively. Mean measurements at each time points are shown as bars, while the fitted exponential function is shown as the solid line. C and D show example time courses of partially bleached integrin and myosin clusters respectively. Lightning symbols in C and D indicate bleached regions.*

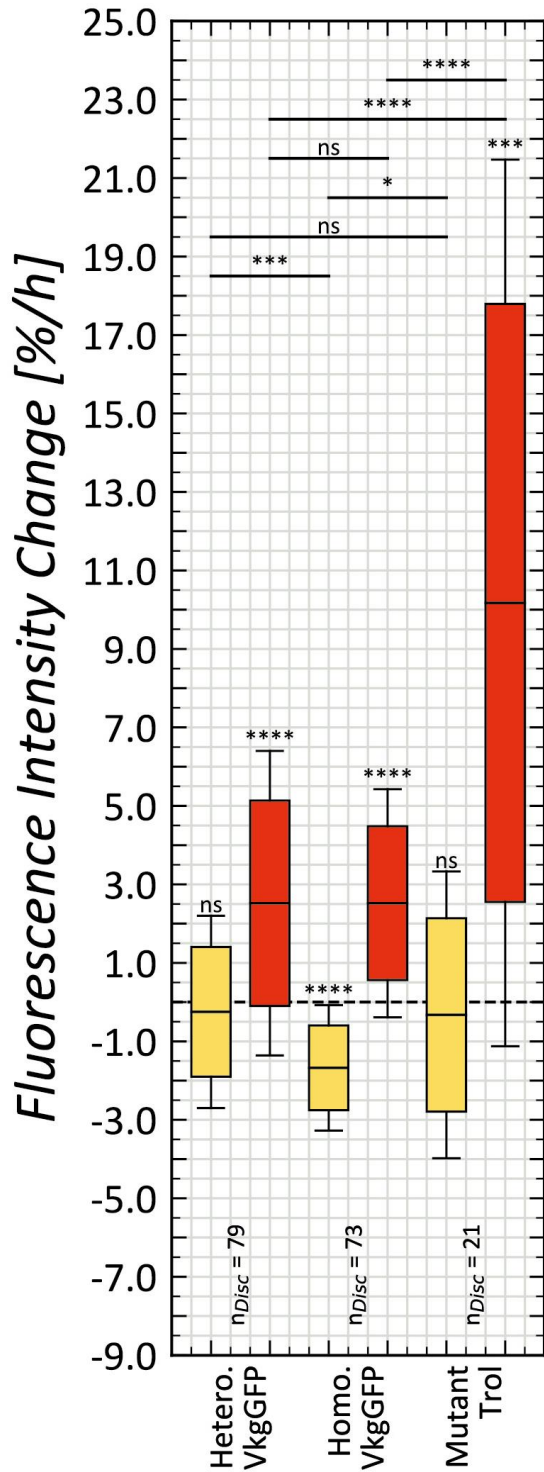


Figure 50. Collagen turnover occurs at timescales on the order of days. Rates of fluorescence intensity change of old collagen (VkgGFP) and new collagen (VkgSCA) are shown for three different conditions; heterozygous VkgGFP, homozygous VkgGFP, and perlecan (Trol) knockout mutant. For homozygous VkgGFP, all endogenously expressed copies of Vkg are labelled with GFP, while for heterozygous VkgGFP only some fraction of endogenously expressed Vkg is labelled with GFP. The Trol knockout mutant uses homozygous VkgGFP.

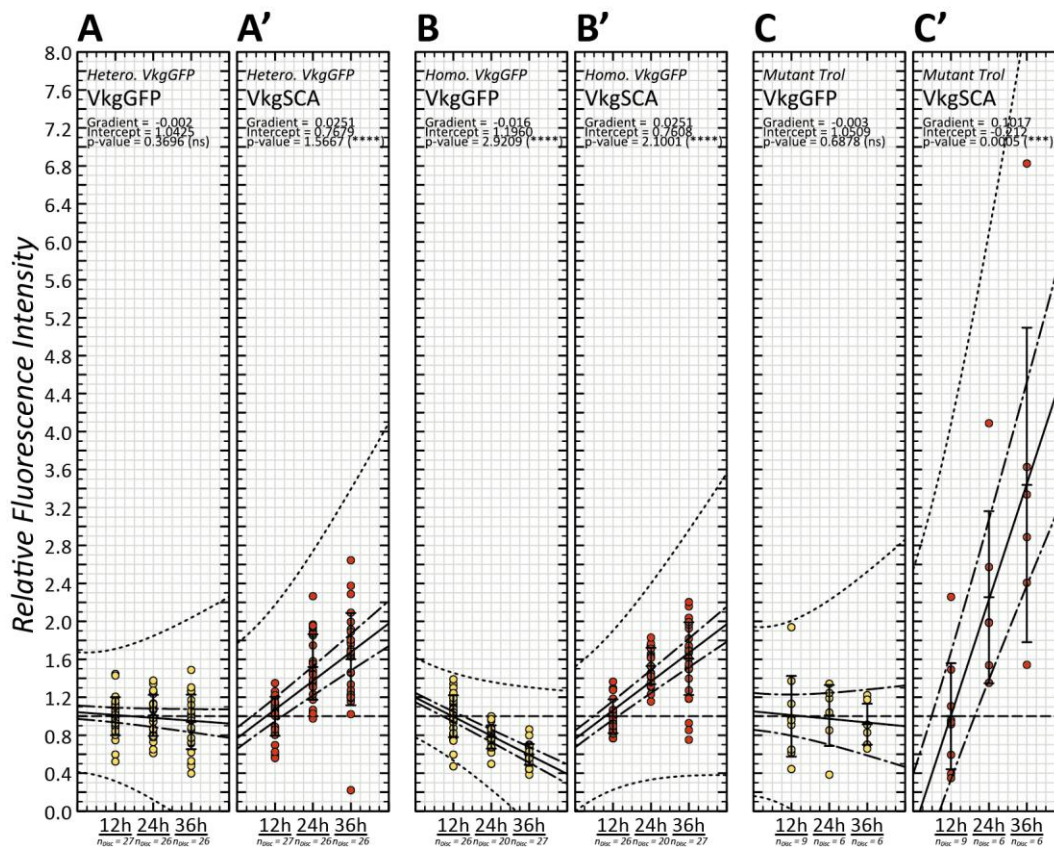


Figure 51. Collagen concentration has a net increase over time per unit area of extra-cellular matrix. **A – A'** show the three dishes contributing to the VkgGFP change measurement with homozygous VkgGFP. **B – B'** shows the three dishes contributing to the VkgSCA measurement with homozygous VkgGFP. For each scatter plot, dots correspond to fluorescence intensity measurements for each wing disc. Fluorescence intensity is normalised to the mean of the 12h measurements. Solid lines indicate linear fit of the data. Dot-dash curves indicate standard error of the fit. Dotted curves indicate standard deviation of the fit. A and A' are old and new collagen dynamics, respectively, for a heterozygous VkgGFP/Vkg background. B and B' are old and new collagen dynamics, respectively, for a homozygous VkgGFP/VkgGFP background. C and C' are old and new collagen dynamics, respectively, for hemizygous perlecan (Trol) knockout mutant in a homozygous VkgGFP/VkgGFP background.

Extra-cellular turnover

Measurements for the turnover of collagen via the Vkg subunit are shown in Figure 50 for three genetic conditions, heterozygous VkgGFP. Homozygous VkgGFP and

perlecan knockout. For homozygous VkgGFP, old collagen is diluted or degraded from the ECM at $(1.7 \pm 0.2)\%$ per hour while new collagen (VkgSCA) incorporates into the ECM at $(2.5 \pm 0.3)\%$ per hour. For heterozygous VkgGFP, old collagen is diluted or degraded from the ECM at $(0.2 \pm 0.3)\%$ per hour, and new collagen is incorporated at $(2.5 \pm 0.4)\%$ per hour. For perlecan knockout in a homozygous VkgGFP background, old collagen is diluted or degraded from the ECM at $(0.3 \pm 0.8)\%$ per hour and new collagen is incorporated at $(10 \pm 2)\%$ per hour. Individual plots of fluorescence intensity change for VkgGFP, VkgSCA and the three genetic conditions are shown in Figure 51. Images showing the spatial distribution of old collagen to new collagen after applying a pulse of new collagen is shown in Figure 52. These images show that new collagen integrates at a faster rate around the pouch and hinge regions, and at a slower rate around the notum region.

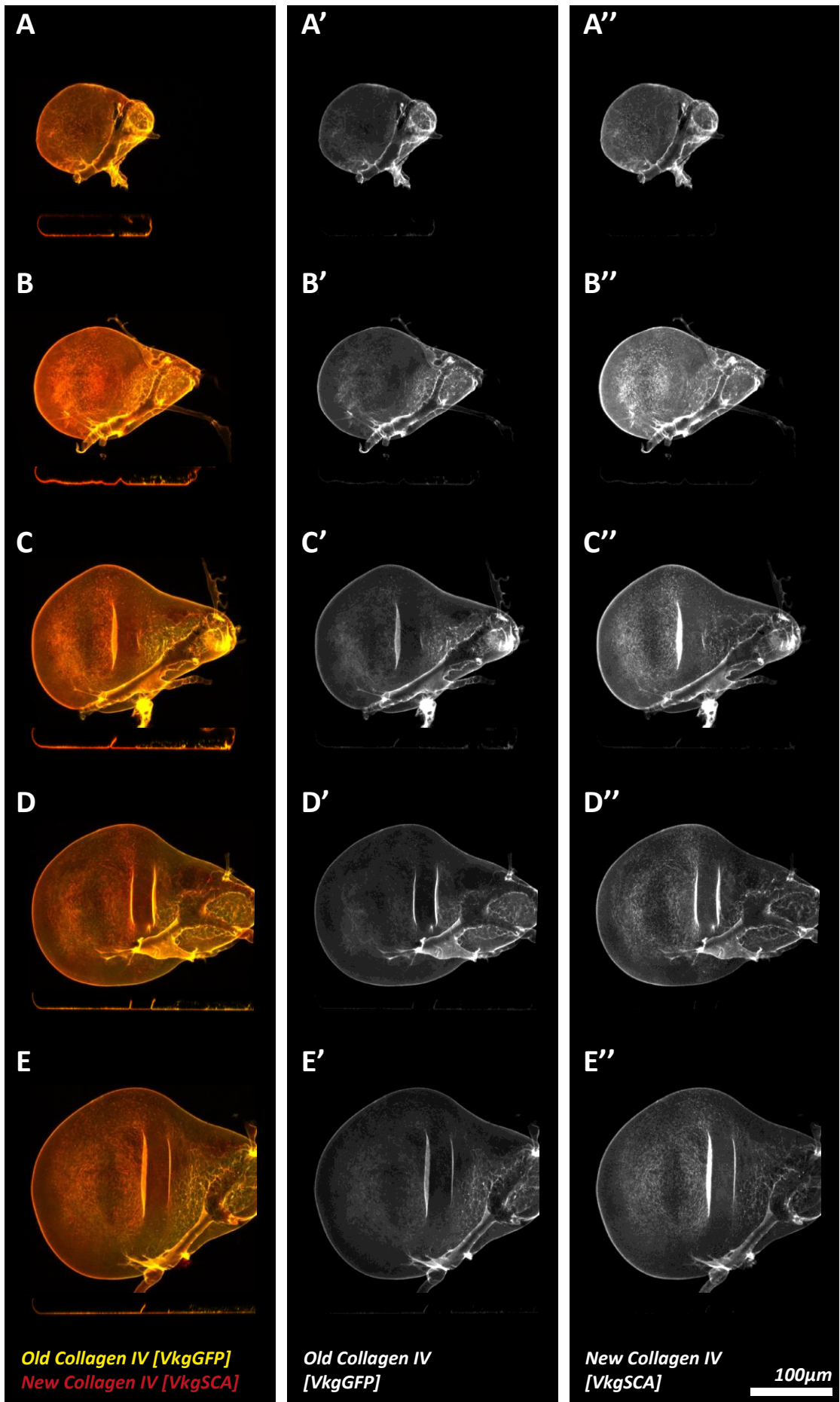


Figure 52. *Collagen turnover occurs at an increased rate in pouch and hinge regions of the wing disc. A – E show summed projection examples of wing discs resulting from driving a pulse of new collagen (VkgSCA) for approximately 12h before dissection. Therefore regions of greater new collagen relative to old collagen (VkgGFP) represent faster integration of new collagen, which is an indicator of turnover rate.*

Images showing the spatial distribution of collagen turnover in perlecan-null mutant wing discs is shown in Figure 53. These wing discs are morphologically very different from wild type wing discs. With the same length pulse of new collagen, approximately 12-16h, the perlecan-null ECM incorporates substantially less new collagen than wild type wing discs, which suggests perlecan is required for incorporation of new collagen. Interestingly some perlecan-null wing discs show patches of ECM that are completely new collagen, indicated with white arrows in Figure 53 B, D. Most of these patches appear bulging out of the perlecan-null wing disc. If the pulse of new collagen is applied for a longer period of time, specifically 48 hours, then some collagen turnover is observed, as shown in Figure 54. New collagen appears to deposit preferentially to the outer, or haemolymph, surface of the ECM Figure 55, which is consistent with collagen depositing from the haemolymph into the ECM.

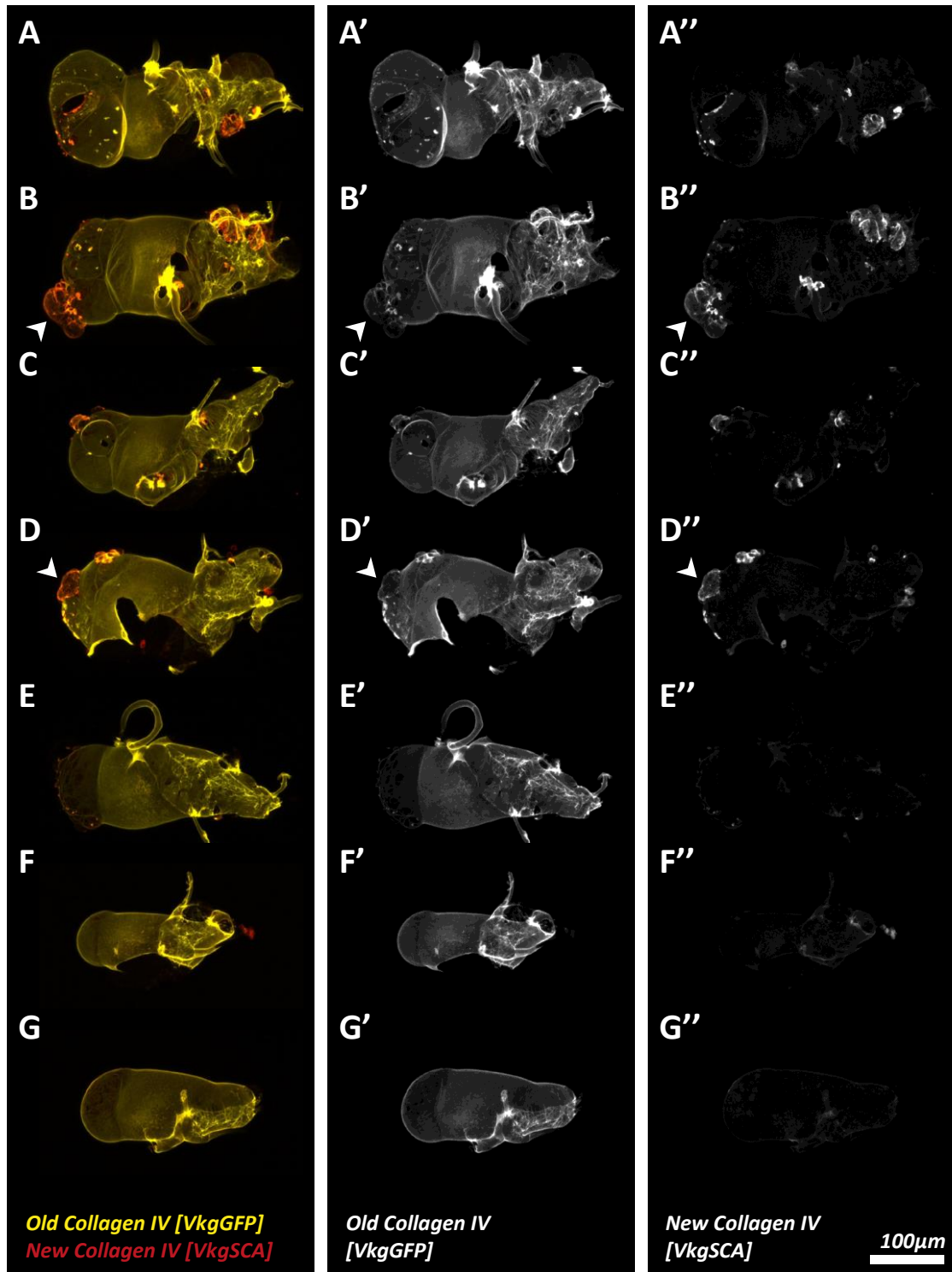


Figure 53. *Loss of perlecan reduces collagen turnover rate.* **A – G** shows summed projections of Troll-null mutant wing discs after driving a pulse of new collagen (VkgSCA) for approximately 12h before dissection. White arrows in **B – B'** and **D – D'** indicate regions of increased new collagen deposition.

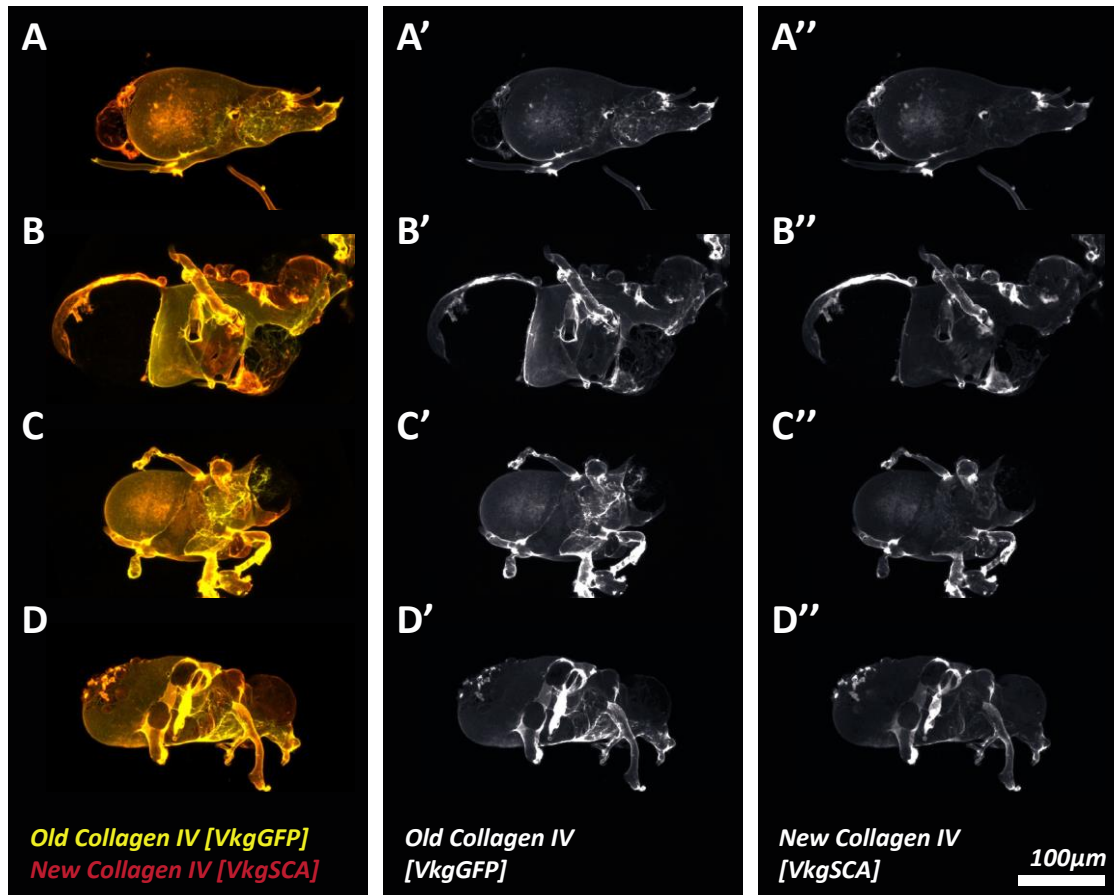


Figure 54. *Without perlecan collagen can still turnover but at a greatly reduced rate. A – D shows summed projections of wing discs after driving a pulse of new collagen (VkgSCA) for approximately 48h before dissection.*

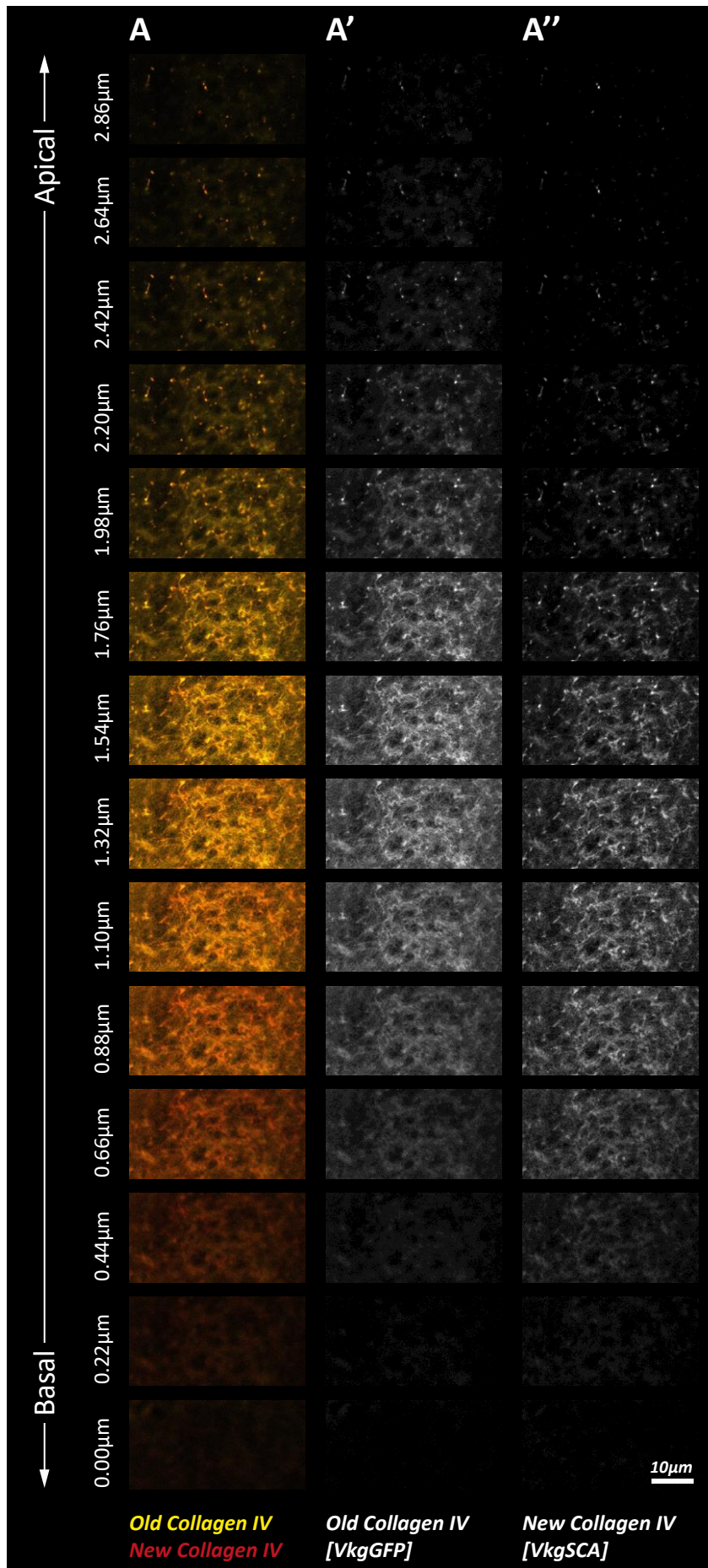


Figure 55. *Collagen turnover rate is greater on the outer surface of the extra-cellular matrix. A* shows slices of the ECM at various depths after driving a pulse of new collagen (VkgSCA) for approximately 12h after dissection. More Apical slices are closer to the basal cell surface while more Basal slices are closer to the haemolymph.

2.4.3 Discussion

Approximately a fifth of the integrins forming a cluster on the basal surface of pouch cells are mobile, Figure 48. Integrins can bind to the ECM directly, and to the cortex indirectly *via* an integrin-associated complex. A simple picture would involve integrins having two binding partners, the ECM and the cortex. There would therefore be four possible integrin states; unbound, bound to ECM, bound to cortex and bound to both ECM and cortex, with two unbinding mechanisms, unbinding from ECM and unbinding from cortex. A simple picture for myosin is two states, unbound and bound to the cortex, with one unbinding mechanism. Multiple unbinding mechanisms are consistent with separate mobile and immobile fractions observed with integrins, while a single unbinding mechanism is consistent with completely mobile fluorescence observed with myosin, Figure 48 A. It is established that the timescale of cortical turnover is on the order of minutes, which should set a minimum possible unbinding rate of anything bound to the cortex. Therefore I expect a minimum unbinding rate of myosin to be on the order of minutes, and the measurement of myosin recovery, shown in Figure 48 B, is consistent with a minutes-timescale. Similarly, I would expect the minimum unbinding rate of integrin from the cortex to be on the order of minutes, and the measurement of integrin mobile fraction recovery is again consistent with a minutes timescale.

Collagen turnover has been measured *in vivo*, with an incorporation rate of approximately 2.5% per hour in both homozygous and heterozygous VkgGFP backgrounds. A combined dilution and degradation rate of approximately 1.7% per hour in a homozygous VkgGFP background and approximately 0.2% per hour in a heterozygous VkgGFP background has also been measured. A reduction in dilution-degradation rate from homozygous to heterozygous backgrounds is likely a result of

the reduction in overall VkgGFP concentration. It may be expected a reduction in overall VkgGFP concentration would only change the error on the rate of change, not the rate of change itself. I think this is not the case because these measurements have not been correctly normalised. The VkgGFP concentration should be normalised to the zero time point before temperature shift, while VkgSCA should be normalised to a time point in the far future where the dynamics after temperature shift have plateaued. Only once this normalisation has been applied can a net rate of change of collagen concentration be calculated. Here, the rate of change of VkgGFP signal is described as a combination dilution and degradation of old collagen. This is because the VkgGFP signal may be both diluted in concentration as the ECM surface area grows, and reduced in concentration as VkgGFP degrades and is lost from the ECM.

Perlecan knockout in a homozygous VkgGFP background leads to a significant, approximately four-fold, increase in new collagen incorporation rate over the homozygous VkgGFP background alone. Conversely old collagen dilution and degradation rate drops to almost zero, but less significantly. Considering both the lack of correct normalisation and the difficulty interpreting the rate of change of VkgGFP signal discussed above, interpretation of this perlecan knockout result is impossible. The hypothesis I wish to test is that perlecan reduces collagen remodelling. This hypothesis is consistent with the more compacted phenotype of the wing disc after perlecan knockdown, Figure 22. A way to test this hypothesis is to repeat the experiment in Figure 51 but normalise measured concentrations correctly. Then extend the conditions tested to include perturbations to cellular growth in an attempt to account for collagen dilution.

More evidence for perlecan regulating collagen remodelling may be found in the morphology of perlecan knockout wing discs. An explanation for the patches of new collagen observed in perlecan knockout wing discs, Figure 53, is that the old collagen ECM has ruptured, perhaps due to excessive tension, leaving basal cell surfaces exposed. New collagen then immediately binds to this exposed cell surface *via* cell-matrix adhesions. The patches of new collagen must appear quickly, somewhere

within the 12 hour pulse. This suggests new ECM may be assembled very quickly by bare cell surface. When the pulse of new collagen is applied for a longer period of time some collagen turnover is observed, Figure 54, showing perlecan is not required for collagen turnover, but at least increases it. As suggested previously, perlecan may be pushing collagen stability from a higher state to a lower state, increasing its rate of unbinding. It may be that collagen is recruited to the ECM *via* two mechanisms, the first a perlecan-dependent mechanism and the second an integrin-dependent mechanism. Some evidence for this is shown in Figure 55, where new collagen preferentially localises to the outer, more-basal surface of the ECM. This suggests a fast-turnover collagen outer layer and a slow-turnover collagen inner layer to the ECM.

The spatial differences in collagen turnover, Figure 52, suggest some spatially defined mechanism or mechanisms of regulation. The ratio of old collagen to new collagen varies fairly continuously across the wing disc ECM. The scale at which continuity occurs should depend on the local control cells have on the turnover mechanism. For example, if a patch of cells were to control collagen turnover by releasing Mmps, then the scale of continuity would depend on how big the patch of cells is and how far the Mmps can diffuse once secreted into the ECM. If collagen turnover were regulated mechanically, by cell growth and proliferation, then it may be expected that small patches of cells whose cell cycles are entrained, which has been observed in the wing disc^[18], would drive local increases in collagen turnover. However, because spatial differences in collagen turnover are fairly smooth, it suggests a mechanism that is spread evenly over this scale.

Spatial differences across the wing disc have so far not been considered thoroughly in the analysis of collagen turnover, or the absolute concentrations of ECM components. It is possible that ECM components vary in a consistent manner between regions of the wing disc. Differences in ECM component concentrations and turnover between wing disc regions may indicate spatial regulation of the ECM. It has been reported that collagen concentration reduces in the middle hinge fold during folding^[62], and the ECM is degraded specifically in the peripheral pouch folds

^[151]. From images obtained for collagen turnover, Figure 52, these reported results appear to be verified. This could be extended to find similar processes in other regions of the wing disc. I would expect regions of ECM with greater Mmp activity to have faster turnover, however too much Mmp may degrade the ECM faster than it can be replaced, reducing its total density. Evidence for this hypothesis could be obtained by correlating spatial differences in Mmp1 and Mmp2 concentration across the wing disc with ECM concentration and turnover. However, published reagents I have tried so far have not provided strong signals for Mmp1 or Mmp2 concentration ^[139, 143], however other published reagents are yet to be tested ^[151].

Another way to determine spatial differences of Mmps is to genetically perturb them and then measure changes to the spatial distribution of ECM concentration and turnover. The difficulty in doing this is genetic. Firstly, the collagen turnover experiments involve the use of many transgenes, §2.4.1, which requires placement of transgenes on both paternal and maternal copies of chromosomes two and three. Further, some transgenes have been recombined onto the same chromosome to fit them in. Recombining transgenes is limited by the ability to know if the transgenes have successfully combined onto one chromosome. The markers exhibited by some transgenes define whether they can be recombined with other transgenes. Therefore sometimes it becomes very difficult to get all necessary transgenes onto the fly. Secondly, there are limitations with combining binary expression systems. Specifically, collagen turnover makes use of the UAS-Gal4 system, however almost all RNA interference lines also use UAS. Hence, the only way to drive knockdowns is temporally with turnover. This is an issue primarily with ECM components, whose knockdown leads to a slow degradation from the ECM, Figure 32. So it would be a measure of turnover as the knocked down component degrades from the ECM, complicating interpretation of the result. Other binary expression systems could be used in parallel, however this would require construction of new RNA interference transgenes. Thirdly, overloading chromosomes with transgenes can lead to unhealthy flies. Combined, these problems limit the complexity of experiments.

One way to circumvent the binary expression problem is to use mutants. Mutants can provide loss-of-function phenotypes without use of binary expression systems. Many loss-of-function mutants are lethal before larval stage, but luckily some mutants for ECM proteins survive. I have already used a Trol mutant in combination with driving a pulse of VkgSCA, Figure 53. Other ECM mutants that could be used are Mmp1 and Mmp2 mutants ^[143], Loxl1 and Loxl2 mutants ^[157], and certain combinations of LanA mutant ^[109]. A concern with using these mutants is their ubiquitous effect on the larva. It is possible that negative effects of these mutants could affect the production of collagen indirectly, for example by reducing their ability to feed. Wing disc specific perturbations are therefore preferred where possible. For lethal mutants of proteins expressed in the wing disc, mitotic recombination can be used to generate double knockout clones. Of particular interest are mutations genes that affect cell-matrix adhesions, such as Mys ^[196] and Dg ^[197]. Other mutations of genes that could affect ECM turnover include growth regulators such as E2f1 ^[19], and contractility regulators such as Rok ^[198] and Flw ^[199]. Some temperature sensitive mutants also exist, such as a temperature sensitive Mys ^[200]. There also exist some overexpression lines, where a copy of the gene has been placed directly under the heat-shock promoter, such as CycE ^[201].

3 Conclusions

As described in the hypothesis, §1.6.2, there were two aims in this work, to understand how the cells interact with the ECM, and to understand how the ECM responds to this interaction. In this work I believe I have made some progress with both these aims. For the first aim, I have found evidence that cellular contractility and the ECM interact to maintain cell shape. For the second aim I have found evidence that the ECM contributes stiffness to the tissue, but also remodels.

3.1 Cell contractility and the ECM

I have first tried to understand the structure of the ECM and how it corresponds to the cortical structure of overlying cells. I have found that the ECM forms a thin sheet along the basal surface of cells, Figure 8. I have found that in the pouch, this ECM sheet delaminates as the wing disc ages, Figure 16, making the ECM appear thicker. I have also found the ECM exhibits high-density fibres than run along its surface, Figure 11, and these fibres appear to correlate with integrin and actin structures at the basal surface of cells, Figure 13, Figure 14, suggesting some interaction between the two. More solid proof of cell-ECM interaction is found when the ECM is degraded, leading to sudden morphological change in the wing disc, Figure 24, including the expansion of basal cell surfaces. Such a drastic morphological change is perhaps surprising, because it suggests a large amount of mechanical energy is being stored in this cell-ECM interaction. This morphological change is dependent on cellular contractility, Figure 25, suggesting the ECM somehow balances contractile forces. Wing disc tissue also becomes softer when either the cortex or ECM is degraded, Figure 43. Interestingly, wing disc tissue also becomes stiffer with age, Figure 44. Together these results show interaction between cellular contractility and the ECM somehow contribute to wing disc morphology. A mechanical explanation

presented for these results is that cellular contractility drives a surface to volume minimisation of the cell, which is counteracted by the stiff ECM.

Much more work is required to determine the validity of this hypothesis. Further work is required to determine if contractility actually drives basal expansion, and if this basal expansion drives ECM tension. For example, genetically inhibiting or promoting contractility during wing disc growth, may slow or accelerate the minimisation of surface to volume ratio, potentially leading to different cell shape. An ECM tension may be measured by ablation experiments. Cell-matrix adhesions may be important in mediating the tension cells apply to the ECM. The significant morphological phenotype observed with loss of integrin adhesion, Figure 23, may be evidence of this importance. A closer look at this phenotype may therefore be enlightening. It would also be interesting to determine if integrins contribute to tissue stiffness. The alternative hypothesis, that fast protein-protein signalling causes a rebalance of forces that drive cell shape change, also needs to be considered. This work could begin with determining if contractile structures such as basal myosin rings, Figure 15, change after ECM degradation. It is likely that the observed morphological change after ECM degradation is a combination of these two hypotheses, so both need to be explored.

3.2 Remodelling of the ECM

I have tentatively measured a turnover rate on the order of days for collagen Figure 50, and I have measured a similar timescale for perlecan dilution and degradation, Figure 32. More work is required to make these measurements rigorous. Firstly by testing the underlying assumptions, such as assumptions about the dynamics of the protein haemolymph concentration. Secondly, a method to deconvolve the contributions of dilution and degradation to the loss of protein signal after knockdown. Once these issues are resolved, these methods of measuring ECM protein dynamics could be used to find potential regulators, and affects on tissue morphology.

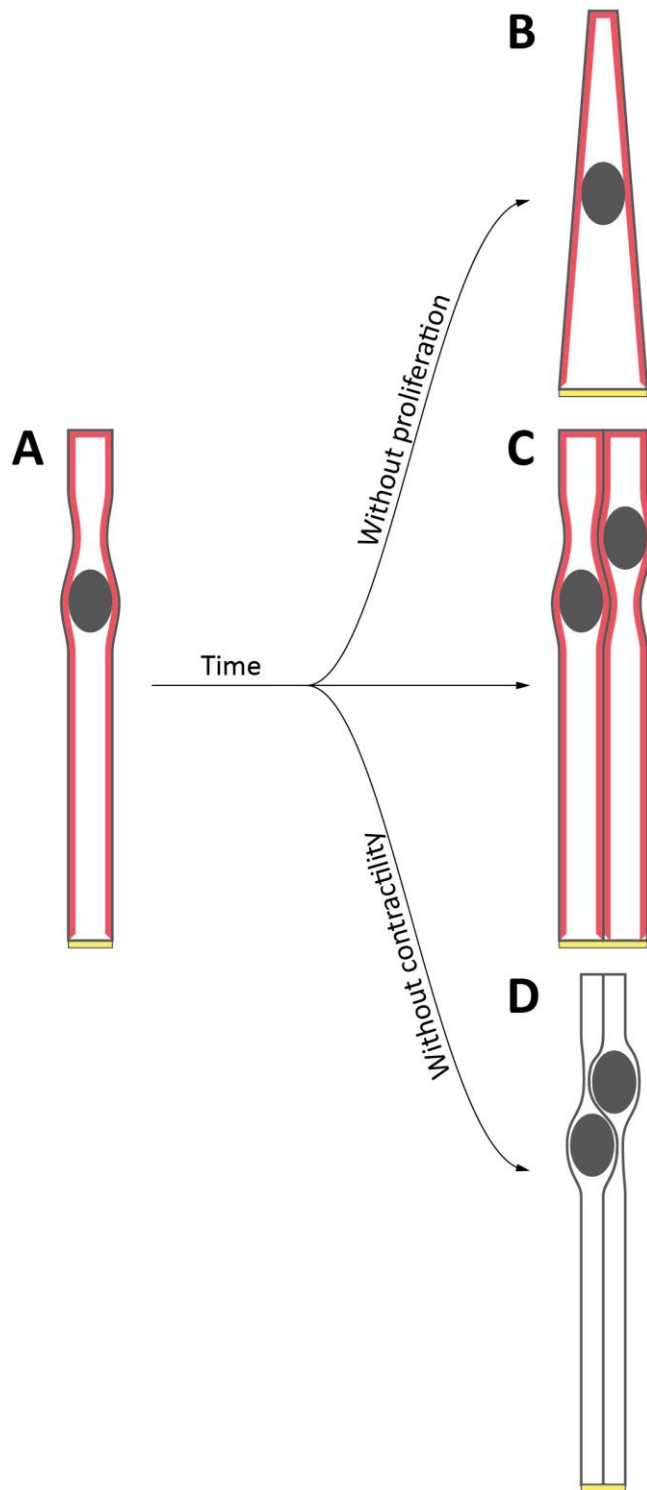


Figure 56. Regulation of extra-cellular matrix area, and therefore cell shape, during tissue growth may depend on both cell contractility and cell proliferation. Given a contractile cell, **A**, if no proliferation occurs then its basal surface and ECM may expand over hours, **B**. If the cell could proliferate but not contract, then the ECM surface area may not grow, compacting cells, **D**. Therefore both proliferation and contractility may be required for correct cell shape, **C**.

Something that can be concluded from measurements of collagen dynamics, Figure 50, is that collagen is dynamic, and so does appear to grow and remodel, incorporating new collagen as it does so. This result may put the interpretation from the previous section in a new light. Minimisation of cellular surface to volume ratio by contractility drives a basal expansion, which is prevented by the stiff ECM on short timescales. On long timescales we now know the ECM, or at least collagen, remodel. Therefore, the basal expansivity of cells may drive an expansive remodelling of the ECM. This expansion of the ECM would allow for some homeostasis of cell basal surface area as they proliferate. This new hypothesis is described in Figure 56.

In terms of proteins that may regulate ECM dynamics, I am particularly interested in perlecan. I expect that phenotypes associated with perlecan such as changes to cell and tissue morphology, and increased tissue stiffness, may be related to ECM remodelling. Tentative measurements of collagen dynamics in a perlecan knockout background suggest perlecan may contribute to regulation of collagen remodelling, Figure 50. However, the issues associated with these measurements discussed previously must first be resolved before a conclusion can be made.

If perlecan does reduce collagen remodelling, this may result in an increased ECM tension as the cells continue to grow. ECM ablations under different perlecan conditions would give a direct measure of ECM tension. Protruding cells in perlecan knockout wing discs, Figure 53, may be a result of ECM tension, and they would be confirmed if cells popped out as a result of ECM ablations. Perturbations to cell growth and proliferation^[19], could also provide more evidence. Supporting evidence would be if increased cell proliferation exacerbates the compacted morphology of perlecan knockdown. Or conversely, supporting evidence would be if reduced cell growth and proliferation rescues the compacted morphology of perlecan knockdown.

When cells of the wing disc are degraded, the ECM remains intact, Figure 30. This suggests the ECM has its own integrity independent of cells, at least *ex vivo*. Also,

when wing discs are cultured for extended periods *ex vivo*, the ECM remains intact Figure 31, suggesting it is stable even without a source of new ECM components. However *in vivo*, factors in the haemolymph and secreted by the wing disc not present *ex vivo* may degrade the ECM. If factors driving ECM degradation or turnover, such as Mmps, are secreted by the wing disc, it is surprising they are not still active *ex vivo*. There are considerable problems culturing wing discs *ex vivo*, primarily defined by a loss of cell proliferation. Therefore it is possible that cessation of cell proliferation is connected to ECM stability *ex vivo*.

3.3 Outlook

Progress has been made towards the aims outlined in §1.6.2. However, further work is required to conclusively determine how these mechanisms function. This work has established techniques to probe the mechanical properties of the tissue and the ECM. In particular, atomic force microscopy has been established as a tool to measure tissue stiffness, and temporal genetic perturbations have been used to measure ECM turnover. The next steps are to apply these techniques in combination with treatments and knockdowns that may further elucidate the mechanisms at play. I am particularly interested in understanding how cells regulate ECM remodelling, and whether remodelling can contribute to wing disc morphology.

4 References

- [1] Lecuit T, *et al.* *Force Generation, Transmission, and Integration during Cell and Tissue Morphogenesis*. Annual Review of Cell and Developmental Biology. 2011. 27:157–184.
- [2] Tlili S, *et al.* *Colloquium: Mechanical formalisms for tissue dynamics*. Eur. Phys. J. E. 2015. 38:33.
- [3] Reddy JN *An Introduction to Continuum Mechanics* (Cambridge University Press)2007.
- [4] Rubinstein M *Polymer Physics* (Oxford University Press)2003.
- [5] Gennes PG de *Scaling Concepts in Polymer Physics* (Cornell University Press)1979.
- [6] Kondo S, *et al.* *Reaction-Diffusion Model as a Framework for Understanding Biological Pattern Formation*. Science. 2010. 329:1616–1620.
- [7] Clark AG, *et al.* *Stresses at the Cell Surface during Animal Cell Morphogenesis*. Current Biology. 2014. 24:R484–R494.
- [8] Mao Y, *et al.* *Tug of war—The influence of opposing physical forces on epithelial cell morphology*. Developmental Biology. 2015. 401:92–102.
- [9] Salbreux G, *et al.* *Actin cortex mechanics and cellular morphogenesis*. Trends in Cell Biology. 2012. 22:536–545.
- [10] Burute M, *et al.* *Spatial segregation between cell–cell and cell–matrix adhesions*. Current Opinion in Cell Biology. 2012. 24:628–636.
- [11] Sagner A, *et al.* *Morphogen interpretation: concentration, time, competence, and signaling dynamics*. Wiley Interdisciplinary Reviews: Developmental Biology. 2017. 6:e271.
- [12] Muiznieks LD, *et al.* *Molecular assembly and mechanical properties of the extracellular matrix: A fibrous protein perspective*. Biochimica et Biophysica Acta (BBA) - Molecular Basis of Disease. 2013. 1832:866–875.
- [13] Lindner JR, *et al.* *The Drosophila Perlecan gene trol regulates multiple signaling pathways in different developmental contexts*. BMC Developmental Biology. 2007. 7:121.
- [14] Crest J, *et al.* *Organ sculpting by patterned extracellular matrix stiffness*. eLife. 2017. 6:e24958.
- [15] Aldaz S, *et al.* *Imaginal discs*. Current Biology. 2010. 20:R429–R431.
- [16] Pastor-Pareja JC, *et al.* *Shaping Cells and Organs in Drosophila by Opposing Roles of Fat Body-Secreted Collagen IV and Perlecan*. Developmental Cell. 2011. 21:245–256.
- [17] Ray RP, *et al.* *Patterned Anchorage to the Apical Extracellular Matrix Defines Tissue Shape in the Developing Appendages of Drosophila*. Developmental Cell. 2015. 34:310–322.
- [18] Day SJ, *et al.* *Measuring dimensions: the regulation of size and shape*. Development. 2000. 127:2977–2987.

- [19] Neufeld TP, et al. *Coordination of Growth and Cell Division in the Drosophila Wing*. Cell. 1998. 93:1183–1193.
- [20] Hariharan IK *Organ Size Control: Lessons from Drosophila*. Developmental Cell. 2015. 34:255–265.
- [21] Lee C-H, et al. *A Regulatory Response to Ribosomal Protein Mutations Controls Translation, Growth, and Cell Competition*. Developmental Cell. 2018. 46:456-469.e4.
- [22] Thummel CS *Molecular Mechanisms of Developmental Timing in C. elegans and Drosophila*. Developmental Cell. 2001. 1:453–465.
- [23] D’Avino PP, et al. *The Ecdysone Regulatory Pathway Controls Wing Morphogenesis and Integrin Expression during Drosophila Metamorphosis*. Developmental Biology. 2000. 220:211–224.
- [24] Lin JI, et al. *Drosophila Ribosomal Protein Mutants Control Tissue Growth Non-Autonomously via Effects on the Prothoracic Gland and Ecdysone*. PLOS Genetics. 2011. 7:e1002408.
- [25] Ginzberg MB, et al. *On being the right (cell) size*. Science. 2015. 348:1245075.
- [26] Gelbart MA, et al. *Volume conservation principle involved in cell lengthening and nucleus movement during tissue morphogenesis*. PNAS. 2012. 109:19298–19303.
- [27] Burke R, et al. *Dpp receptors are autonomously required for cell proliferation in the entire developing Drosophila wing*. Development. 1996. 122:2261–2269.
- [28] Johnston LA, et al. *Drosophila myc Regulates Cellular Growth during Development*. Cell. 1999. 98:779–790.
- [29] Bielmeier C, et al. *Interface Contractility between Differently Fated Cells Drives Cell Elimination and Cyst Formation*. Current Biology. 2016. 26:563–574.
- [30] Schwank G, et al. *Growth regulation by Dpp: an essential role for Brinker and a non-essential role for graded signaling levels*. Development. 2008. 135:4003–4013.
- [31] Rogulja D, et al. *Regulation of Cell Proliferation by a Morphogen Gradient*. Cell. 2005. 123:449–461.
- [32] Hufnagel L, et al. *On the mechanism of wing size determination in fly development*. PNAS. 2007. 104:3835–3840.
- [33] Mao Y, et al. *Differential proliferation rates generate patterns of mechanical tension that orient tissue growth*. The EMBO Journal. 2013. 32:2790–2803.
- [34] Fulford A, et al. *Upstairs, downstairs: spatial regulation of Hippo signalling*. Current Opinion in Cell Biology. 2018. 51:22–32.
- [35] Goñi FM *The basic structure and dynamics of cell membranes: An update of the Singer–Nicolson model*. Biochimica et Biophysica Acta (BBA) - Biomembranes. 2014. 1838:1467–1476.
- [36] Diz-Muñoz A, et al. *Use the force: membrane tension as an organizer of cell shape and motility*. Trends in Cell Biology. 2013. 23:47–53.
- [37] Stewart MP, et al. *Hydrostatic pressure and the actomyosin cortex drive mitotic cell rounding*. Nature. 2011. 469:226–230.
- [38] Jacinto A, et al. *Actin in development*. Mechanisms of Development. 2003. 120:1337–1349.

- [39] Röper K, et al. *Contribution of sequence variation in Drosophila actins to their incorporation into actin-based structures in vivo*. Journal of Cell Science. 2005. 118:3937–3948.
- [40] Rogers SL, et al. *Molecular requirements for actin-based lamella formation in Drosophila S2 cells*. The Journal of Cell Biology. 2003. 162:1079–1088.
- [41] Hsiao JY, et al. *Arp2/3 Complex and Cofilin Modulate Binding of Tropomyosin to Branched Actin Networks*. Current Biology. 2015. 25:1573–1582.
- [42] Lammel U, et al. *The Drosophila FHOD1-like formin Knittrig acts through Rok to promote stress fiber formation and directed macrophage migration during the cellular immune response*. Development. 2014. 141:1366–1380.
- [43] Homem CCF, et al. *Diaphanous regulates myosin and adherens junctions to control cell contractility and protrusive behavior during morphogenesis*. Development. 2008. 135:1005–1018.
- [44] Barkó S, et al. *Characterization of the Biochemical Properties and Biological Function of the Formin Homology Domains of Drosophila DAAM*. J. Biol. Chem. 2010. 285:13154–13169.
- [45] Szikora S, et al. *The formin DAAM is required for coordination of the actin and microtubule cytoskeleton in axonal growth cones*. J Cell Sci. 2017. 130:2506–2519.
- [46] Dollar G, et al. *Unique and Overlapping Functions of Formins Frl and DAAM During Ommatidial Rotation and Neuronal Development in Drosophila*. Genetics. 2016. 202:1135–1151.
- [47] Quinlan ME, et al. *Regulatory interactions between two actin nucleators, Spire and Cappuccino*. J Cell Biol. 2007. 179:117–128.
- [48] Tanaka H, et al. *Formin3 is required for assembly of the F-actin structure that mediates tracheal fusion in Drosophila*. Developmental Biology. 2004. 274:413–425.
- [49] Patel AA, et al. *Drosophila and human FHOD family formin proteins nucleate actin filaments*. J. Biol. Chem. 2018. 293:532–540.
- [50] Bilancia CG, et al. *Enabled Negatively Regulates Diaphanous-Driven Actin Dynamics In Vitro and In Vivo*. Developmental Cell. 2014. 28:394–408.
- [51] Gates J, et al. *Enabled plays key roles in embryonic epithelial morphogenesis in Drosophila*. Development. 2007. 134:2027–2039.
- [52] Külshammer E, et al. *The actin cross-linker Filamin/Cheerio mediates tumor malignancy downstream of JNK signaling*. J Cell Sci. 2013. 126:927–938.
- [53] Okenve-Ramos P, et al. *Fascin links Btl/FGFR signalling to the actin cytoskeleton during Drosophila tracheal morphogenesis*. Development. 2014. 141:929–939.
- [54] Huelsmann S, et al. *Evidence for the mechanosensor function of filamin in tissue development*. Scientific Reports. 2016. 6:32798.
- [55] Janody F, et al. *Actin capping protein α maintains vestigial-expressing cells within the Drosophila wing disc epithelium*. Development. 2006. 133:3349–3357.
- [56] Lin C-M, et al. *Capulet and Slingshot share overlapping functions during Drosophila eye morphogenesis*. Journal of Biomedical Science. 2012. 19:46.

- [57] Fernández BG, et al. *Actin-Capping Protein and the Hippo pathway regulate F-actin and tissue growth in Drosophila*. *Development*. 2011. 138:2337–2346.
- [58] Heintzelman MB, et al. *Cloning of a Secretory Gelsolin from Drosophila melanogaster*. *Journal of Molecular Biology*. 1993. 230:709–716.
- [59] Clément R, et al. *Viscoelastic Dissipation Stabilizes Cell Shape Changes during Tissue Morphogenesis*. *Current Biology*. 2017. 27:3132–3142.e4.
- [60] Deng W-M, et al. *Dystroglycan is required for polarizing the epithelial cells and the oocyte in Drosophila*. *Development*. 2003. 130:173–184.
- [61] Maître J-L, et al. *The role of adhesion energy in controlling cell–cell contacts*. *Current Opinion in Cell Biology*. 2011. 23:508–514.
- [62] Sui L, et al. *Differential lateral and basal tension drive folding of Drosophila wing discs through two distinct mechanisms*. *Nat Commun*. 2018. 9:1–13.
- [63] Savin T, et al. *On the growth and form of the gut*. *Nature*. 2011. 476:57–62.
- [64] Martin-Bermudo MD, et al. *Uncoupling integrin adhesion and signaling: the β PS cytoplasmic domain is sufficient to regulate gene expression in the Drosophila embryo*. *Genes Dev*. 1999. 13:729–739.
- [65] Brower DL, et al. *Related cell-surface antigens expressed with positional specificity in Drosophila imaginal discs*. *PNAS*. 1984. 81:7485–7489.
- [66] Stark KA, et al. *A novel alpha integrin subunit associates with betaPS and functions in tissue morphogenesis and movement during Drosophila development*. *Development*. 1997. 124:4583–4594.
- [67] Hughes AL *Evolution of the Integrin α and β Protein Families*. *J Mol Evol*. 2001. 52:63–72.
- [68] Tanentzapf G, et al. *Multiple factors contribute to integrin-talin interactions in vivo*. *J Cell Sci*. 2006. 119:1632–1644.
- [69] Devenport D, et al. *Mutations in the Drosophila α PS2 integrin subunit uncover new features of adhesion site assembly*. *Developmental Biology*. 2007. 308:294–308.
- [70] Bunch TA, et al. *Drosophila PS2 integrin mediates RGD-dependent cell-matrix interactions*. *Development*. 1992. 116:239–247.
- [71] Gotwals PJ, et al. *Drosophila PS1 integrin is a laminin receptor and differs in ligand specificity from PS2*. *PNAS*. 1994. 91:11447–11451.
- [72] Brown NH, et al. *Developmentally regulated alternative splicing of Drosophila integrin PS2 α transcripts*. *Cell*. 1989. 59:185–195.
- [73] Zusman S, et al. *Analyses of PS integrin functions during Drosophila development*. *Development*. 1993. 118:737–750.
- [74] Graner MW, et al. *Splice Variants of the Drosophila PS2 Integrins Differentially Interact with RGD-containing Fragments of the Extracellular Proteins Tigrin, Ten-m, and D-Laminin α 2*. *J. Biol. Chem*. 1998. 273:18235–18241.
- [75] Ellis SJ, et al. *The Talin Head Domain Reinforces Integrin-Mediated Adhesion by Promoting Adhesion Complex Stability and Clustering*. *PLOS Genetics*. 2014. 10:e1004756.

- [76] Brown NH, et al. *Talin Is Essential for Integrin Function in Drosophila*. *Developmental Cell*. 2002. 3:569–579.
- [77] Dominguez-Gimenez P, et al. *Integrin-ECM interactions regulate the changes in cell shape driving the morphogenesis of the Drosophila wing epithelium*. *Journal of Cell Science*. 2007. 120:1061–1071.
- [78] Delon I, et al. *The integrin adhesion complex changes its composition and function during morphogenesis of an epithelium*. *Journal of Cell Science*. 2009. 122:4363–4374.
- [79] Green HJ, et al. *Novel functions for integrin-associated proteins revealed by analysis of myofibril attachment in Drosophila*. *eLife*. 2018. 7:e35783.
- [80] Bulgakova NA, et al. *Cell adhesion in Drosophila: versatility of cadherin and integrin complexes during development*. *Current Opinion in Cell Biology*. 2012. 24:702–712.
- [81] Ellis SJ, et al. *In vivo functional analysis reveals specific roles for the integrin-binding sites of talin*. *Journal of Cell Science*. 2011.:jcs.083337.
- [82] Maartens AP, et al. *Drosophila vinculin is more harmful when hyperactive than absent, and can circumvent integrin to form adhesion complexes*. *J Cell Sci*. 2016. 129:4354–4365.
- [83] Tanentzapf G, et al. *An interaction between integrin and the talin FERM domain mediates integrin activation but not linkage to the cytoskeleton*. *Nature Cell Biology*. 2006. 8:601–606.
- [84] Alatortsev VE, et al. *Vinculin gene is non-essential in Drosophila melanogaster*. *FEBS Letters*. 1997. 413:197–201.
- [85] Franco-Cea A, et al. *Distinct developmental roles for direct and indirect talin-mediated linkage to actin*. *Developmental Biology*. 2010. 345:64–77.
- [86] Klapholz B, et al. *Alternative Mechanisms for Talin to Mediate Integrin Function*. *Current Biology*. 2015. 25:847–857.
- [87] Zervas CG, et al. *A central multifunctional role of integrin-linked kinase at muscle attachment sites*. *J Cell Sci*. 2011. 124:1316–1327.
- [88] Clark KA, et al. *Analysis of PINCH function in Drosophila demonstrates its requirement in integrin-dependent cellular processes*. *Development*. 2003. 130:2611–2621.
- [89] Vakaloglou KM, et al. *Functional analysis of parvin and different modes of IPP-complex assembly at integrin sites during Drosophila development*. *J Cell Sci*. 2012. 125:3221–3232.
- [90] Vakaloglou KM, et al. *IPP Complex Reinforces Adhesion by Relaying Tension-Dependent Signals to Inhibit Integrin Turnover*. *Cell Reports*. 2016. 14:2668–2682.
- [91] Chountala M, et al. *Parvin Overexpression Uncovers Tissue-Specific Genetic Pathways and Disrupts F-Actin to Induce Apoptosis in the Developing Epithelia in Drosophila*. *PLOS ONE*. 2012. 7:e47355.
- [92] Yuan L, et al. *Analysis of integrin turnover in fly myotendinous junctions*. *J Cell Sci*. 2010. 123:939–946.
- [93] Bulgakova Natalia A., et al. *Diverse integrin adhesion stoichiometries caused by varied actomyosin activity*. *Open Biology*. 2017. 7:160250.

- [94] Chen G-C, et al. *Regulation of Rho and Rac Signaling to the Actin Cytoskeleton by Paxillin during Drosophila Development*. *Molecular and Cellular Biology*. 2005. 25:979–987.
- [95] Grabbe C, et al. *Focal adhesion kinase is not required for integrin function or viability in Drosophila*. *Development*. 2004. 131:5795–5805.
- [96] Tsai P-I, et al. *Fak56 functions downstream of integrin alphaPS3betanu and suppresses MAPK activation in neuromuscular junction growth*. *Neural Development*. 2008. 3:26.
- [97] Torgler CN, et al. *Tensin Stabilizes Integrin Adhesive Contacts in Drosophila*. *Developmental Cell*. 2004. 6:357–369.
- [98] Cha IJ, et al. *Drosophila tensin plays an essential role in cell migration and planar polarity formation during oogenesis by mediating integrin-dependent extracellular signals to actin organization*. *Biochemical and Biophysical Research Communications*. 2017. 484:702–709.
- [99] Schneider M, et al. *Perlecan and Dystroglycan act at the basal side of the Drosophila follicular epithelium to maintain epithelial organization*. *Development*. 2006. 133:3805–3815.
- [100] Greener MJ, et al. *Conservation of components of the dystrophin complex in Drosophila* 11New database accession numbers: AF277386, AF277387, AF277388, AF277389, AF277390, AF277391, AF277392, AF277393. *FEBS Letters*. 2000. 482:13–18.
- [101] Poulton JS, et al. *Dystroglycan down-regulation links EGF receptor signaling and anterior–posterior polarity formation in the Drosophila oocyte*. *PNAS*. 2006. 103:12775–12780.
- [102] Yatsenko AS, et al. *A Putative Src Homology 3 Domain Binding Motif but Not the C-terminal Dystrophin WW Domain Binding Motif Is Required for Dystroglycan Function in Cellular Polarity in Drosophila*. *J. Biol. Chem*. 2007. 282:15159–15169.
- [103] Kucherenko MM, et al. *Genetic Modifier Screens Reveal New Components that Interact with the Drosophila Dystroglycan-Dystrophin Complex*. *PLOS ONE*. 2008. 3:e2418.
- [104] Marrone AK, et al. *New Dystrophin/Dystroglycan interactors control neuron behavior in Drosophila eye*. *BMC Neuroscience*. 2011. 12:93.
- [105] Yurchenco PD *Basement Membranes: Cell Scaffoldings and Signaling Platforms*. Cold Spring Harb Perspect Biol. 2011. 3:a004911.
- [106] Wilmes AC, et al. *Biosynthesis and assembly of the Collagen IV-like protein Pericardin in Drosophila melanogaster*. *Biology Open*. 2018. 7:bio030361.
- [107] Fogerty FJ, et al. *Tiggrin, a novel Drosophila extracellular matrix protein that functions as a ligand for Drosophila alpha PS2 beta PS integrins*. *Development*. 1994. 120:1747–1758.
- [108] Urbano JM, et al. *Drosophila laminins act as key regulators of basement membrane assembly and morphogenesis*. *Development*. 2009. 136:4165–4176.
- [109] Henchcliffe C, et al. *Genetic analysis of laminin A reveals diverse functions during morphogenesis in Drosophila*. *Development*. 1993. 118:325–337.
- [110] Martin D, et al. *wing blister, A New Drosophila Laminin α Chain Required for Cell Adhesion and Migration during Embryonic and Imaginal Development*. *The Journal of Cell Biology*. 1999. 145:191–201.

- [111] Tashiro K, et al. *A synthetic peptide containing the IKVAV sequence from the A chain of laminin mediates cell attachment, migration, and neurite outgrowth.* J. Biol. Chem. 1989. 264:16174–16182.
- [112] Hunter DD, et al. *Primary sequence of a motor neuron-selective adhesive site in the synaptic basal lamina protein s-laminin.* Cell. 1989. 59:905–913.
- [113] Brown KL, et al. *Building collagen IV smart scaffolds on the outside of cells.* Protein Science. 2017. 26:2151–2161.
- [114] Momota R, et al. *Drosophila type XV/XVIII collagen, Mp, is involved in Wingless distribution.* Matrix Biology. 2011. 30:258–266.
- [115] Haigo SL, et al. *Global Tissue Revolutions in a Morphogenetic Movement Controlling Elongation.* Science. 2011. 331:1071–1074.
- [116] Wang X, et al. *Type IV collagens regulate BMP signalling in Drosophila.* Nature. 2008. 455:72–77.
- [117] Ma M, et al. *Basement Membrane Manipulation in Drosophila Wing Discs Affects Dpp Retention but Not Growth Mechanoregulation.* Developmental Cell. 2017. 42:97-106.e4.
- [118] Harmansa S, et al. *A nanobody-based toolset to investigate the role of protein localization and dispersal in Drosophila.* eLife. 2017. 6:e22549.
- [119] Yan D, et al. *Shaping Morphogen Gradients by Proteoglycans.* Cold Spring Harb Perspect Biol. 2009. 1:a002493.
- [120] Strigini M, et al. *A Hedgehog activity gradient contributes to AP axial patterning of the Drosophila wing.* Development. 1997. 124:4697–4705.
- [121] Strigini M, et al. *Wingless gradient formation in the Drosophila wing.* Current Biology. 2000. 10:293–300.
- [122] Han C, et al. *Drosophila glypicans Dally and Dally-like shape the extracellular Wingless morphogen gradient in the wing disc.* Development. 2005. 132:667–679.
- [123] Yan D, et al. *The Core Protein of Glypican Dally-Like Determines Its Biphasic Activity in Wingless Morphogen Signaling.* Developmental Cell. 2009. 17:470–481.
- [124] Kirkpatrick CA, et al. *The function of a Drosophila glypican does not depend entirely on heparan sulfate modification.* Developmental Biology. 2006. 300:570–582.
- [125] Kleinschmit A, et al. *Drosophila heparan sulfate 6-O endosulfatase regulates Wingless morphogen gradient formation.* Developmental Biology. 2010. 345:204–214.
- [126] Gallet A, et al. *Cellular Trafficking of the Glypican Dally-like Is Required for Full-Strength Hedgehog Signaling and Wingless Transcytosis.* Developmental Cell. 2008. 14:712–725.
- [127] Bischoff M, et al. *Cytonemes are required for the establishment of a normal Hedgehog morphogen gradient in Drosophila epithelia.* Nature Cell Biology. 2013. 15:1269–1281.
- [128] Schulz JG, et al. *Drosophila syndecan regulates tracheal cell migration by stabilizing Robo levels.* EMBO reports. 2011. 12:1039–1046.
- [129] Voigt A, et al. *Perlecan participates in proliferation activation of quiescent Drosophila neuroblasts.* Developmental Dynamics. 2002. 224:403–412.

- [130] Grigorian M, et al. *The proteoglycan Trol controls the architecture of the extracellular matrix and balances proliferation and differentiation of blood progenitors in the Drosophila lymph gland*. *Developmental Biology*. 2013. 384:301–312.
- [131] Friedrich MVK, et al. *Perlecan domain V of Drosophila melanogaster*. *European Journal of Biochemistry*. 2000. 267:3149–3159.
- [132] Zang Y, et al. *Plasma membrane overgrowth causes fibrotic collagen accumulation and immune activation in Drosophila adipocytes*. *eLife*. 2015. 4:e07187.
- [133] Park Y, et al. *Drosophila Perlecan modulates FGF and Hedgehog signals to activate neural stem cell division*. *Developmental Biology*. 2003. 253:247–257.
- [134] Kamimura K, et al. *Perlecan regulates bidirectional Wnt signaling at the Drosophila neuromuscular junction*. *J Cell Biol*. 2013. 200:219–233.
- [135] Dai J, et al. *Dissection of Nidogen function in Drosophila reveals tissue-specific mechanisms of basement membrane assembly*. *PLOS Genetics*. 2018. 14:e1007483.
- [136] Wolfstetter G, et al. *Characterization of Drosophila Nidogen/entactin reveals roles in basement membrane stability, barrier function and nervous system patterning*. *Development*. 2019. 146:dev168948.
- [137] Portela M, et al. *Drosophila SPARC Is a Self-Protective Signal Expressed by Loser Cells during Cell Competition*. *Developmental Cell*. 2010. 19:562–573.
- [138] Shahab J, et al. *Loss of SPARC dysregulates basal lamina assembly to disrupt larval fat body homeostasis in Drosophila melanogaster*. *Developmental Dynamics*. 2015. 244:540–552.
- [139] LaFever KS, et al. *Both Drosophila matrix metalloproteinases have released and membrane-tethered forms but have different substrates*. *Scientific Reports*. 2017. 7:44560.
- [140] Wei S, et al. *Drosophila TIMP Is a Potent Inhibitor of MMPs and TACE: Similarities in Structure and Function to TIMP-3*. *Biochemistry*. 2003. 42:12200–12207.
- [141] Srivastava A, et al. *Basement membrane remodeling is essential for Drosophila disc eversion and tumor invasion*. *PNAS*. 2007. 104:2721–2726.
- [142] Pézeron G, et al. *Notch directly regulates the cell morphogenesis genes Reck, talin and trio in adult muscle progenitors*. *J Cell Sci*. 2014. 127:4634–4644.
- [143] Page-McCaw A, et al. *Drosophila Matrix Metalloproteinases Are Required for Tissue Remodeling, but Not Embryonic Development*. *Developmental Cell*. 2003. 4:95–106.
- [144] Zhang S, et al. *An MMP liberates the Ninjurin A ectodomain to signal a loss of cell adhesion*. *Genes Dev*. 2006. 20:1899–1910.
- [145] Glasheen BM, et al. *Distinct functions for the catalytic and hemopexin domains of a Drosophila matrix metalloproteinase*. *PNAS*. 2009. 106:2659–2664.
- [146] Beaucher M, et al. *Metastatic ability of Drosophila tumors depends on MMP activity*. *Developmental Biology*. 2007. 303:625–634.
- [147] Jia Q, et al. *Mmp1 and Mmp2 cooperatively induce Drosophila fat body cell dissociation with distinct roles*. *Scientific Reports*. 2014. 4:7535.

- [148] Guha A, et al. *Regulation of Drosophila matrix metalloprotease Mmp2 is essential for wing imaginal disc:trachea association and air sac tubulogenesis*. *Developmental Biology*. 2009. 335:317–326.
- [149] Uhlirova M, et al. *JNK- and Fos-regulated Mmp1 expression cooperates with Ras to induce invasive tumors in Drosophila*. *The EMBO Journal*. 2006. 25:5294–5304.
- [150] Pastor-Pareja JC, et al. *An innate immune response of blood cells to tumors and tissue damage in Drosophila*. *Disease Models & Mechanisms*. 2008. 1:144–154.
- [151] Sui L, et al. *The Dorsocross T-box transcription factors promote tissue morphogenesis in the Drosophila wing imaginal disc*. *Development*. 2012. 139:2773–2782.
- [152] Meyer H, et al. *Drosophila metalloproteases in development and differentiation: The role of ADAM proteins and their relatives*. *European Journal of Cell Biology*. 2011. 90:770–778.
- [153] Lieber T, et al. *kuzbanian-mediated cleavage of Drosophila Notch*. *Genes Dev*. 2002. 16:209–221.
- [154] Ismat A, et al. *The secreted AdamTS-A metalloprotease is required for collective cell migration*. *Development*. 2013. 140:1981–1993.
- [155] Skeath JB, et al. *The extracellular metalloprotease AdamTS-A anchors neural lineages in place within and preserves the architecture of the central nervous system*. *Development*. 2017. 144:3102–3113.
- [156] Lucero HA, et al. *Lysyl oxidase: an oxidative enzyme and effector of cell function*. *Cell. Mol. Life Sci*. 2006. 63:2304–2316.
- [157] Molnar J, et al. *Drosophila Lysyl Oxidases Dmlox1-1 and Dmlox1-2 Are Differentially Expressed and the Active DmLOXL-1 Influences Gene Expression and Development*. *J. Biol. Chem*. 2005. 280:22977–22985.
- [158] Kim SN, et al. *ECM stiffness regulates glial migration in Drosophila and mammalian glioma models*. *Development*. 2014. 141:3233–3242.
- [159] Bhawe G, et al. *Peroxidasin forms sulfilimine chemical bonds using hypohalous acids in tissue genesis*. *Nature Chemical Biology*. 2012. 8:784–790.
- [160] McCall AS, et al. *Bromine Is an Essential Trace Element for Assembly of Collagen IV Scaffolds in Tissue Development and Architecture*. *Cell*. 2014. 157:1380–1392.
- [161] Morin X, et al. *A protein trap strategy to detect GFP-tagged proteins expressed from their endogenous loci in Drosophila*. *PNAS*. 2001. 98:15050–15055.
- [162] Metaxakis A, et al. *Minos as a Genetic and Genomic Tool in Drosophila melanogaster*. *Genetics*. 2005. 171:571–581.
- [163] Sarov M, et al. *A genome-wide resource for the analysis of protein localisation in Drosophila*. *eLife*. 2016. 5:e12068.
- [164] Lowe N, et al. *Analysis of the expression patterns, subcellular localisations and interaction partners of Drosophila proteins using a pigP protein trap library*. *Development*. 2014. 141:3994–4005.
- [165] Handke B, et al. *Towards Long Term Cultivation of Drosophila Wing Imaginal Discs In Vitro*. *PLOS ONE*. 2014. 9:e107333.

- [166] Dye NA, *et al.* *Cell dynamics underlying oriented growth of the Drosophila wing imaginal disc.* *Development.* 2017. 144:4406–4421.
- [167] Restrepo S, *et al.* *Cultivation and Live Imaging of Drosophila Imaginal Discs.* *Drosophila: Methods and Protocols*, *Methods in Molecular Biology.*, ed Dahmann C (Springer New York, New York, NY)2016., pp 203–213.
- [168] Williams JA, *et al.* *Pattern formation in a secondary field: a hierarchy of regulatory genes subdivides the developing Drosophila wing disc into discrete subregions.* *Development.* 1993. 117:571–584.
- [169] Brand AH, *et al.* *Targeted gene expression as a means of altering cell fates and generating dominant phenotypes.* *Development.* 1993. 118:401–415.
- [170] del Valle Rodríguez A, *et al.* *Power tools for gene expression and clonal analysis in Drosophila.* *Nature Methods.* 2012. 9:47–55.
- [171] Perrimon N, *et al.* *In vivo RNAi: Today and Tomorrow.* *Cold Spring Harb Perspect Biol.* 2010.:a003640.
- [172] Perkins LA, *et al.* *The Transgenic RNAi Project at Harvard Medical School: Resources and Validation.* *Genetics.* 2015. 201:843–852.
- [173] Meyer EJ, *et al.* *Interkinetic Nuclear Migration Is a Broadly Conserved Feature of Cell Division in Pseudostratified Epithelia.* *Current Biology.* 2011. 21:485–491.
- [174] Ley K, *et al.* *Integrin-based therapeutics: biological basis, clinical use and new drugs.* *Nature Reviews Drug Discovery.* 2016. 15:173–183.
- [175] disintegrin in UniProtKB.
- [176] Eble JA, *et al.* *Vipera lebetina Venom Contains Two Disintegrins Inhibiting Laminin-binding β 1 Integrins.* *J. Biol. Chem.* 2003. 278:26488–26496.
- [177] Marcinkiewicz C, *et al.* *Significance of RGD Loop and C-Terminal Domain of Echistatin for Recognition of α IIb β 3 and α v β 3 Integrins and Expression of Ligand-Induced Binding Site.* *Blood.* 1997. 90:1565–1575.
- [178] Smith JB, *et al.* *Characterization of a monomeric disintegrin, ocellatusin, present in the venom of the Nigerian carpet viper, *Echis ocellatus* 1.* *FEBS Letters.* 2002. 512:111–115.
- [179] McGuire SE, *et al.* *Spatiotemporal Gene Expression Targeting with the TARGET and Gene-Switch Systems in Drosophila.* *Sci. STKE.* 2004. 2004:pl6–pl6.
- [180] Diaz-de-la-Loza M-C, *et al.* *Apical and Basal Matrix Remodeling Control Epithelial Morphogenesis.* *Developmental Cell.* 2018. 46:23-39.e5.
- [181] Wolfstetter G, *et al.* *The role of LamininB2 (LanB2) during mesoderm differentiation in Drosophila.* *Cell. Mol. Life Sci.* 2012. 69:267–282.
- [182] Borchiellini C, *et al.* *The function of type IV collagen during Drosophila muscle development.* *Mechanisms of Development.* 1996. 58:179–191.
- [183] Kc P, *et al.* *Cardiac tissue-derived extracellular matrix scaffolds for myocardial repair: advantages and challenges.* *Regen Biomater.* 2019. 6:185–199.

- [184] Royou A, et al. *Reassessing the Role and Dynamics of Nonmuscle Myosin II during Furrow Formation in Early Drosophila Embryos*. MBoC. 2003. 15:838–850.
- [185] Kondo T, et al. *Mitotic cell rounding accelerates epithelial invagination*. Nature. 2013. 494:125–129.
- [186] Theret DP, et al. *The Application of a Homogeneous Half-Space Model in the Analysis of Endothelial Cell Micropipette Measurements*. J Biomech Eng. 1988. 110:190–199.
- [187] Aoki T, et al. *The pipette aspiration applied to the local stiffness measurement of soft tissues*. Annals of Biomedical Engineering. 1997. 25:581–587.
- [188] Hutter JL, et al. *Calibration of atomic-force microscope tips*. Review of Scientific Instruments. 1993. 64:1868–1873.
- [189] Crick SL, et al. *Assessing Micromechanical Properties of Cells with Atomic Force Microscopy: Importance of the Contact Point*. Biomech Model Mechanobiol. 2007. 6:199–210.
- [190] Stephen Timoshenko author *Theory of plates and shells / by S. Timoshenko ...* (McGraw-Hill Book Company, Inc, New York)1940. First edition.
- [191] Johnson KL *Contact Mechanics* by K. L. Johnson. Cambridge Core. 1985.
- [192] Harris AR, et al. *Experimental validation of atomic force microscopy-based cell elasticity measurements*. Nanotechnology. 2011. 22:345102.
- [193] Krueger D, et al. *Downregulation of basal myosin-II is required for cell shape changes and tissue invagination*. The EMBO Journal. 2018. 37:e100170.
- [194] Goehring NW, et al. *Polarization of PAR Proteins by Advective Triggering of a Pattern-Forming System*. Science. 2011. 334:1137–1141.
- [195] Fritzsche M, et al. *Analysis of turnover dynamics of the submembranous actin cortex*. MBoC. 2013. 24:757–767.
- [196] Bunch TA, et al. *Characterization of mutant alleles of myospheroid, the gene encoding the beta subunit of the Drosophila PS integrins*. Genetics. 1992. 132:519–528.
- [197] Bellen HJ, et al. *The BDGP Gene Disruption Project: Single Transposon Insertions Associated With 40% of Drosophila Genes*. Genetics. 2004. 167:761–781.
- [198] Winter CG, et al. *Drosophila Rho-Associated Kinase (Drok) Links Frizzled-Mediated Planar Cell Polarity Signaling to the Actin Cytoskeleton*. Cell. 2001. 105:81–91.
- [199] Sun Y, et al. *Regulation of somatic myosin activity by Protein Phosphatase 1 β controls Drosophila oocyte polarization*. Development. 2011. 138:1991–2001.
- [200] Deak II, et al. *Mutations affecting the indirect flight muscles of Drosophila melanogaster*. Development. 1982. 69:61–81.
- [201] Richardson H, et al. *Ectopic cyclin E expression induces premature entry into S phase and disrupts pattern formation in the Drosophila eye imaginal disc*. Development. 1995. 121:3371–3379.